EXPERIMENTATION AND MODELING OF HOT PRESSING BEHAVIOUR OF VENEER-BASED COMPOSITES

by

Brad Jianhe Wang

B.Sc., Nanjing Forestry University, 1985
M.Eng., Nanjing Forestry University, 1988
M.Sc., The University of British Columbia, 1998

A THESIS SUBMITTED IN PARTIAL FULFILMENT OF
THE REQUIREMENTS FOR THE DEGREE OF

DOCTOR OF PHILOSOPHY

in

The Faculty of Graduate Studies

(Forestry)

THE UNIVERSITY OF BRITISH COLUMBIA

April 2007

ABSTRACT

To understand the unique hot pressing behaviour of veneer-based composites, the key objectives of this research were to: 1) characterize air permeabilities of veneers and gluelines; 2) examine fundamentals of veneer contacts for bonding; 3) explore mechanics of veneer compression; and 4) develop the first hot pressing simulation model to predict heat and mass transfer and panel densification in veneer-based composites.

To determine the mechanism of heat transfer, transverse air permeabilities of aspen (*Populus tremuloides*) veneers, phenol formaldehyde (PF) gluelines and aspen plywood/strandboard were first investigated. The laminate permeability theory was adopted to determine the relative contribution of the veneers and gluelines to panel permeability. A concept of effective porosity was also proposed based on the classic Carman-Kozeny theory to explain the difference in panel permeability and resulting hot pressing behaviour. It was concluded that veneer compression rather than glueline curing serves as the main barrier to gas and moisture movement, resulting in a negligible rate of transverse heat convection during hot pressing.

By examining veneer compression behaviour under various temperature and moisture content (MC) conditions, a revised wood transverse compression theory was proposed to include the first stage of "progressive contact" and define true yield displacement, and a novel method was developed for assessing veneer surface roughness/quality on an area basis. Through analyses of veneer contact area (glue coverage) under changing loads, the minimum compression required for achieving adequate veneer-to-veneer contacts was determined. Furthermore, the Greenwood and Tripp's contact theory was modified to explain how veneer surface roughness and compression affect panel bonding contacts. This led to the establishment of an optimum panel densification target for performance plywood/LVL products and shed a light on how to help prevent panel delamination.

Finally, the revised compression theory was applied to characterize veneer compressive stress-strain relationship, creep and springback behaviour during hot pressing. By introducing a concept of wood-glue mix layers and applying theories of heat and mass transfer and solid mechanics, a one-dimensional hot pressing model was successfully developed and validated. The model can predict the changes of temperature, MC, gas pressure and vertical density profile during hot pressing. The outcome of this research provides insight into the plywood/LVL hot pressing processes.

TABLE OF CONTENTS

LIST OF TABLES

LIST OF FIGURES

ACKNOWLEDGEMENTS

I offer my sincere gratitude to Forintek Canada Corp. and Faculty of Forestry of UBC, who have rendered me this opportunity to continue my education and study in this field.

I owe particular thanks to my academic supervisor Dr. Simon Ellis of UBC for his instruction and guidance, and research supervisor Dr. Chunping Dai of Forintek for his valuable advice and help throughout this research.

Thanks also go to my committee members Dr. Stavros Avramidis and Dr. Gregory Smith of UBC for their help and valuable feedback. Further, I thank my External Examiner, Dr. Ying Hei Chui, for his critical review of my dissertation and insightful feedback, and my University Examiners, Dr. Reza Vaziri and Dr. Thomas Maness, for their helpful correction and feedback, as well as Ms. Teresa Jones and Ms. Max Read at Faculty of Graduate Studies for their coordination and help.

In addition, I would like to thank Professor Changming Yu for his useful discussion during this study. Other help from Peter Ens, Xiaoyan Zhou, Francine Côté and Heng Xu is also readily acknowledged.

Finally, special thanks are owed to my family: son – Jason, daughter – Kelly, parents and wife for giving me motivation and support throughout my years of education.

DEDICATION

To my son Jason and daughter Kelly

CO-AUTHORSHIP STATEMENT

In Chapter II, Brad Jianhe Wang conducted the experimental design, prepared the materials for the permeability tests, performed the data analysis and drew the conclusions. As well, Brad Jianhe Wang prepared the manuscripts. Xiaoyan Zhou helped perform some of the permeability tests. Drs. Chunping Dai and Simon Ellis provided guidance to this study.

In Chapter III, Brad Jianhe Wang conducted the experimental design, prepared equipment and materials for the compression tests, performed the data analysis and drew the conclusions. As well, Brad Jianhe Wang prepared the manuscripts. Drs. Chunping Dai and Simon Ellis provided guidance during the course of this study.

In Chapter VI, Brad Jianhe Wang conducted the experimental design, prepared the materials for the hot pressing studies, performed the data analysis and drew the conclusions. As well, Brad Jianhe Wang developed the VPress® computer program and prepared the manuscripts. Professor Changming Yu joined the discussion and provided some help in establishing heat and mass transfer equations. Drs. Chunping Dai and Simon Ellis provided guidance for this modeling work.

CHAPTER I RATIONALE, CONCEPTS AND RESEARCH OUTLINE

1.1 Introduction

Wood composites can be mainly classified into two categories: veneer-based and non veneer-based. The former include laminated veneer lumber (LVL) and plywood; and the latter include fiberboard, medium density fiberboard (MDF), particleboard and oriented strand board (OSB). Due to its unidirectional structure and smaller strength variation than sawn lumber and glulam beams, LVL has become one of the main engineered wood composite products in North America for I-joist flanges, headers and beams with annual output exceeding 2.5 million m^3. On the other hand, the traditional plywood industry faces more challenges from OSB for applications such as subfloors and underlayments, wall and roof sheathing. Over the past decades, the Canadian wood resource has changed as second-growth species dominate and plantation species, such as trembling aspen (*Populus tremuloides*) and hybrid poplar, become mature (Knudson and Wang 2002). To stay competitive, plywood and LVL producers strive to reduce manufacturing costs and extract higher value from these species.

From a structural standpoint, OSB is made of short and discontinuous elements or strands which are generally coated with discrete resin spots and are then deposited onto a mat for consolidation. Due to this nature of formation, the mat is generally loose and porous. High densification is needed to compress the mat, to reduce between-strand voids and in turn to create adequate strand-to-strand contacts for bonding development. In contrast, plywood and LVL are made of solid veneer sheets covered with continuous glue layers (or films) or gluelines. In these veneer panels, the layered structure is much more striking. To create adequate veneer-to-veneer contacts for bonding, a relatively low densification is needed to overcome veneer surface irregularities such as roughness. Due to these essential differences, OSB is more permeable and requires high compression whereas plywood and LVL are less permeable and only require low compression.

From a manufacturing standpoint, hot pressing is a critical stage in wood composites production. It not only affects productivity and material recovery but also determines panel quality and performance. However, due to the difference in constituent elements and panel structure, the hot-pressing processes are quite different between non-veneer and veneer-based wood composites. Generally speaking, during OSB hot-pressing, as shown in Figure 1.1, three stages can be defined. In the first stage, the press platen is usually controlled by position while the mat reaches

maximum pressure. Mat thickness is controlled by the layer stress-strain relationships and creep responses. In the second stage, the mat reaches the target thickness which is then maintained for glue curing, but the mat pressure drops due to the combined effect of thermo-hydro softening and viscoelastic stress relaxation. During the third stage, the press opens for degassing and the mat springback results.

As shown in Figure 1.2, during plywood/LVL hot pressing, three distinct stages can also be identified. During the first stage, the press is quickly closed to generate intimate veneer-to-veneer contacts. By holding a constant pressure in the second stage, adequate bonds are achieved sequentially from surface to core while panel thickness decreases and a certain degree of panel densification results. The plywood/LVL manufacturing productivity is mainly controlled by the time needed for the innermost glueline to reach a target curing temperature. In the third stage, the panel is pressed under a predefined decompression cycle to avoid blisters/blows during which the innermost glueline temperature continues to rise to cure the glue and springback results.

To help understand the manufacturing process, over the past decades, tremendous efforts have been devoted to the hot-pressing simulation of non veneer-based wood composites, resulting in various simulation models with different levels of complexity (Kelly 1977; Humphery and Bolton 1989; Bolton and Humphrey 1994; Lenth and Kamke 1996; Carvalho *et al.* 1998; Haas *et al.* 1998; Wang and Winistorfer 2000; Haas and Fruhwald 2000, 2001; Dai *et al.* 2001; Dai and Yu 2005; Thoemen and Humphrey 2006). In most cases, responses of temperature, gas pressure and moisture content (MC) have been addressed. The mat consolidation or deformation has been the focus of other studies (Wolcott *et al.* 1990; Dai and Steiner 1993, 1994a, 1994b, 1994c, 1997; Dai 2001; Suo and Bowyer 1994; Lang and Wolcott 1996; Winistorfer and Young 1996; Xu 1999; Dai *et al.* 2000; Clouston and Lam 2001; Dai *et al.* 2002). Hooke's law modified with a nonlinear strain function was generally used to define the stress development during mat consolidation (Wolcott *et al.* 1990; Dai and Steiner 1993). The OSB compressibility was found to be associated with the stress-strain behaviour of each layer (Suo and Bowyer 1994). When viewing an average mat stress-strain relationship, the early stage of consolidation was generally seen as insignificant during OSB pressing. But as pointed out by Lang and Wolcott (1996), it could be crucial to the effective production of low density OSB panels. By realizing the effect of resulting density on panel performance, these models can simulate the formation of panel vertical

density profile (VDP) and/or horizontal density profile (HDP) during hot-pressing (Harless *et al.* 1987; Suchsland and Xu 1989; Xu 1999; Wong 1999; Dai *et al.* 2000; Carvalho *et al.* 2001; Dai *et al.* 2002).

Compared to OSB, plywood and LVL have different quality concerns which require different ways to control hot pressing variables. Currently, veneer surface quality, as generally measured by roughness, thickness (average and variance), and lathe checks (depth and frequency), has become an increasing concern to the plywood industry. Although there are methods for measuring the above three veneer quality criteria, their effects on gluebond performance have not been fully established. Since veneer surface quality changes from species to species, mill-to-mill and log-to-log, most of the studies have so far been qualitative in nature. In addition, the wide variations in veneer and pressing control variables in these studies also make quantitative comparisons very difficult. To date, only a few studies have aimed to quantify the effect of veneer surface roughness on bond quality and glue consumption (Faust and Rice 1986; Faust and Rice 1987; Neese *et al.* 2004). Both veneer roughness and lathe checks were found to influence gluebond quality measured by percent wood failure and shear load (Neese *et al.* 2004). To deal with increasing rough veneer resulting from declining log quality, plywood/LVL producers generally use higher glue spread and platen pressure to achieve target gluebond performance (Faust 1987). This practice would inevitably result in an increase in glue cost and a reduction in material recovery.

Due to the lack of technical information, the optimization of plywood/LVL hot pressing operations is still more or less trial and error. Zavala seems to be the only one who experimentally investigated the physical process of hot-pressing of 5-ply Douglas-fir plywood panels (Zavala 1986; Zavala and Humphery 1996). Based on his experimental results, it was speculated that due to the sealing effect of curing gluelines to gas and MC, the heat transfer by convection is limited and hence heat conduction is dominant during pressing. However, a numerical simulation of plywood hot pressing was not developed. Although the influence of gluelines on plywood properties was preliminarily studied (Okuma 1976), their effect on plywood hot pressing has not been studied. The effect of pressing pressure and veneer MC on compression of poplar LVL was experimentally studied (Zhang *et al.* 1994), which provides strong evidence concerning how hot pressing operations affect material recovery and product performance. Recently, the hot-pressing behaviour and strength properties of 13-ply aspen LVL

and 5-ply Douglas-fir and spruce plywood were studied (Wang 2001a; Wang 2001b; Wang *et al.* 2002; Wang 2003). These studies demonstrated that the level of glue spread significantly affected the hot pressing time needed for the innermost glueline to reach a target temperature due to the MC concentration near the glueline, which generally accounts for 50% to 80% of total MC in the panel. Moreover, during the pressing even at the decompression stage, gas was largely entrapped inside the panel as its pressure generally kept increasing, indicating a low panel transverse permeability. However, the permeability change of the veneer and glueline during hot pressing has so far not been quantified.

In summary, the literature clearly indicates that compared to non veneer-based wood composites, veneer-based composites have distinct characteristics in terms of both structures and manufacturing processes. Work on modeling wood composites has so far been focused on non veneer-based composites. A numerical simulation of the hot-pressing process of plywood/LVL products is currently not available.

1.2 Methodologies for Plywood/LVL Hot Pressing Simulation

The goal of this research is to simulate the hot-pressing behaviour of plywood/LVL products. Figure 1.3 shows the methodologies in a flowchart for developing a plywood/LVL hot pressing simulation model. First of all, the plywood/LVL hot pressing operation will be conceptualized by making hypotheses. Then, the key variables in plywood/LVL hot-pressing will be determined. In the meantime, theories in heat and mass transfer, solid mechanics and numerical methods will be adopted to describe the complex phenomenon during hot pressing. Using aspen veneer as an example, the model input parameters will be determined based on current pressing operations, veneer property analysis and experimental material characterization. Subsequently, the model will be validated through a comparison between predictions and experimental results.

As shown in Figure 1.4, plywood/LVL hot pressing involves a number of key variables from the veneer, panel lay-up and pressing control. The veneer variables include those from tree growth characteristics such as density and those from veneer processing such as veneer surface quality, thickness, MC, and visual grade or stress grade. The panel lay-up variables consist of number of plies, stacking sequence, ply orientation and glue spread level whereas the pressing control variables include platen temperature, platen pressure, target innermost glueline temperature,

target panel thickness and pressing time. The hot pressing simulation consists of two key modules: heat and mass transfer model to predict temperature, gas pressure and MC; and panel densification model to predict panel density profile and stiffness.

1.3 Key Fundamental Issues

To improve plywood/LVL manufacturing productivity, material recovery and panel quality and performance, a more fundamental understanding of heat and mass transfer and panel densification during hot pressing is needed. As shown in Figure 1.5, veneers and gluelines are the two basic constituent elements for plywood and LVL products in which the glueline is relatively thin but has much higher density than the veneer. This is due to the higher density of solids and water from the glue as compared to the wood veneer. To maintain the integrity of the products, during hot pressing, continuous gluelines need to be formed to create veneer-to-veneer bonds, and all gluelines, especially at the innermost, must be adequately cured. The former depends heavily upon the amount of glue spread, veneer surface roughness/quality and panel densification whereas the latter generally determines duration of the pressing time, namely manufacturing productivity. A low level of glue spread or low panel densification allows existence of veneer-to-veneer gaps, resulting in inadequate bonding sites and low gluebond performance. On the other hand, a high level of glue spread not only increases glue cost and chance of defective bonding, but also prolongs the pressing time required for a full glue cure due to high water concentration at or near the gluelines. Quantitatively, as shown in Figure 1.6, the pressing time will increase by about 15% when glue spread level increases from 100 g/m^2 to 200 g/m^2 (Wang 2006), which indicates that the glueline plays an important role in heat and mass transfer.

Since veneers and gluelines are in a layered form and more or less continuous, curing process is sequential from panel surface to core. In such a case, heat conduction and convection could occur simultaneously. The former is through interfacial thermal contacts whereas the latter is associated with the movement of air and vapour through the panel thickness with its magnitude determined by the transverse permeability of veneers and gluelines.

In the meantime, glue-coated veneers are consolidated under heat and pressure to create veneer-to-veneer contacts in a progressive manner. However, as shown in Figure 1.7, machined veneer

surface, either peeled or sliced, generally displays a typical 3-D roughness profile with many peaks and valleys. Due to the variation of veneer surface roughness, the contact area of different veneer-to-veneer pairs may not be the same under the same pressure. Good gluebonds can only be developed when veneer-to-veneer contacts are adequate at a certain level of veneer compression or panel densification. With further increasing panel densification, panel stiffness could be enhanced but material recovery will inevitably decrease. So far, no work has been done to tackle such fundamental issues as: 1) how the permeabilities of veneers and gluelines change during plywood/LVL hot pressing; 2) how veneer-to-veneer contacts are achieved for bonding development; and 3) how veneers behave physically and mechanically with increasing compression. As a result, information has been dramatically lacking concerning how to balance manufacturing productivity, material recovery, panel quality and performance.

1.3.1 Glueline Permeability in Relation to Heat and Mass Transfer

The mechanisms of heat and mass transfer through layered veneer structure and strand mattresses could be quite different. Currently, how gluelines affect heat and mass transfer during plywood/LVL hot-pressing remains unknown; and a quantitative analysis of heat and mass transfer for plywood/LVL has not been available. In comparison with non veneer-based wood composites, it was only speculated that the glueline acts as a main barrier to gas and MC movement, resulting in a negligible convection effect (Bolton and Humphrey 1988; Zavala and Humphrey 1996). Through characterization of air permeability of veneers and gluelines, their sealing effect can be ascertained; the relative strength of heat conduction and convection during hot pressing can be quantified. As a result, the mechanism of heat and mass transfer during plywood/LVL hot pressing can be determined. If the sealing effect of the veneers and gluelines is not significant, the convection effect should be considered.

1.3.2 Fundamentals of Veneer Contact for Bonding

The key in the wood composite manufacturing process is to promote bonding through developing intimate element-to-element contacts from consolidation. Due to the natural complexity of 3-D veneer surface roughness profile, a fundamental understanding of veneer-to-veneer contacts has not been available. For plywood, gluebond performance is a key quality concern which is generally evaluated by percent wood failure and shear strength. These properties were shown to be affected by veneer surface roughness, degree of glue cure (or

pressing time), lathe checks and annual ring characteristics (Chow and Hancock 1968; Neese *et al.* 2004; Devallance 2005). Rough veneer generally reduced surface-to-surface contacts, allowing gaps in the glueline that might weaken the cohesive strength of the bond. Coupled with a larger thickness variation, rough veneer generally enhanced both over-penetration and dryout (Neese *et al.* 2004). The overall effects of veneer surface roughness were to reduce the gluebond quality or percent wood failure dramatically compared to smooth veneer (Faust 1987). When conditions for dryout or over-penetration are present, rough veneer reduced gluebond quality more than would normally be expected (Faust and Rice 1987).

In general, the percent wood failure can be increased by reducing veneer surface roughness whereas shear strength can be enhanced by reducing lathe check frequency (Devallance 2005). Currently, a common problem facing the plywood/LVL industry is panel delamination, for which a major cause is poor quality gluebonds with a low percent wood failure resulting from rough veneer. To date, the effect of veneer surface roughness on interfacial veneer-to-veneer contacts, transverse compressibility and material recovery has so far not been studied. To establish the required plywood/LVL densification, the concept of contact area can be used to analyze the bond development. However, no literature has been available to quantitatively link the panel gluebond quality to the veneer-to-veneer contact area. As a result, characterizing veneer contact area could provide insight into how much panel densification is required to achieve target panel gluebond performance while maximizing material recovery.

Panel densification affects not only material recovery and panel gluebond performance but also panel stiffness and strength (Zhang *et al.* 1994). In some cases, panel densification in hot pressing can surpass the level required for achieving adequate veneer-to-veneer contacts. Particularly, this is the case for LVL manufacturing in which panel stiffness and strength are primary concerns. However, due to the variation in species, cell structure and surface roughness/quality, the optimum levels of panel densification have not yet been established. On one hand, a fair amount of panel densification is required to eliminate veneer surface irregularities (mainly roughness) to create adequate veneer-to-veneer contacts for bonding development. Excessive densification, on the other hand, could cause negative effects such as heavier products, more thickness loss, higher dimensional changes in service (Wellons *et al.*

1983) and lower gluebond performance resulting from wood cell wall buckling and yielding or fracture.

Realizing the effect of constituent veneer elements on product performance, a model was once developed to predict the bending stiffness and strength of structural plywood (Booth 1990; Booth and Hettiarachchi 1990). However, how panel densification affects plywood/LVL gluebond quality and overall performance has not been experimentally studied. For plywood products, which are generally made from visually graded veneer, the target is to achieve required panel gluebond performance (or target percent wood failure) while minimizing panel thickness loss. To maximize material recovery and reduce manufacturing cost, a minimum level of panel densification could be experimentally determined based on investigation of the veneer-to-veneer contact area. In contrast, for LVL products, which are generally made from stress graded veneer, the goal is to achieve target product performance such as stiffness and strength while increasing manufacturing productivity and material recovery. An optimum range of panel densification could be rigorously established based on an analysis of veneer transverse compression behaviour.

In addition to above experimental approaches, a theoretical analysis is deemed necessary to advance further understanding of veneer-to-veneer contacts and describe how the contact area is affected by veneer surface roughness, the load applied and level of compression. The theory of contact mechanics could be applied to model the veneer-to-veneer contact area and pressure as a function of veneer surface roughness and panel densification.

1.3.3 Mechanics of Veneer Compression

Panel densification in the hot pressing process is generally controlled by the coupled mechanism of veneer thermo-hydro softening and viscous creeping (Wellons *et al.* 1983; Dodig and Jayne 1993; Leijten 1994). To understand how veneers are densified during hot-pressing and their effect on panel performance, veneer transverse compression behaviour under ambient conditions and changing MC and temperature environments needs to be investigated. As well, veneer viscous creep behaviour under constant loads (or pressures) needs to be determined. Through experimental investigations, veneer instantaneous and time-dependent compressive stress-strain relationships can be established. Furthermore, veneer elastoplastic (springback) behaviour

determines final irrecoverable deformation of the panel after press unloading. Through compression and springback tests, veneer springback ratio and thickness recovery can be determined in relation to temperature, MC and compression level. These results should be used to determine the changes of veneer layer deformation during hot-pressing and final density profile of plywood/LVL products.

To develop a theoretical panel densification model, veneer transverse compressive stress-strain behaviour should be determined over a wide range of temperature, MC and compression strain. A modified Hooke's law with a non-linear strain function has shown success in modeling of the stress-strain relationship for non veneer-based panels such as OSB and MDF. The underlying assumption was that the non-linear strain function is dependant only on the cellular structure or deformation process; therefore, this method can separate the effect of temperature and MC on the wood compression Young's modulus from its general deformation behaviour. However, as mentioned, the constituent elements, panel structure and pressing methods are quite different among these products. For OSB and MDF, the entire compression appears more essential. By comparison, for plywood/LVL, the early compression or relatively small compression is generally more crucial. As a result, whether the modified Hooke's law is adequate to describe veneer compressive stress-strain relationship for plywood/LVL hot pressing simulation needs to be explored.

1.4 Research Objectives

While improving the fundamental understanding of the plywood/LVL hot-pressing process, this research will address the following specific objectives:

1) to characterize air permeability of veneers and gluelines;
2) to examine fundamentals of veneer-to-veneer contacts in terms of veneer surface roughness, load applied and densification; and
3) to investigate mechanics of veneer compression.

The ultimate goal of this research is to develop a theoretical model to predict heat and mass transfer and panel densification during hot-pressing. To determine the hot-pressing time required for a full glue cure and how panel density profile is formed, quantifying temperature, MC and deformation at or near glueline zones is essential. On the basis of defining wood-glue mix layers

through the panel thickness, a finite-difference based plywood/LVL hot-pressing model can be developed to simulate the changes of temperature, MC, gas pressure and panel density throughout the pressing cycle. The model should be able to evaluate the sensitivity of the main variables that affect hot-pressing time (productivity), panel compression (material recovery) and vertical density profile (panel performance).

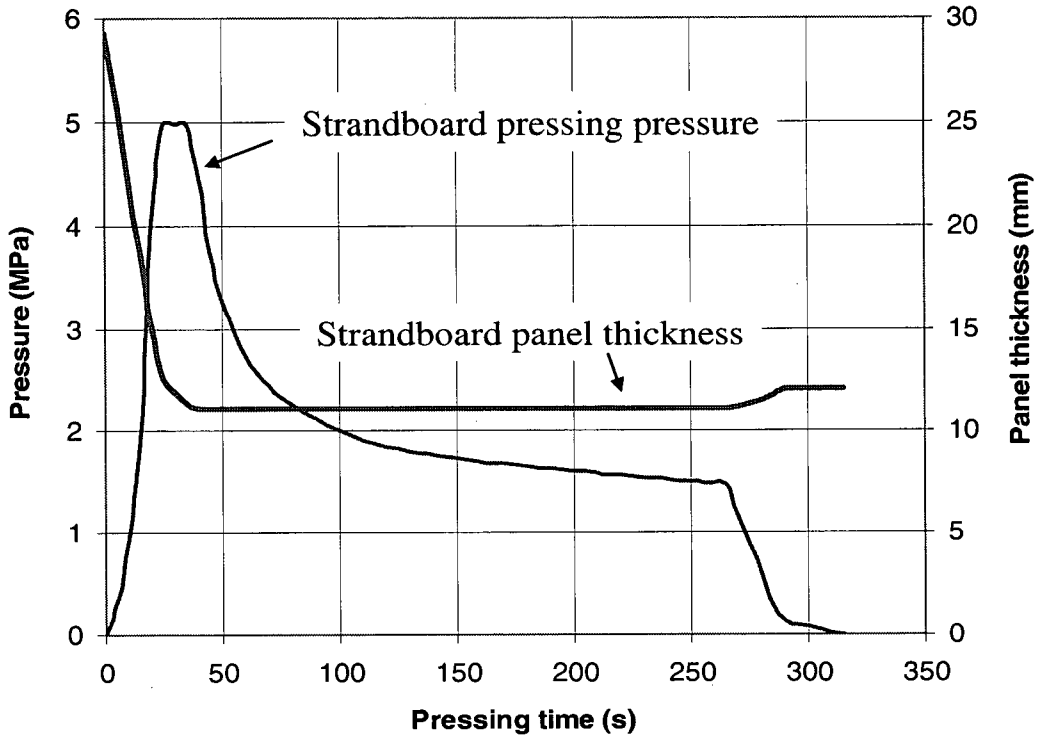

Figure 1.1 Typical pressing schedule for OSB

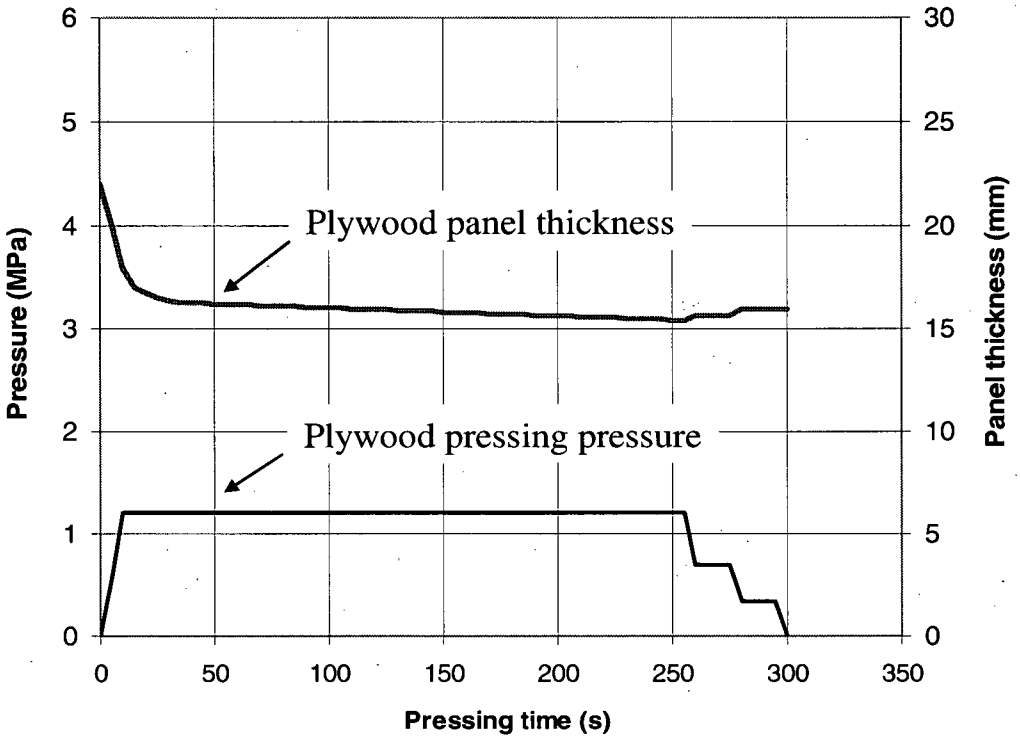

Figure 1.2 Typical pressing schedule for plywood

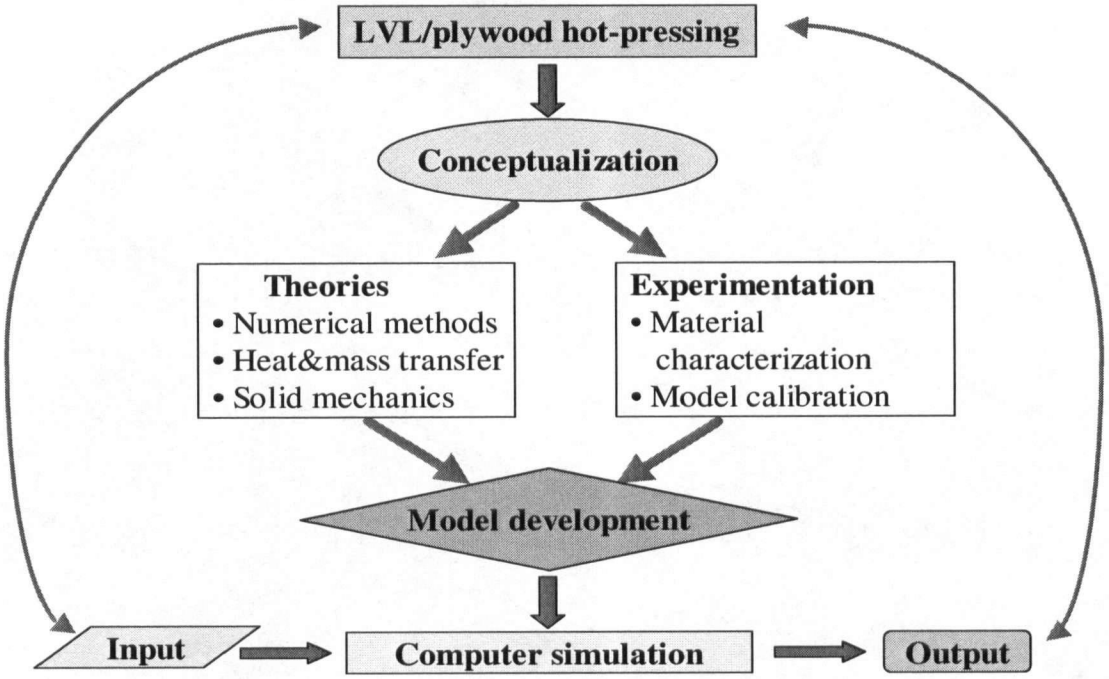

Figure 1.3 Methodologies for plywood/LVL hot-pressing simulation

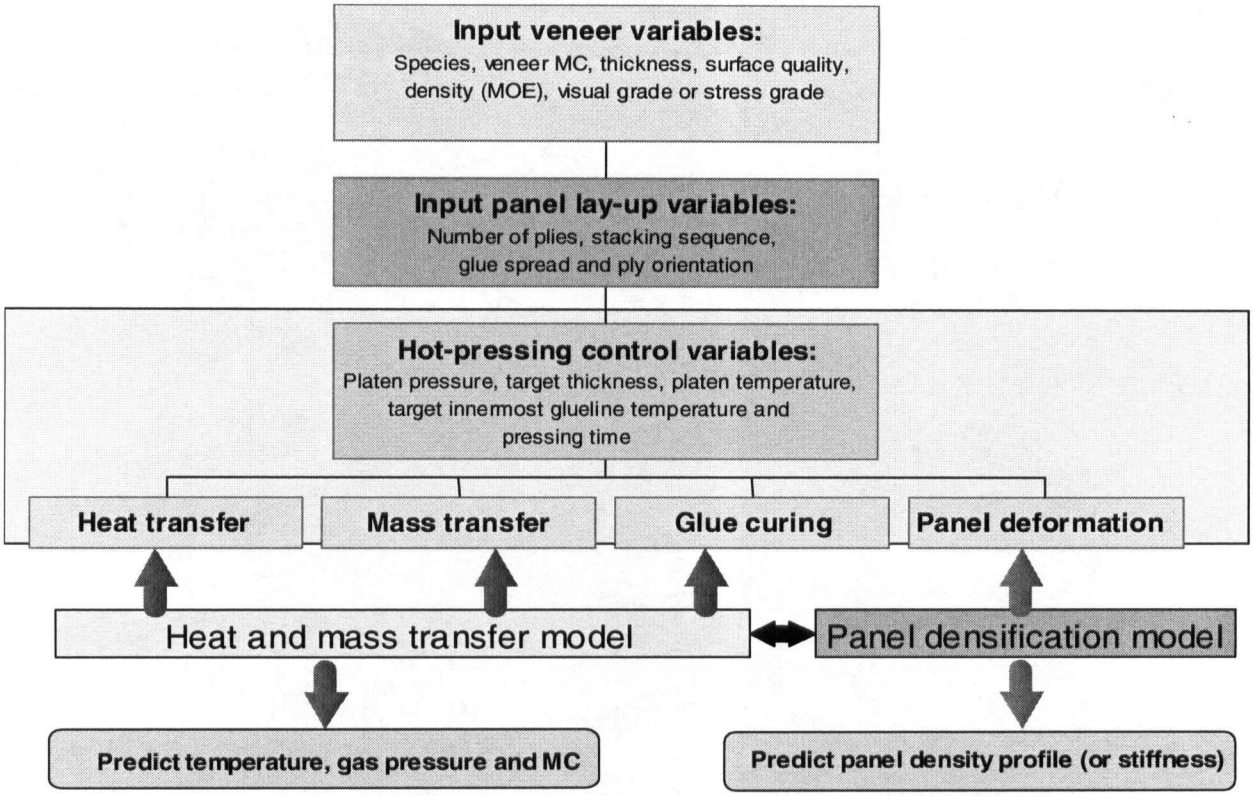

Figure 1.4 Simulation modules for plywood/LVL hot-pressing

(a)

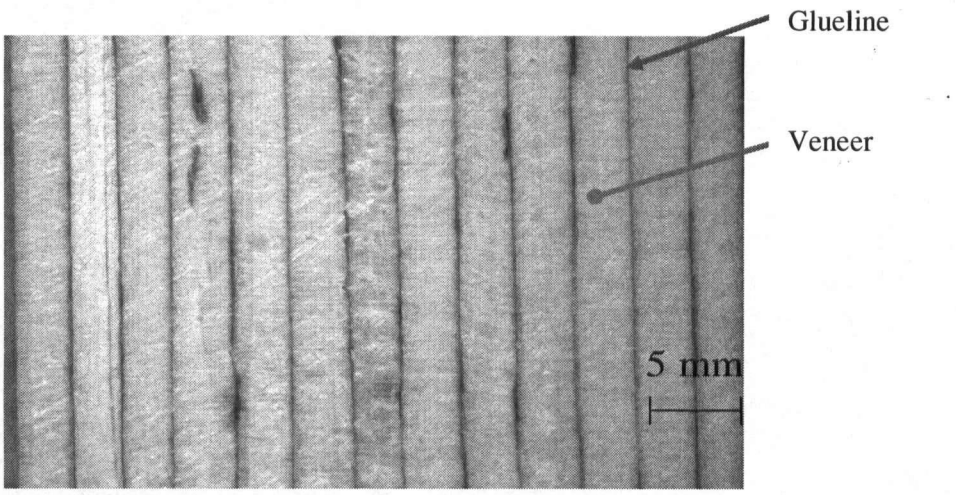

(b)

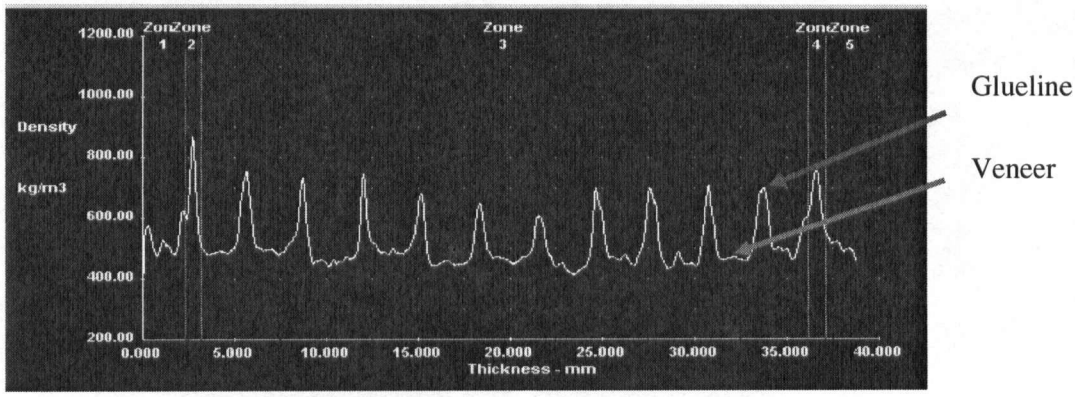

Figure 1.5 Two basic elements in veneer-based composites: veneer and glueline.

(a) A cross-section of 13-ply aspen LVL

(b) A vertical density profile (VDP) of that section

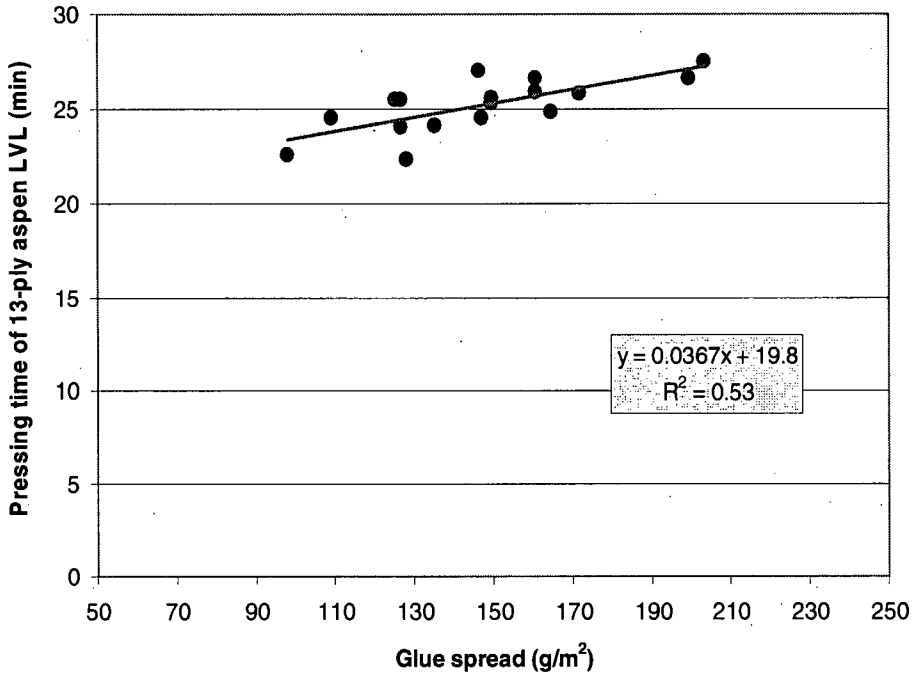

Figure 1.6 The effect of glue spread level on pressing time of 13-ply aspen LVL

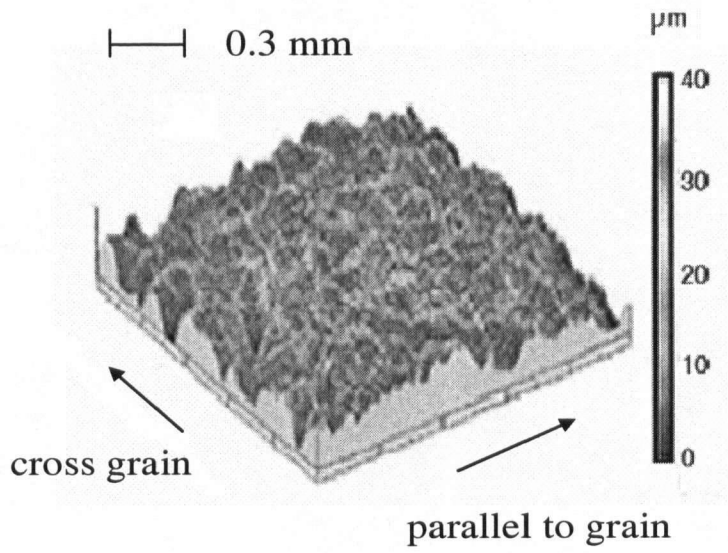

Figure 1.7 Typical 3-D veneer surface roughness profile (tight side)

1.5 Bibliography

Bodig, J. and B. A. Jayne. 1993. Mechanics of wood and wood composites. Kriegen publishing company, Malabar, Florida. 712 pp.

Bolton, A. J. and P. E. Humphrey. 1988. The hot-pressing of dry-formed wood-based composites (Part I). Holzforschung. 42: 403-406.

Bolton, A. J. and P. E. Humphrey. 1994. The permeability of wood-based composite materials. Part 1. A review of the literature and some unpublished work. Holzforschung. 48: 95-100.

Booth, L. G. 1990. Predicting the bending strength of structural plywood. Part 1: a theoretical model. J. Inst. Wood Sci. 12(1): 14-47.

Booth, L. G. and M. T. P. Hettiarachchi. 1990. Predicting the bending strength of structural plywood. Part 2: an experimental verification. J. Inst. Wood Sci. 12(2): 48-58.

Carvalho, L. M. H. and C. A. V. Costa. 1998. Modelling and simulation of the hot-pressing process in the production of MDF. Chem. Eng. Comm. 170: 1-21.

Carvalho, L. M. H., M. R. N. Costa and C. A. V. Costa. 2001. Modelling rheology in the hot-pressing of MDF: Comparison of mechanical models. Wood and Fiber Sci. 33(3): 395-411.

Chow, S. Z. and W. V. Hancock. 1968. Method for determining degree of cure of phenolic resin. Forest Prod. J. 19(4):24-29.

Clouston, P. L. and F. Lam. 2001. Computational modeling of strand-based wood composites. J. of Engi. Mech. 127(8):844-851.

Dai, C. 2001. Viscoelastic behaviours of wood composite mats during consolidations. Wood and Fiber Sci. 33(3):353-363.

Dai, C. and P. R. Steiner. 1993. Compression behaviour of randomly-formed wood flake mats. Wood and Fiber Sci. 25(4): 349-358.

Dai, C. and P. R. Steiner. 1994a. Spatial structure of wood composites in relation to processing and performance characteristics. Part II. Modelling and simulation of a randomly-formed flake layer network. Wood Sci. and Tech. 28(2):135-146.

Dai, C. and P. R. Steiner. 1994b. Spatial structure of wood composites in relation to processing and performance characteristics. Part III. Modelling and simulation of a random multi-layered flake mat. Wood Sci. and Tech. 28(3):229-239.

Dai, C. and P. R. Steiner. 1994c. Analysis and implications of structure in short fibre wood composites. In: Proceedings of the Second Pacific Rim Bio-based Composites Symposium. Vancouver, Canada. 17-24.

Dai, C. and P. R. Steiner. 1997. On horizontal density variations in randomly-formed short-fibre wood composite boards. Composites. 28A: 57-64.

Dai, C., C. Yu and P. Hubert. 2000. Modeling vertical density profile in wood composite boards. Proceedings of the 5th Pacific Rim Bio-based Composites Symposium. Canberra, Australia. pp. 220-226.

Dai, C., C. Yu and B. J. Wang. 2001. Modeling of OSB hot pressing processes. Forintek Canada Corp. Report –1062.18pp.

Dai, C. and C. Yu. 2004. Heat and mass transfer in wood composite panels during hot-pressing: Part I. A physical-mathematical model. Wood and Fibre Sci. 36(34):585-597.

Dai, C., C. Mei and H. Korai. 2002. Density and property relationships of wood strand composites. 6th Pacific Rim Bio-based Composites Symposium. Pullman. USA. pp. 458-466.

Devallance, D. B. 2005. Douglas-fir plywood gluebond quality as influenced by veneer roughness, lathe checks, and annual ring characteristics. June 19-22. Posters at 59th International Convention of Forest Prod. Soc. Quebec City, Quebec, Canada.

Faust, T. D. and J. T. Rice. 1986. Effects of veneer surface roughness on the bond quality of southern pine plywood. Forest Prod. J. 36(4):57-62.

Faust, T. D. and J. T. Rice. 1987. Effects of a variable glue application rate strategy on bond quality and resin consumption in the manufacture of southern pine plywood. Forest Prod. J. 37(7/8):64-70.

Faust, T. D. 1987. Real-time measurement of veneer surface roughness by image analysis. Forest Prod. J. 37(6):34-40.

Haas, G. V., A. Steffen and A. Fruhwald. 1998. Permeability of fiber, particle and strand mats for gas. Holz als Roh- und Werkstoff. 56:386-392.

Haas, G. V. and A. Fruhwald. 2000. Compression behaviour of fiber, particle and strand mats. Holz als Roh- und Werkstoff. 58:317-323.

Haas, G. V. and A. Fruhwald. 2001. Rheological behaviour of fiber, particle and strand mats. Holz als Roh- und Werkstoff. 58:415-418.

Harless, P. E., F. G. Wagner, P. H. Short, R. D. Seale, P. H. Mitchell and D. S. Ladd. 1987. A model to predict the density profile of particleboard. Wood and Fiber Sci. 19(1): 81-92.

Humphery, P. E. and A. J. Bolton. 1989. The hot pressing of dry-formed wood-based composites: Part II. A simulation model for heat and moisture transfer, and typical results. Holzforschung. 43(3): 199-206.

Kelly, M. 1977. Critical review of relationships between processing parameters and physical properties of particleboard. General Technical Report FPL-10. US FPL: Madison, Wis.

Knudson, R. M. and B. J. Wang. 2002. Manufacture of LVL and plywood from short rotation hybrid poplar. Forintek Canada Corp. Report-2019. 91pp.

Lang, E. and M. P. Wolcott. 1996. A model for viscoelastic consolidation of wood-strand mats. Part II. Static stress-strain behaviour of the mat. Wood and Fiber Sci. 28(3):369-379.

Leijten, A. 1994. Properties of densified veneer. Pacific Timber Engineering Conference, Gold Coast Australia. 648-657.

Lenth, C. and F. A. Kamke. 1996. Investigations of flakeboard mat consolidation Part II. Modelling mat consolidation using theories of cellular materials. Wood and Fiber Sci. 28 (3): 309-319.

Neese, J. L., J. E. Reeb and J. W. Funck. 2004. Relating traditional surface roughness measures to gluebond quality in plywood. Forest Prod. J. 54(1):67-73.

Okuma, M. 1976. Plywood properties influenced by the glueline. Wood Sci. and Tech. 10: 57-68.

Suchsland, O. and H. Xu. 1989. A simulation of the horizontal density distribution in a flakeboard. Forest Prod. J. 39(5): 29-33.

Suo, S. and J. Bowyer. 1994. Simulation modelling of particleboard density profile. Wood and Fiber Sci. 26(3):397-441.

Thoemen, H. and P. E. Humphrey. 2006. Modeling the physical processes relevant during hot pressing of wood-based composites. Part I. Heat and mass transfer. Holz als Roh- und Werkstoff. 64:1-10.

Wang, B. J. 2001a. Characterizing aspen veneer for LVL/plywood products Part I: Stress grade of veneer. Forintek Canada Corp. General Report-2019(5).14pp.

Wang, B. J. 2001b. Characterizing aspen veneer for LVL/plywood products Part II: Pressing strategies and strength. Forintek Canada Corp. General Report-2019(6). 41pp.

Wang, B. J. and C. Dai. 2001. Characterizing veneer stress grades for plywood/LVL products. Symposium on utilization of agricultural and forestry residues. Nanjing, P. R. China. 270-276.

Wang, B. J., C. Dai and S. Ellis. 2002. Hot-pressing behaviour and strength properties of laminated veneer lumber made from stress graded aspen veneer. Proceedings of the 6th Pacific Rim Bio-Based Composites Symposium. Portland, Oregon, USA. 423-435.

Wang, B. J. 2003. Hot-pressing behaviour of 5-ply Douglas-fir and spruce plywood. Forintek Report-2019(7). 28 pp.

Wang, B. J. 2006. Improving productivity, recovery and quality of veneer products with new pressing method. Funded by Forest Innovation Investment (FII-MDP-07-0015), B. C. Canada. Unpublished results.

Wang, S. and P. M. Winistorfer. 2000. Consolidation of flakeboard mats under theoretical laboratory pressing and simulated industrial pressing. Wood and Fiber Sci. 32(4):527-538.

Wellons, J. D., R. L. Krahmer, M. D. Sandoe and R. W. Jokerst. 1983. Thickness loss in hot-pressed plywood. Forest Prod. J. 33(1):27-34.

Winistorfer, P. and T. M. Young. 1996. Modelling and comparing vertical density profiles. Wood and Fiber Sci. 28(1):133-141.

Wolcott, M. P., F. A. Kamke and D. A. Dillard. 1990. Fundamental aspects of wood deformation pertaining to manufacture of wood-based composites. Wood and Fiber Sci. 26(4):496-511.

Wong, E. D. 1999. Effects of density profile on the mechanical properties of particleboard and fiberboard. Review article.

Xu, W. 1999. Influence of vertical density distribution on bending MOE of wood composite panels: A theoretical consideration. Wood and Fiber Sci. 31(3): 277-282.

Zavala, D. 1986. Analysis of process operative within plywood during hot-pressing. Ph.D dissertation. Oregon State University.

Zavala, D. and P. Humphery. 1996. Hot pressing veneer-products: the interaction of physical process. Forest Prod. J. 46 (1): 69-77.

Zhang, H. J., Y. H. Chui and M. H. Schneider. 1994. Compression control and its significance in the manufacture and effects on properties of poplar LVL. Wood Sci. and Tech. 28(4):285-290.

CHAPTER II CHARACTERIZING AIR PERMEABILITIES OF VENEERS AND GLUELINES[1]

2.1 Introduction

Permeability is a measure of the ease with which fluids move through a porous material under the influence of a pressure gradient. Wood is permeable because it is a cellular material and the void spaces are interconnected by pits. These pits are openings between longitudinal tracheid lumens of softwoods or between the lumens of hardwood vessels and fibers (Siau 1995). Wood permeability has a remarkable effect on drying, the production of panels, and all kinds of chemical treatment of wood. Thus far, tremendous efforts have been devoted to this topic in terms of species and their growth conditions, such as the flow directions of vapour and ways to increase permeability (Lin 1972; Kuroda and Siau 1988; Bolton and Humphrey 1994; Bao *et al.* 2001).

During the hot pressing of wood composites, a panel's transverse (vertical) air permeability determines the degree of penetration and diffusion of hot gas, a mixture of air and vapour, from surface layers to the core at the stage of panel consolidation and curing. This parameter also influences the ease of gas evaporation at the stage of degassing. The first inward gas movement will affect the rate of core temperature rise and hence efficiency of hot-pressing. During the later stage of pressing, the outward gas movement will allow core gas pressure to release to avoid blisters or blows. Furthermore, the permeability is an important factor related to structural durability since it affects moisture content (MC), sorption and desorption, the ease of post-treatment and the degree of formaldehyde emission in service.

Realizing its critical importance, some work has been done to characterize the transverse air permeability in terms of element geometry, mat density and forming characteristics for strandboard, medium density fiberboard (MDF) and particleboard (Bolton 1988; Bolton and Humphrey 1994; von Haas 1998). Recently, a theoretical permeability model was developed for

[1] A version of this chapter has been published in two papers.
1. Wang, B. J., X. Zhou, C. Dai and S. Ellis. 2004. The Permeability of Veneer-Based Wood Composites Pertaining to Hot-Pressing Process. Proceedings of the 7th Pacific Rim Bio-Based Composites Symposium. Nanjing, P. R. China. Volume II. 91-100.
2. Wang, B. J., X. Zhou, C. Dai and S. Ellis. 2006. Air permeability of Aspen Veneer and Glueline: Experimentation and Implications. Holzforchung. Vol.60:304-312.

strandboards based on the classic Carman-Kozeny theory (Dai *et al.* 2005). It was found that strandboard mat permeability was mainly controlled by voids between strands instead of those inside strands. Mat density had a primary effect and strand size had a secondary effect on mat porosity and permeability. The between-strand voids in the final products were about 2.5-10.0% of panel volume depending on the board density. These results were helpful to determine the rate of heat convection during hot pressing. However, for veneer-based composites, such as plywood and LVL, veneer plies and gluelines are more or less continuous. The governing mechanism of the product permeability may be quite different from that of strandboard. Due to the complexity caused by water vapour and panel compression, the real-time glueline permeability has never been measured. As discussed in Chapter 1, to date, no studies have been conducted on permeabilities of the veneer and glueline and their effect on panel hot pressing. It was only speculated that during plywood hot-pressing, the heat convection was limited due to the very low permeability of curing gluelines, and therefore, the main heat transfer was supposed to be heat conduction (Zavala and Humphrey 1996).

To improve the fundamental understanding of the hot-pressing processes for veneer-based composites, the objectives of this work were: 1) to investigate experimentally the transverse (vertical) air permeabilities of veneers and gluelines; 2) to measure and compare the permeabilities of veneer panels and strandboards; and 3) to determine the effect of the permeabilities of veneers and gluelines on plywood hot pressing. By excluding the effect of the panel compression, the change of the glueline permeability from uncured state to cured state was examined. Based on the permeability tests of the veneer and veneer panels, the main factors affecting panel permeability were identified. The theory for permeability through laminates was applied to determine the relative contribution of veneers and gluelines to panel permeability and to clarify their role in heat and mass transfer. Furthermore, the classic Carman-Kozeny theory was adopted to determine the effective porosity in the veneer panels. Finally, the effect of the permeability on panel hot pressing behaviour was demonstrated through manufacturing of plywood and strandboard panels.

2.2 Materials and Methods

Trembling aspen (*Populus tremuloides*) was chosen because it is an emerging species in North America for plywood/LVL manufacturing. As shown in Figure 2.1, this wood is a diffuse-porous hardwood having a rather uniform diameter of vessels throughout the growth ring (Mei and Dai 2003). Ten 1.22 m (4 -ft) long fresh aspen logs (34.3 cm in average diameter) were acquired from a mill in Eastern Canada. Then, four logs were randomly selected and each of them was cut into four 30.5 cm (12 -in) blocks for peeling 3.2 mm (1/8 -in) thick veneer with a mini-lathe. Before peeling, the boundary of sapwood and heartwood of each block was determined based on their colour difference delineated on the end grain of the blocks. After peeling, five hundred 30.5 x 30.5 -cm (12 x 12 -in) veneer sheets were sampled and marked sequentially from veneer ribbons and separated into the following three groups: sapwood, sapwood/heartwood mix and heartwood. Subsequently, these veneer sheets were dried in an oven (103°C) to a target MC of 3% on an oven dry basis. Half of the veneer sheets (250 sheets with odd number) were used to cut 60 mm diameter veneer disks. Four to ten veneer disks were generated from each veneer sheet. In total, about 1200 veneer disks were prepared with 450, 200 and 550 disks being from the sapwood, sapwood/heartwood mix and heartwood veneer, respectively. The remaining half (250 sheets with even number) were used for making two-ply 30.5 x 30.5 -cm (12 x 12 -in) veneer panels.

For preparing plywood with dimensions of 5-ply 15.5 mm (5/8 -in) 61x 61-cm (24 x 24 -in), three aspen logs were peeled using a 122 cm (4 -ft) lathe for 3.2 mm (1/8 -in) thick veneer. Veneer ribbons were then clipped into 122 x 61 -cm (48 x 24 -in) sheets. Fifty 61 x 61 -cm veneer sheets were cut and dried down to a target MC of 5% on an oven dry basis.

For preparing strandboards with dimensions of 11 mm (7/16 -in) 32 x 32 -cm and 61x 61 -cm, three remaining aspen logs were peeled using the 122 cm lathe for 0.75 mm (0.03 -in) thick veneer. After peeling, veneer ribbons were clipped into 122 x 61 -cm (48 x 24 -in) sheets, which were further trimmed into uniform 101.6 x 25.4 x 0.75 -mm (4.0 x 1.0 x 0.03 -in) veneer strands along the grain direction. Then strands were dried to a target MC of 5% on an oven-dry basis, blended with 2% (w/w) powered phenol formaldehyde (PF) resin and hand-formed into randomly oriented strand mats.

2.2.1 Permeability Measurements on Veneers and Gluelines

Permeability is a function of the porous structure of the medium, and is numerically equal to the rate of flow of a fluid of unit viscosity through a unit cube of the material with a unit pressure differential between two parallel faces. The measurements of transverse (vertical) air permeability were performed using the apparatus represented in Figure 2.2. According to Darcy's law for gases (Dullien 1992), the formula for calculating air permeability is as follows:

$$K = \frac{\mu \cdot L \cdot Q \cdot P_2}{F \cdot \Delta P \cdot \bar{P}} \qquad (2\text{-}1)$$

where K = permeability (m^2);

μ = viscosity of fluid ($Pa \cdot s$), for gas at room temperature $\mu = 1.846 \times 10^{-5}\ Pa \cdot s$;

L = length in flow direction (m);

F = cross-sectional area of the specimen (m^2);

Q = volumetric flow rate at pressure P_2 (m^3 /s);

ΔP = pressure differential = $P_1 - P_2$ (Pa);

$\bar{P}$ = arithmetic average pressure = $(P_1 + P_2)/2$ (Pa);

P_1 = given air pressure (Pa); and

P_2 = pressure at which Q was measured (Pa).

To determine the effect of various factors on permeabilities of veneer panels, a t-test was adopted. The t-test is commonly used to assess whether the means of two groups, i.e., treated and control, are statistically different from each other (Montgomery 2005). The t-value is calculated as a ratio of the difference between the two means over the standard error of the difference. This t-value is positive if the first mean is larger than the second and negative if it is smaller. By comparing the computed t-value with a critical value in a standard table of significance, a judgement can be made whether a significant difference exists between the means of the two groups.

To determine the effect of sapwood/heartwood composition on veneer permeability, 16 disk pairs (two-ply veneer assemblies) were randomly selected from the sapwood/heartwood mix veneer, and 20 disk pairs each were randomly selected from the pure sapwood and heartwood veneer, respectively. To identify the difference in microscopic structure, the scanning electron

micrograph (SEM) photographs of aspen sapwood and heartwood were taken. In the meantime, to identify the effect of glue curing on panel permeability, the permeability of each disk pair was measured for the three veneer types in the following sequence: 1) without glue, 2) uncured (liquid) glue, and 3) cured glue. The glue spread was 160 g/m^2 per single glueline, which is the amount normally used by the plywood/LVL industry. Before and after applying glue, the thickness and weight of each disk pair were measured and average thickness and density were calculated. To create a continuous glueline between the two veneer plies without over-densification, each disk pair was clamped under a pressure of about 68.9 KPa (10 psi). In the third case, each disk pair was clamped and put in an oven at a 155°C temperature for 200 s to ensure a full glue cure. The SEM photographs of the cured glueline were taken in the longitudinal-radial plane (L-R) and tangential-radial plane (T-R). The t-tests were conducted to identify if significant differences in permeability existed 1) between the sapwood and heartwood veneer, and 2) due to glue spread and curing.

To determine the glueline permeability, films of commercial plywood PF glue (45% solids content) were made using permeable paper towels as the substrate at seven glue spread levels: 100, 110, 120, 128, 145, 160 and 170 g/m^2. Glue films were fully cured in an oven with a temperature of 103°C for 1 h. Two perforated plastic disks were used to sandwich the glue films to perform the permeability tests.

To determine the effect of veneer compression on the panel permeability, 14 sapwood veneer and 14 heartwood veneer disks were randomly selected and then paired to form 14 sapwood-heartwood veneer assemblies (two-ply veneer panels). The veneer assemblies were subjected to: 0%, 5%, and 23% compression ratios (CR) without glue using 155°C platen temperature and 120 s pressing time. The permeability of each veneer assembly was measured at each of the three CR levels to determine the effect of veneer compression on permeability.

2.2.2 Permeability Measurements on Veneer Panels and Strandboards

To investigate the effect of veneer panel density on permeability, thirty 30.5 x 30.5 -cm veneer sheets were selected from sapwood, heartwood, and sapwood/heartwood mix veneer, respectively. Then the thickness and weight of each veneer sheet were measured. Using a small press, fifteen 30.5 x 30.5 -cm two-ply veneer panels were made from sapwood, heartwood and

sapwood/heartwood mix veneer, respectively. The pressing temperature and time were 155°C and 120 s, respectively. A commercial plywood PF glue (45% solids content) was used with a glue spread of 160 g/m^2 per single glueline. During the pressing, a thickness control was used to achieve a target CR from 5 to 25% with a 5% increment. Note that the plywood and LVL industry commonly uses this range of CR for panel manufacturing. After pressing, the panels were stacked for 24 h and then trimmed into a size of 28 x 28 -cm. The thickness and weight of each panel were measured to calculate the panel density and actual panel CR. From each panel, six disks (60 mm in diameter) were cut for measuring permeability.

To reduce the effect of density gradient on strandboard permeability, a special pressing method was used to achieve uniform vertical density distribution (Dai *et al.* 2005). Eight 32 x 32 -cm one-layer homogeneous strandboards (nominal thickness 11 mm or 7/16 -in) were made with the following eight target density levels: 450, 500, 550, 600, 650, 700, 750 and 800 kg/m^3. Ten disk specimens (60 mm in diameter) were cut from each panel for the permeability tests. Since the strandboard had a homogeneous one-layer structure, its permeability was considered to be independent of panel thickness. Therefore, the permeability data between the 11 mm thick strandboards and two-ply veneer panels can be compared in terms of average and standard deviation.

2.2.3 Plywood and Strandboard Hot Pressing

To investigate the effect of panel permeability on hot pressing behaviour, three 5-ply 15.9 mm (5/8 -in) thick 61 x 61 -cm plywood panels were made in the following pressing conditions: pressing (platen) pressure, 1.21 MPa (175 psi); platen temperature, 155°C; pressing time, 300 s; glue spread, 160 g/m^2 per single glueline with a commercial plywood PF glue (45% solids content). As well, three 11 mm (7/16 -in) 61 x 61 -cm one-layer random structure strandboards were made in the following pressing conditions: platen temperature, 205°C; target panel density, 675 kg/m^3; closing time, 25 s; maximum pressing (mat) pressure, 5 MPa; and total pressing time, 320 s, with press opening commencing at 265 s. Note that 11 mm thick strandboards are commonly produced in the North America with a similar pressing time to the 5-ply plywood panels. Since the one-layer random structure strandboard is seen as homogeneous, its transverse (vertical) permeability can be assumed to be independent of the panel thickness. During the pressing, two coupled thermocouple-gas pressure sensors were placed at the center section: one

on the surface layer (about 3 mm from the surface for strandboards and the first glueline from the surface for plywood panels) and the other at the core to monitor the changes of temperature and gas pressure. The pressing schedules are shown in Figure 2.3. The temperature and gas pressure responses with regard to pressing time were compared between the plywood panels and strandboards.

2.3 Results and Discussion

2.3.1 Effect of Wood Composition and Glueline on Panel Permeability

The results concerning the permeability of the disk pairs (two-ply veneer assemblies) are summarized in Table 2.1 in terms of the three aspen veneer types (sapwood, sapwood/heartwood mix and heartwood) and glue curing. For all three veneer types, the permeability of disk pairs dropped from the uncured to the cured state of glue. The t-tests (Table 2.2) demonstrate that the aspen heartwood veneer was significantly denser than the aspen sapwood veneer ($p < 0.05$), and the permeability of the heartwood veneer was significantly lower than that of the sapwood veneer ($p < 0.05$). On average, without applying glue, the permeability of the sapwood veneer was about twice of that of the heartwood veneer. This could be due to more extensive tylose formation and extractives in the aspen heartwood. The pits were clearly evident in both aspen sapwood and heartwood veneer (Figure 2.4). However, compared to the sapwood veneer, the heartwood veneer seemed to have more tyloses.

As shown in Figure 2.5, the permeabilities of all aspen veneer disk pairs are compared in terms of glue curing. The average permeability value had the same order of magnitude among the following three cases: 1) without glue; 2) uncured glue; and 3) cured glue. The t-test results are listed in Table 2.3 for comparison of the differences in permeability of the total veneer among the above three cases. Since the p-value calculated was greater than 0.05, there was no statistical difference between case 1 (without glue) and case 2 (uncured glue). There was no difference between case 1 (without glue) and case 3 (cured glue) either. Although case 3 (cured glue) had lower permeability than case 2 (uncured glue) ($p < 0.05$), the reduction in permeability from the uncured to the cured state was only about 15%. This demonstrates that the sealing effect of the glueline was limited during the course of curing. The results are consistent with those obtained from plastic films such as polyethylene and polyvinyl chloride, providing evidence that the

permeability decreases only slightly with increasing degree of polymerization (Hennessy *et al.* 1966).

Figure 2.6 shows SEM photographs of the glueline in the longitudinal-radial plane (L-R) and tangential-radial plane (T-R). Although the glueline was cured and continuous, micro cracks inevitably occurred through the very thin glueline. These cracks provide a passage for flowing air and vapour. Obviously, the extent of glueline cracking decreases with increasing glue spread. As illustrated in Figure 2.7, the permeability of the cured plywood PF glue films decreased with increasing glue spread level. This result is in agreement with that obtained by Hennessy *et al.* (1966), who investigated the effect of coating weight variations on the permeability of polyvinylidene chloride (PVDC) -coated polyester films. Based on our results, the permeability of the cured glue films can decrease by about 50% over a normal glue spread level of 150 to 170 g/m^2 per single glueline in plywood/LVL, with an average value of approximately 3.0×10^{-14} m^2.

2.3.2 Effect of Compression on Veneer Permeability

Veneer compression had a significant effect on permeability. As shown in Figure 2.8, the average permeability of the two-ply unglued veneer assemblies at an average 5% CR was approximately two-fold higher than that of the veneer panels at an average 23% CR. Compared to the control (with 0% CR), the veneer permeability was reduced by about 70% for an average 5% CR and 92% for an average 23% CR. The results indicate that the veneer permeability was significantly affected by a small compression (deformation) within a CR range of 3-7%. Since the pits in the vessels serve as the main passage for the air and vapour in the transverse (vertical) direction, the compression may have resulted in a significant increase in the pit closure, leading to a low gas flow.

The logarithmic plots are presented in Figure 2.9 concerning the permeability and actual CR of the two-ply veneer panels (30.5 x 30.5 -cm) made from the sapwood and heartwood veneer, respectively. In general, the relationship between the permeability and CR of the veneer panels followed an exponential or a power function. The permeability of the veneer panels decreased in a log-linear manner with the CR, and the permeabilities of sapwood and heartwood veneer panels differed increasingly with CR, with the former being higher than the latter. On average, the permeability of the sapwood veneer panels was about four times higher than that of the

heartwood veneer panels for the CR range tested. These results imply that 1) panels made from the sapwood veneer are more permeable and treatable; and 2) blows and blisters could be reduced during hot pressing by segregating sapwood and heartwood veneer and manipulating panel lay up and compression.

2.3.3 Predicting Permeability of Veneer Panels

The glued two-ply veneer panel can be considered as a multi-layer laminate comprising two veneer plies and one glueline (glue film). These components represent three barriers arranged in series. According to the theory for permeability through laminates (Dullien 1992), the overall permeability of the two-ply veneer panel can be calculated from the sum of the reciprocals of the permeability of the separate components in the laminate panel:

$$\frac{t}{K} = \frac{t_{veneer1}}{K_{veneer1}} + \frac{t_{glueline}}{K_{glueline}} + \frac{t_{veneer2}}{K_{veneer2}} \qquad (2\text{-}2)$$

where K = permeability of the glued two-ply veneer panel,

$K_{veneer1}$ and $K_{veneer2}$ = permeabilities of veneer plies 1 and 2, respectively,

t = total thickness of the veneer panel,

$t_{veneer1}$ and $t_{veneer2}$ = average thickness of veneer plies 1 and 2, respectively,

$t_{glueline}$ = average thickness of the glueline, which was about 0.16 mm, 5% of 3.2 mm thick aspen veneer estimated from the SEM images.

$K_{glueline}$ = average permeability of the glueline (glue film), which was about 3.0 x 10^{-14} m^2 from Figure 2.7.

It was assumed that veneer plies 1 and 2 are identical. Hence, the permeability of the glued two-ply panel can be estimated by:

$$K = \frac{2.05 K_{veneer} K_{glueline}}{2K_{glueline} + 0.05 K_{veneer}} \qquad (2\text{-}3)$$

As shown in Table 2.4, the predicted and measured permeability values of the two-ply veneer panels are compared. It was assumed that cured PF glueline (film) was not compressible and its permeability remained the same (3.0 x 10^{-14} m^2) under different panel CRs. The permeability of the cured PF glueline was on average about 20% of that of non-compressed aspen wood veneer

(0% CR). However, the permeability values were somewhat closer when veneers were subjected to 5% CR. At higher CR, such as at 23%, the permeability of the cured glueline became higher than that of the veneer. Since the thickness of the glueline was only about 5% of that of the veneer normally peeled, the influence of the glueline on panel permeability was limited. Contrary to the hypothesis of Zavala and Humphrey (1996), the glueline does not act as a main barrier to the gas and moisture movement during plywood hot-pressing. In addition, the predicted and measured permeabilities agreed reasonably well with an error within ±15%; therefore, the theory for permeability through laminates, as demonstrated with the two-ply veneer panel, can be successfully used to predict the permeability of veneer-based wood composites with different lay-ups.

2.3.4 Comparison of Permeabilities between Veneer Panels and Strandboards

Figure 2.10 shows the comparison of permeabilities between the aspen two-ply panels and strandboards on a logarithmic scale. This demonstrates that at the same panel density, the strandboards exhibited much higher permeability than the veneer panels. Moreover, the permeabilities of the veneer panels tended to decrease more rapidly with panel density than those of strandboards. The reason for the much greater permeability is that products such as strandboards contain a high level of interconnected voids between constituents (Dai *et al.* 2005), whereas plywood relies on flow through voids across the wood cell walls. Note that compared to plywood/LVL products, OSB is about 40 -50% denser. The average density is about 0.450 g/cm^3 for commercial aspen veneer panels as compared to 0.675 g/cm^3 for commercial aspen strandboards. As shown in Table 2.5, at their respective commercial density levels, the average permeability values of veneer panels and strandboards seemed to be close but the permeability variation of veneer panels was about one third that of strandboards, mainly due to the presence of layered and uniform structure. The horizontal density variation in OSB is much greater than plywood due to random strand formation (Dai *et al.* 2005).

2.3.5 Analysis of Effective Porosity in Veneer Panels

The Carman-Kozeny theory (Kozeny 1927; Carman 1956) used to model permeability of strand-based products (Dai *et al.* 2005) was also employed here. Based on the analogy of flow through hydraulic channels, the generic form of the Carman-Kozeny equation for permeability K is (Dullien 1992):

$$K = \frac{\phi^3}{k^*(1-\phi)^2 S_0^{\ 2}} \qquad (2\text{-}4)$$

where ϕ = porosity,

S_0 = specific surface area based on solid's volume, and

$k^* = k_0 (L_e/L)^2$, which is often referred to as Kozeny constant or tortuosity, where k_0 is a constant, and L_e and L are the effective microscopic flow length and the macroscopic flow length, respectively. The best value of k^* to fit most of experimental data is 5 (Dullien 1992).

Two key parameters need to be determined: effective porosity and specific surface area. For wood composite products, total porosity is determined by panel density and cell wall density (≈ 1500 kg/m^3) whereas the effective porosity is the portion of the total porosity which is interconnected and directly contributes to the panel permeability. For veneer-based composite products, the transverse permeability is mainly determined by interconnected pits with effective porosity ϕ_e since gas flow inside a panel is limited by pits dispersed in the tracheids (softwood) or vessels (hardwood). Since a veneer is rectangular in shape, its specific surface area S_0 is:

$$S_0 = \frac{2(lb + lt' + bt')}{lbt'} = 2(\frac{1}{l} + \frac{1}{b} + \frac{1}{t'}) \qquad (2\text{-}5)$$

For veneer plies, the length l and the width b are usually an order of magnitude greater than the thickness t'. Note that the veneer thickness t' depends on the veneer initial thickness t and the CR. Equation (2-5) can therefore be approximated by:

$$S_0 \approx \frac{2}{t'} = \frac{2}{(1-CR)t} \qquad (2\text{-}6)$$

By combining Equations (2-4) and (2-6), the modified Carman-Kozeny equation for predicting the permeability of veneer panels becomes:

$$K = \frac{1}{20}\left[\frac{1-CR}{1-\phi_e}\right]^2 \phi_e^{\ 3} t^2 \qquad (2\text{-}7)$$

This equation provides a fundamental model for permeability based on the classic Carman-Kozeny theory and the structure of veneer panels. In practice, the value of the effective porosity ϕ_e is very difficult to measure. Therefore, one merit of this model is that it allows evaluation of the change in effective porosity ϕ_e based on measurement of the permeability of veneer panels. Figure 2.11 shows that the total porosity of veneer panels ranged from 50 to 70% but the

effective porosity ranged only from 0.05 to 0.50%. The effective porosity of veneer panels also decreased significantly with increasing panel density; however, at a density of approximately 0.60 g/cm^3, it started to level off, probably due to blockage of the passage for air and vapour between the pits. As shown in Figure 2.12, at the same panel density, OSB panels had a greater effective porosity than veneer panels. As well, due to the horizontal density variation, OSB panels had a larger variation in effective porosity than veneer panels. Further, the effective porosity in OSB panels was found to range from 0.05 to 0.70%, which was mainly from between-strand voids varying from 2.5 -10.0%. As a result, it seemed that less than 10% of the between-strand voids in OSB panels were interconnected.

2.3.6 Permeability Implications for Heat and Mass Transfer

Compared to veneer panels, strandboards show greater variation for both horizontal and vertical density distribution. As demonstrated, strandboards have about two-fold greater variation in permeability than veneer panels, although these panel types as commercial products have almost the same average transverse air permeability. During hot-pressing of strandboards, areas of high transverse (vertical) and lateral (horizontal) permeability can serve as the main passage for gas and moisture flow. Although lateral permeability is much greater than transverse permeability, its role in degassing could still be limited, since the panel thickness is much smaller than the panel length and width. Thus, the rate of convection during strandboard hot-pressing could be mainly controlled by the localized spots with higher transverse permeability. However, during hot-pressing of veneer panels, it is the veneer compression (or deformation) that results in layered and uniform barriers to gas and moisture movement rather than the curing glueline. These barriers cause a sealing effect and lead to a low rate of convection within the panel. Compared to veneer panels, gas and moisture can move more easily in strandboards, since their dissipation is mainly controlled by the localized peak air permeability within the panel.

Figures 2.13 and 2.14 compare the typical temperature and gas pressure responses between 15.9 mm (5/8 -in) thick aspen 5-ply plywood and 11 mm (7/16 -in) thick aspen strandboard in two typical locations (surface-center and core-center). For both the surface and the core, the temperature responses were very smooth in the plywood, but uneven in the strandboard. Although the trends for temperature rising were similar for strandboard and plywood, the stronger convective flow of air and vapour in the strandboard led to temperature fluctuation on

the surface and in the core. For strandboard, at the beginning of the pressing, the temperature rising on the surface was faster than that in the core; however, after a period of time, the temperature rising in the core became faster than that on the surface. During press opening, temperature both on the surface and in the core decreased, apparently due to the localized peak transverse permeability. In contrast, for plywood, temperature increases on the surface and in the core were smoother. During the decompression cycle, temperature both on the surface and in the core continued to rise.

For gas pressure (Figure 2.14), the responses were also dramatically different between plywood and strandboard. In general, for both products, at the beginning of the pressing, the gas pressure on the surface increased more rapidly than that in the core due to the higher temperature on the surface. In strandboard, at a pressing time of about 100 s, gas pressures on the surface and in the core approached the same value. During press opening, gas pressures dropped sharply in both locations and the pressure in the core was only slightly higher than that on the surface, probably due to the existence of spots of higher transverse permeability in the strandboard. In contrast, for plywood, the gas pressures on the surface and in the core generally followed different trends with no overlap, and the pressures during the decompression cycle did not decrease notably. The following reasons are conceivable: 1) the surface plies have relatively higher compression and lower transverse permeability, and 2) layers with uniformly low permeability are formed within the panel which prevent the movement of gas and MC.

2.4 Conclusions

In veneer-based wood composites such as plywood/LVL, compression (or deformation) was the most important factor affecting air permeability, followed by the veneer sapwood/ heartwood composition, glue spread level and degree of glue curing. Panel permeability reduced substantially by about 70% with as little as 5% CR. On average, the permeability of sapwood veneer panels was about 4 times higher than that of heartwood veneer panels. The permeability of the PF glueline decreased during glue curing, but its reduction from the uncured to the cured state was only about 15%. The permeability of cured gluelines (films) decreased with increasing glue spread. At the normal glue spread level for plywood, average permeability of the cured glueline was about 20% of that for the non-compressed veneer, but was close to that of the veneer with 5% CR. Since the thickness of the cured glueline was only about 5% of that of the

veneer normally peeled, the net contribution of the glueline to panel permeability was low. Therefore, during panel hot pressing, it is veneer compression rather than curing glueline that acts as the main barrier to gas and moisture movement. The rate of convection is negligible, and thus heat conduction is dominant.

At the same panel density, strandboards exhibited much higher permeability than veneer panels. With increasing panel density, veneer panel permeability tended to decrease more rapidly. Although these panel types as commercial products showed almost the same average permeability, the veneer panels showed about two-fold less variation because of the formation of layered and uniform gas and moisture barriers. Based on the classic Carman-Kozeny theory, a concept of effective porosity was proposed to quantify the actual contribution of voids to panel permeability. For veneer panels, the effective porosity was only 0.05 - 0.50% compared to total panel voids ranging from 50 to 70%.

Due to the difference in permeability, the responses of the temperature and gas pressure during hot pressing of plywood and strandboard were essentially different. During plywood hot pressing, the gas pressure on the surface layer was generally higher than that in the core, and gas pressure and temperature did not decrease notably at the decompression stage. These results should be helpful for developing optimum pressing strategies to increase manufacturing efficiency and panel quality.

Table 2.1 The permeability test results of aspen veneer disk pairs (two-ply veneer assemblies) in terms of sapwood/heartwood composition and glue curing

Veneer type	Permeability of veneer disk pairs (10^{-14} m^2)			Density of veneer disk pairs (g/cm^3)		Number of samples
	Without glue	Uncured glue	Cured glue	Without glue	Cured glue	
Sapwood veneer	17.6 (7.86)*	21.5 (8.16)	19.2 (6.79)	0.433 (0.019)	0.434 (0.020)	20
Heartwood veneer	9.27 (6.33)	7.51 (5.70)	6.19 (4.50)	0.446 (0.011)	0.445 (0.010)	20
Sapwood/heartwood mix veneer	17.4 (3.35)	19.2 (3.74)	14.7 (2.91)	0.435 (0.032)	0.435 (0.031)	16
Overall aspen veneer	14.6 (7.36)	15.8 (8.84)	13.2 (7.53)	0.434 (0.023)	0.435 (0.022)	56

Note: * number in the brackets are standard deviations.

Table 2.2 Comparison of the density and permeability between aspen sapwood and heartwood veneer

Comparison	Veneer density (g/cm^3)		Veneer permeability (m^2)	
	Heartwood	Sapwood	Heartwood	Sapwood
Mean	0.445	0.434	0.93×10^{-13}	1.76×10^{-13}
Variance	0.0001	0.0004	4.01×10^{-27}	6.17×10^{-27}
Observations	20	20	20	20
Pearson Correlation	0.103	$t>t_{critical}$	0.221	$\|t\|>t_{critical}$
Hypothesized Mean Difference	0		0	
df	19		19	
t Stat	2.28		-4.19	
P(T<=t) two-tail	0.034		0.00049	
t Critical two-tail	2.09		2.09	

Table 2.3 The t-test results to identify changes in glueline permeability

Comparison of permeability (m^2)	Between		Between		Between	
	Without glue	Uncured glue	Uncured glue	Cured glue	Without glue	Cured glue
Mean	1.46×10^{-13}	1.58×10^{-13}	1.58×10^{-13}	1.32×10^{-13}	1.46×10^{-13}	1.32×10^{-13}
Variance	5.42×10^{-27}	7.81×10^{-27}	7.81×10^{-27}	5.67×10^{-27}	5.42×10^{-27}	5.67×10^{-27}
Observations	56	56	56	56	56	56
Pearson Correlation	0.725	$\lvert t \rvert < t_{critical}$	0.857	$t > t_{critical}$	0.709	$t < t_{critical}$
Hypothesized mean difference	0		0		0	
df	55		55		55	
t Stat	-1.53		4.27		1.76	
P(T<=t) two-tail	0.133		0.0000778		0.0839	
t Critical two-tail	2.00		2.00		2.00	

Table 2.4 Comparison of the predicted and measured permeability for the two-ply aspen veneer panels

Average panel CR	Average panel density (g/cm^3)	Measured permeability (10^{-14} m^2)*	Average permeability (10^{-14} m^2)			Prediction error (%)
			Veneer ply	Glueline	Predicted	
0%	0.435	13.20 (5.80)	14.60	3.0	13.30	-0.8
5%	0.458	4.02 (1.20)	3.43	3.0	3.42	14.9
23%	0.565	1.01 (0.40)	1.10	3.0	1.12	-10.9

Note: * values in brackets indicate standard deviations.

Table 2.5 Comparison of the permeability between aspen veneer panels and strandboards at their respective commercial density levels

Panel	Average panel density (g/cm^3)	Permeability (10^{-14} m^2)	
		Average	Standard deviation
Veneer panel	0.450	4.95	1.80
Strandboard	0.675	5.20	5.50

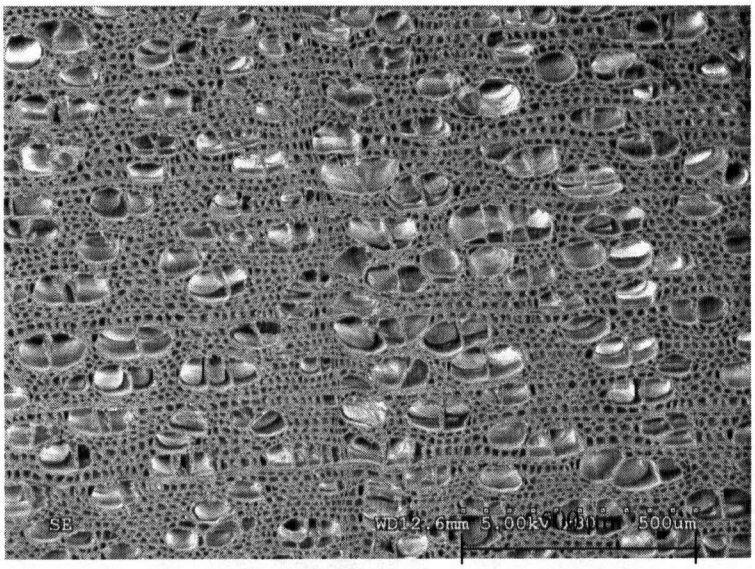

Figure 2.1 Microscopic structure of trembling aspen wood (courtesy of Mei and Dai 2003).

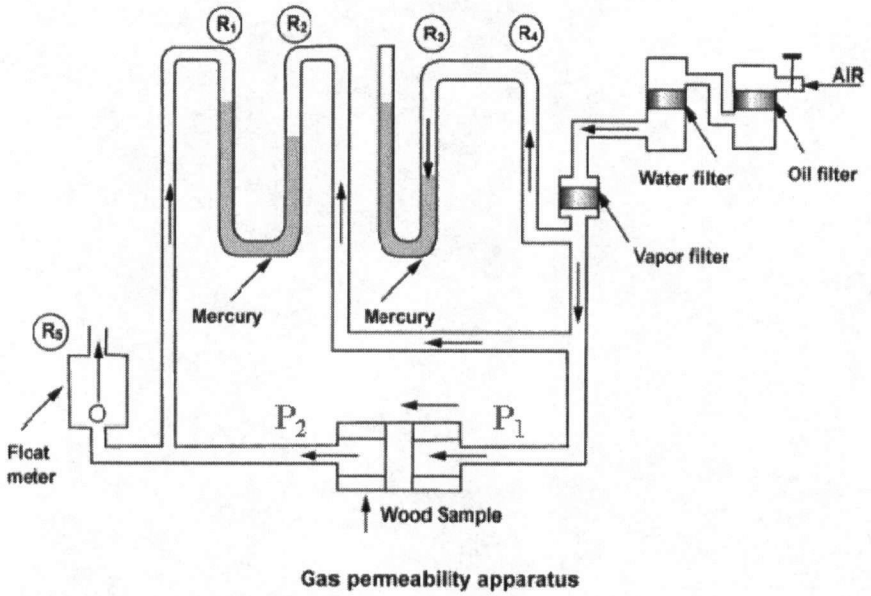

Figure 2.2 Schematic of the permeability measurement apparatus for wood samples (courtesy of Cai and Oliveira 2005).

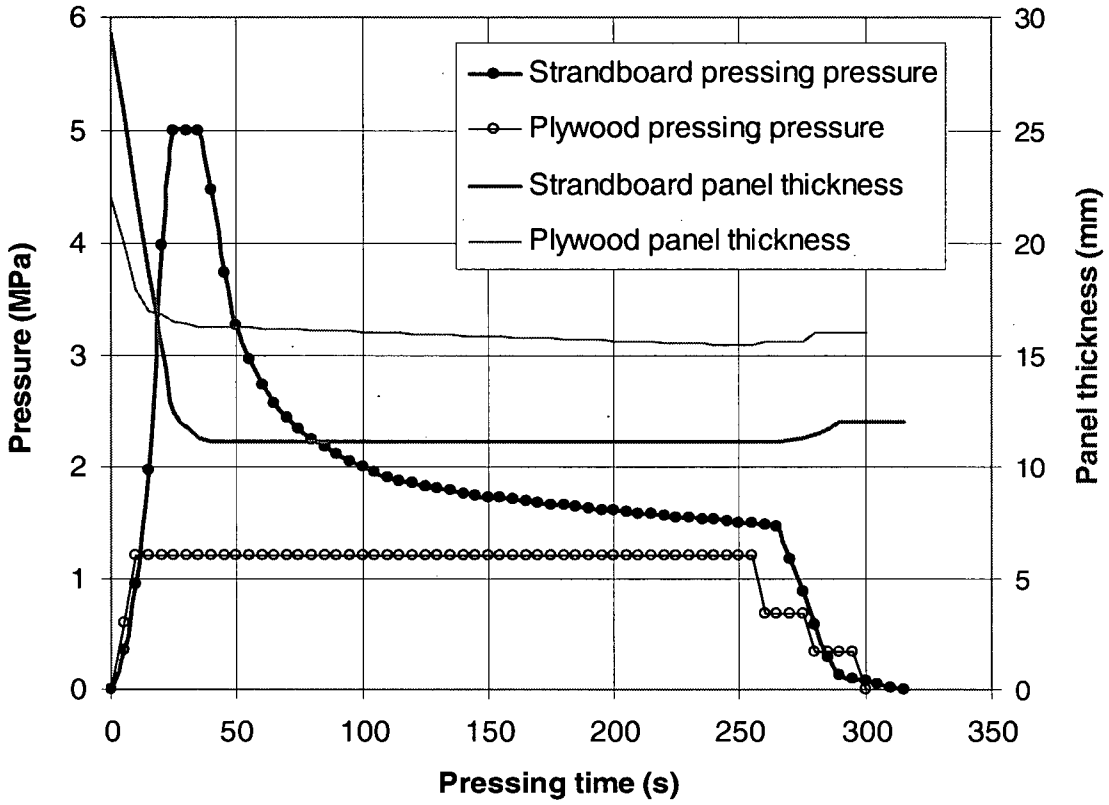

Figure 2.3 Typical pressing schedules for aspen plywood and strandboard

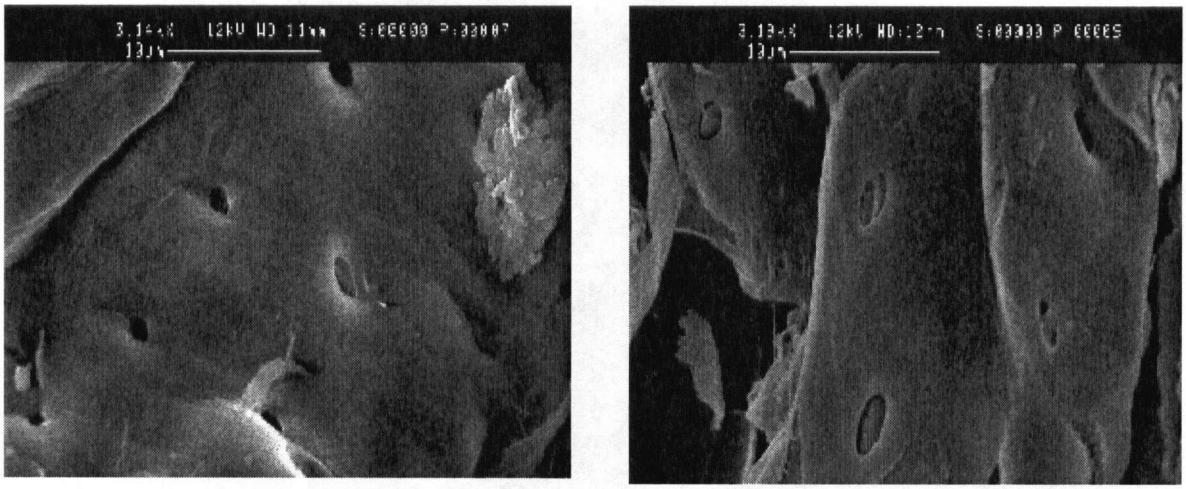

a) Sapwood b) Heartwood

Figure 2.4 Pits in trembling aspen sapwood and heartwood veneer

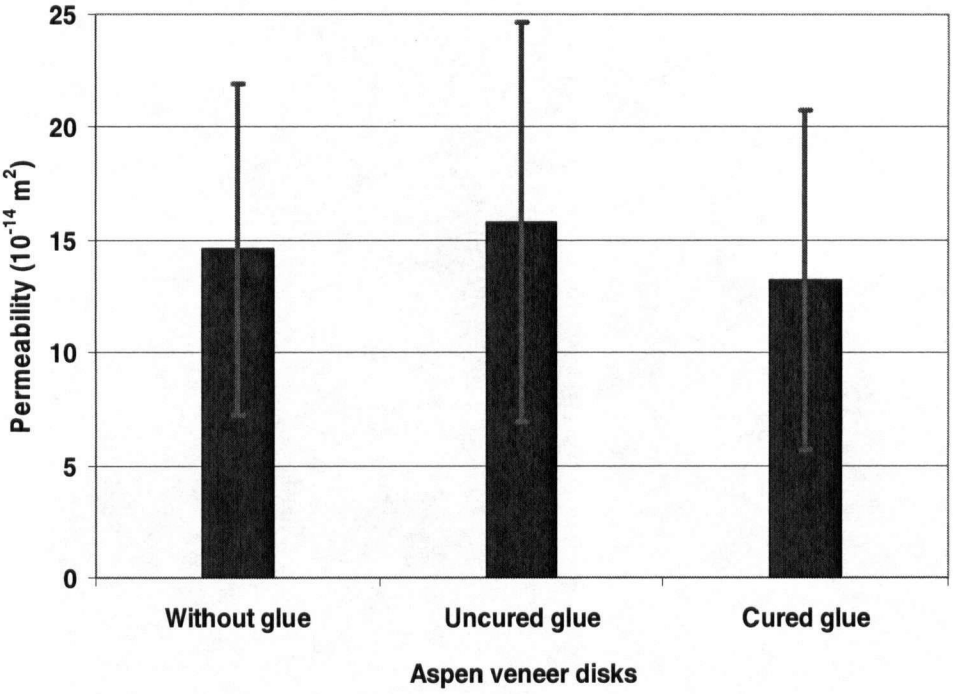

Figure 2.5 Comparison of the permeability of aspen veneer disk pairs with regard to glue curing (error bar: ±one standard deviation)

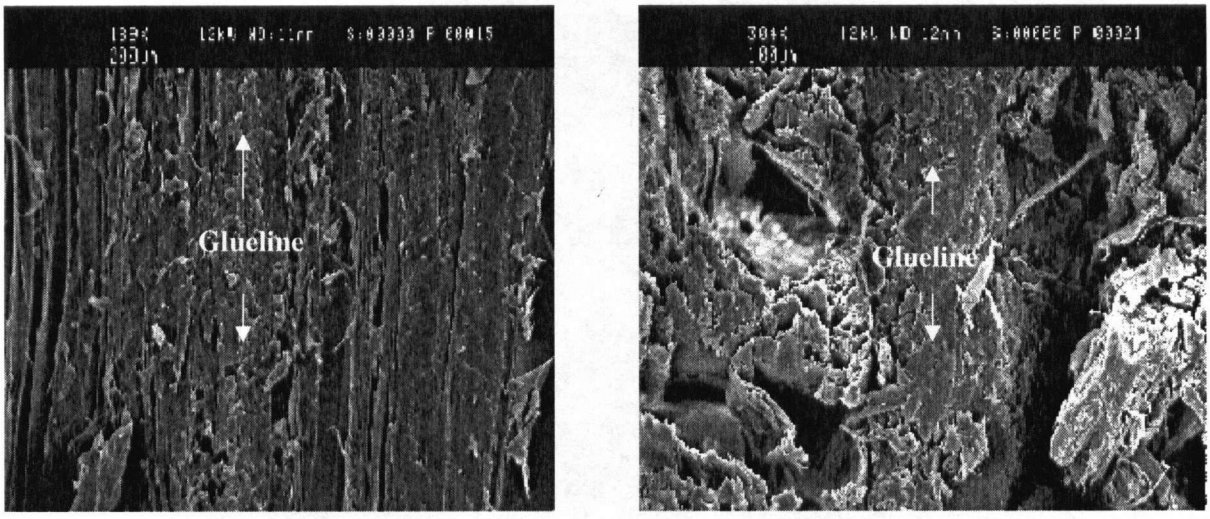

Longitudinal-radial (L-R) plane

Transverse-radial (T-R) plane

Figure 2.6 SEM photographs of the glueline in the L-R and T-R planes

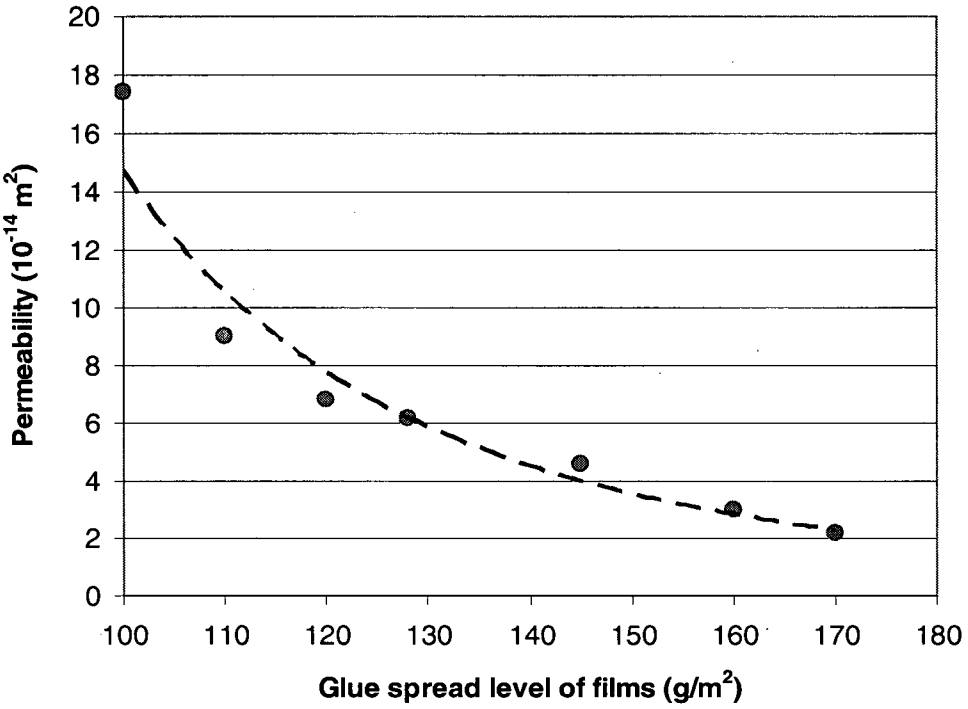

Figure 2.7 Changes in the permeability of the glue film (glueline) at different glue spread levels

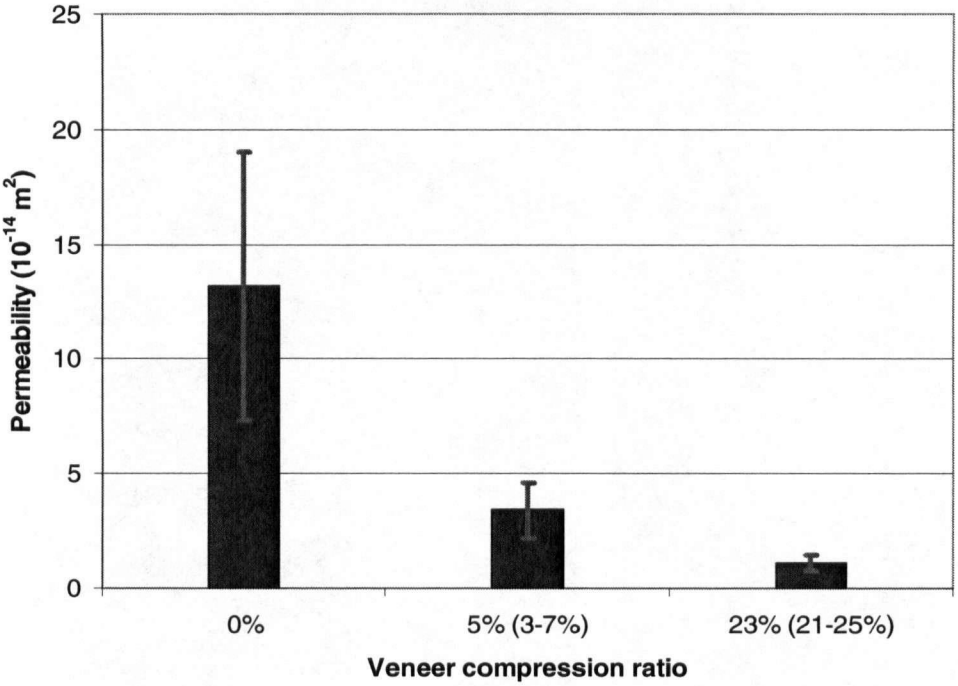

Figure 2.8 Comparison of the permeability of the unglued aspen veneer disk pairs with regard to compression ratio (error bar: ±one standard deviation)

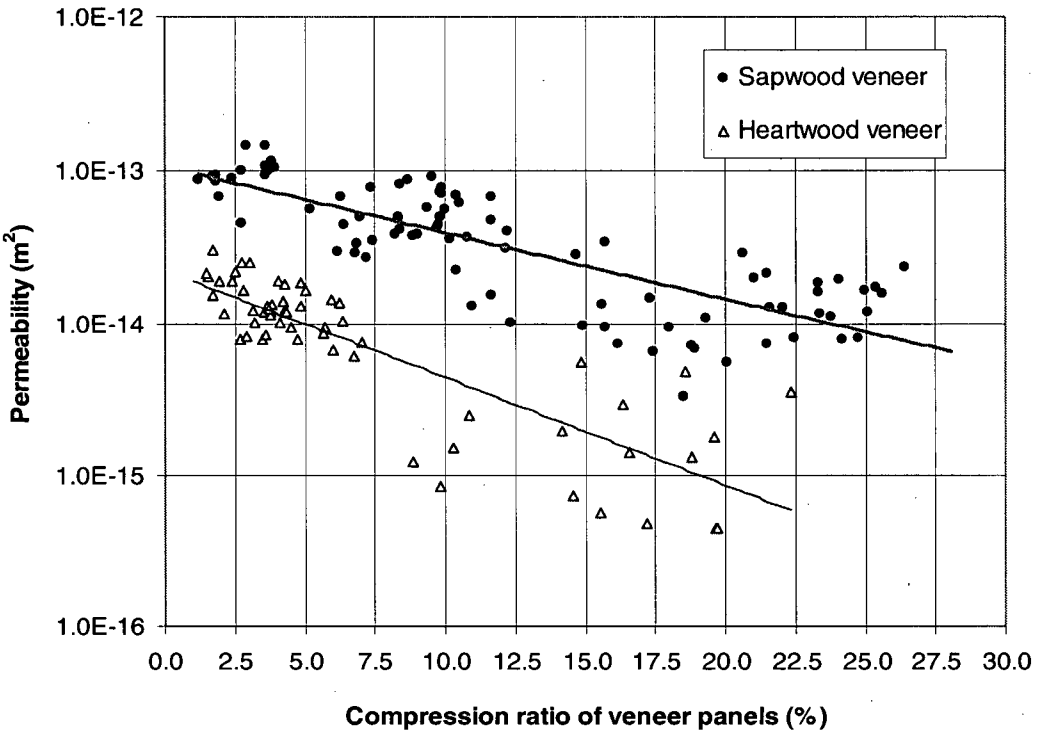

Figure 2.9 Logarithmic plots comparing the permeability of the two-ply veneer panels made from sapwood and heartwood veneer in terms of compression ratio

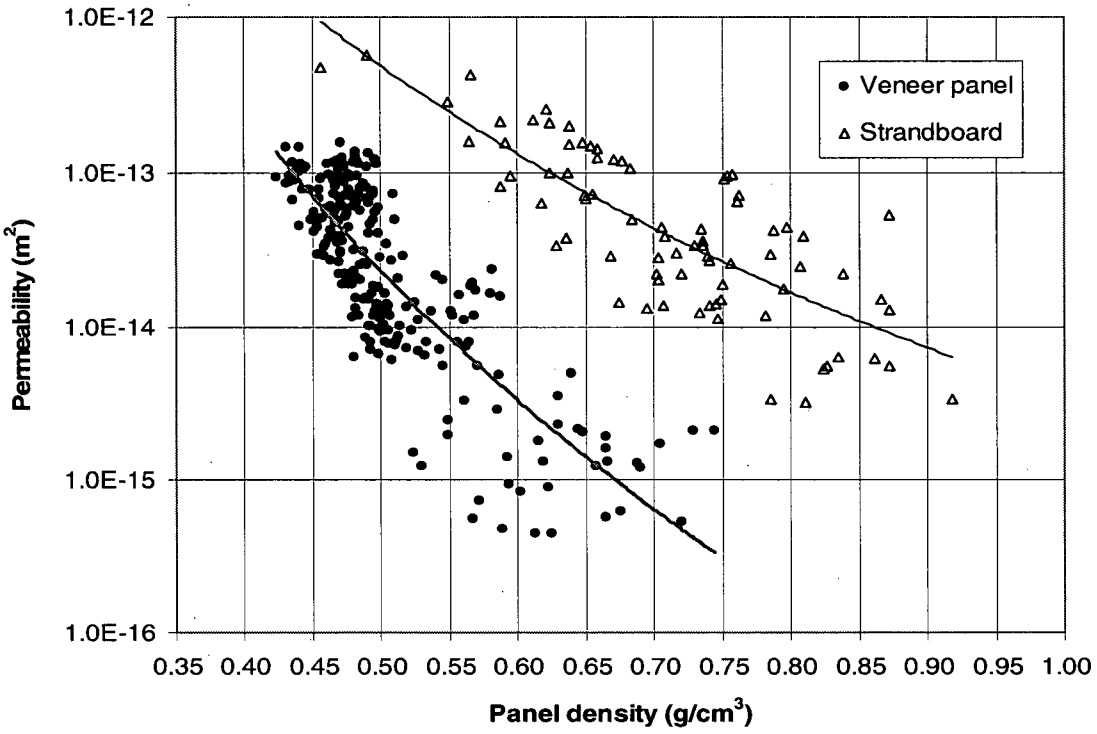

Figure 2.10 Logarithmic plots comparing the permeability between aspen veneer panels and strandboards

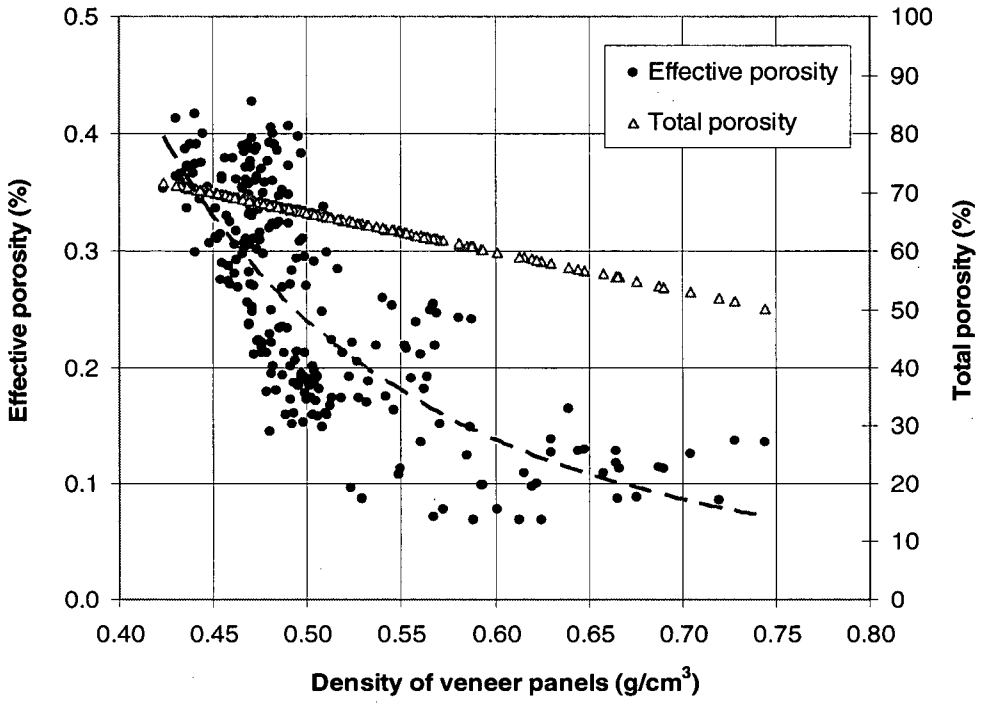

Figure 2.11 Relationship between effective porosity, total porosity and density for aspen veneer panels

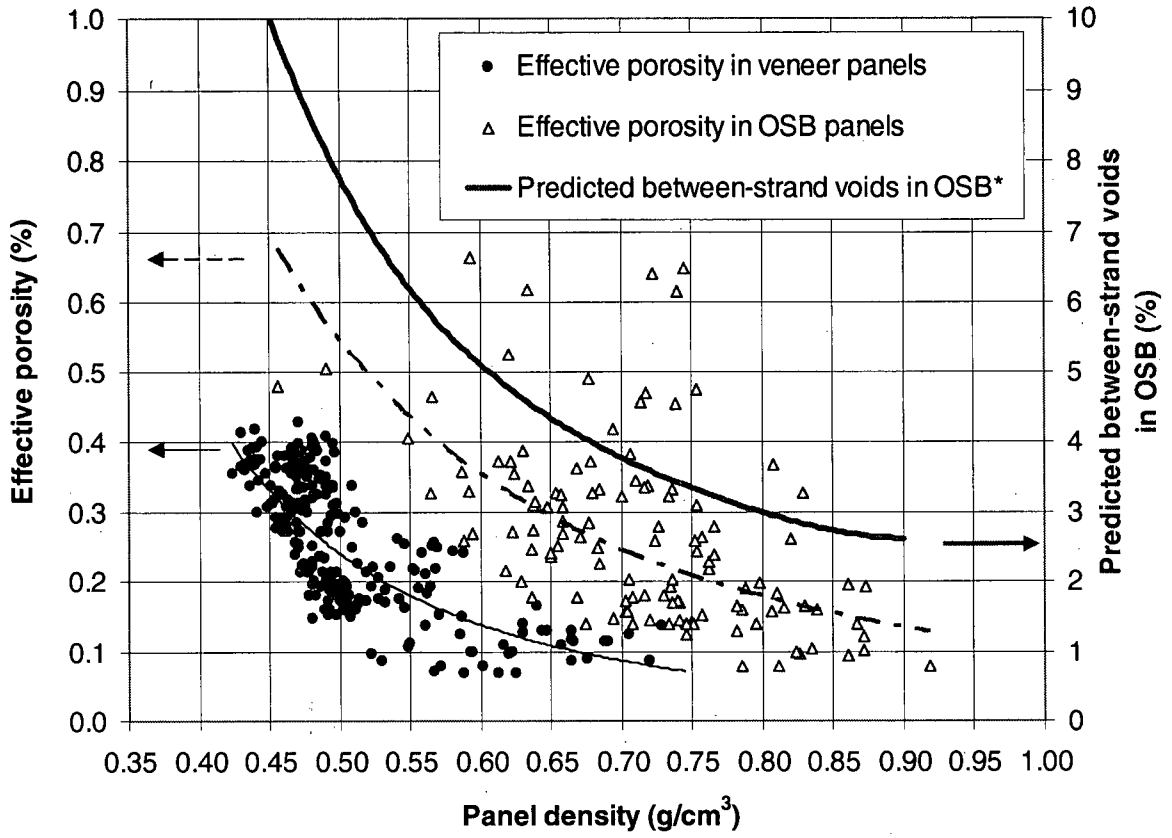

Figure 2.12 Logarithmic plots comparing effective porosity between aspen veneer panels and OSB [Note: * data cited from Dai *et al.* (2005)]

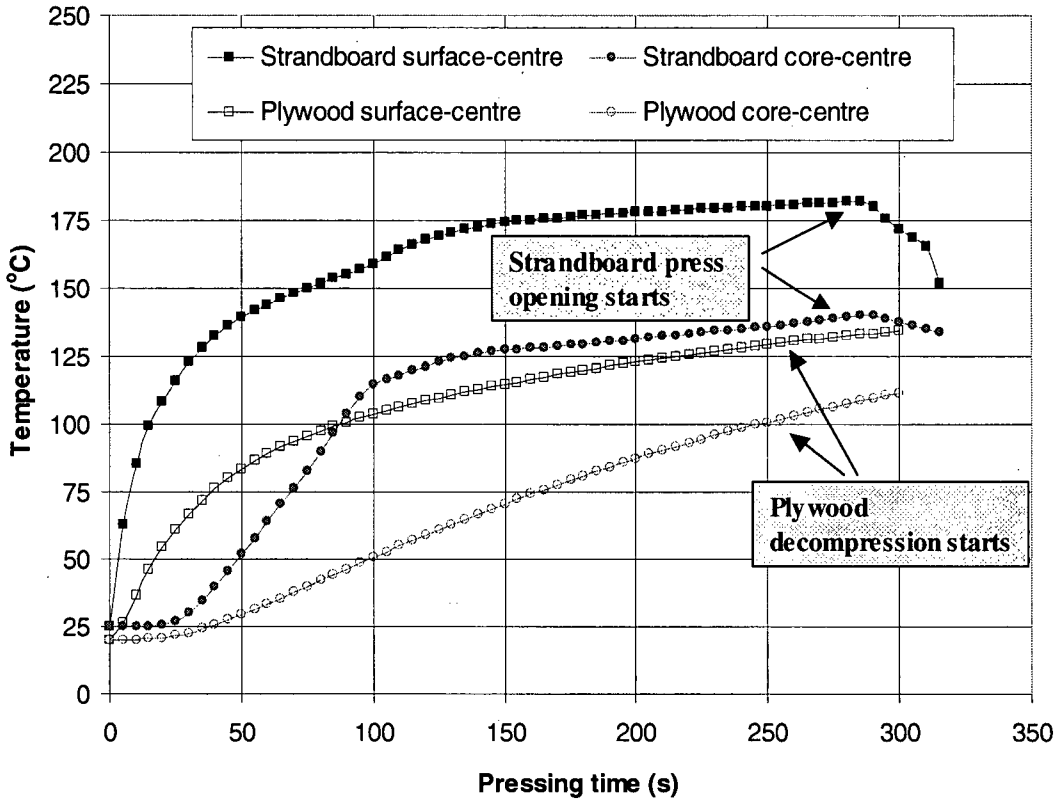

Figure 2.13 Comparison of the temperature response between aspen plywood and strandboard

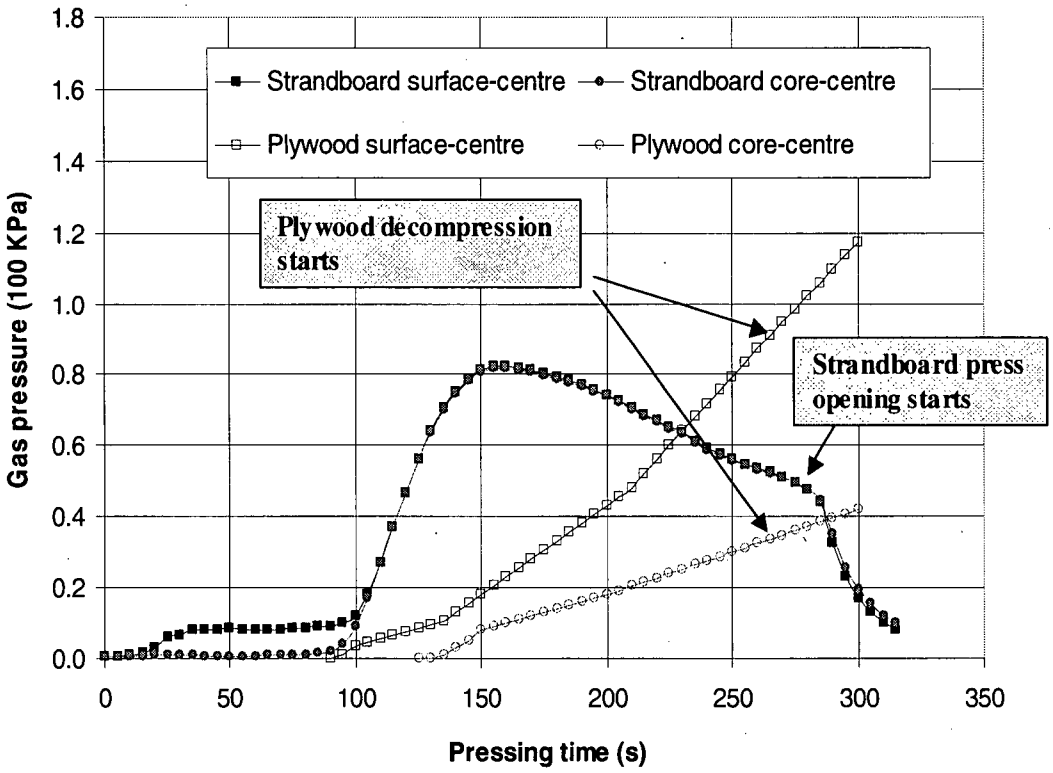

Figure 2.14 Comparison of the gas pressure response between aspen plywood and strandboard

2.5 Bibliography

Bao, F., J. Lu and Y. Zhao. 2001. Effect of bordered pit torus position on permeability in ChineseYezospruce. Wood and Fiber Sci. 33(2):193-199.

Bolton, A. J. 1988. The hot pressing of dry-formed wood-based composites. Part I. A review of the literature, identifying the primary physical process and the nature of their interaction. Holzforschung. 42(6):403-406.

Bolton, A. J. and P. E. Humphrey. 1994. The permeability of wood-based composite materials. Holzforschung 48: 95-100.

Cai, L. and L. Oliveira. 2005. Study on permeability of wet wood and normal wood of sub-alpine fir. Proceedings of 9th International IUFRO Wood Drying Conference. Nanjing, P. R. China. pp.63-68

Carman, P. C. 1956. Flow of gas through porous media. Butterworths, London.

Dai, C., C. Yu and X. Zhao. 2005. Heat and mass transfer in wood composite panels during hot pressing: Part 2. Modeling void formation and mat permeability. Wood and Fiber Sci. 37(2):242-257.

Dullien, F. A. 1992. Porous media: fluid transport and pore structure. 2nd Edition. Academic Press, New York.

Hennessy, B. J., J. A. Mead and T. C. Stening. 1966. The permeability of plastics films. Published by The Plastics Institute. England. 62pp.

Kozeny, J. 1927. Uber Kapillare Leitung des Wassers im Boden. Sitzungsberichte der Akadamie der Wissenschaften in Wien, Abteilung, Illa, 136:271-206.

Kuroda, N. and J. F. Siau. 1988. Evidence of nonlinear flow in softwoods from wood permeability measurements. Wood and Fiber Sci. 20(1):112-169.

Lin, R. T. 1972. Air permeability of wood measured by a pseudo-steady-state method. Wood Sci. 5(2):125-131.

Mei, A. and C. Dai. 2003. On compression behaviour of aspen wood and horizontal density variation of strandboard. A presentation at Forintek Canada Corp. (unpublished).

Montgomery, D. C. 2005. Introduction to statistical quality control. Fifth Edition. John Wiley & Sons, Inc. USA.

Siau, J. F. 1995. Wood: Influence of moisture on physical properties. Department of Wood Science and Forest Products, Virginia Polytechnic Institute and State University. ISBN No: 0-9622181-0-3. 227pp.

von Haas, G. 1998. Investigations of the hot pressing of wood-composite-mats under special consideration of the compression-behaviour, the permeability, the temperature-conductivity and the sorption-speed. Ph.D thesis, University of Hamburg, Germany.

Zavala, D. and P. E. Humphrey. 1996. Hot pressing veneer-based products: the interaction of physical process. Forest Prod. J. 46(1): 69-77.

CHAPTER III FUNDAMENTALS OF VENEER-TO-VENEER CONTACTS: EXPERIMENTATION[2]

3.1 Introduction

Wood is an anisotropic cellular material. Machined surfaces of wood composite elements such as veneers, strands or fibers are rough to various degrees. Surface roughness affects wood composites manufacturing in which wood elements are consolidated to form intimate contacts and then adequate bonding under heat and pressure with the least amount of resin required.

Currently, roughness is evaluated by surface texture parameters defined in standards such as ASME Standard B46.1-2002 and ISO 4287-1997 (ASME 2003). Two main methods for surface roughness/quality measurement use conventional stylus profilometer and optical scanning. The conventional stylus profilometer is widely accepted as the most accurate contact-type roughness device for laboratory and off-line use, whereas the optical method is generally accepted as the most effective non-contact surface profilometer in quality and process control. To quantify surface roughness, two key parameters are generally used. One is the roughness average R_a, which is the arithmetic average of the absolute value of the profile height deviations recorded within the evaluation length and measured from the mean line. The other is the root mean square (RMS) roughness R_q, which is the RMS average of the profile height deviations taken within the evaluation length and measured from the mean line. However, R_a and R_q are derived from a single roughness profile based on point measurements. Also, they are amplitude-based not spacing-based, hence they may not adequately characterize the surface roughness/quality of wood materials (Sandak and Tanaka 2003; Sandak *et al.* 2004). As shown in Figure 3.1, the shapes of the two profiles of veneer surface roughness are dramatically different but they have the same R_a. Neese *et al.* (2004) investigated whether traditional two-dimensional, amplitude-based measures for characterizing surface roughness can be used to predict percent wood failure and load at failure. It was determined that the only statistically significant relationship was between the loose-side roughness measurements and percent wood failure giving an R^2 of 0.68.

[2] A version of this chapter has been published in two papers in series.
1. Wang, B. J., C. Dai and S. Ellis. 2006. Veneer surface roughness and compressibility pertaining to plywood/LVL manufacturing. Part I. Experimentation and implication. Wood and Fiber Sci. Vol. 38 (3): 535-545
2. Wang, B. J., S. Ellis and C. Dai. 2006. Veneer surface roughness and compressibility pertaining to plywood/LVL manufacturing. Part II. Optimum panel densification. Wood and Fiber Sci. Vol. 38 (4): 727-735

At present, both methods are very slow (0.3 to 0.6 mm/s), tedious and labour intensive for assessing wood surface roughness/quality and are generally suitable for only small samples (8 to 15 mm in length). Since a single line measurement might deviate from the complete surface profile of wood due to its natural variability, many line-scans need to be done to generate a three-dimensional surface map for an accurate assessment. Further, the data reduction process is rather complicated from the measured profile. As a result, these two methods are limited for an off-line and laboratory use and cannot yet be fully utilized for on-line applications. Although image methods have been used to measure veneer surface roughness at the production speed (about 0.5 m/s), the algorithm used, filter level, veneer vibration and variation of wood colour might significantly affect the accuracy of roughness measurements (Faust 1987).

There is no commonly accepted quantitative parameter for characterizing surface roughness/quality of wood veneers or strands. No specific roughness measurement standard has been recommended and widely used in the wood industry (Fujiwara *et al.* 2004). To date, some studies have been done to quantify the effect of veneer surface roughness on required glue application and gluebond performance (Faust and Rice 1986; Faust and Rice 1987; Neese *et al.* 2004). Although the initial upward curvilinear stress-strain relationship was observed through compression tests of four wood species with different anatomical characteristics, it was speculated that this was probably due to the irregularities such as those caused by drying stresses in the wood specimen surface (Bodig 1965). Bodig and Jayne (1982) further characterized the stress-strain curve for wood composites with four regions, namely, initial alignment, linear elastic, curvilinear and post-failure. The first region, generally ignored in the analysis of data, was caused by specimen misalignment in the testing apparatus and surface roughness. However, all these observations were mainly based on wood compression in the parallel to the grain direction, which had little connection to wood composite manufacturing. Note that it is the wood transverse (mainly radial) compression behaviour that directly affects bonding contact of wood constituent elements and resulting panel densification. Wolcott *et al.* (1989) examined the transverse compression behaviour of small wood specimens and found that yield stress was not affected by specimen height but an increase of specimen height resulted in a decrease of yield strain. They attributed these observations to surface roughness or non-parallelism of the specimen. However, due to the variation of veneer surface roughness, thickness (average and variance) and lathe checks (depth and frequency), information still lacks concerning how veneer

surface roughness/quality affects panel transverse compressibility, gluebond quality and material recovery.

During plywood/LVL hot pressing, the glue-coated veneer constituents are heated and compressed between two platens to eliminate veneer surface roughness to create close veneer-to-veneer contacts and then to form bonds. Effective bonds are achieved sequentially from panel surface to core under pressure and temperature with a certain level of panel densification. This densification, generally controlled by veneer transverse compression under changing temperature and MC, will not only directly affect material recovery but also panel gluebond quality and bending performance. As discussed in Chapter 1, for veneer-based composites such as plywood/LVL, the densification level required for achieving adequate bonding contacts should be relatively low compared to non veneer-based composites such as OSB. Since the target (or goal) for plywood and LVL manufacture is not the same, different levels of panel densification should also apply. To date, the fundamentals of veneer-to-veneer contacts for bonding have not been clear. No work has been performed to determine: 1) how veneer-to-veneer contact area changes with veneer surface roughness and pressing load; 2) how veneer-to-veneer contact area changes with panel compression ratio (CR) and density; and 3) how veneer-to-veneer contact area quantitatively links with panel gluebond quality. As a result, a trial and error method is still prevailing to determine the hot pressing parameters for plywood/LVL manufacturing, resulting in reduced material recovery and inconsistent panel performance. The question still remains concerning how to establish the optimum panel densification for plywood/LVL manufacturing to balance material recovery, panel gluebond quality and performance.

The goal of this study was to improve the fundamental understanding of the plywood/LVL manufacturing processes. The specific objectives were to: 1) develop a new method to measure veneer surface roughness/quality; 2) determine the relationship between contact area, veneer surface roughness and pressing load; 3) establish the relationship between contact area, veneer surface roughness and density; 4) quantify the impact of veneer surface roughness/quality, temperature and MC on minimum compression required for bonding contact; and 5) establish the optimum panel densification for plywood/LVL manufacturing. Through systematic transverse compression tests of trembling aspen (*Populus tremuloides*) veneer, a threshold load was established under which the transition from the initial non-linear stage to the linear stage

occurred. Note that this load was established by a visual interpretation rather than any specific mathematical approach. Then, a concept of the minimum compression required was proposed for achieving adequate veneer-to-veneer or veneer-to-plate contacts. After that, the correlation was established between veneer surface roughness and the minimum compression required. Meanwhile, the relationship was determined between the contact area and 1) veneer surface roughness and the pressing load, and 2) panel CR and density. In addition, the effect of veneer surface roughness, temperature and MC on the minimum compression required and yield displacement was examined. Based on the results, a novel method was developed for characterizing veneer surface roughness/quality, and a revised wood transverse compression theory was proposed with inclusion of the first stage of progressive contact. Furthermore, within-sheet and between-sheet variations in aspen veneer thickness, density and compressibility were revealed. Based on the frequency distribution of the minimum compression required and yield displacement from the veneer compression tests, an optimum range of aspen panel densification was identified for manufacturing high performance plywood/LVL. Finally, through testing of the two-ply aspen veneer panels, such a densification range identified was examined in terms of panel gluebond performance, stiffness and dimensional stability.

3.2 Materials and Methods

One hundred and fifty 3.2 mm (1/8 -in) thick rotary-cut dried aspen veneer sheets (1.2 x 1.2 -m) were randomly selected from a mill in Eastern Canada and delivered to Forintek's Vancouver laboratory. The average veneer MC was about 3% on an oven-dry basis. Among them, 120 veneer sheets were visually separated into the three groups: smooth, medium rough and rough. Ten 1.2 x 1.2 -m veneer sheets were randomly selected from each group for cutting one hundred 30 x 30 -mm veneer specimens. These 100 specimens from each group were marked and kept in plastic bags for compression tests. Before the tests, five-point veneer thickness, weight, length and width of each specimen were measured to calculate veneer density.

One 1.2 m long fresh trembling aspen log (30.5 cm in diameter) was acquired from the same mill. The log was sliced into 2.5 mm (1/10 -in) thick veneer. Five sliced aspen veneer sheets (about 1.2 x 0.2 -m) were randomly selected and then dried down to an average MC of 3% on an oven dry basis.

3.2.1 New Method for Assessing Veneer Surface Roughness

Ten 30 x 30 -mm specimens were randomly selected from each roughness group. At the ambient temperature (20°C), the compression tests of these thirty specimens were conducted on a universal Instron test machine in the transverse (thickness) direction at a load rate of 2 mm/min until the load reached the maximum (about 975 kg). This maximum load ensured the 30 x 30 -mm specimens reached a stage of cell wall densification. Before starting the compression test, a load level of about 2.5 kg was applied to each 30 x 30 -mm veneer specimen to create an initial contact between veneer and compression steel plates. In this way, the slack in the universal test machine can be largely eliminated. For each test, the load-displacement curve was recorded and then plotted. Based on these load-displacement curves, an average threshold load can be identified under which the transition of the load-displacement curves from a non-linear stage to a linear stage occurs. The displacement measured prior to the linear elastic stage under the threshold load can be named the minimum compression required. For each specimen, the minimum compression required under the average threshold load and yield displacement were determined.

To quickly evaluate veneer surface roughness/quality and compressibility, a novel method was developed to measure an averaged quality criterion over any given area. To demonstrate the new method, two 30 x 30 -mm aspen veneer specimens (one smooth and the other rough) were selected. They had the same wood density (0.47 g/cm^3) and average MC (3%). Figure 3.2 shows the load-displacement curves of these two aspen veneer specimens. At the linear elastic stage, they displayed almost the same magnitude of slopes (compression MOE) but with different levels of delay in displacement, namely d_1 and d_2, prior to the linear elastic stage. This delayed elasticity at the early stage of compression is believed to be mainly caused by different levels of veneer surface roughness/quality. As shown in Figure 3.2, the threshold load was established by a visual identification of the initiation of the straight line (constant slope) portion of the linear elastic stage. For 30 x 30 -mm aspen veneer specimens at the ambient temperature and 3% average MC, this threshold load was about 120 kg.

For viscous-elastic and porous materials like wood, non-linear load-displacement relationship occurs at the early stage of the compression. It is proposed that by measuring displacement of

wood veneer under transverse compression at a predetermined threshold load, veneer surface roughness/quality can be evaluated. Figure 3.3 shows the apparatus required for this method.

To evaluate the accuracy of the method proposed for roughness measurement, five 30 x 30 -mm veneer specimens were randomly selected from each of the three roughness groups. The surface roughness of these 15 veneer specimens was evaluated using a SJ-400 surface roughness tester, a stylus profilometer. The stylus of the tester traced the minute irregularities of the veneer surface by measuring vertical stylus displacement as the detector traversed the surface irregularities (Mitutoyo 2004). The roughness was evaluated across the grain on both tight and loose sides of each specimen. The overall veneer roughness parameter R_a was the square root of R_a at the tight side and R_a at the loose side. The overall veneer roughness parameter R_q was calculated similarly. After measuring veneer roughness, compression tests were conducted at the ambient temperature following the same method established to determine the minimum compression required and yield displacement for each specimen. Then the correlation between the R_a and R_q and the minimum compression required was established.

3.2.2 Veneer Compressibility Tests

The purpose of veneer compressibility tests was to: 1) understand how veneer-to-veneer contact area and veneer-to-plate contact area are affected by the load applied; 2) examine how the contact area is influenced by veneer (or panel) compression; 3) determine the sensitivity of the new roughness assessment method to veneer temperature and MC; and 4) explore the variation of veneer compressibility and then establish an optimum range of panel densification.

3.2.2.1 Relationship between the veneer-to-veneer contact area and the load applied

Eight, ten and twelve 30 x 30 -mm specimens were randomly selected from each of the three roughness groups: smooth, medium rough and rough, respectively. Then, the roughness of each specimen was measured on both sides using the SJ-400 tester. These specimens were paired for each of the three roughness groups. For each pair, a plywood phenol formaldehyde (PF) glue (45% solids content) was uniformly spread onto the tight side of one veneer specimen at an application rate of 160 g/m^2. Parallel veneer-ply was generated by stacking two veneer specimens in a loose-to-tight pattern. The assembly time was about 3 min. Before starting the compression test, a load level of about 2.5 kg was applied to 30 x 30 -mm veneer specimens to create an initial contact for veneer-to-veneer and veneer-to-plate. At the ambient temperature, the

compression test of each parallel veneer-ply was conducted in a load-control mode and stopped when the load reached a desired level from 20 to 220 kg. During the compression, glue was transferred from the tight side of one specimen to the loose side of the other, displaying the contact area (glue coverage map) when the parallel veneer-ply was brought into contact at varying load levels. After stopping compression, the thickness and weight of each parallel veneer-ply were measured to calculate its CR and density. Then each parallel veneer-ply was carefully detached and the contact area in dark colour was visually estimated. Subsequently, the correlation between the contact area and the load applied was established.

3.2.2.2 Relationship between the veneer-to-plate contact area and the load applied

One 3.2 mm thick 1.2 x 1.2 -m dried aspen veneer sheet each was selected from the smooth group and rough group, respectively. Twenty-four 63.5 x 63.5 -mm (2.5 x 2.5 -in) veneer specimens were cut from each sheet for compression tests at the ambient temperature. Before performing tests, the five-point veneer thickness, weight, length and width were measured on each piece of veneer to calculate veneer density. A plywood phenol formaldehyde (PF) glue was uniformly spread onto a smooth steel plate (125 x 125 -mm) at an application rate of 160 g/m^2. The loose side of each veneer specimen was placed face-down on the glue-covered plate. Prior to the compression test, a load level of about 10 kg was applied to 63.5 x 63.5 -mm veneer specimens. This load level was equivalent to the 2.5 kg applied to 30 x 30 -mm veneer specimens for eliminating machine slacks to create an initial contact between the veneer and the steel plate. The compression tests were started in a load-control mode at a load rate of 2 mm/min and manually stopped when the load reached a desired target from 50 to 975 kg in order to establish the relationship between the contact area and the load applied. During the test, glue was transferred to the loose side of the veneer, displaying the contact area (glue coverage map) when the veneer and the steel plate were brought into contact to various degrees. After completing the test, the veneer specimens were carefully removed from the plate. The thickness and weight of each veneer specimen were measured to calculate the CR and density. Using an image analysis software program, the glue coverage map of each specimen was taken and the contact area (in dark color) was evaluated in terms of the percentage of the specimen size. The correlation between the contact area and the load applied was established.

3.2.2.3 Relationship between the contact area and panel CR and density

By combining the results from specimens of parallel veneer-ply (Section 3.2.2.1) and single veneer (Section 3.2.2.2), the relationship between contact area and veneer (and panel) density was established.

3.2.2.4 Sensitivity of the method proposed to veneer temperature and MC

Sliced aspen veneer was chosen because its surface was rather smooth with no lathe checks. This was done to minimize the effect of surface roughness, thickness variation and lathe checks. In total, two hundred 30 x 30 -mm veneer specimens were cut from the five selective sheets (1.2 x 0.2 -m): half were wrapped with the plastic bags to keep a MC level of 3% and the remaining half were left unwrapped for one week to achieve an average MC level of about 6% based on oven dry weight at the ambient environment. The compression tests of these sliced veneer specimens were conducted using an apparatus with a temperature control. As shown in Figure 3.4, the apparatus can be affixed to an Instron test machine for compression tests. Before starting the compression test, a load level of 2.5 kg was applied to 30 x 30 -mm veneer specimens to create an initial contact between the veneer and compression steel platens. The tests were conducted at the following four temperature levels: 20°C, 50°C, 100°C and 150°C. For each temperature level, ten specimens were compressed to a maximum load of about 650 kg. Since the threshold load changes with the temperature, an average threshold load was determined based on the ten load-displacement curves at each temperature level. The minimum compression required under the threshold load and yield displacement were evaluated for each specimen. The t-tests were conducted to compare the minimum compression required and yield displacements at different veneer temperature levels.

3.2.2.5 Variation of veneer compressibility

To investigate the difference in compressibility between smooth veneer and rough veneer, two 3.2 mm thick dried 1.2 x 1.2 -m aspen veneer sheets, one smooth and the other rough, were visually selected from 150 dried aspen veneer sheets (1.2 x 1.2 -m) obtained as described in Section 3.2. First, an area of 300 x 300 -mm was marked and a 30 x 30 -mm matrix was then drawn on the marked area. Then, one hundred 30 x 30 -mm veneer specimens were cut from each sheet and labelled sequentially. After that, the five-point veneer thickness, weight, length and width of each specimen were measured to calculate veneer density. At the time of testing,

the average MC of veneer specimens was about 5%. Under the ambient temperature (20°C), the transverse compression tests were conducted using an Instron machine for each specimen following the same procedures as described before. The t-tests were conducted to determine whether there was a significant difference in dry veneer density, thickness, the minimum compression required and yield displacement between the two sheets. As well, the correlation between the minimum compression required and veneer thickness and density was investigated.

To establish an optimum range of panel densification, thirty-five aspen veneer sheets (1.2 x 1.2 -m) were randomly selected. First, three hundred and fifty 30 x 30 -mm aspen veneer specimens were cut and marked for compression tests with ten specimens from each sheet. These specimens were then compressed in an Instron machine with a load control mode. At the time of testing, the average veneer MC was 5%. The five-point veneer thickness, weight, length and width of each specimen were measured to calculate veneer density. The testing procedures were the same as described before. Based on the load-displacement curve, the minimum compression required at the threshold load of 120 kg and the yield displacement were derived respectively for each veneer specimen to establish their frequency distribution.

3.2.3 Veneer Panel Manufacturing

To validate the optimum range of densification in terms of panel performance, seventy 86 x 60 -cm (34 x 24 -in) veneer sub-sheets were cut with two from each of the 35 sheets (1.2 x 1.2 -m) selected for the compressibility tests mentioned above. The average veneer MC was 5%. The veneer thickness (nine points with eight being on edges and one being in center), weight, length and width of each sub-sheet were first measured to calculate veneer density. Then, ten lines were drawn along the grain direction at the loose side of each veneer sheet with a lateral interval of 5-cm. A portable Metriguard 239 stress wave timer was used to measure stress wave time along these ten lines for each sheet (Metriguard Inc. 2005). The modulus of elasticity (MOE) was calculated for each veneer sheet based on average veneer stress wave time and veneer density. After that, 33 two-ply veneer assemblies (86 x 60 -cm) were prepared in a loose-to-tight pattern along the same grain direction. For each panel, a commercial plywood phenol formaldehyde (PF) glue (45% solids content) was uniformly spread onto the loose side of one veneer sheet at an application rate of 160 g/m^2. A press (96 x 96 -cm) was used with 155°C platen temperature and 180 s pressing time. The platen pressure was held constant from 0.69 MPa (100 psi) to 2.41 MPa

(350 psi) with an increment of 0.17 MPa (25 psi). For each platen pressure, 3 panels (replicates) were made. During press unloading, blows were carefully monitored. After pressing, all 33 panels were hot stacked for 24 h. The nine-point thickness and weight of each panel were measured to calculate panel density. Subsequently, ten readings of the stress wave time were measured at two sides of each veneer panel to calculate the average stress wave time. Based on the average stress wave time and panel density, the panel MOE was calculated. Hence, the MOE ratio of the panel over the veneer was determined. In addition, ten 81 x 25 -mm specimens were cut from each panel for dry shear tests. After testing, percent wood failure and failure mode were determined for each shear specimen. Furthermore, ten 150 x 150 -mm specimens were cut for water absorption (WA) and thickness swell (TS) tests after 24-h water soaking. The weight and 9-point thickness before and after soaking were measured to calculate WA and TS.

3.3 Results and Discussion

3.3.1 Accuracy of the New Method for Roughness Assessment

The 15 specimens used for the roughness measurements appeared to have two density groups: low density (average 0.42 g/cm^3, ranging from 0.40 to 0.43 g/cm^3) and high density (average 0.52 g/cm^3, ranging from 0.51 to 0.53 g/cm^3). One aspen veneer specimen was out of the magnitude range of the roughness tester. Figure 3.5 shows the plots of the load-displacement curves for three typical veneer specimens with different levels of density and roughness. It can be seen that the optimum threshold load for 30 x 30 -mm specimens was about 120 kg, and the effect of the veneer density was mainly revealed in the linear-elastic range with different slopes. Compared to the smooth veneer (small R_a), the rough veneer (large R_a) had larger displacement before the linear elastic range started.

For each of the 15 specimens, the displacement under the threshold load was derived from its load-displacement curve. Figure 3.6 shows that the correlation between the roughness parameters R_a and R_q and the displacement derived was very good with R^2 values of 0.87 and 0.85, respectively. This indicates that the displacement obtained under the threshold load is a good indication of overall veneer surface roughness on an area averaging basis. Since the roughness measurement is taken with a single compression, the method proposed is fast, reasonably accurate and suitable for evaluating veneer surface roughness/quality. The variation unaccounted for by the correlation is probably due to the two-dimensional nature of the stylus tracing

measurement since the roughness parameters were derived from the single line measurement on each side of the veneer specimen. It is expected that the correlation could be further improved through multi-line measurements using the stylus profilometer.

3.3.2 Contact Area in Relation to Veneer Surface Roughness and Load Applied

3.3.2.1 Veneer-to-veneer contacts

It was found that for glued aspen parallel veneer-ply specimens (30 x 30 -mm), the threshold load was about 105 kg which was lower than 120 kg determined for unglued aspen veneer specimens (30 x 30 -mm). This could be mainly due to the fact that the PF coated specimens had a greater MC at the surface. The higher the MC, the lower the threshold load for determining the displacement to assess veneer surface roughness.

Figure 3.7 shows the three typical glue coverage maps indicative of the contact areas at the three different load levels for 30 x 30 -mm aspen rough parallel veneer-ply specimens. The higher the load applied, the larger the contact area. Figure 3.8 shows the relationship between the contact area and the load applied for the total 15 aspen parallel veneer-ply specimens. The correlation between the contact area and the load applied followed a polynomial or power pattern whereas the correlation between the non-contact area (100-contact area) and the load applied followed an exponential pattern. This result was in good agreement with that found from the paper-press contact during paper manufacturing (Provatas and Uesaka 2003). Under a small load from 20 to 40 kg, the difference in contact area between the smooth, medium rough and rough veneer was relatively small. However, under a larger load, the smooth veneer seemed to have a larger contact area than the rough veneer. At a threshold load of about 105 kg, the contact area reached about 80%. Thus, about 80% of the effect of surface roughness or irregularities could be eliminated at the threshold load level.

3.3.2.2 Veneer-to-plate contacts

As shown in Figure 3.9, the correlation between the contact area and the load applied was also good with a power pattern for both smooth and rough 63.5 x 63.5 -mm veneer specimens. In general, at the same load, the smooth veneer had a higher contact area than the rough veneer. As shown in Figure 3.10, the correlation between the contact area and the load applied was established for the combination of the smooth and rough veneer. For 63.5 x 63.5 -mm veneer

specimens, the contact area reached about 86% at a threshold load level of about 470 kg, which is equivalent in pressure to 105 kg established for 30 x 30 -mm parallel veneer-ply specimens. At their respective threshold loads, the contact area for the 63.5 x 63.5 -mm veneer specimens was slightly higher than that for the 30 x 30 -mm parallel-ply veneer specimens. This is because the 63.5 x 63.5 -mm veneer specimen was in contact with smooth surface of the plate. The plate can be conceived of as the veneer with a perfectly smooth surface. The results again demonstrate that for a given area, the threshold load determined from the load-displacement curves would eliminate the major effect of veneer surface roughness or irregularities to achieve a contact area equal to or greater than 80%. Since plywood products require a minimum 80% wood failure for quality assurance, it is believed that the displacement of wood veneer under the threshold load defines the minimum compression required to achieve adequate veneer-to-veneer or veneer-to-plate contacts for bonding development. As a result, this minimum compression required not only reveals the roughness/quality and compressibility of wood veneer but also benchmarks the inherent material recovery when manufacturing into quality veneer products.

3.3.2.3 Effect of temperature and MC on veneer compressibility

Figure 3.11 shows the load-displacement curves of the 30 x 30 -mm, 2.5 mm thick sliced aspen veneer specimens over a temperature range of 20 to 150°C. In general, the higher the temperature, the lower the threshold load required to achieve the minimum compression required. On average, it is this threshold load level, rather than the minimum compression required, that changes with the temperature of the veneer specimens. Table 3.1 summarizes the t-test results for comparison of temperatures of 20°C and 150°C. Note that the threshold load at 150°C was only about 50 kg as compared to about 120 kg at 20°C. Statistically, the results demonstrate that for this sliced aspen veneer, there was no significant difference in the minimum compression required and yield displacement between the two temperature levels ($p > 0.05$). Thus, it is believed that the minimum compression required is mainly determined by wood surface roughness, and the yield displacement is primarily dependent on both surface roughness and cellular structure of the wood while the threshold load changes in relation to temperature and MC.

Figure 3.12 shows the effect of MC on the minimum compression required and yield displacement. The range between the minimum compression required and the yield displacement

could be defined as the optimum range of veneer compression pertaining to plywood/LVL manufacturing. Overall, the temperature and MC mainly affected material compression modulus (E) and the threshold load level required to achieve the required compression, but they did not affect the minimum compression required and yield displacement for the range of MC and temperature tested. This phenomenon could also be explained by the modified Hooke's law as follows:

$$\sigma = \varphi(\varepsilon) E \varepsilon \qquad (3\text{-}1)$$

where ε is the compression strain, σ is the applied stress (platen pressure), E is the veneer compression modulus, which is the function of veneer density, MC and temperature, and $\varphi(\varepsilon)$ is the strain function. When veneer temperature and MC increase, the slope at the second stage (linear elastic) of the stress-strain curve becomes less steep, hence the compression E reduces. This will result in a reduced load or stress because the veneer is more easily compressed. However, in this case, the level of compression required to achieve adequate contacts and cell wall buckling and yielding or fracture would stay unchanged. The implication is that the minimum compression required of wood veneer can be measured at any combinations of temperature and MC as long as the threshold load is re-examined. Similarly, the yield displacement of wood veneer can be rigorously determined from the compression tests as long as the initial non-linear stage for progressive contact is taken into account. In practice, it is more convenient to measure the minimum compression required (indication of surface roughness/quality) and yield displacement under the ambient temperature and oven dry conditions.

3.3.3 Contact Area in Relation to Veneer Surface Roughness and Density

3.3.3.1 Veneer-to-veneer contacts

Figure 3.13 shows the correlation between veneer-to-veneer contact area and CR for 30 x 30 - mm aspen parallel veneer-ply specimens with an R^2 of 0.58. Based on the limited data points from smooth, medium rough and rough veneer, it seemed that the required CR for achieving 80% target veneer-to-veneer contact area was about 10.5%.

3.3.3.2 Veneer-to-plate contacts

Figure 3.14 shows the relationship between veneer-to-plate contact area and CR for 63.5 x 63.5 - mm aspen veneer specimens with the rough veneer having a higher R^2. Based on the

compression results from the smooth and rough veneer specimens, it was found that the rougher veneer generally required more compression to achieve the same contact area. Overall, as shown from the trend line for all data points, the required CR for achieving a target 80% contact area was about 11.0%.

By combining the data from the compression tests of veneer-to-veneer and veneer-to-plate for all roughness categories, the relationship between the contact area and veneer (panel) density was established. As shown in Figure 3.15, the relationship followed a polynomial pattern with an R^2 of 0.86. Note that the data points were widely spread due to the variation of veneer density. For this aspen veneer, the average veneer density before compression (ρ_0) was 0.440 g/cm^3 with a standard deviation of 0.036 g/cm^3. A target 80% contact area was achieved when density of veneer (panel) after compression (ρ_1) reached about 0.495 g/cm^3. At this density level, the average CR required was 11.2%, which was calculated with the formula as follows:

$$CR = (1 - \frac{\rho_0}{\rho_1}) * 100\% \qquad (3\text{-}2)$$

Note that the ratio of panel density (ρ_1) over veneer density before compression (ρ_0) is sometime defined as compaction ratio (CR'). Based on Equation (3-2), there is a one-to-one relationship between CR' and CR as follows:

$$CR' = \frac{1}{1-CR} \qquad (3\text{-}3)$$

When CR is 11.2%, the CR' is about 1.13.

3.3.4 Variation of Veneer Compressibility

The load-displacement curves for two hundred 30 x 30 -mm veneer specimens, half from smooth veneer sheet and the remaining half from the rough veneer sheet, were obtained. The data were then reconstructed in a 10 x 10 matrix and then plotted. The t-tests (Table 3.2) demonstrate that the smooth veneer was significantly denser than the rough veneer ($p < 0.05$), and the rough veneer was significantly thicker than the smooth veneer ($p < 0.05$). Note that for the area of 300 x 300 -mm, there was a significant within-sheet variation in both density and thickness. On average, the smooth veneer had the larger variation in density but smaller variation in thickness compared to the rough veneer. The t-tests (Table 3.3) also show that both the minimum compression required and yield displacement of the smooth veneer were significantly smaller

than those of the rough veneer ($p < 0.05$). On average, the minimum compression required of the rough veneer was about 35% higher than that of the smooth veneer. This indicates that the rough veneer requires more compression to achieve adequate veneer-to-veneer contacts. In addition, the yield displacement of the rough veneer was about 5% larger than that of the smooth veneer. This indicates that the rough veneer could sustain more compression before the cell wall buckling and yielding or fracture. Furthermore, the within-sheet variation of the minimum compression required and yield displacement of the rough veneer was larger compared to those of the smooth veneer.

Figures 3.16 and 3.17 show the correlation between the minimum compression required and veneer thickness and density for these two hundred 30 x 30 -mm veneer specimens, respectively. Neither veneer thickness nor veneer density seemed to have any effect on the minimum compression required. Recall that the correlation between the minimum compression required and roughness parameters R_a and R_q gave R^2 values of 0.87 and 0.85, respectively. It is concluded that along with some effect of veneer thickness variation and lathe checks, the minimum compression required was a main indicator of the veneer surface roughness/quality.

Figure 3.18 shows the frequency distribution of the minimum compression required (d_{min}) for the three hundred and fifty 30 x 30 x 3.2 -mm representative aspen veneer specimens. It demonstrates that for the population of this mill-peeled aspen veneer, in order to achieve a target 80% contact area, the minimum compression required is about 0.35 mm. At this compression level, about 82% of the population of veneer specimens have gone through the first stage of progressive contact, creating about 80% contact area. The remaining 18% of the population of veneer specimens still have not achieved 80% contact area, which could still be acceptable based on the standard requirements of plywood products. Note that for this nominal 3.2 mm thick aspen veneer, the average dry veneer thickness was 3.07 mm. As a result, to make quality plywood/LVL products, the actual CR required was about 11.3%, which was very close to those identified from the compression tests for veneer-to-veneer and veneer-to-plate. Note that the CR is veneer thickness dependent. If the actual veneer thickness is 3.3 mm, the actual CR required (CR_{min}) will be reduced to about 10.6%.

Figure 3.19 shows the frequency distribution of the yield displacement (d_{max}) for this aspen veneer. The average yield displacement was 0.63 mm with a standard deviation of 0.10 mm. At the compression level of 0.55 mm, about 15% of veneer population would experience cell wall buckling and yielding or fracture. In general, the wood cell wall buckling and yielding or fracture will result in more panel thickness loss and less dimensionally stable products in service. It could also lead to lower shear strength, and sometime reduced tensile and bending strength. For performance LVL products, an upper level of compression ratio (CR_{max}) can be determined as follows:

$$CR_{max} = \frac{d'_{max}}{t_{actual}} * 100\% \qquad (3\text{-}4)$$

where d'_{max} is the upper compression level for the LVL manufacturing, which can be determined from the frequency distribution of the yield displacement for this aspen veneer. And t_{actual} is the average veneer thickness measured. For this nominal 3.2 mm thick mill peeled aspen veneer, d'_{max} was about 0.55 mm, t_{actual} was 3.07 mm, hence the resulting CR_{max} was about 18.0%.

For plywood products, to reduce the thickness loss while achieving the target percent wood failure, the optimum panel CR for this aspen veneer is about 11.3%. Similarly, for LVL products, to increase panel quality, material recovery and dimensional stability, the optimum range of panel CR appears to be from 11.3% to 18.0%.

3.3.5 Panel Performance in Relation to Compression Ratio

Thirty-three two-ply aspen panels, made with 11 different platen pressures from 0.69 MPa (100 psi) to 2.41 MPa (350 psi), had a range of panel CRs from 2.0 to 25.7% when average veneer MC was about 5%. Note that of the total 33 panels made, seven panels with the CR greater than 18.0% had serious blows during press opening. This is probably because at a CR greater than 18.0%, not only is the transverse permeability of veneer substantially reduced due to the closure of inter-connected pits, but also the lateral air permeability is significantly reduced due to the buckling and yielding or fracture of the cell walls. As shown in Figure 3.20, at a CR of 23%, most of the aspen early wood cell walls were buckled (Mei and Dai 2003). According to classic Carman-Kozeny theory (Dullien 1992; Nield and Bejan 1998), the lateral permeability is not only related to the effective porosity but also is proportional to the square of equivalent hydraulic

diameter of the porous media. It is anticipated that the buckled or fractured cell walls will block the air or moisture movement from vessel to vessel (or fibre to fibre) along the grain direction due to a drastic reduction in both effective porosity and equivalent hydraulic diameter. Although blows occur only locally within the panel, they are always seen as the severe product failure in the panel production. Note also that the surface of panels with CR greater than 18.0% was not smooth, which may result from within-sheet variation of springback behaviour after press unloading. As the panel CR reached or exceeded 18.0%, a portion of the veneer would experience transverse compression at the plastic stage. It is envisioned that the amount of veneer springback after compression differed between the linear elastic stage and the plastic stage. As shown in Figure 3.21, on average, the MOE ratio of the panel over the veneer increased with the increase of panel CR within the range tested. However, as shown in Figure 3.22, the 24-h panel thickness swell (TS) increased dramatically with increasing panel CR. The higher the panel CR, the larger the panel TS because the buckled or fractured cell walls can freely recover to their original shape from water penetration. As well, the relationship between the panel shear strength and CR appeared to be a polynomial pattern. The panel shear strength first increased notably with the panel CR due to the increased interfacial veneer-to-veneer bonding contacts. At a panel CR level of about 13.7%, the maximum shear strength resulted with an average value of about 3.2 MPa. After that, the panel shear strength reduced significantly with the panel CR probably due to the weakening effect of wood from buckled or fractured cell walls. The panel CR ranging from 11.3% to 18.0% resulted in high shear strength which was over 3.0 MPa. These results demonstrate that the maximum allowable panel CR for the normal panel manufacturing should be about 18.0% at which most of wood cell walls are not buckled or fractured. This maximum panel CR recommended agreed well with that identified through the compression tests of the three hundred and fifty 30 x 30 -mm representative aspen veneer specimens. At a panel CR level of about 11.3%, the MOE ratio of the panel over the veneer was about 1.18, and the panel 24-h TS was about 10% whereas the average shear strength was greater than 3.0 MPa with about 92% wood failure. As a result, for this mill peeled aspen veneer, the optimum range of panel densification should be from 11.3 to 18.0% for achieving superior panel performance in bending, gluebond (shear) and dimensional stability. Note that the results presented dealt with aspen parallel-ply instead of aspen cross-ply. Under the same platen pressure, the compression from aspen cross-ply assembly (plywood) was found to be only slightly smaller than that from aspen

parallel-ply assembly (LVL) (Wang 2003). This implies that under the same pressing conditions, the difference in bonding contacts between aspen plywood and LVL could be relatively small.

3.4 Significance and Implications

3.4.1 Revised Wood Transverse Compression Theory

The new method developed for evaluating veneer surface roughness/quality and compressibility have several implications on both theory and practice. In theory, the general wood transverse compression theory needs to be modified. A load-displacement curve in compression for one 30 x 30 -mm 3.2 mm thick aspen veneer specimen is shown in Figure 3.23. The revised wood transverse compression theory includes four stages instead of commonly defined three (Fukuyama and Takemura 1962; Wolcott *et al.* 1989; Ellis and Steiner 2002; Zhou and Dai 2005). The first stage may be referred to as "progressive contact" period, in which the contact area increases nonlinearly with the load applied. It is this stage that directly reveals the interfacial contacts of veneer-to-veneer or veneer-to-plate and the minimum compression required for achieving adequate contacts (equal to or greater than 80% of contact area). As well, with the inclusion of the first stage, the yield displacement needs to be re-defined.

In practice, the method provides a fast and objective way of evaluating surface roughness/quality of wood veneer in terms of its compression behaviour. For plywood and LVL, the implication is that the veneer is required to reach the critical compression level, namely the minimum compression required, to achieve the target 80% veneer-to-veneer contacts for developing adequate bonding sites while maximizing material recovery. As well, in order to increase material recovery for manufacturing performance plywood/LVL products, there are constraints to avoid both veneer under-densification and over-densification. The optimum range of veneer compression seems to be between the minimum compression required and the yield displacement. Beyond the yield displacement, the cell walls of wood veneer start to buckle or fracture, which may result in reduced panel bonding strength and dimensional stability. Without inclusion of the initial stage of progressive contact, there would be no baseline to deal with the variation in wood surface roughness/quality. Since both the minimum compression required and yield displacement are independent of temperature and MC, the material recovery of wood veneer can be benchmarked with regard to its surface roughness/quality when manufacturing into quality plywood/LVL products.

3.4.2 Optimum Panel Densification

Based on the revised wood transverse compression theory, and the distribution of the minimum compression required and yield displacement of wood veneer, an optimum range of panel compression ratio (CR) can be established to balance panel gluebond quality, performance and material recovery. The case study demonstrated that veneer surface roughness/quality has a great impact on the panel densification required for achieving adequate bonding contacts. Based on the veneer compression tests, the required CR for aspen veneer panels to achieve adequate interfacial contacts generally ranges from 6 to 16% for the nominal 3.2 mm (1/8 -in) thick veneer (Figure 3.14). Such a wide range provides an opportunity for the industry to reduce panel thickness loss while achieving target gluebond performance. Currently, owing to the larger variation in dry veneer surface roughness and thickness, plywood mills are generally using a larger-than-normal platen pressure for panel manufacturing. To deal with increased rougher veneer, the glue spread level has to increase with additional glue cost. It is hoped that through improved process control in plywood/LVL manufacturing, veneer surface roughness and thickness variation can be reduced or better controlled. As an option, veneers could also be segregated into several roughness classes in the production line. As a result, the required panel CR can be significantly reduced in the plywood/LVL manufacturing for increased material recovery and reduced glue consumption. It is conservatively estimated that with a 1% increase in recovery from improved control of the panel CR alone, a typical plywood and LVL mill can realize about $300,000 annual savings with an annual capacity of 250 million ft^2 (on a 3/8 -in basis).

3.5 Conclusions

A novel method was developed to characterize surface roughness/quality of wood veneer in terms of its compression behaviour. Based on the concept of this method, the surface roughness/quality of wood veneer can be quickly assessed on an area basis. The method could also be applied to other wood composite elements such as wood strands.

Through extensive transverse compression tests under ambient and controlled temperature and MC environments for aspen veneer, the relationship between contact area, veneer surface roughness and the load applied was established. As well, the critical importance of veneer surface roughness/quality on contact area was revealed. The results demonstrate that the general wood transverse compression theory needs to be revised to include four stages instead of the

commonly defined three. The first stage, which has long been overlooked but is critically important, could be named "progressive contact". During this stage, the contact area increases nonlinearly with the load applied. It is this stage that directly reveals the interfacial veneer-to-veneer contacts during compression and the minimum compression required for achieving adequate contacts. The results also indicate that the yield displacement needs to be re-defined with the inclusion of the first stage. Furthermore, the results show that both the minimum compression required and yield displacement of wood veneer were independent of temperature and MC, which helps benchmark the material recovery of wood veneer with regard to veneer surface roughness/quality when manufacturing into quality plywood/LVL products.

With the revised wood transverse compression theory, the compression behaviour of wood constituent elements can be directly linked to the performance of resulting panel products. The optimum panel densification can be established in terms of veneer surface roughness/quality and compressibility for performance plywood/LVL manufacturing. As a case study with nominal 3.2 mm thick mill peeled aspen veneer, the correlation between the contact area and panel CR was first established. Then, the required panel CR and density were identified for achieving target 80% contact area. Through the compression tests of 30 x 30 -mm aspen veneer specimens, within-sheet and between-sheet variations in density, thickness and compressibility were revealed. Furthermore, based on the frequency distribution of the minimum compression required and yield displacement of representative aspen veneer specimens, the optimum range of aspen panel densification was identified with a CR ranging from 11.3 to 18.0%. Finally, through manufacturing the two-ply aspen veneer panels with different platen pressures, such densification range identified was validated for improved panel quality, increased material recovery and dimensional stability while achieving superior panel bending and gluebond (shear) performance.

Table 3.1 Comparison of the minimum compression required (d_{min}) and yield displacement (d_{max}) at two temperatures for sliced aspen veneer

Comparison	d_{min} (T=20 °C)*	d_{min} (T=150°C)**	d_{max} (T=20°C)	d_{max} (T=150°C)
Mean	0.230	0.217	0.494	0.490
Variance	0.0014	0.0008	0.015	0.020
Observations	10	10	10	10
Hypothesized mean difference	0	$t < t_{critical}$	0	$t < t_{critical}$
df	9		9	
t Stat	1.31		0.06	
P(T<=t) one-tail	0.11		0.48	
t critical one-tail	1.83		1.83	
P(T<=t) two-tail	0.22		0.96	
t critical two-tail	2.26		2.26	

Note: * d_{min} was derived at a threshold load of 120 kg.
**d_{min} was derived at a threshold load of 50 kg.

Table 3.2 The t-test results comparing smooth and rough veneer in terms of dry density and thickness

Comparison	Dry density (g/cm^3)		Dry thickness (mm)	
	Smooth sheet	Rough sheet	Smooth sheet	Rough sheet
Mean	0.482	0.429	3.063	3.085
Variance	0.0007	0.0006	0.0025	0.0046
Observations	100	100	100	100
Hypothesized Mean Difference	0	$t > t_{critical}$	0	$\|t\| > t_{critical}$
df	99		99	
t Stat	18.08		-2.67	
P(T<=t) one-tail	0.0		0.004	
t Critical one-tail	1.66		1.66	
P(T<=t) two-tail	0.0		0.009	
t Critical two-tail	1.98		1.98	

Table 3.3 The t-test results comparing smooth and rough veneer in terms of minimum compression required and yield displacement

Comparison	Minimum compression required (mm)		Yield displacement (mm)	
	Smooth sheet	Rough sheet	Smooth sheet	Rough sheet
Mean	0.234	0.320	0.578	0.611
Variance	0.0023	0.0062	0.0121	0.0127
Observations	100	100	100	100
Hypothesized Mean Difference	0	$\lvert t \rvert > t_{critical}$	0	$\lvert t \rvert > t_{critical}$
df	99		99	
t Stat	-9.06		-2.11	
P(T<=t) one-tail	0.0		0.019	
t Critical one-tail	1.66		1.66	
P(T<=t) two-tail	0.0		0.038	
t Critical two-tail	1.98		1.98	

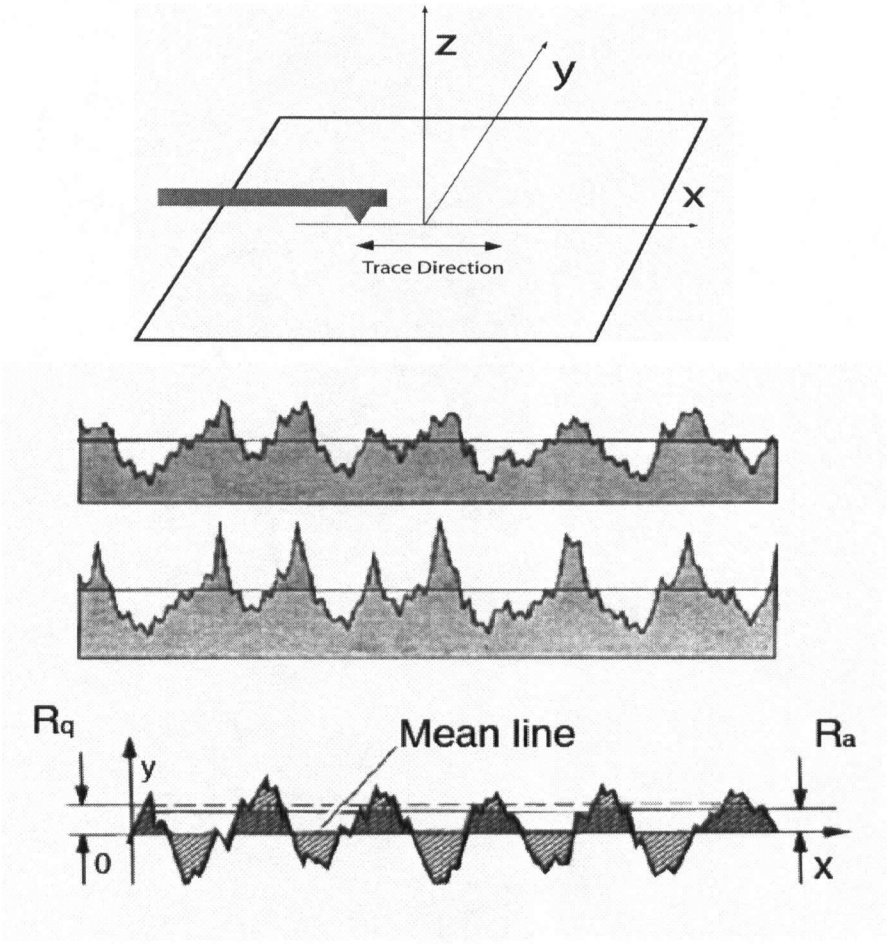

Figure 3.1 Veneer surface roughness profiles and the two key roughness parameters

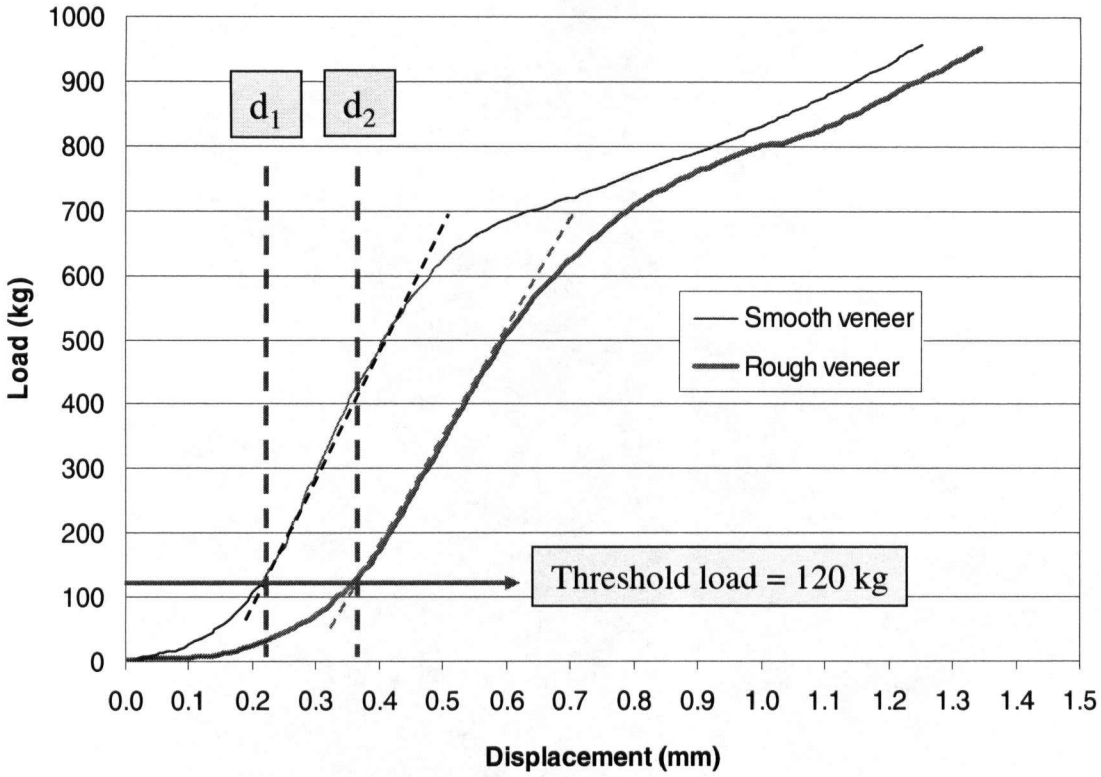

Figure 3.2 Effect of veneer surface roughness on compression indicated by the early stage load-displacement curve

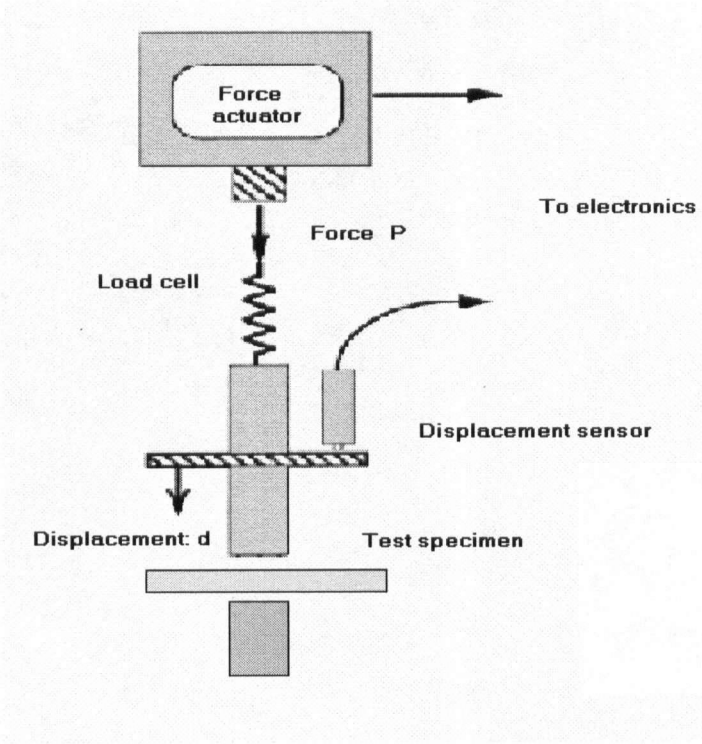

Figure 3.3 Method for evaluating veneer surface roughness/quality in terms of compressibility

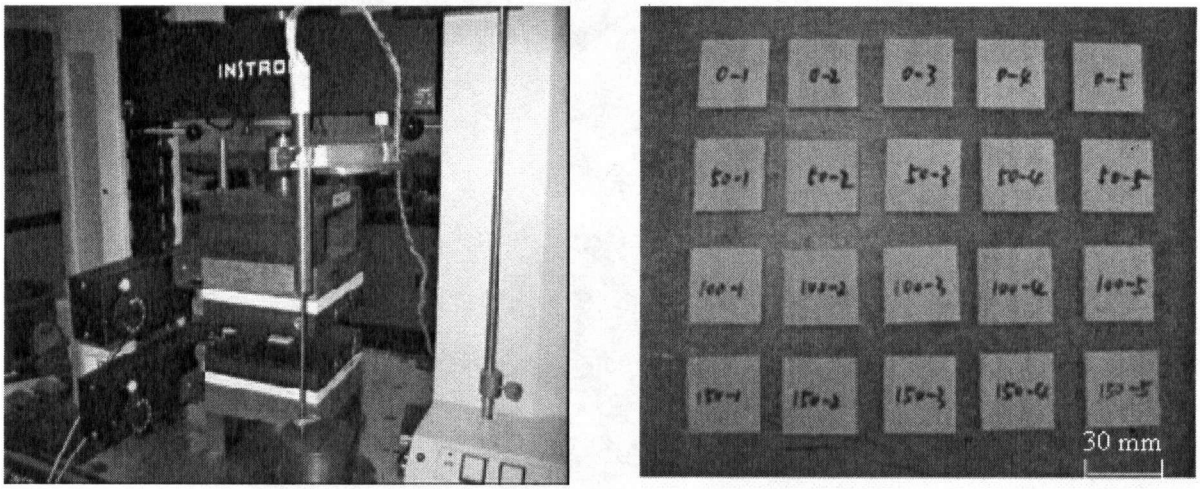

(a) Testing apparatus

(b) 30 x 30 -mm samples

Figure 3.4 Veneer compressibility tests at different levels of temperature and MC

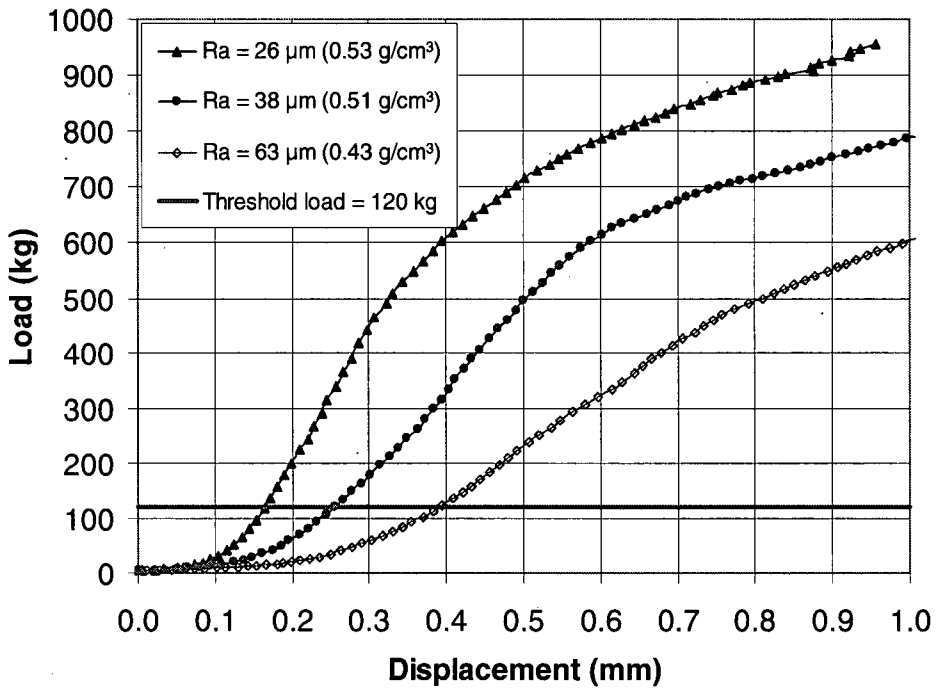

Figure 3.5 Load-displacement curves for aspen veneer in terms of roughness and density

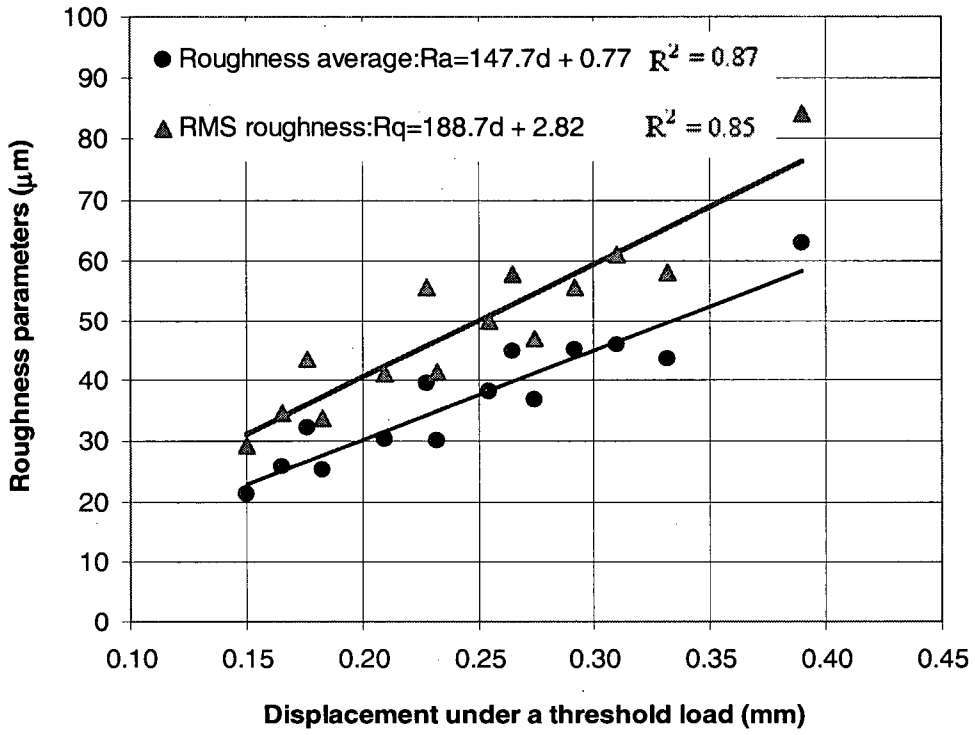

Figure 3.6 The correlation between the two key roughness parameters and displacement under a threshold load

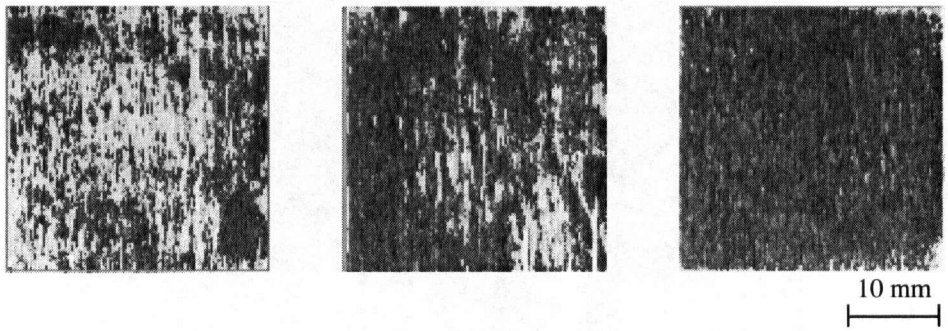

a) 48% (40 kg) b) 78% (98 kg) c) 92% (210 kg)

Figure 3.7 Measurement of the contact area in terms of the load applied for 30 x 30 -mm aspen rough veneer

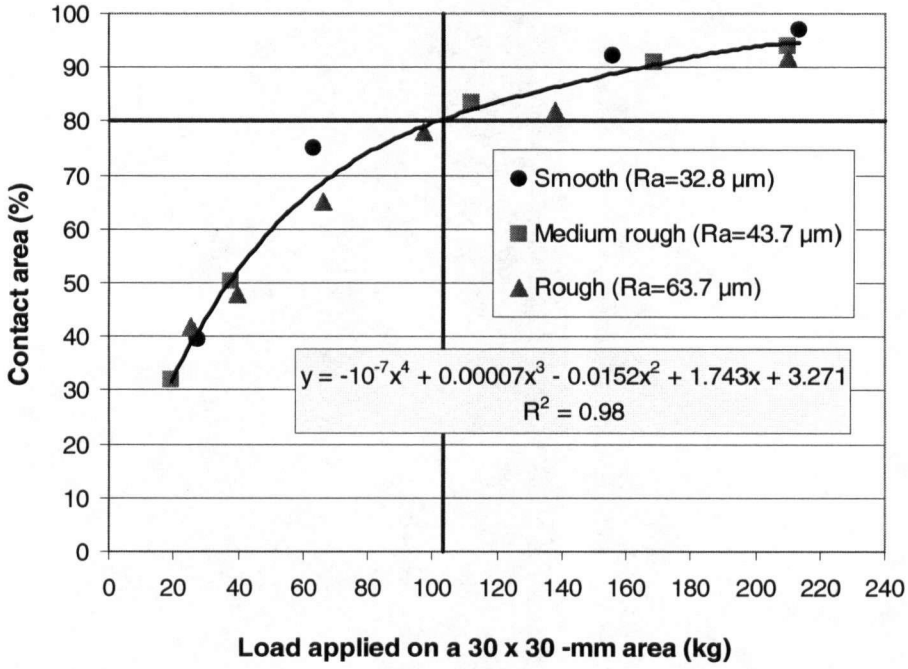

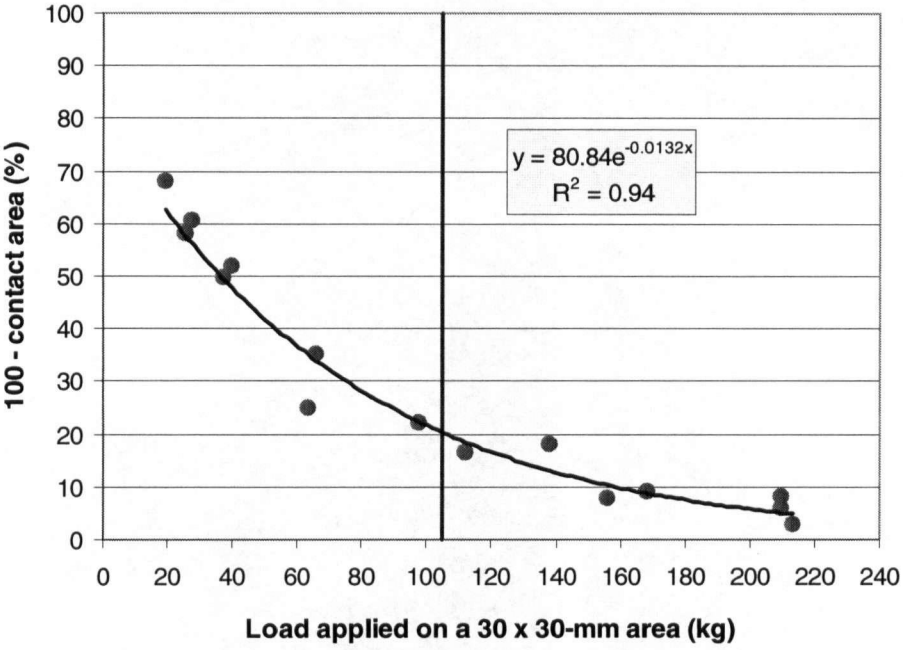

Figure 3.8 The relationship between the contact area and the load applied for aspen parallel veneer-ply specimens (upper: polynomial or power; bottom: exponential)

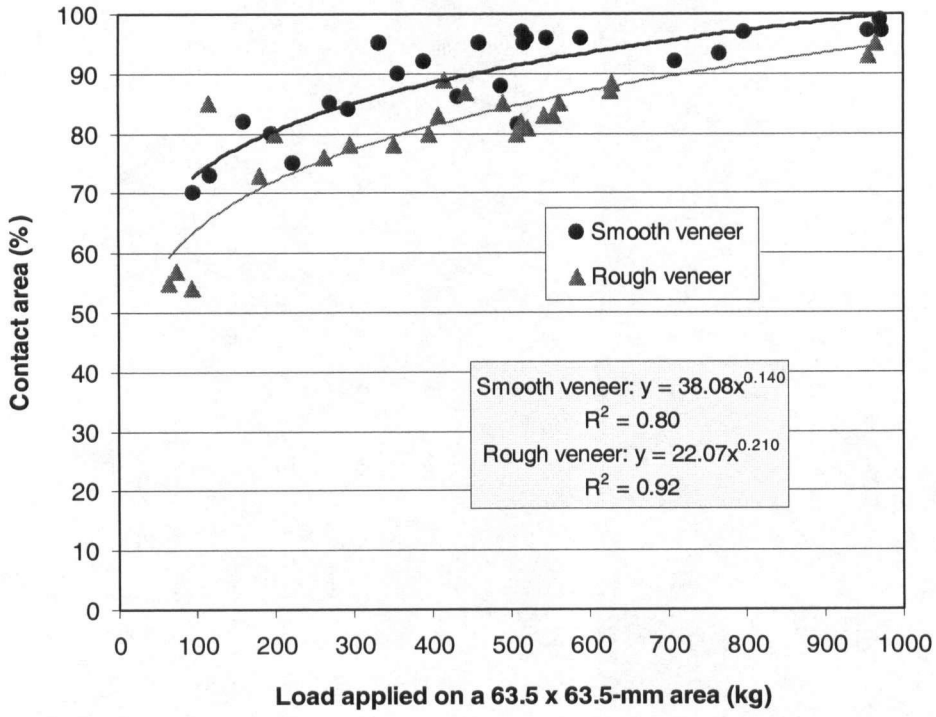

Figure 3.9 The effect of veneer surface roughness on veneer-to-plate contact area at different loads

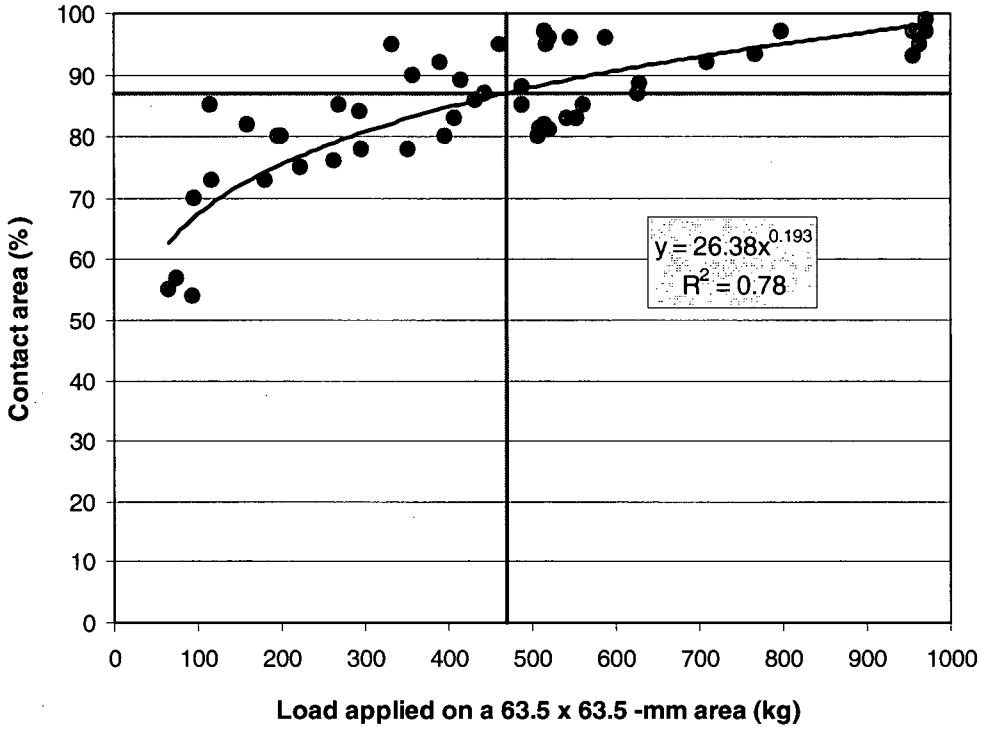

Figure 3.10 The relationship between veneer-to-plate contact area and the load applied for aspen veneer

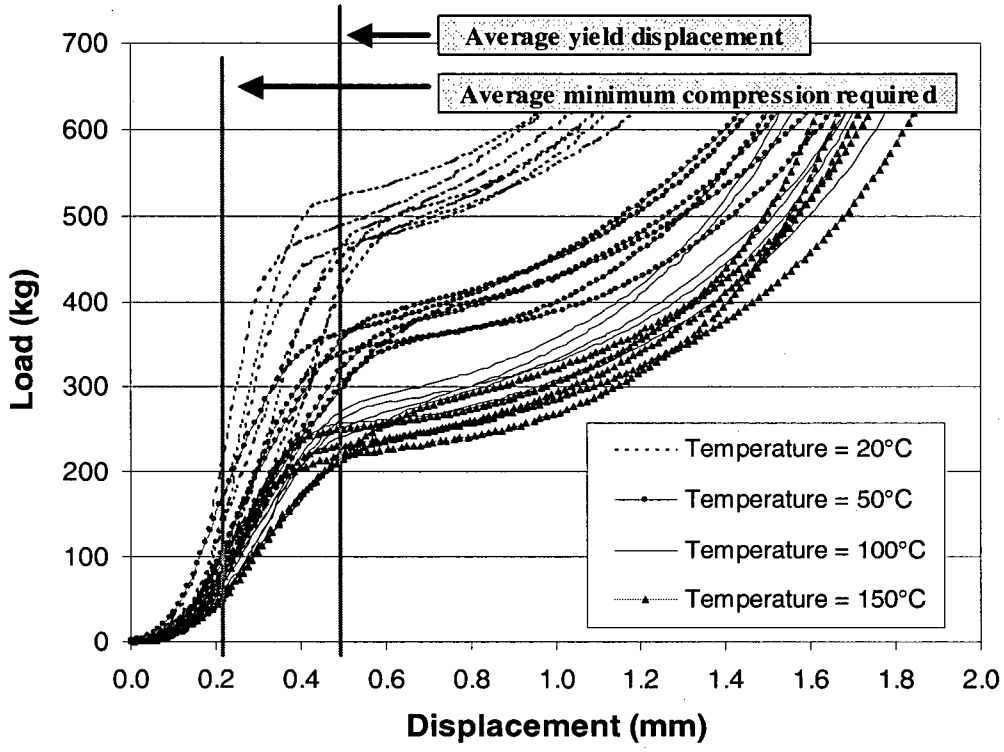

Figure 3.11 The average minimum compression required and average yield displacement over a temperature range for 30 x 30 x 2.5 -mm sliced aspen veneer

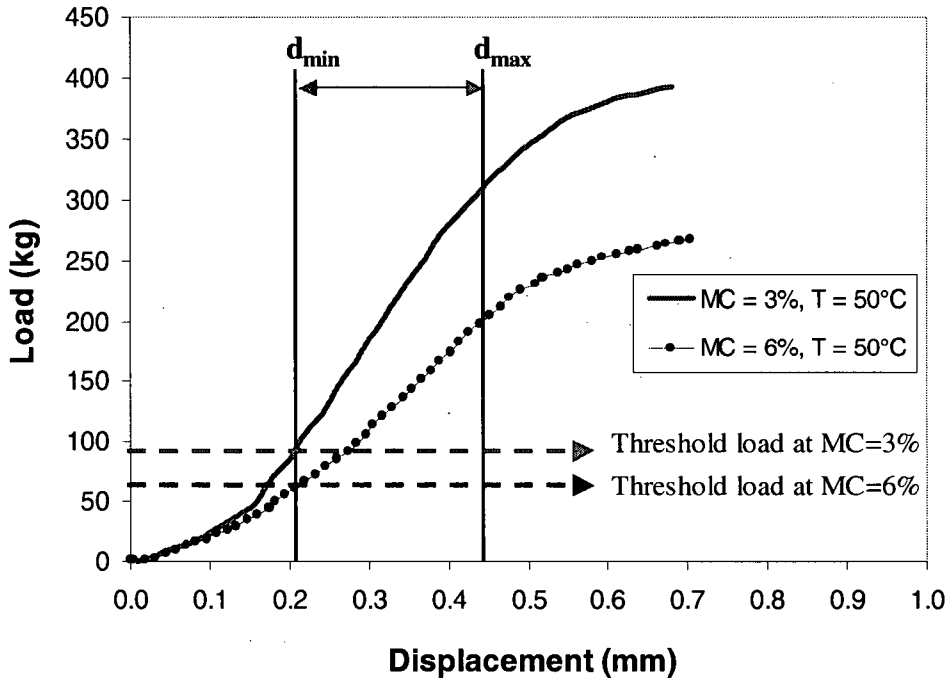

Figure 3.12 The effect of MC on the minimum compression required (d_{min}) and yield displacement (d_{max}) of 30 x 30 x 2.5 -mm sliced aspen veneer

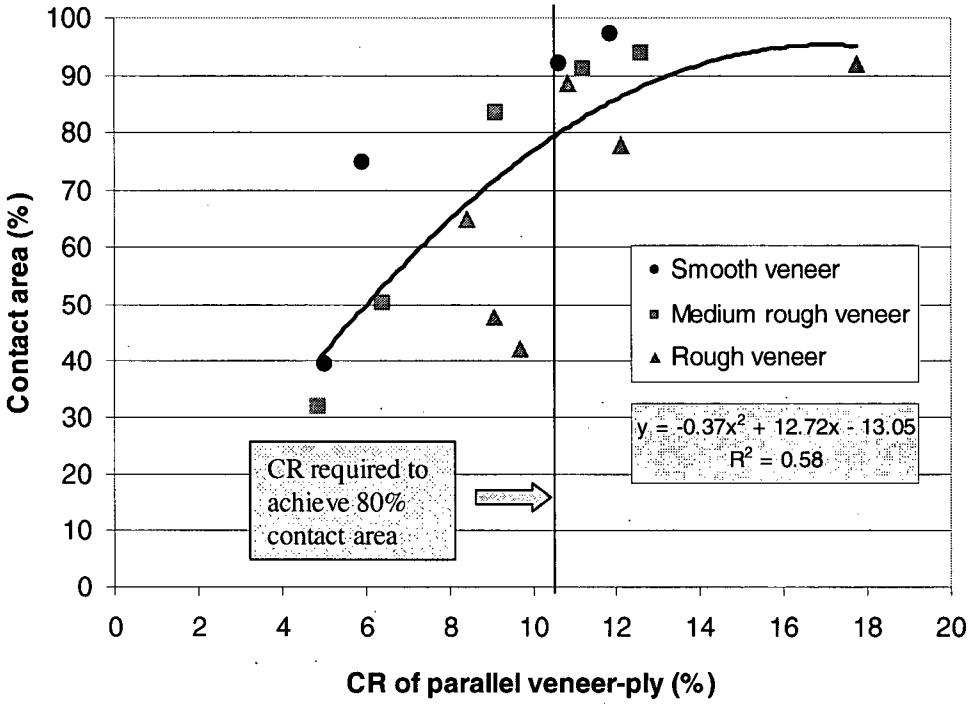

Figure 3.13 The relationship between veneer-to-veneer contact area and compression ratio (CR) for parallel veneer-ply in terms of veneer roughness

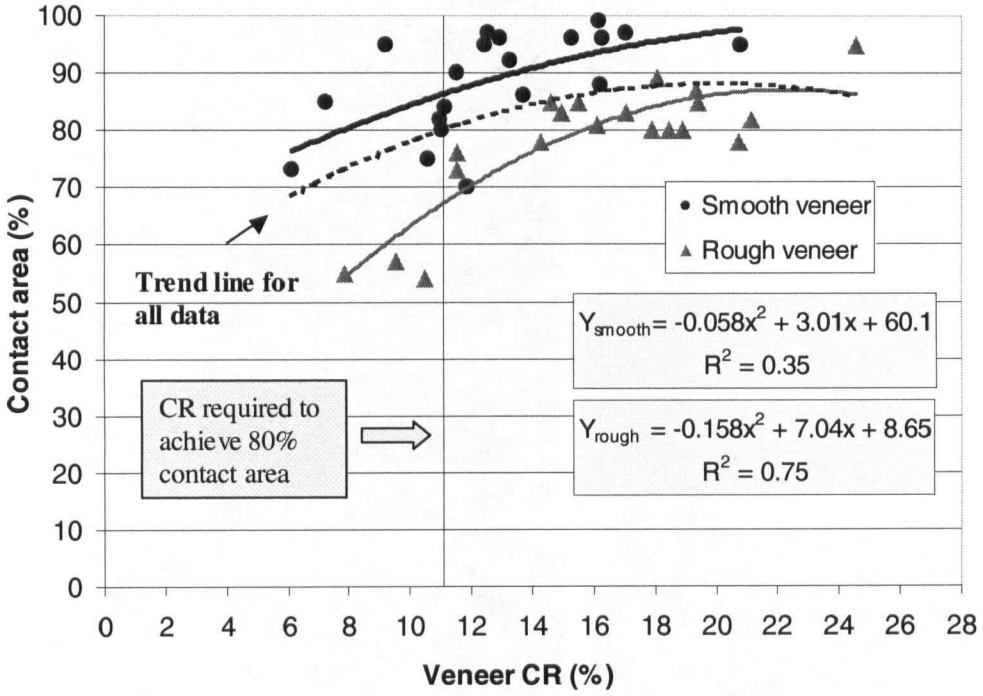

Figure 3.14 The relationship between veneer-to-plate contact area and veneer compression ratio (CR) in terms of veneer roughness

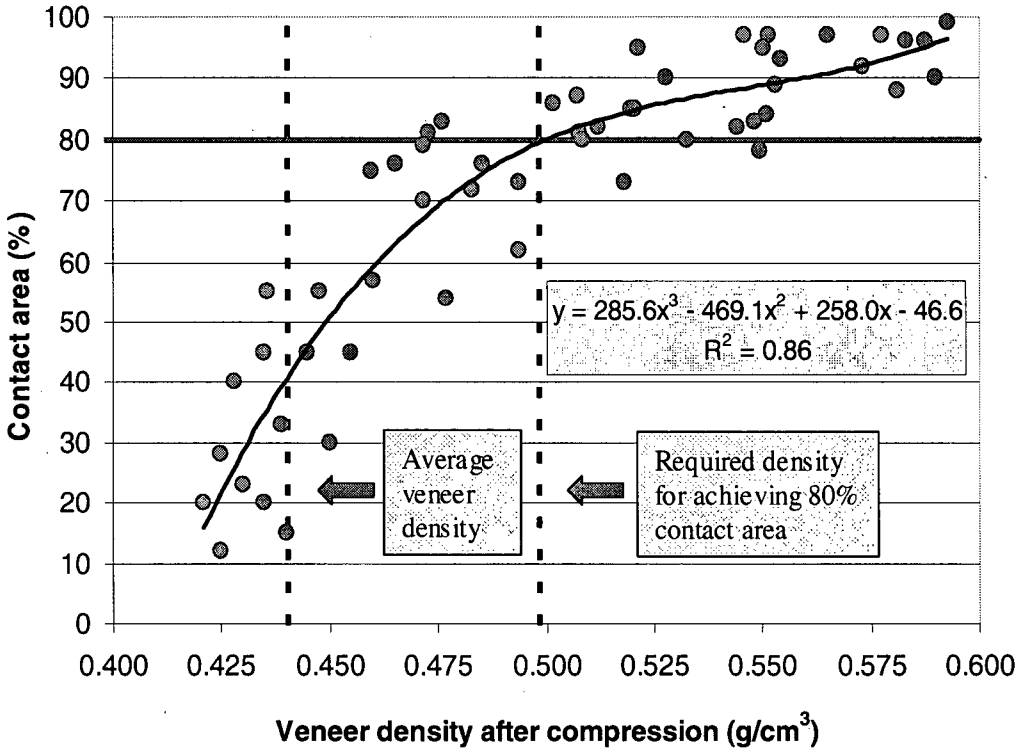

Figure 3.15 The relationship between the contact area and veneer (panel) density

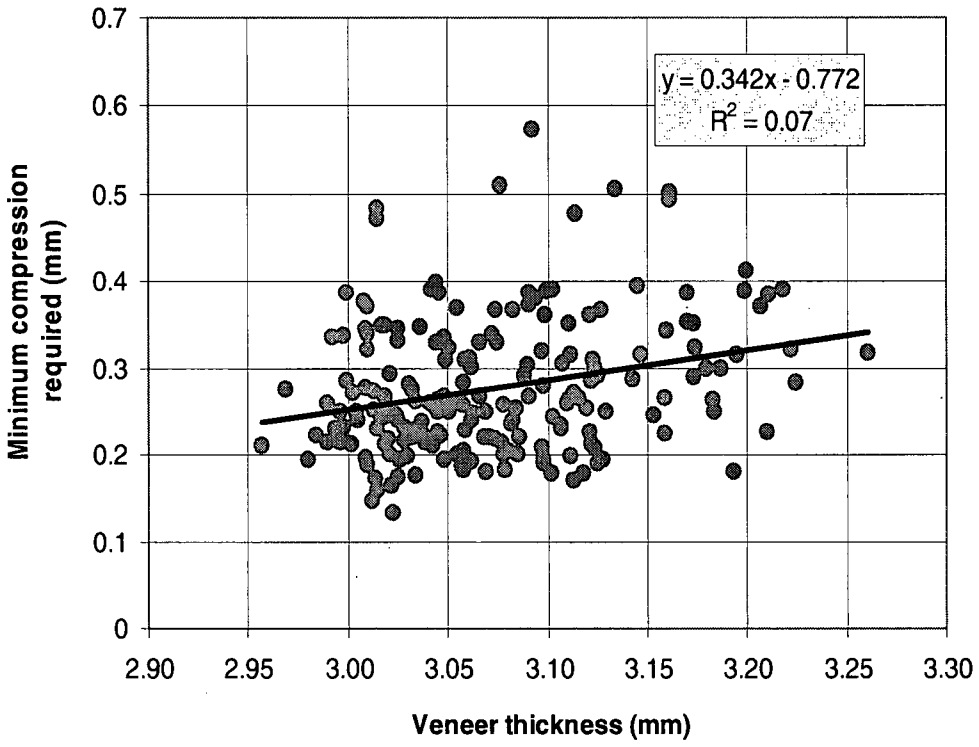

Figure 3.16 The correlation between the minimum compression required and veneer thickness

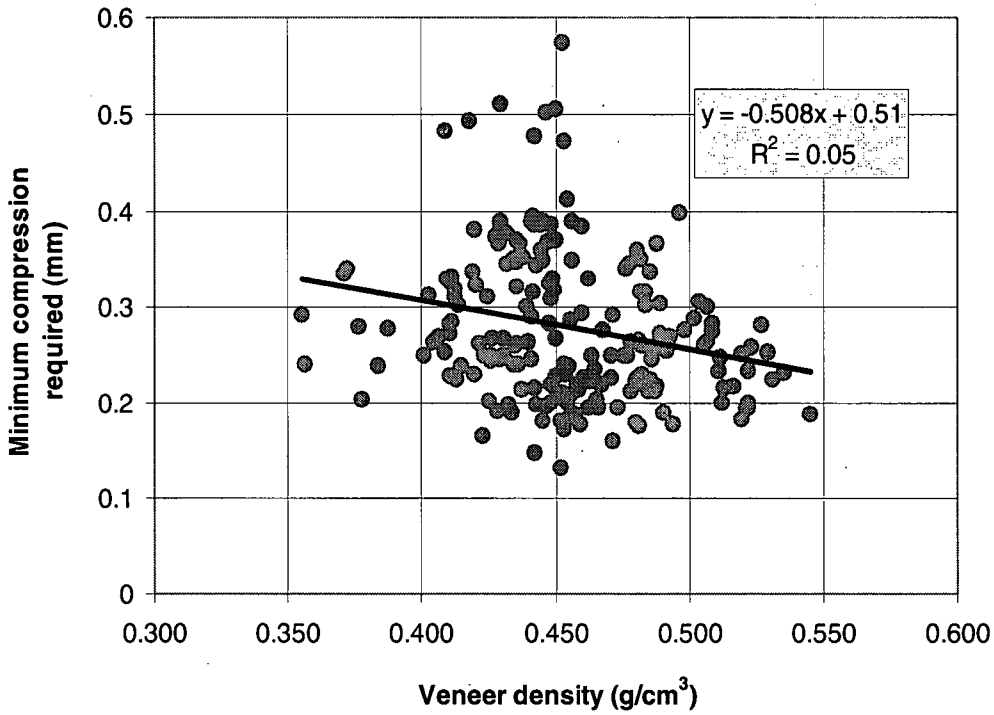

Figure 3.17 The correlation between the minimum compression required and veneer density

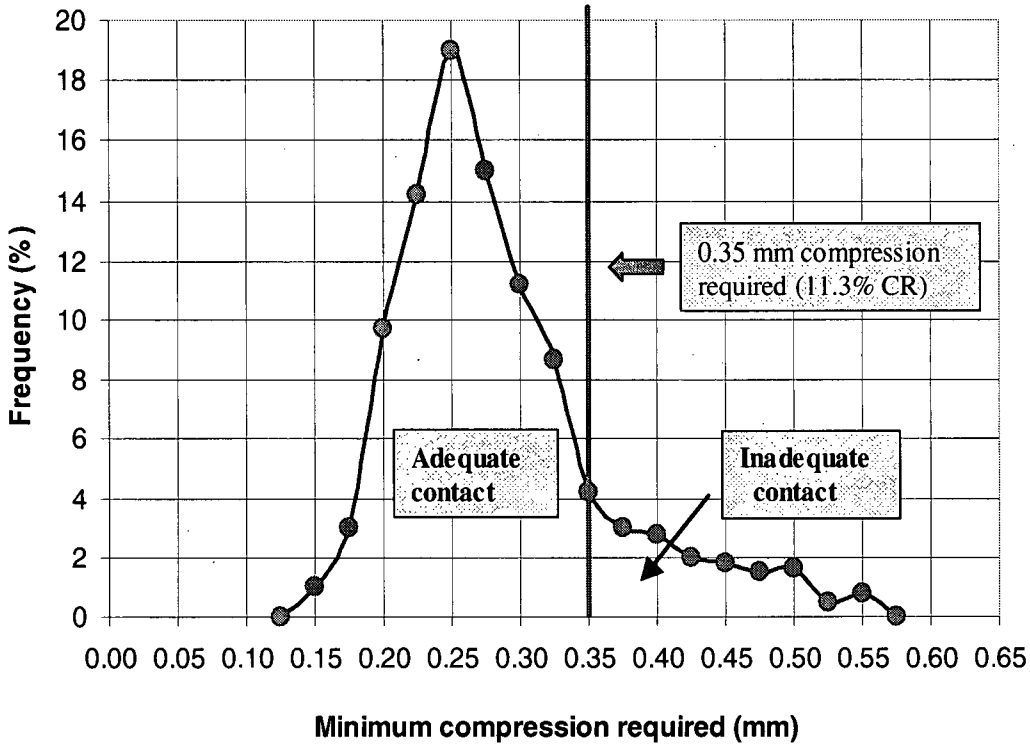

Figure 3.18 Frequency distribution of the minimum compression required for nominal 3.2 mm thick mill peeled aspen veneer

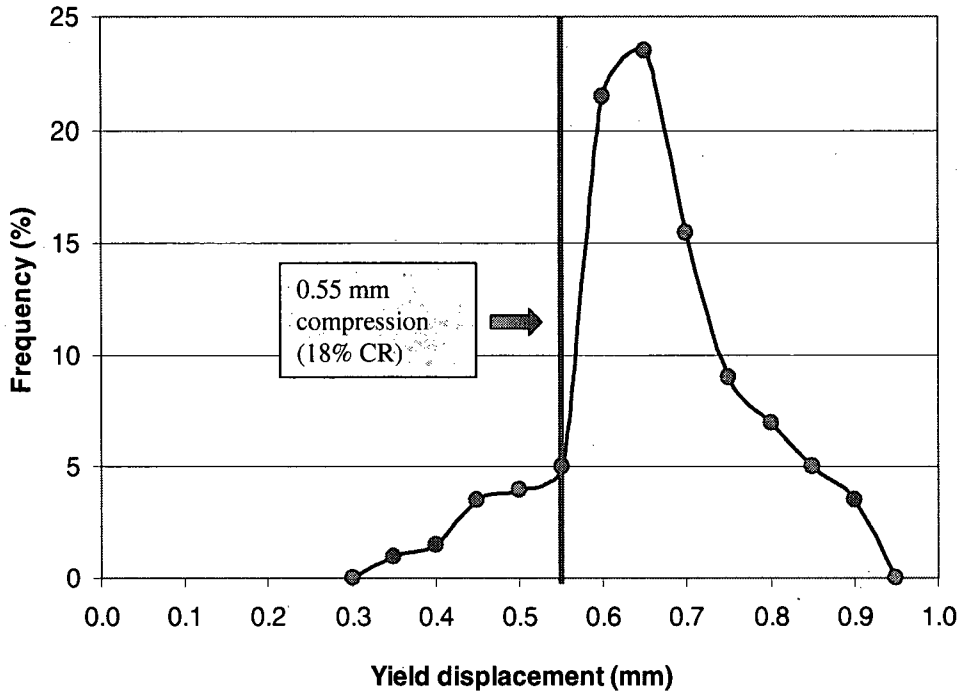

Figure 3.19 Frequency distribution of the yield displacement for nominal 3.2 mm thick mill peeled aspen veneer

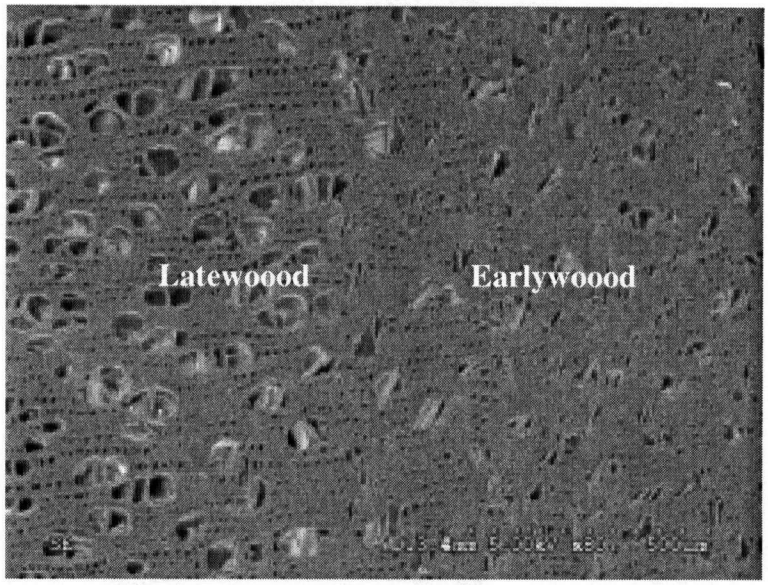

Figure 3.20 SEM photographs of aspen wood at 23% compression ratio (CR) (courtesy of Mei and Dai 2003)

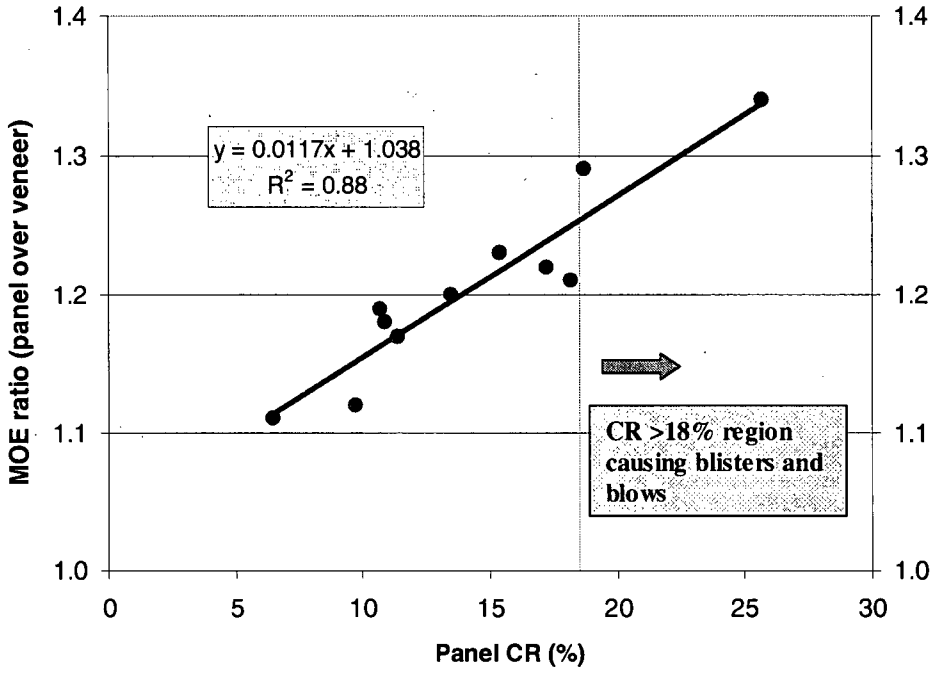

Figure 3.21 The changes of MOE ratio of the panel over veneer with regard to panel compression ratio (CR)

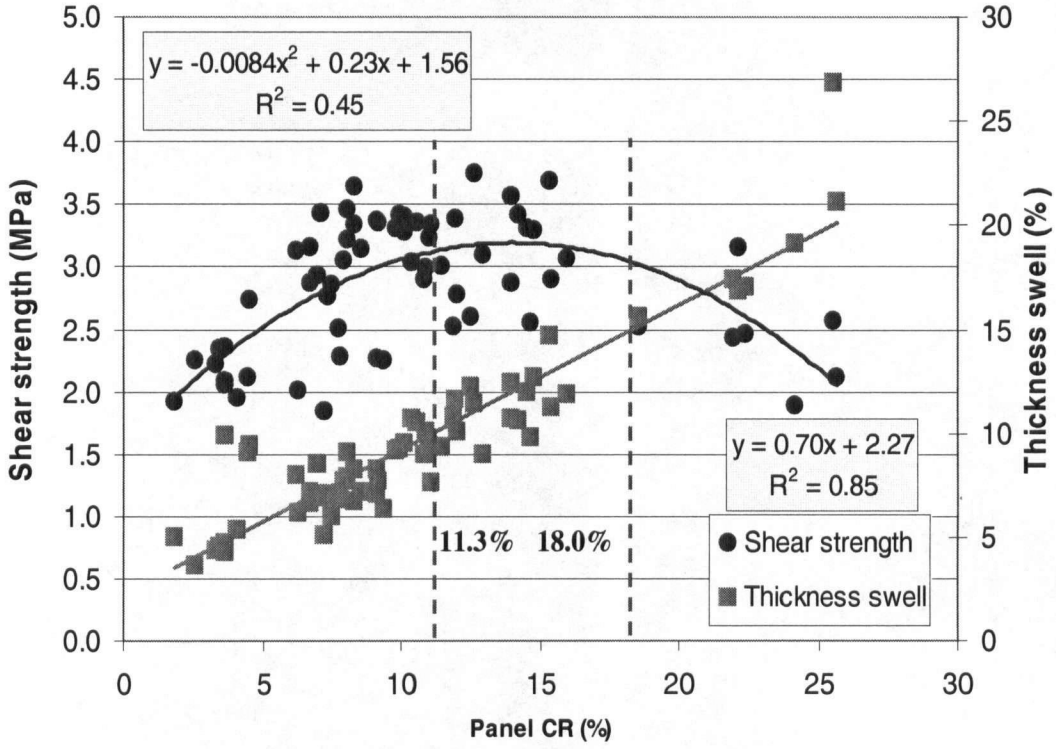

Figure 3.22 The changes of shear strength and thickness swell with regard to panel compression ratio (CR)

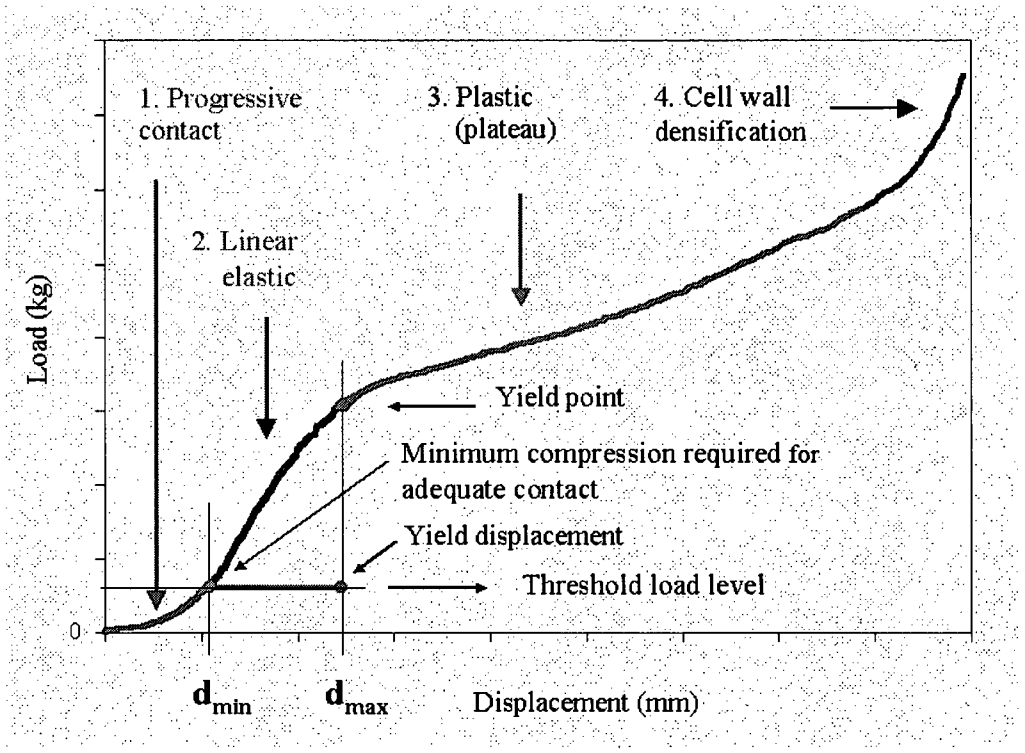

Figure 3.23 Revised wood transverse compression theory with four stages

3.6 Bibliography

ASME Standard B46.1-2002. 2003. Surface texture (surface roughness, waviness, and lay). American Society of Mechanical Engineers, New York, NY. (Revision of ASME B46. 1-1995).

Bodig, J. 1965. The effect of anatomy as the initial stress-strain relationship in transverse compression. Forest Prod. J. 15 (5):197-202.

Bodig, J. and B. A. Jayne. 1982. Mechanics of wood and wood composites. Krieger Publishing Company. Malabar, Florida, USA.

Ellis, S. and P. Steiner. 2002. The behaviour of five wood species in compression. IAWA Journal.Vol.23(2):201-211.

Faust, T. D. and J. T. Rice. 1986. Effects of veneer surface roughness on the bond quality of southern pine plywood. Forest Prod. J. 36(4):57-62.

Faust, T. D. and J. T. Rice. 1987. Effects of a variable glue application rate strategy on bond quality and resin consumption in the manufacture of southern pine plywood. Forest Prod. J. 37(7/8):64-70.

Faust, T. D. 1987. Real-time measurement of veneer surface roughness by image analysis. Forest Prod. J. 37(6):34-40.

Fujiwara, Y., Y. Fujii, and Y. Sawada. 2004. Assessment of wood surface roughness: comparison of tactile roughness and three dimensional parameters derived using a robust Gaussian regression filter. J. Wood Sci. 50: 35-40.

Fukuyama, M. and T. Takemura. 1962. The effect of temperature on compressive properties perpendicular to grain of wood. Journal of the Japan Wood Res. Soc. 8(4): 170-176.

Mei, A. and C. Dai. 2003. On compression behaviour of aspen wood and horizontal density variation of strandboard. A presentation at Forintek Canada Corp. (unpublished).

Metriguard Inc. 2005. User manual of model 239 stress wave timer.

Mitutoyo. 2004. SJ-400 --- Surface Roughness Tester. User's Manual.

Neese, J. L., J. E. Reeb and J. W. Funck. 2004. Relating traditional surface roughness measures to gluebond quality in plywood. Forest Prod. J. 54(1):67-73.

Provatas, N. and T. Uesaka. 2003. Modelling paper structure and paper-press interactions. Journal of Pulp and Paper Sci. 29(10):332-340.

Sandak, J. and C. Tanaka. 2003. Evaluation of surface smoothness by laser displacement sensor I: effect of wood species. J. Wood Sci. 49: 305-311.

Sandak, J., C. Tannka and T. Ohtani. 2004. Evaluation of surface smoothness by a laser displacement sensor II. Comparison of lateral effect photodiode and multielement array. J. Wood Sci. 50: 22-27.

Wolcott, M. P., B. Kasal, F. A. Kamke and D. A. Dillard. 1989. Testing small wood specimens in transverse compression. Wood and Fiber Sci. 21(3): 320-329.

Zhou, X. and C. Dai. 2005. Interaction of temperature and moisture content on flake compression. Proceedings of the 7th Pacific Rim Bio-Based Composites Symposium. Volume II. 116-125. Nanjing, P.R. China.

Faust, T. D. and J. T. Rice. 1986. Effects of veneer surface roughness on the bond quality of southern pine plywood. Forest Prod. J. 36(4):57-62.

Faust, T. D. and J. T. Rice. 1987. Effects of a variable glue application rate strategy on bond quality and resin consumption in the manufacture of southern pine plywood. Forest Prod. J. 37(7/8):64-70.

Neese, J. L., J. E. Reeb and J. W. Funck. 2004. Relating traditional surface roughness measures to gluebond quality in plywood. Forest Prod. J. 54(1):67-73.

Wang, B. J. 2003. Optimization of plywood/LVL hot-pressing operations. Funded by Forintek Canada Corp. Project no. 2019. Unpublished results.

Wang, B. J. and C. Dai. 2005. Hot-pressing stress graded aspen veneer for laminated veneer lumber (LVL). Holzforschung. 59(1):10-17.

CHAPTER IV FUNDAMENTALS OF VENEER-TO-VENEER CONTACTS: MODELING

4.1 Introduction

Wood is a viscoelastic and compressible material. Due to its roughness, the contact between surfaces is generally discontinuous. When two rough wood surfaces are pressed into contact, initially, they touch only a small fraction of the nominal area, namely at the high spots of the two surfaces. Then they deform progressively, the contact area becomes larger and new contact points are created. Depending on the localized compression level, the deformation could be elastic, elastic-plastic and plastic.

The characteristics of veneer surface were found to be truly relevant to its behaviour when pressed into contact, and veneer surface roughness had a significant effect on panel gluebond performance and resulting material recovery (Faust and Rice 1987; Neese *et al.* 2004). In the previous Chapter, a revised wood compression theory was proposed, and a new method was developed to characterize surface roughness and compressibility of wood elements such as veneers and strands. The contact area of veneer-to-veneer and veneer-to-plate was experimentally investigated. It was demonstrated that the contact area increased non-linearly with the pressing load applied. Under the same load, the contact area was generally larger with the smoother veneer than with the rougher veneer. However, in the study, since veneers were visually sorted into the two or three categories, i.e., smooth and rough or medium rough, the results were still semi-empirical. Although many height (amplitude) and spacing-based roughness parameters can be derived from a single 2-D profile (ASME 2003), these are obviously not sufficient to predict the contact area due to the 3-D nature of the surface. To accurately predict veneer-to-veneer contacts, 3-D characterization of veneer surface is deemed to be necessary. However, with the conventional roughness measurement methods, it is very tedious and labour intensive to generate a true 3-D veneer surface profile or map (refer to Figure 1.6). So far, the correlation between 3-D roughness parameters and resulting veneer compression behaviour has never been studied. Although some work has been done to characterize the contacts of one rough surface and a flat or two nominally flat rough surfaces (Greenwood and Williamson 1966; Greenwood 1967; Greenwood and Tripp 1970-1971), none of the models dealt with wood materials. Therefore, a theoretical analysis appears essential to describe how veneer-to-veneer contacts are affected by veneer surface roughness and compression level.

To advance the fundamental understanding of how veneer surface roughness affects contact area for bonding, contact mechanics, classic Hertz theory, Greenwood and Tripp's theory and the revised wood compression theory were applied (Greenwood and Tripp 1970-1971; Johnson 1985). A mathematical model was developed to predict the contact area in terms of veneer surface roughness and nominal compression. To describe veneer-to-veneer contacts which permit compression in both separation and compression modes, four stages of contacts between the two non-conforming wood surfaces were also proposed. Meanwhile, veneer-to-veneer contact area was experimentally investigated under different loads through an image analysis of glue coverage. Based on the experimental results, some key input parameters to the modified Greenwood and Tripp's contact model were determined to predict contact area during veneer compression.

4.2 Modeling of Veneer-to-Veneer Contact

4.2.1 Characteristics of Random Rough Surfaces

As demonstrated in Chapter 3, for any 2-D surface profile (Figure 3.1), a center-line is established by finding the straight line from which the mean square deviation is a minimum. This implies that the area of the trace above the center-line is equal to that below it. The average roughness is then defined by

$$R_a = \frac{1}{L}\int_0^L |z(x)|dx \qquad (4\text{-}1)$$

where z(x) is the height of the surface above the center-line and L is the sampling length. A statistically more meaningful measure of average roughness is the root mean square R_q or standard deviation σ' of the height of the surface from the center-line, i.e.,

$$\sigma'^2 = \frac{1}{L}\int_0^L z(x)^2 dx \qquad (4\text{-}2)$$

The relationship between σ' and R_a depends on the nature of the surface. For a normal random profile $\sigma' = \sqrt{\frac{\pi}{2}}\, R_a$ (Johnson 1985).

The R_a value by itself gives no information about the shape of the surface profile, i.e., about the distribution of the deviations from the mean. However, if we denote by $\phi(z)$ the probability that the height of a particular point on the surface will lie between z and z + dz, then the probability

that the height of a point on the surface is greater than z is given by the cumulative probability function: $\Phi(z) = \int_{z}^{\infty} \phi(z)dz$. This yields an S-shaped curve identical with the bearing area curve.

One simplifying feature of surface roughness is that although the height of a particular asperity is random, the distribution of the asperity heights is rather close to normal (Johnson 1985). It has been found that many real (randomly rough) surfaces exhibit a height distribution which is close to the normal probability function.

$$\phi(z) = \frac{1}{\sqrt{2\pi\sigma}} \exp(-\frac{z^2}{2\sigma^2}) \qquad (4\text{-}3)$$

where σ is the standard deviation (or RMS) from the mean height. The cumulative probability

$$\Phi(z) = 0.5 - \frac{1}{\sqrt{2\pi}} \int_{0}^{z/\sigma} \exp(-\frac{z^2}{2\sigma^2}) d(\frac{z}{\sigma}) \qquad (4\text{-}4)$$

can be found in statistical tables.

4.2.2 Stages of Contacts between Two Random Rough Surfaces

The characteristics of random rough surfaces have a significant effect on their compression behaviour when pressed into contact. A contact is said to be conforming if the surfaces of the two bodies fit exactly or even closely together without deformation. Bodies which have dissimilar profiles are said to be non-conforming. When two non-conforming bodies are brought into contact they touch initially at a single point or along a line (Johnson 1985). As shown in Figure 4.1, the separation is defined as the vertical distance between the two mean lines of the profiles. In theory, without consideration of lateral expansion, there would be four stages for two non-conforming bodies: before contact (separation h>>0), start to contact (separation h > 0), certain contact with zero separation (h = 0) and full contact after compression (separation h < 0).

4.2.3 Hertz Theory of Elastic Contact

When a normal compressive load is applied to the two elastic bodies, the point of contact will spread into an area. Hertz was the first to investigate the normal contact of two elastic bodies (Johnson 1985). A theory of contact was developed to predict how contact area, deformation (compression) and maximum pressure grow with the load applied in terms of curvature and elastic modules of the bodies. For elastic bodies, the contact area was found to be proportional to

the (load)$^{2/3}$. The assumptions made in the Hertz theory of elastic contact were parabolic profiles, elliptical contact area, frictionless surfaces and elastic half-space.

4.2.4 Contact of One Nominally Flat Rough Surface and a Plane

To deal with real contact of two plate-type materials, Hertz's contact theory was further expanded and statistical rules were applied. The simplest of this type is the contact of one nominally flat rough surface and a plane. So far, most models of surface contact consider the surface roughness to be on one of the contacting surfaces only (Greenwood 1967; Johnson 1985). In the frictionless contact of elastic bodies, the contact stresses depend only on the relative profile of their two surfaces, i.e. upon the shape of the gap between them before loading. In general, they can be replaced by a flat, rigid surface in contact with a body having an effective modulus and a profile which results in the same undeformed gap between the surfaces. Assuming that the two surfaces have RMS roughnesses σ_1' and σ_2', respectively, the equivalent contact should be between a rigid flat plane with a deformable surface of equivalent roughness σ' given by

$$\sigma' = \sqrt{\sigma_1'^2 + \sigma_2'^2} \qquad (4\text{-}5)$$

The mean level of the surface is taken as the centerline and the distance between the centerline and the rigid flat plane is seen as the separation. Based on these approximations, the contact area, total load required and stress can be determined in terms of the distribution function of summit heights of the surface, curvature of the summits, effective modulus and separation (Johnson 1985).

4.2.5 Contact of Two Nominally Flat Rough Surfaces

In reality, most of the contacts deal with two nominally flat rough plane surfaces. By expanding actual single contact laws to generalized laws with a consideration of radial misalignment, and replacing distribution of asperity heights by distribution of sums of pairs of heights, the solution for contact of only one surface being rough can be applied to that for both surfaces being rough. Greenwood and Tripp (1970-1971) proposed a general theory of contacts between two rough plane surfaces and applied this to generic metal materials. In the area of wood composite processing, the model dealing with two rough surfaces is more practical and applicable, since machined wood (veneer) surface is generally rougher compared to metal surface.

To simplify the analysis, two rough surfaces are represented by identical asperities differing only in their heights above the mean line of the plane (Greenwood and Tripp 1970-1971). As shown in Figure 4.2, the contacts between two such surfaces are considered in which the pairs of asperities are not aligned so that the usual contact will be between the shoulders of the two hills. Following functions and parameters were defined: the distribution of asperity heights $\phi(z)$, and the shape of each asperity with respect to its peak z = S(x, y) = S(λ), where λ and z are the horizontal and vertical distances from the peak. Considering a particular asperity on the first surface with height Δ_1' and all the asperities of height Δ_2' on the second surface, a typical pair of asperities will be a horizontal distance r away. Since all asperities are assumed to have the same shape, the contact will first occur midway between their centers, namely a distance r/2 from the individual centers if they are convex, at which point the heights above the respective mean planes will be Δ_1' – S(r/2) and Δ_2' – S(r/2). To create contacts, the separation h of the mean planes must be smaller than the sum of these heights, i.e.

$$h < \Delta_1' + \Delta_2' - 2S(r/2) \qquad (4\text{-}6)$$

Hence the deformation or compression at the contact can be defined as

$$\Delta = \Delta_1' + \Delta_2' - 2S(r/2) - h \qquad (4\text{-}7)$$

Without considering the lateral expansion during loading, the contact area A and the load applied P in the vertical direction will depend only on the deformation Δ and the misalignment r. If the surface density of asperity peaks on either surface is denoted as ω, the number of asperities with heights in the range Δ_2' to $\Delta_2' + d\Delta_2'$ situated between r and r + dr from the first asperity will be

$$2\pi r\, \omega\, dr\, \phi(\Delta_2')d\Delta_2' \qquad (4\text{-}8)$$

Hence the load applied on the first asperity due to the second surface will be

$$\int_{\Delta_2}\int_{r} 2\pi\omega P(\Delta, r)\phi(\Delta_2')rdrd\Delta_2' \qquad (4\text{-}9)$$

where the r integration will, in principle, be limited by the extent of the surfaces but in practice may be taken from 0 to ∞. If the nominal area of contacts is A', there will be $A'\omega\phi(\Delta_1')d\Delta_1'$ asperities on the first surface with heights between Δ_1' to $\Delta_1' + d\Delta_1'$. Thus, the total load required between the two surfaces becomes

$$P(h) = 2\pi\omega^2 A' \int_{\Delta_1'\Delta_2'} \int\int P(\Delta, r)\phi(\Delta_1')\phi(\Delta_2')rdrd\Delta_1'd\Delta_2' \qquad (4\text{-}10)$$

According to Greenwood and Tripp (1970-1971), the load between a pair of asperities with given heights does not depend on the individual heights Δ_1' and Δ_2' but only on their sum $(\Delta_1' + \Delta_2')$, and therefore only the statistical distribution of the sum of pairs of heights can affect P(h). The distribution of the sum can be established from the individual distributions $\phi(\Delta_1')$ and $\phi(\Delta_2')$ by the standard derivation of mathematical statistics. By defining $\Delta_1' + \Delta_2' = \Delta'$, and assuming it has a distribution $\varphi(\Delta')$, the total load required is then

$$P(h) = 2\ \pi\omega^2 A' \int_{\Delta'} \int P(\Delta, r)\varphi(\Delta')rdrd\Delta' \qquad (4\text{-}11)$$

Now, $\Delta = \Delta_1' + \Delta_2' - 2S(r/2) - h = \Delta' - h - 2S(r/2)$ where $\Delta' - h$ is the overlap between the peaks of the pair of asperities considered. Because of misalignment, the peaks may overlap without being any contacts. Further, if we define the result of the r-integration as

$$P_0(\Delta' - h) = 2\pi\omega \int_0^\infty P(\Delta' - h - 2S(r/2), r)rdr \qquad (4\text{-}12)$$

then

$$P(h) = \omega A' \int_h^\infty P_0(\Delta' - h)\varphi(\Delta')d\Delta' \qquad (4\text{-}13)$$

In the same way, according to Greenwood and Tripp (1970-1971), if we write

$$A_0(\Delta' - h) = 2\pi\omega \int_0^\infty A(\Delta' - h - 2S(r/2), r)rdr \qquad (4\text{-}14)$$

the total contact area is

$$A(h) = \omega A' \int_h^\infty A_0(\Delta' - h)\varphi(\Delta')d\Delta' \qquad (4\text{-}15)$$

For simplicity, it was assumed that the surfaces are covered with paraboloidal asperities to conform to general Hertz approximation. The asperity shape is then $z = S(\lambda) = \lambda^2/2R'$ where R' is the radius of curvature at the peak. Thus $2S(r/2) = r^2/4R'$. Because of the misalignment, the Hertz theory for the contact of two paraboloids can be only approximately applied, since the normal load is not acting vertically and there must also be a tangential component. However, according to Greenwood and Tripp (1970-1971), the tangential component was generally

negligible due to the slopes of real surfaces. By applying Hertz's theory concerning the relationship between load and elastic modulus and radius of curvature for two contact bodies (Johnson 1985), Equation (4-12) becomes

$$P_0(\Delta' - h) = 2\pi\omega \int_0^{\infty} P(\Delta' - h - 2S(r/2), r) r dr$$

$$= \frac{8}{3}\pi\omega E^* (\frac{R'}{2})^{\frac{1}{2}} \int_0^{\infty} (\Delta' - h - \frac{r^2}{4R'})^{\frac{3}{2}} r dr$$

$$= \frac{16\sqrt{2}}{15}\pi\omega E^* R'^{\frac{3}{2}} (\Delta' - h)^{\frac{5}{2}} \qquad (4\text{-}16)$$

Then the total load required is

$$P(h) = \omega A' \int_h^{\infty} P_0(\Delta' - h)\varphi(\Delta')d\Delta' = \frac{16\sqrt{2}}{15}\pi\omega^2 E^* R'^{\frac{3}{2}} A' \int_h^{\infty} (\Delta' - h)^{\frac{5}{2}} \varphi(\Delta')d\Delta' \qquad (4\text{-}17)$$

By defining $\Delta' = s\sigma'$, we have

$$P(h) = \frac{16\sqrt{2}}{15}\pi(\omega R'\sigma')^2 E^* \sqrt{\frac{\sigma'}{R'}} A' F_{5/2}(\frac{h}{\sigma'}) \qquad (4\text{-}18)$$

where $F_n(\mu) = \int_{\mu}^{\infty} (s-\mu)^n \varphi'(s) ds$, in which $\varphi'(s)$ is the standardized height distribution with $\varphi'(s)\,ds = \varphi(\Delta')d\Delta'$; E^* is the composite elastic modulus, given by $\frac{1}{E^*} = \frac{1-\nu_1^2}{E_1} + \frac{1-\nu_2^2}{E_2}$, in which E_1 and E_2 are Young's moduli, ν_1 and ν_2 are Poisson's ratios of surfaces 1 and 2, respectively. By further defining $k' = \frac{2\sqrt{2}}{3}(\omega R'\sigma')E^* \sqrt{\frac{\sigma'}{R'}}$, the nominal stress for contacts between two nominally flat rough surfaces can be calculated as

$$\sigma(h)_{two} = \frac{8\pi}{5}(\omega R'\sigma')k' F_{5/2}(\frac{h}{\sigma'}) \qquad (4\text{-}19)$$

Unlike generic metal materials, wood is an anisotropic material with a significant difference of Young's modulus in different loading directions. Therefore, in Equation (4-18), transverse compression Young's modulus (E) should be used for wood due to its anisotropic behaviour. Note that asperity heights generally follow a normal distribution. By statistics, if the height

distribution on each surface is normal with standard deviation σ_1', the distribution of sums of heights is also normal with standard deviation $\sigma' = \sqrt{2}\,\sigma_1'$ based on Equation (4-5).

Similarly, according to Greenwood and Tripp (1970-1971), the total contact area A(h) is given by

$$A(h) = \omega A' \int_h^{\infty} A_0(\Delta' - h)\varphi(\Delta')d\Delta' = \pi^2(\omega R'\sigma')^2 A' F_2(\frac{h}{\sigma'}) \qquad (4\text{-}20)$$

Therefore, at the separation of h, the percent contact area (%) can be calculated by

$$\text{Contact area (\%)} = \frac{A(h)}{A'}\ (100\%) = \pi^2(\omega R'\sigma')^2 F_2(\frac{h}{\sigma'})\ \ (100\%) \qquad (4\text{-}21)$$

with the expected number of contacts

$$N(h) = 4\ \pi(\omega R'\sigma')\omega A' F_1(\frac{h}{\sigma'}) \qquad (4\text{-}22)$$

Equations (4-19), (4-21) and (4-22) expressed stress (σ), percent contact area (A%) and number of contacts (N) in terms of integrals of the distribution of asperity heights. According to Greenwood and Tripp (1970-1971), these equations were generally used for general metal materials. The prediction was limited to a minimum of zero separation, namely, $h \geq 0$, with a maximum contact area up to 1%. It was found that $\omega R'\sigma'$ was reasonably constant with a value of around 0.05, and k' was around 100 MPa for metal materials. For wood materials, as shown in Figure 4.1, the compression was generally up to the last stage with a negative separation or compression. When a negative separation occurs ($\frac{h}{\sigma'} < 0$), $F_n(\frac{h}{\sigma'})$ can be solved by a mathematical tool (Mathematica 2007). For example, when $\frac{h}{\sigma'} = -2$, we have

$$F_2(-2) = \frac{1}{\sqrt{2\pi}}\int_{-2}^{\infty}(s+2)^2\varphi'(s)ds = \frac{1}{\sqrt{2\pi}}\int_{-2}^{\infty}(s+2)^2 e^{-s^2/2}ds$$

$$\approx 0.1995\, e^{-s^2/2}\,[5e^{s^2/2}\sqrt{2\pi}\ \text{erf}(s/\sqrt{2}) - 2(s+4)]\Big|_{-2}^{\infty} \qquad (4\text{-}23)$$

where erf (s) is an error function, given by

$$\text{erf}(s) = \frac{2}{\sqrt{\pi}}\int_0^s e^{-t^2}dt \approx \frac{2}{\sqrt{\pi}}(s - \frac{1}{3}s^3 + \frac{1}{10}s^5 - \frac{1}{42}s^7 + \frac{1}{216}s^9 + \cdots) \qquad (4\text{-}24)$$

Hence, F_2 (-2) $\approx$ 10.5. If $\frac{h}{\sigma}$ is negative and large, $F_n(\frac{h}{\sigma})$ is approximately equal to $(-\frac{h}{\sigma})^n$ (Greenwood and Tripp 1970 -71).

4.2.6 Factors Affecting Contact Area and Stress

Based on Equation (4-21), theoretically, the contact area is dependent on the equivalent RMS roughness of two surfaces, separation, area density of asperities and radius of the asperities. At the same separation, the larger the area density of asperities or radius of the asperities, the larger the contact area. In contrast, based on Equation (4-19), aside from the effect of the above four variables, the resulting nominal stress is also dependent on k', a parameter measuring the modulus and surface asperities of the materials. Note that k' is determined by the following four surface and material variables, namely, area density of asperities, radius of the asperities, equivalent RMS roughness and composite elastic modulus. If any of the above four variable increases, k' will increase. At the same separation, the larger the k', the larger the stress. As discussed in Chapter 3, unlike metal materials, the revised wood compression theory defines four stages of compression instead of the commonly defined three. At the first stage, the load increases non-linearly with increasing displacement to create adequate contacts, namely 80% or above, until a threshold load is reached. Therefore, from a contact viewpoint, the first stage of progressive contact is critical to wood veneer as compared to the linear elastic stage to metal materials.

As discussed, wood veneer is much more compressible than metal materials, during the first stage of progressive contact, the deformation could be elastic, elastic-plastic and plastic for individual asperities depending on localized stress levels. As a result, Equation (19) may not be suitable for wood veneer to predict the resulting nominal stress. This is due to the fact that elastic deformation was assumed in theoretical modeling. The resulting (global) stress for wood veneer could be accurately predicted by summing up the product of localized contact area and stress. Based on Equation (21), the contact area is governed by surface roughness and compression level and independent of material elastic modulus. As long as the compression level and shape/distribution of surface asperities are identical, the predicted contact area for metal

materials and wood veneer should be the same. As a result, Equation (21) could be applicable to wood veneer for predicting the contact area.

4.3 Experimental

In this study, the experimental investigations served as two purposes: 1) to determine input parameters for the contact model; and 2) to validate the model prediction of the contact area.

Two 3.2 mm thick 1.2 x 1.2 -m dried aspen veneer sheets were selected with a MC of 3%. Fifty 63.5 x 63.5 -mm (2.5 x 2.5 -in) veneer specimens, each of them having almost same level of surface roughness based on visual identification, were cut from each sheet. Before performing tests, the five-point thickness, weight, length and width of each specimen were measured to calculate veneer density. Then, five 63.5 x 63.5 -mm (2.5 x 2.5 -in) veneer specimens from each sheet were randomly selected for measuring veneer roughness using a SJ-400 Surface Roughness Tester (Mitutoyo 2004). The measurements were taken across the grain at both tight and loose sides of each specimen. The equivalent RMS roughness parameter σ' for each veneer specimen was determined, which was the square root of R_q at the tight side and R_q at the loose side of each specimen. After that, these ten specimens were compressed in an Instron machine at ambient temperature (20°C) to establish the stress-strain curves. During compression, a load rate of 2 mm/min was used. The compression was stopped when the load reached a maximum limit of 975 kg.

To experimentally investigate how veneer-to-veneer contact area and stress change with the nominal compression, 45 pairs of veneer specimens were formed with one from each sheet. A plywood phenol formaldehyde (PF) glue was uniformly spread onto the tight side of one specimen at an application rate of 160 g/m^2. Based on the tight-to-loose construction, the loose side of the other veneer specimen was placed face-down to the glue-covered specimen. Before starting the compression test, a load level of about 10 kg was applied onto 63.5 x 63.5 -mm two-ply veneer panels to create an initial contact for veneer-to-veneer. The compression tests were conducted in a load-control mode at a load rate of 2 mm/min and then stopped when the load reached a desired target from 25 to 975 kg. During the compression, glue was transferred to the loose side of the upper veneer specimen, displaying the glue coverage map (contact area) when two-ply veneer panels were brought into contact at various degrees. The maximum deformation

of each two-ply veneer panel was recorded. The veneer-to-veneer compression (negative separation) was approximately one-third of the maximum deformation since there were three contact interfaces during compression of the two-ply veneer panels. After stopping the compression, the upper veneer specimen was carefully removed. Using an image analysis software program, the glue coverage map of each upper veneer specimen was taken and the contact area in dark color was evaluated in terms of the percentage of the specimen size. The stress was calculated based on the maximum load applied and area of the veneer specimen.

4.3.1 Determination of Model Parameters

To theoretically predict the contact area during veneer compression, one must know the area density of veneer asperities, average radius of veneer asperities and veneer equivalent RMS roughness. On average, based on the measurements of the ten aspen veneer specimens, the equivalent veneer RMS roughness parameter σ' for these two sheets was 50 μm with a standard deviation of 3 μm. Figure 4.3 shows the typical 2-D roughness profiles for both tight and loose sides of one aspen veneer specimen. On average, the frequency of peaks per millimeter (η_p) was approximately 4, the RMS roughness σ' was 50 μm (0.05 mm), and average radius of the asperities R' was close to 50 μm (0.05 mm). Hence, according to Johnson (1985), the area density of asperities can be calculated as:

$$\omega \approx 1.8 * \eta_p^2 = 1.8 * (4\ /\text{mm})^2 = 28.8\ /\text{mm}^2$$

Then we have $\omega R'\sigma' \approx 0.072$. Note that this value, generally assumed constant in contact mechanics, was slightly larger than 0.05 for generic metal materials (Johnson 1985).

4.3.2 Measurement of Contact Area and Stress from Veneer Compression

Figure 4.4 shows the relationship between the contact area, stress and nominal compression of veneer-to-veneer for the forty-five pairs of 63.5 x 63.5 -cm (2.5 x 2.5 -in) aspen veneer panels. The relationship between the stress and nominal compression followed a power pattern. In contrast, the relationship between the contact area and nominal compression displayed a polynomial pattern. Initially at a very low applied stress, the contact area increased quickly. However, it tended to level off when 85-90% contact area was achieved. Note that the dispersion of data points may result from the variation of actual veneer surface roughness since the average equivalent RMS roughness (50 μm) was used to calculate $\frac{h}{\sigma'}$.

4.4 Typical Prediction of Contact Area

Since all model parameters are determined, the typical prediction of the contact area from the model can be examined. Recall from Figure 4.1, at the third stage of contact, namely certain contacts with zero separation (h = 0), if $\frac{h}{\sigma'} = 0$, $F_2(\frac{h}{\sigma'}) = 0.5$.

Therefore, the contact area is calculated as follows:

Contact area (%) = $\pi^2(\omega R'\sigma')^2 F_2(\frac{h}{\sigma'})$ (100%) = 2.6%

At the fourth stage of contact (Figure 4.1), namely a full contact after compression ($\frac{h}{\sigma'} < 0$ and large), we have $F_n(\frac{h}{\sigma'}) \approx (-\frac{h}{\sigma'})^n$. If $\frac{h}{\sigma'} = -4.4$, $F_2(\frac{h}{\sigma'}) \approx 19.5$.

Therefore, the contact area is computed as follows:

Contact area (%) = $\pi^2(\omega R'\sigma')^2 F_2(\frac{h}{\sigma'})$ (100%) $\approx$ 100%

The results demonstrate that the contact area is surface roughness dependent. Theoretically, in order to achieve a full 100% contact area, the amount of compression seems to be approximately 4.4 times of the surface equivalent RMS roughness (50 μm).

Figure 4.5 shows the theoretical prediction of contact area in relation to nominal veneer-to-veneer compression. Based on this model, it seems that the contact area increased nonlinearly with increasing nominal compression. Due to the nature of an integration of normal distribution of asperity heights, the contact area seems to approach to its maximum value. Note particularly that using nominal compression in the model can successfully deal with the variation of veneer surface roughness for generic prediction whereas the compression ratio (CR), generally used in the manufacturing of wood composites, is essentially thickness and surface roughness dependent.

Figures 4.6 shows how contact area changes in terms of veneer compression ratio (CR) and surface roughness based on the model prediction. Three veneer roughness grades were simulated, namely, smooth, medium rough and rough. Their three equivalent RMS roughness (σ') values were based on the roughness measurement results in Chapter 3 (see Figure 3.8). In order to achieve an 80% or higher contact area, the CR required was about 5.0%, 7.0% and 10.0% for the smooth, medium rough and rough veneer, respectively. This implies that processing the rough

veneer will inevitably result in a lower material recovery when manufacturing into quality veneer products. As a result, it seems to be beneficial to sort veneer based on its surface roughness. For a typical plywood/LVL mill with an annual capacity of 250 million ft^2 (on a 3/8" basis), every reduction of 1% CR will translate to about $300,000 savings.

4.5 Model Validation

As shown in Figure 4.7, the comparison was made for the contact area between the measured and predicted in terms of nominal compression. In general, it was found that the real contact area measured from the glue coverage map, before it reached about 50%, was larger compared to the theoretical prediction. This is probably due to the fact that during compression, the glue could flow or move and veneers would experience some lateral expansion with a mixture of elastic and plastic deformation whereas in the theoretical model, only elastic deformation was assumed. With increasing nominal compression, the predicted contact area tended to be larger than the measured contact area. This is probably because: 1) the theoretical model assumed that all asperities had identical (parabolic) shapes, differing only in heights from their mean lines of the plane; and 2) in reality, roughness is not uniformly random as defined by the normal distribution in the model. As shown early in Figure 4.3, veneer surface roughness is more abnormal. Further research is needed to modify the model to consider veneer lateral expansion, plastic deformation and glue movement, and so on.

4.6 Conclusions

Contact mechanics, classic Hertz theory and Greenwood and Tripp's theory were adopted to characterize contact area of the two nominally flat rough surfaces in relation to surface roughness parameters and nominal separation. To simulate veneer-to-veneer contacts which permit compression in both separation and compression (negative separation) modes, four stages of contacts between the two non-conforming wood surfaces were proposed in terms of the two surface roughness profiles and the separation between the two mean lines of planes. The Greenwood and Tripp's theory, generally used for generic metal materials, was extended to the stage of compression. In the meantime, the veneer-to-veneer contact area was experimentally investigated under different loads through an image analysis of glue coverage. Some key inputs to the modified Greenwood and Tripp's model were determined to predict the contact area during veneer compression. The model demonstrated that the contact area was mainly

determined by surface density of asperity peaks, average radius of the asperities, equivalent RMS surface roughness and nominal separation (or compression). Compared to the measured contact area, the predicted contact area was somehow underestimated before it reached about 50%, which could be mainly due to the fact that the model developed did not consider veneer plastic deformation, lateral expansion and glue transfer during compression. However, with increasing nominal compression, the predicted contact area tended to be larger than the measured contact area. Further research is warranted to modify the theoretical model for improved prediction of the contact area and resulting stress.

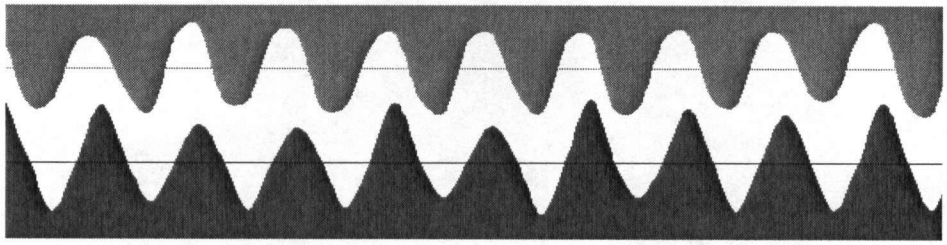

a) Before contact (separation h>>0)

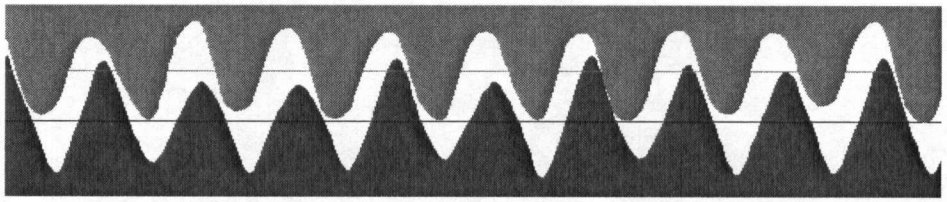

b) Start to contact (separation h>0)

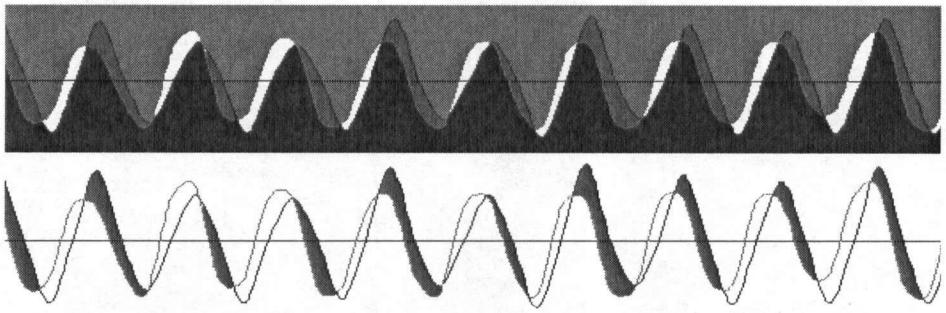

c) Certain contacts with zero separation (separation h = 0)

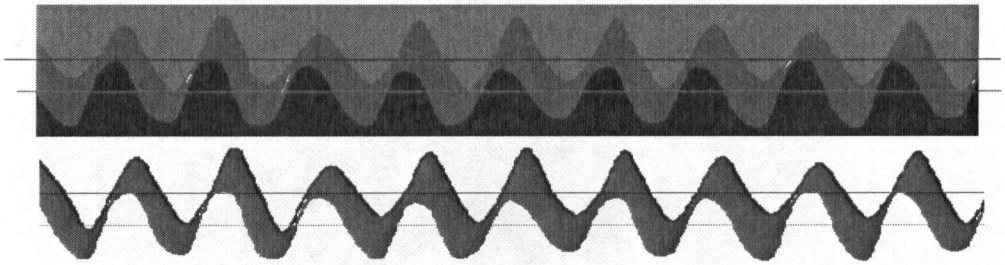

d) Full contacts after compression (separation h < 0)

Figure 4.1 Stages of the contact between two non-conforming body surfaces

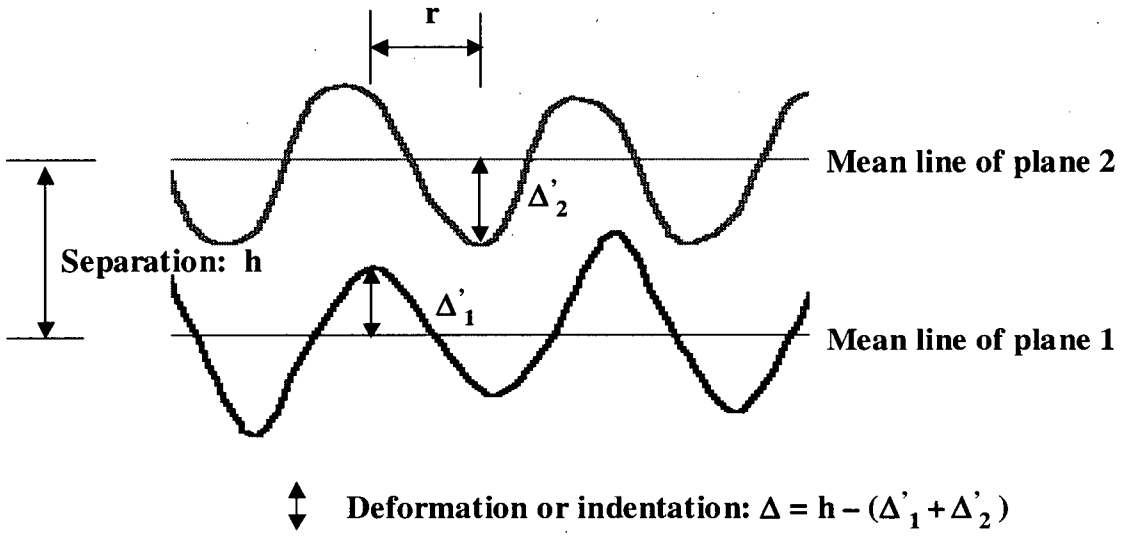

Figure 4.2 Contacts of two nominally flat rough surfaces

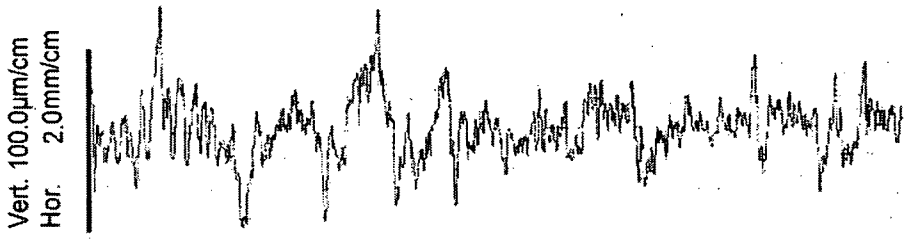

Veneer loose side: R_q= 39 µm

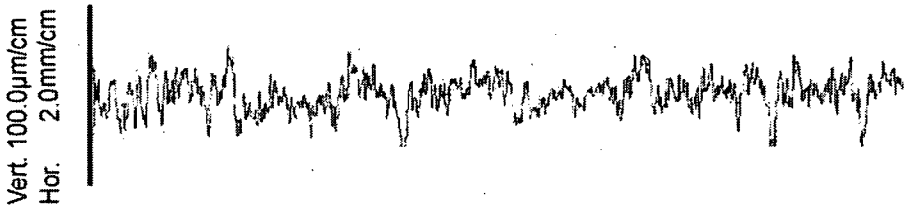

Veneer tight side: R_q= 32 µm

Figure 4.3 Typical 2-D veneer surface roughness profiles at the loose side and tight side

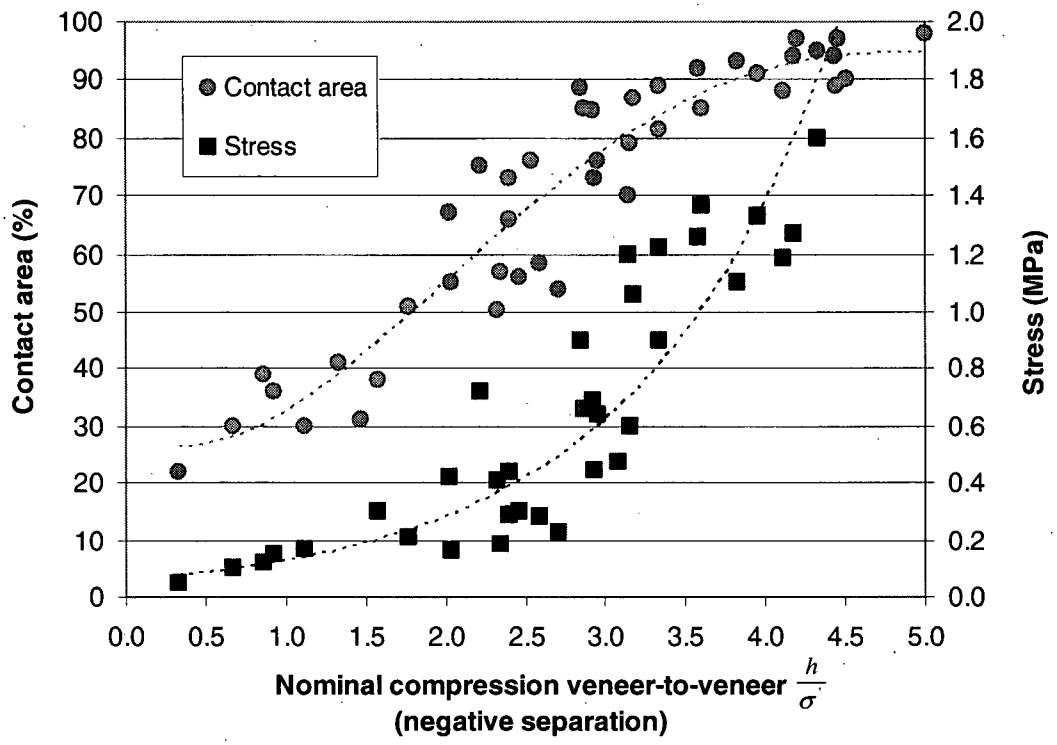

Figure 4.4 The relationship between contact area, stress and nominal veneer-to-veneer compression

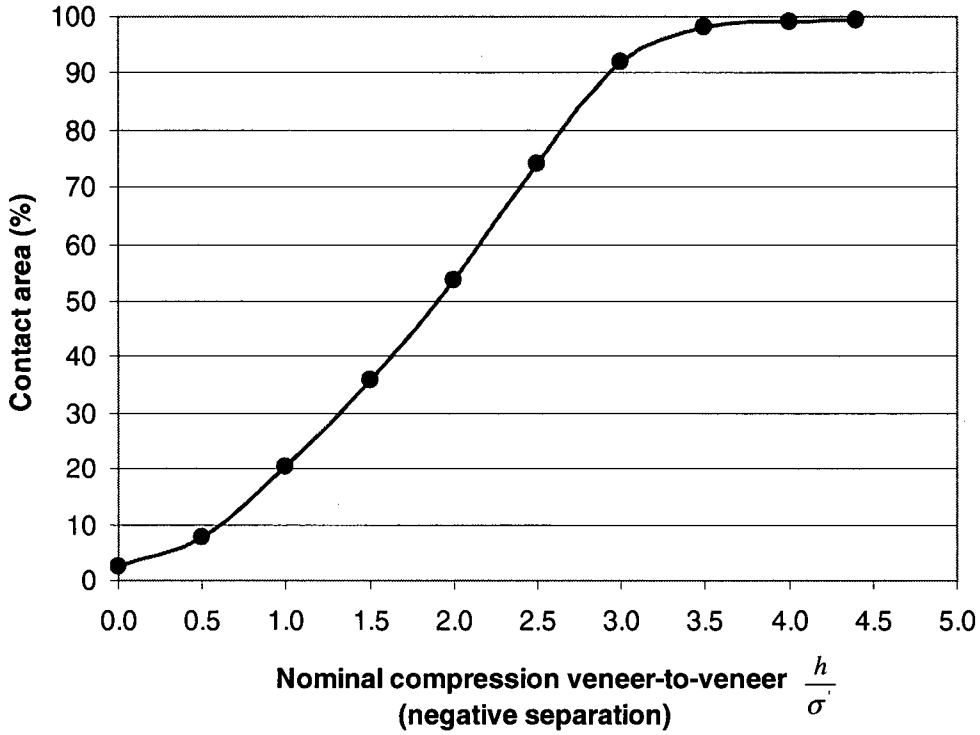

Figure 4.5 The theoretical prediction of contact area in relation to nominal veneer-to-veneer compression

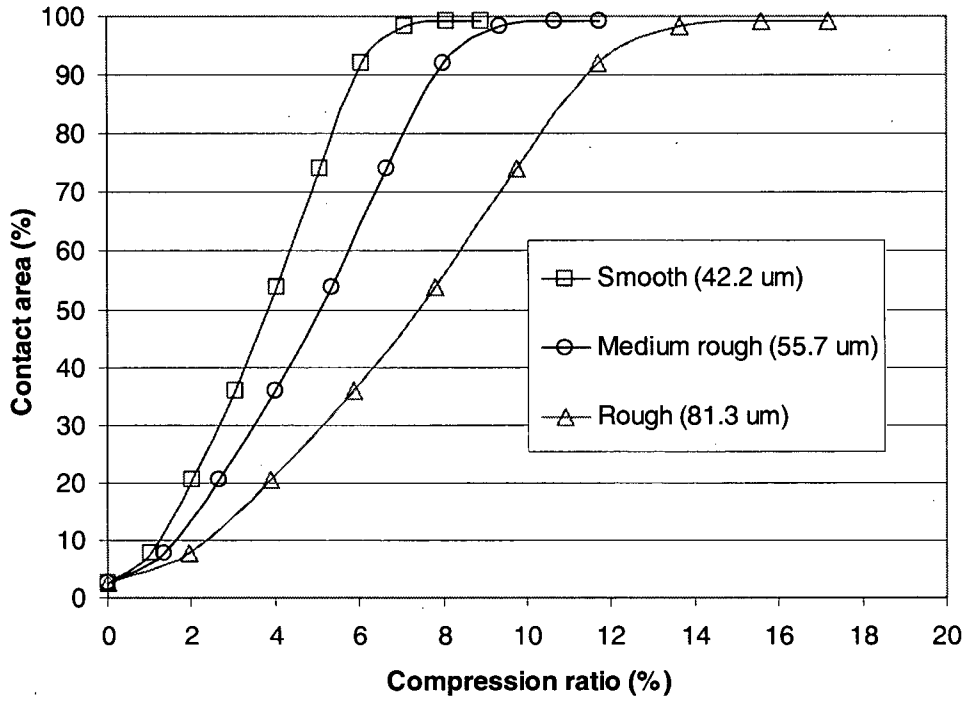

Figure 4.6 The theoretical prediction of contact area in terms of veneer compression ratio (CR) and surface roughness

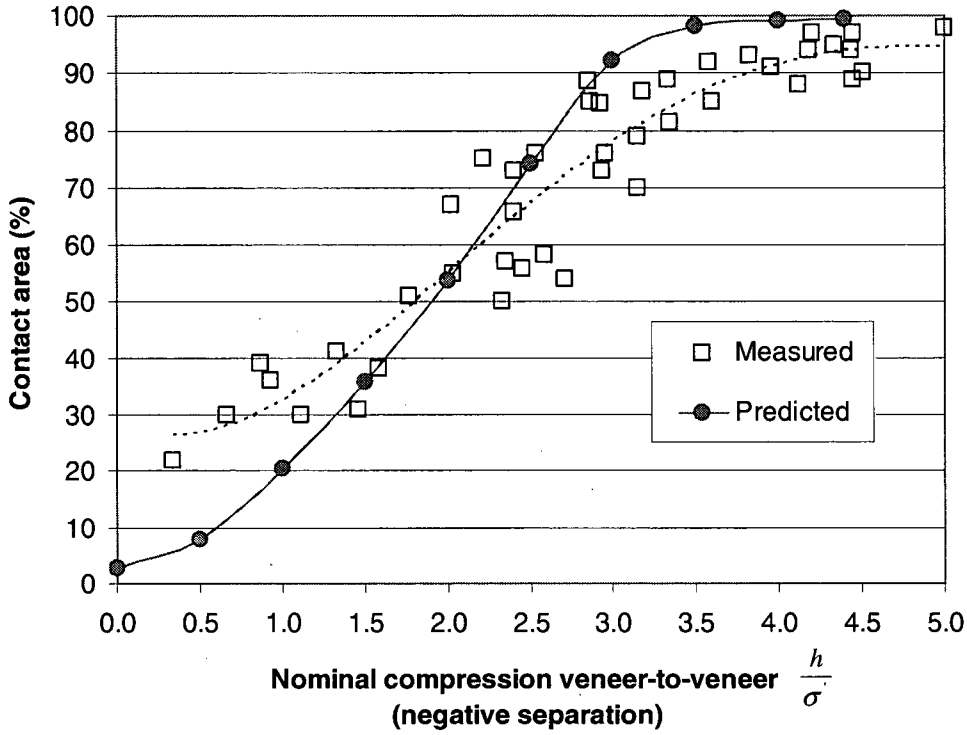

Figure 4.7 Comparison of predicted and measured contact area in relation to nominal veneer-to-veneer compression

4.7 Bibliography

ASME B46.1-2002. 2003. Surface texture (surface roughness, waviness, and lay). The American Society of Mechanical Engineers. Three Park Avenue, New York. NY 10016-5990. USA.

Faust, T. D. and J. T. Rice. 1987. Effects of a variable glue application rate strategy on bond quality and resin consumption in the manufacture of southern pine plywood. Forest Prod. J. 37(7/8):64-70.

Greenwood, J. A. 1967. On the area of contact between a rough surface and a flat. J. Lubric. Technology, Trans. Am. Soc. Mech. Engineers. 1, 81.

Greenwood, J. A., and J. H. Tripp 1970-1971. The contact of two nominally flat rough surfaces. Proc. Inst. Mech. Eng., Vol. 185. 625-633.

Greenwood, J. A. and J. B. P. Williamson. 1966. Contact of nominally flat surfaces. Proceedings, Royal Society, A295, 300.

Johnson, K. L. 1985. Contact mechanics. Cambridge University Press.

Mathematica® (Version 5.2). 2007. Wolfram Research, Inc. Campaign, USA.

Mitutoyo. 2004. SJ -400 --- Surface roughness tester. User's Manual.

Neese, J. L., J. E. Reeb and J. W. Funck. 2004. Relating traditional surface roughness measures to gluebond quality in plywood. Forest Prod. J. 54 (1):67-73.

CHAPTER V MECHANICS OF VENEER COMPRESSION

5.1 Introduction

As discussed in Chapters 3 and 4, the surfaces of wood veneers are rough to various degrees. Depending on the level of roughness, the stress-strain relationship during veneer transverse (radial) compression could be significantly different. At the early stage, a non-linear stress-strain relationship occurs for achieving progressive veneer-to-veneer contacts. Then elastic deformation prevails and if the applied pressure is discontinued, the veneer will largely recover to its original thickness. Once the yield point is exceeded, cell wall elastic buckling and plastic bending (yielding) or brittle fracture (crushing) start to occur depending on test conditions and the nature of the cell wall materials. A plastic plateau is subsequently reached where large deformation is possible with only a small increase in applied pressure, resulting in irreversible deformation (or strain hardening). This plateau ends where the densification zone starts, which coincides with the compression of the collapsed cell walls.

Wood veneer is a cellular and porous material, which exhibits both viscoelastic (creep) and elasto-plastic (springback) behaviour during compression (Wolcott *et al.* 1990; Dai 2001). At the microscopic level, the relative thickness of the cell walls, thus the relative density, determines the mechanical properties of wood. Veneer compression Young's modulus (E), determined by cell wall bending, varies generally as the density to the third power. In contrast, veneer compression strength (or yield stress), determined by the plastic bending (yielding) and/or buckling of the cell walls, varies as the square of the density (Gibson and Ashby 1997). The transverse compression properties of wood veneer play a key role in the plywood/LVL hot-pressing. During hot pressing, the multi-ply veneer assemblies are consolidated and then densified under a combination of changing temperature and moisture content (MC). Under a constant pressure, the creep-induced deformation occurs. In addition, the deformation from thermo-softening of individual veneer plies also results due to the coupled effect of temperature and MC on veneer compression E. As heat is transferred from the platen to the veneer assemblies, veneers closer to the platens will soften and deform more than those in the inner region. The inner region is generally stiffer and can generally resist more deformation. Thus, an initial density gradient forms across the panel thickness. Subsequently during press unloading, depending on the stage of veneer compression, different rates of springback result. Therefore,

two major steps in controlling final product thickness and density profile are the pressing stage when density profile is created from creep deformation and thermo-hydro softening and the springback as the panel unloads and exits the press.

As discussed in Chapter 1, for oriented strand board (OSB) and particleboard made from discontinuous wood elements such as strands and particles, a high compression ratio (CR) (about 40-60%) is generally required to remove the void space that separates the individual wood elements, thereby providing contacts between strands or particles and promoting bonding (Dai and Steiner 1993; Lang and Wolcott 1996a). By comparison, for plywood and LVL, the key is to bring continuous veneer elements into adequate contacts by overcoming surface irregularities such as roughness for bonding development. The panel structure after hot pressing is still dictated by the two distinct elements: veneer and glueline. For such products, a high CR is generally not required (Wellons *et al.* 1983). The normal CR ranges are only from 3 to 15%. Indeed, in the plywood/LVL manufacture, the amount of veneer compression, veneer creeping and springback behaviour are closely related to panel performance and material recovery. The knowledge on how veneers deform across the panel thickness is essential to determine the platen pressure required to achieve the target thickness. So far, only a few researchers have investigated the creep and stress relaxation of wood strands (fibers) and mats at ambient conditions (von Haas 1998; Dai *et al.* 2000; Dai 2001; Carvalho *et al.* 2001), and non-linear behaviour of strands and particles during compression of OSB and particleboard under isothermal or cold pressing (Dai and Steiner 1993; Lenth and Kamke 1996; Lang and Wolcott 1996a; Lang and Wolcott 1996b; Wang and Winistorfer 2000). The resulting models simulated the stress-strain behaviour of OSB and particleboard by separating the effect of temperature and MC on the mechanical properties of wood from the general deformation behaviour of wood. Although the effect of temperature and MC gradients on the mechanical properties of wood was studied, the springback behaviour of wood was not considered in these studies (Harless *et al.* 1987; Suo and Bowyer 1994; Zhou and Dai 2004). Dai *et al.* (2000) analyzed the implications of the mat elasto-plasticity on formation of vertical density profile, and concluded that the springback due to resin pre-cure was the main reason for the low density surface. Godbille (2002) investigated both compression and springback behaviour of wood to simulate the mechanical behaviour of particleboard during hot pressing. The general approach was to use a modified Hooke's law, as discussed in Chapters 1 and 3, to describe the stress-strain relationship for whole range of wood transverse compression,

and use a single non-linear strain function to determine the wood deformation during hot pressing. This strain function can be obtained from compression tests scaled by the corresponding compression Young's modulus E, which is the function of veneer temperature (T) and MC. In the case of unloading, the strain function was approximated to a linear term to take strain hardening into consideration (Godbille 2002).

While the strain function derived generally fitted with the experimental data with a reasonable accuracy, a large discrepancy was found for the strain level up to the yield point (approximately 20%) (Godbille 2002; Zhou and Dai 2004). This could be acceptable for non veneer-based wood composites such as OSB and particleboard due to their higher level of compression required and significant number of constituent elements used in the mats. However, for veneer-based wood composites such as plywood and LVL, veneer surface roughness affects the initial non-linear stress-strain relationship; the compression in the veneer assemblies is generally from the early stage of progressive contact to the stage of plastic deformation (plateau) with a majority of compression being in the linear elastic stage. As a result, the modified Hooke's law may not be adequate to describe the veneer stress-strain relationship. Compared to discontinuous wood elements such as strands and particles which are randomly deposited in the mat, veneer plies are rather large and continuous which are assembled in a more controlled manner. For OSB and particleboard, the effect of wood density is more or less averaged or masked. When the modified Hooke's law was applied, a single strain function could generally be accepted for a wide range of wood density. In contrast, for plywood and LVL, veneer sheets are sometime classified into distinct density groups especially when different species are used and/or stress grading is performed. Note that wood density not only significantly affects veneer compression E and yield stress but the strain function as well, since the latter is determined by the cell structure. If the modified Hooke's law is used, various strain functions may be needed over a wide range of density. To better describe the veneer compression stress-strain relationship, it seems essential to determine the effect of wood density on veneer compression behaviour in conjunction with MC and temperature, and use a model to describe the stress-strain relationship at different stages of compression. This could help develop a solid understanding of the mechanics of veneer compression, which forms the main topic of this Chapter.

So far, no information has been available to describe the mechanical behaviour of wood under the initial stage of progressive contact; and no work has been performed concerning the time-dependent creep and springback behaviour of wood veneer. Meanwhile, no models have been developed to describe the mechanical behaviour of the veneer during hot pressing. In this work, extensive experiments were conducted to investigate the effect of wood density, temperature and MC on veneer transverse compression behaviour. A regression model based on a response surface methodology (RSM) was established for veneer compression E and yield stress. As well, creep tests were conducted to investigate the deformation of the veneer under the predetermined pressures. In addition, veneer specimens were loaded to different stages of compression to ascertain the springback behaviour, thickness recovery and dimensional stability. Furthermore, loading and unloading tests were conducted to examine the springback behaviour of the veneer. Based on the results, an analytical model was developed to describe the mechanical and deformation behaviour of the veneer during transverse (radial) compression, and was further used in developing the panel densification module for plywood/LVL hot pressing.

5.2 Experimental

5.2.1 Materials

The source of veneer materials was the same as described in Chapter 3. Among a total of 150 (3.2 mm thick) rotary-cut random aspen dried veneer sheets (1.2 x 1.2 m), 120 veneer sheets were taken and then visually separated into the three roughness groups for the compression tests performed in Chapter 3. The remaining 30 veneer sheets were used to cut 1) 900 specimens (30 x 30 -mm) for the compression tests with 30 specimens from each sheet, and 2) 90 specimens (30 x 30 -cm) for the creep test with 3 specimens from each sheet. These 900 specimens were kept in plastic bags for compression tests. The average veneer MC was about 3% on an oven-dry basis. The 5-point thickness and weight of each specimen were measured to calculate veneer density. For each of these 90 (30 x 30 -cm) specimens, the 9-point thickness and weight were measured. They were wrapped in a plastic bag for the creep test.

5.2.2 Veneer Compression as Affected by Surface Roughness and Density

The experimental results were obtained from the compression tests as described in Chapter 3. In those tests, fifteen 30 x 30 -mm dried aspen veneer specimens were randomly selected from the three roughness groups with known roughness and density. These specimens were compressed at

the ambient temperature (20°C) to a maximum load of 975 kg to record the load-displacement curve for each specimen. Subsequently, based on the area and thickness of each veneer specimen, the stress-strain relationship was plotted.

5.2.3 Veneer Compression in Terms of Veneer Density, MC and Temperature

To investigate the effect of wood density, MC and temperature on veneer transverse (radial) compression, a response surface methodology (RSM) was used. This method has been widely used to evaluate veneer yield and quality (Warren and Hailey 1980) and optimize pulping processes (Khuri and Cornell 1996; Jimenez *et al.* 2000; Rosli *et al.* 2003). A second-order central composite design (CCD) was adopted to design the experiment, which involves devising the composition of the experimental conditions and subsequently developing a regression model. This design consists of factorial design points with eight (2^k, k = 3) runs, two center points and six axial or star points to estimate the first- and second-order interaction terms of a polynomial, which meets the general requirements that every variable in the mathematical model can be estimated from a fairly small number of experiments. In this study, three independent veneer variables were selected as: veneer density (X_1), MC (X_2) and temperature (X_3), whereas the two dependent variables were veneer compression modulus (E) and yield stress. Table 5.1 shows the 16 experimental runs of veneer compression tests dealing with the three levels of each variable. Each variable was normalized from -1 to +1 in order to facilitate direct comparison of the coefficients and visualization of the effects of the individual independent variables on the response (or dependent) variable. This normalization approach also results in more accurate estimates of the regression coefficients as it reduces interrelationships between linear and quadratic terms.

For veneers with actual values of density (ρ*), MC (MC*) and temperature (T*), their respective coded values, namely, ρ, MC and T, can be calculated as follows:

$$\rho = -1 + \frac{\rho^* - 0.35}{0.075} \qquad (5\text{-}1)$$

$$MC = -1 + \frac{MC^* - 0.5}{4.5} \qquad (5\text{-}2)$$

$$T = -1 + \frac{T^* - 20}{65} \qquad (5\text{-}3)$$

Table 5.2 compares the actual value of each variable with its coded value. Note that the middle level of each variable was chosen as the average value whereas the upper and lower levels of each variable generally covered the range of variation for aspen veneer in the plywood/LVL manufacturing. Before the test, veneer specimens were pre-selected based on the three density levels specified in Table 5.2. For each experimental run, three replicates were used. In total, forty-eight 30 x 30 -mm veneer specimens were compressed under the different combinations of density, temperature and MC.

Experimental results were fitted to the following second-order polynomial:

$$Y = a_0 + \sum_{i=1}^{3} a_i X_i + \sum_{i=1}^{3} b_i X_i^2 + \sum_{i=1, j=1}^{3} c_{ij} X_i X_j \qquad (i < j) \qquad (5\text{-}4)$$

where X_1, X_2 and X_3 are the three independent variables which influence the response Y; and a_0, a_i (i = 1-3), b_i (i = 1-3) and c_{ij} (i = 1-3; j = 1-3; i < j) are unknown coefficients.

The experimental set up for the compression test was described early in Figure 3.2. Attachments for an Instron universal tester were designed to allow testing of the veneer in compression at various levels of temperatures. The attachments consisted of two identical aluminium blocks (15.2 x 15.2 -cm) equipped with an electric heater and a thermocouple probe connected to a controller so that the mechanical properties of the veneer can be measured at different temperatures. Veneer specimens (30 x 30 -mm) were first seasoned to the three designated MC levels in an environmental chamber then placed between the two preheated blocks in the tester. The controlled temperature of the heating block was set according to the experimental run. Before starting the test, a load level of about 2.5 kg was applied onto each specimen and the LVDT extensometer was zeroed. Based on the readings from the probe, the temperature of the veneer specimen would reach the target in about 10 to 20 s. After that, isothermal compression testing started with a loading rate of 2 mm/min (0.08 in/min). The MC of the veneer specimen was measured upon completion of each experiment to account for the loss during its preheating between the two heated blocks. In order to limit vapourization during compressing at 150°C which is higher than the boiling point of water, veneer specimens were wrapped in a thin foil of aluminium for the testing.

The load-displacement curves of aspen veneer were obtained at different combinations of veneer density, temperature and MC. Then, based on the area and thickness of each specimen, the stress-strain relationship was established to compute the veneer compression modulus (E) and estimate the yield stress. Average compression E and yield stress were calculated for each experimental run.

5.2.4 Veneer Creeping Tests

Under a constant platen pressure, veneers will exhibit viscoelastic (creep) behaviour. For general viscoelastic materials, the basic constitutive equation between applied stress and strain according to the definition is (Christensen 1971):

$$\sigma = \mu \frac{d\varepsilon_v}{dt} \qquad (5\text{-}5)$$

where ε_v is viscous strain, t is pressing time, μ is viscous coefficient of the veneer reflecting the relationship between strain ε_v and pressing time t, and σ is the pressure applied. Equation (5-5) is a first order linear ordinary differential equation. To solve it, an initial condition is needed such that ε_v is equal to zero when time t is zero. So we can obtain the solution for the creep strain as follows:

$$\varepsilon_v = \frac{\sigma}{\mu} t \qquad (5\text{-}6)$$

However, μ changes with pressing time, which causes complexity to determine creep strain. Instead, an experimental approach is generally used to determine the creep strain with time by curve fitting (Bodig and Jayne 1982).

To understand the time-dependent viscoelastic behaviour of aspen veneer under a constant applied pressure, experiments were conducted by suddenly applying and maintaining different levels of pressures (stresses) onto 30 x 30 -cm aspen veneer specimens. By the time of testing, veneer average MC was 5%. The tests were conducted with a 96 x 96 -cm computer controlled press at an ambient temperature (20°C). At each stress level, three replicates were used. The veneer specimens were pre-selected to have identical thickness (3.25 mm) and density (0.425 g/cm^3) to eliminate the potential effect of veneer density. According to the literature, the highest creep strain was associated with the cell-wall yield point where wood starts buckling. The creep in both the linear range and the highly densified range was considerably lower than that in the

cell-wall buckling and yielding range (Dai 2001). In this study, three stress loading levels were selected as 1.21 MPa (175 psi), 1.38 MPa (200 psi) and 1.55 MPa (225 psi), which were normally used in aspen plywood and LVL manufacturing. The time of holding was set to 17 min. A high stress level for achieving cell wall buckling and yielding at the ambient temperature (20°C) was not pursued due to the hydraulic pressure limitation of the press.

Of the large number of methods used to portray creep and relaxation behaviour of composite materials, empirical curve fitting is among the simplest, which requires that an appropriate equation be chosen to describe the data. Among a number of equations used to describe the creep behaviour of composites, a parabolic representation can be effectively used to demonstrate the empirical approach to creep behaviour. The equation takes the following form according to Bodig and Jayne (1982):

$$\varepsilon_\gamma = \varepsilon_a + \beta t^m \qquad (5\text{-}7)$$

where ε_a is instantaneous (elastic) strain, t is time and β and m are constants.

Rearranging and taking logarithms gives

$$\log(\varepsilon_\gamma - \varepsilon_a) = \log\beta + m\log t \qquad (5\text{-}8)$$

By plotting $\log(\varepsilon_\gamma - \varepsilon_a)$ as a function of $\log t$, the parameters β and m can be determined.

5.2.5 Veneer Compression and Springback Tests

To investigate the elasto-plastic (springback) behaviour of aspen veneer during transverse (radial) compression, the compression tests were first conducted under the following four different temperatures: 20°C, 50°C, 100°C and 150°C. Ten replicates were used for each temperature level. Veneer MC was approximately 6%. For each veneer specimen (30 x 30 -mm), the weight was first measured, and then eight spots on edges plus one spot in the center were marked for thickness measurement. Subsequently, the average veneer thickness and density were determined. The apparatus described in Section 5.2.3 was used and same procedures were followed. The veneer compression tests were started and stopped until the maximum load reached approximately 650 kg. At this load level, all veneer specimens reached the stage of cell wall densification at different temperatures. After unloading, the thickness and weight of each veneer specimen were measured. Irrecoverable strain was determined for each specimen. Subsequently, all specimens were soaked in the cold water for 2 h. The thickness of each specimen was measured again at the same spots to determine the 2-h thickness swell.

Assuming original veneer thickness is t_0, at the end of the compression, the veneer thickness is reduced to t_c. During and after unloading, the veneer thickness bounces back to t_s. Subsequently, after 2-h cold water soaking, final wet thickness of veneer is t_w. Hence the thickness recovery after compression (R_t) before soaking can be calculated as:

$$R_t = \frac{t_s}{t_0} * 100\% \qquad (5\text{-}9)$$

The compression strain (ε) is defined as:

$$\varepsilon = \frac{t_0 - t_c}{t_0} \qquad (5\text{-}10)$$

The irrecoverable strain after compression (ε_p) is computed as:

$$\varepsilon_p = \frac{t_0 - t_s}{t_0} = 1 - R_t \qquad (5\text{-}11)$$

As well, the springback ratio (S_t) can be calculated as:

$$S_t = \frac{t_s - t_c}{t_0 - t_c} * 100\% \quad = (1 - \frac{t_0 \varepsilon_p}{t_0 - t_c}) * 100\% \qquad (5\text{-}12)$$

Furthermore, the 2-h veneer thickness swell (TS_{2h}) can be determined as:

$$TS_{2h} = \frac{t_w - t_s}{t_s} * 100\% \qquad (5\text{-}13)$$

Finally, the irrecoverable strain after compression (ε_p) can be calculated based on compression strain (ε) and springback ratio (S_t) as follows:

$$\varepsilon_p = (1 - S_t) * \varepsilon \qquad (5\text{-}14)$$

Therefore, if the compression strain and the springback ratio are known, the irrecoverable strain can be determined.

To compare the thickness recovery and springback ratio between the first stage of progressive contact and the second stage of linear elastic, compression tests of veneer specimens (30 x 30 - mm) were conducted at the ambient temperature (20°C). Ten replicates were used. For each veneer specimen (30 x 30 -mm), the weight was first measured, and then eight spots on edges plus one spot in the center were marked for thickness measurement. Subsequently, the average

veneer thickness and density were determined. Veneer average MC was approximately 6%. For the progressive contact, the compression tests were stopped prior to the start of the linear elastic stage based on the shape of load-displacement curve. During compression, the maximum strain was recorded. After unloading, the thickness of each specimen was measured again from the same spots to calculate the irrecoverable strain.

To further investigate the springback behaviour of aspen veneer, loading and unloading tests were conducted at different levels of strain. The purpose of the tests is to determine the amount of springback at the end of compression. The apparatus and procedures described in Section 5.2.3 were again used and adopted. The following four temperature levels were used: 20°C, 50°C, 100°C and 150°C. Two average MC levels, namely 3% and 6%, were selected. The strain levels were selected to represent different stages of the compressive stress-strain relationship, namely, L1 (linear elastic), L2 (early plastic, right crossing the yield point), L3 (plastic, plateau) and L4 (cell wall densification). A full factorial design was conducted with 32 experiments (3 replicates each). Before conducting loading and unloading tests, for each veneer specimen (30 x 30 -mm), the weight was first measured, and then eight spots on edges plus one spot in the center were marked for thickness measurement. Subsequently, the average veneer thickness and density were determined. Following the shape of the load-displacement curve, the compression stages can be easily determined. For each specimen, the compression test was started until the maximum strain level reached the predetermined stage and then the load was entirely removed. After unloading, the thickness of each specimen was measured from the same spots.

5.3 Results and Discussion

5.3.1 Veneer Stress-Strain Relationship in Terms of Surface Roughness and Density

As shown in Figure 5.1, veneer surface roughness has a substantial effect on the initial stage of veneer transverse (radial) compression, namely progressive contact. The stress-strain relationship exhibited a non-linear (exponential) pattern. The fit of an exponential equation to the experimental data was found to be very good for different levels of veneer roughness. For these veneer specimens compressed at the ambient temperature (20°C) and 3% MC, the threshold pressure was about 1.31 MPa. The rougher the veneer surface, the larger the strain level prior to the start of the linear-elastic stage. Based on the measurements from the representative veneer

specimens, the initial strain level prior to the start of the linear elastic stage was found to range from 0.05 to 0.12 depending on veneer surface roughness.

Figure 5.2 shows the effect of veneer density on the compressive stress-strain relationship. In general, the deformation of wood is non-uniform and occurs by the progressive collapse of cells from the surface inwards, although the unit step is still the plastic collapse of a cell (Gibson and Ashby 1997). Five specimens were classified into the two density groups: high (0.51 - 0.53 g/cm^3) and medium (0.42 - 0.43 g/cm^3). Veneer density mainly affected the linear-elastic stage of veneer transverse compression. The higher the veneer density, the steeper the slope. As well, for the two compression curves at the same density level of 0.42 g/cm^3, the slopes seemed to be identical but the two strain levels prior to the start of the linear elastic stage were quite different due to their different levels of surface roughness. Furthermore, the shape of stress-strain relationship appeared to be different between the high density veneer and medium density veneer.

5.3.2 Effect of Veneer Density, MC and Temperature on Compression Modulus and Yield Stress

Table 5.3 summarizes the experimental results for the 16 runs of the compression tests. The veneer compression modulus (E) was calculated based on the stress-strain relationship at the linear elastic stage. Using a statistical software program (JMP 2000), a second-order RSM model for the effect of wood density, temperature and MC on veneer compression E was developed as follows:

$$E = 30.21 + 19.89\,\rho - 6.07\,MC - 12.95\,T - 3.29\,\rho * MC - 5.14\,\rho * T - 1.34\,MC * T + 11.94\,\rho^2 + 1.94\,MC^2 + 2.94\,T^2 \quad (5\text{-}15)$$

As well, a second-order RSM model for the effect of veneer density, temperature and MC on yield stress was developed as follows:

$$\sigma_Y = 3.12 + 0.74\,\rho - 0.27\,MC - 1.01\,T - 0.10\,\rho * MC + 0.15\,\rho * T + 0.1\,MC * T + 0.19\,\rho^2 - 0.16\,MC^2 + 0.54\,T^2 \quad (5\text{-}16)$$

The results concerning analysis of variance for veneer compression E are shown in Table 5.4. The empirical regression model for veneer compression E gave an R^2 of 0.986 and a standard

error of estimate (SEE) of 4.06. Based on Table 5.4, the model fitted the experimental data very well. In Equation (5-15), all three variables use coded values from -1 to 1.

Similarly, the results concerning analysis of variance for yield stress are shown in Table 5.5. The empirical regression model for the yield stress gave an R^2 of 0.940 and a standard error of estimate (SEE) of 0.43. Based on Table 5.5, the model also fitted the experimental data very well. In Equation (5-16), all three variables use coded values from -1 to 1.

Based on the regression models, veneer compression *E* and yield stress can be predicted at any combination of veneer density, MC and temperature with a high accuracy. As an example, for veneers with dry density 0.40 g/cm^3 and 5% MC at 85°C, the coded value for density, MC and temperature are -0.333, 0 and 0, respectively. Based on Equations (5-15) and (5-16), the predicted veneer compression *E* and yield stress are 24.9 MPa and 2.8 MPa, respectively.

Figure 5.3 shows the prediction profiler of the three variables in terms of the veneer compression *E* and yield stress. The significance level of each variable was determined by the maximum difference (absolute value) in the veneer compression *E* or yield stress at the three designated levels of the variable. In general, the larger the difference, the more important the variable. It was evident that for the veneer compression *E*, the wood density had the largest effect, followed by veneer temperature and MC within the range tested; In contrast, for yield stress, the temperature had the largest effect, followed by veneer density and MC within the range tested. Both veneer compression *E* and yield stress notably decreased with decreasing veneer density and increasing veneer temperature and MC.

Figure 5.4 shows the response of the veneer compression *E* in relation to MC and temperature when veneer dry density is 0.40 g/cm^3 (a) and 0.45 g/cm^3 (b). At each density level, the response appeared to be a curvilinear pattern with some interactions existing between MC and temperature.

5.3.3 Veneer Creeping Behaviour during Compression

Figure 5.5 shows the experimental results regarding the aspen veneer thickness change with time at the three stress (pressure) levels. At the ambient temperature (20°C) and 5% MC, the first stress (pressure) level situates at the end of the first stage of non-linear progressive contact (right prior to the linear elastic stage). The second and third stress levels represent linear elastic stage of the compressive stress-strain relationship. Figure 5.6 plots the creep strain with time. Note that the instantaneous strain is the sum of strain from eliminating surface roughness and strain from elastic deformation. Veneer surface roughness had a significant effect on the instantaneous strain. In general, the higher the pressure applied, the greater the reduction of thickness at the initial stage up to 1 min and in turn the instantaneous strain. During this stage, the effect of veneer surface roughness was largely eliminated. Obviously, the actual creep started after the surface was ironed out. It seemed that the low stress (pressure) level of 1.21 MPa resulted in the lowest instantaneous strain but the highest creep strain rate compared to the other two stress (pressure) levels. This is probably due to the effect of residual roughness. Recall that from Figure 5.1, at a threshold pressure level of approximately 1.31 MPa, the linear elastic stage starts with elimination of the major effect of veneer surface roughness. On average, for these aspen veneer specimens tested (mill peeled), surface roughness-induced strain was found to be equal or greater than 0.10. The difference in strain rates between 1.38 MPa and 1.55 MPa stress (pressure) levels seemed to be very small. Overall, the strain level due to veneer creeping was about 0.015-0.020.

By fitting the experimental data, the following parameters were yielded as shown in Table 5.6. The parameter m was more stable with a value of about 0.30 whereas the parameter β changed from 0.007 to 0.009 with the stress level from 1.21 MPa to 1.55 MPa.

5.3.4 Behaviour of Veneer after Compression

Figure 5.7 shows the compressive stress-strain relationship of aspen veneer with the following four stages of transverse compression: progressive contact, linear elastic, plastic and cell wall densification. The tests were conducted at the four different temperatures, namely 20°C, 50°C, 100°C and 150°C with an average veneer MC level of 3%. In general, the linear-elastic stage 2 exhibited the compression behaviour from cell wall bending. The plastic stage 3 was controlled by the non-uniform plastic yielding of the cells, which generally starts at the surface of the loading platen and propagating inwards through the veneer thickness (Gibson and Ashby 1997).

Note that all specimens were pressed to the stage of cell wall densification. When veneer specimens are pressed beyond the elastic region, the maximum strain imposed on the specimens generally determines the amount of irrecoverable deformation.

As shown in Figure 5.8, the springback ratios with different compression strains are dramatically different. The springback ratio reduced from about 85% to 30% with a range of compression strain from 0.3 to 0.8. Figure 5.9 shows the change of irrecoverable strain with regard to compression strain. Their relationship appeared to be an exponential pattern. In general, the higher the compression strain, the higher the irrecoverable strain. However, this level of irrecoverable strain was not stabilized or fixed in the wet environment. As shown in Figure 5.10, 2-h cold water soaking tests after compression demonstrated that there was a strong relationship between the thickness swell (TS) and irrecoverable strain level. The higher the irrecoverable strain after the compression, the higher the TS. This type of dimensional instability will impact the engineered applications of veneer-based composite products. In general, higher compression strain not only causes lower material recovery but also poorer dimensional stability. Since the maximum compression strain in plywood/LVL products is generally situated between the linear-elastic stage and the early plastic stage, the information on springback behaviour of veneer compression at different stages is essential to help improve material recovery and product performance.

5.3.5 Springback Behaviour of Veneer at Different Compression Stages

Figure 5.11 compares the thickness recovery and springback ratio between the first stage of progressive contact and the second stage of linear elastic. On average, at ambient temperature (20°C) and 3% MC, when the maximum compressive strain was at the first stage (<=10%) with an average of 7.5%, the average springback ratio was about 75% and the thickness recovery was about 98%. In contrast, when the maximum compressive strain was at the second linear-elastic stage (between 10 and 18%), the average springback ratio was about 95% and the thickness recovery was about 99%. The results indicated that the first stage of progressive contact exhibited mixed behaviour of plasticity and elasticity.

Typical representations of loading and unloading curves of aspen veneer are shown in Figures 5.12 and 5.13. The tests were conducted under 150°C temperature and 6% MC. Note that the

density of veneer specimens was 0.42 and 0.43 g/cm^3, respectively, for loading and unloading at the linear elastic stage (stage 2) and early plastic stage (right crossing the yield point). There was a significant difference in both thickness recovery and springback ratio between the linear elastic stage and the early plastic stage. The springback ratio was 63% for the compression at the linear stage compared to 57% for the compression at the early plastic stage. The irrecoverable strain with the maximum compression strain below the yield point was about 0.082 (thickness recovery 91.8%) whereas this strain with the maximum strain at the early plastic stage was about 0.202 (thickness recovery 81.8%). The difference in the irrecoverable strain was about 0.12. In the case of linear elastic, the irrecoverable strain was caused by veneer surface roughness and plasticity from thermo-softening. In contrast, in the case of early plastic stage, the irrecoverable strain was caused by veneer surface roughness and plasticity from cell wall buckling and yielding and thermo-softening. At the temperature of 150°C, a large proportion of the compression strain beyond the yield point was not recoverable. This indicates that to effectively enhance the densification, the compression strain should exceed the yield point. However, the detrimental effect of this densification is the reduced material recovery, lowered shear strength and increased thickness swell as demonstrated in Chapter 3.

Similarly, as shown in Figure 5.13, there was also a significant difference in both thickness recovery and springback ratio between the 3rd plastic stage and the 4th cell wall densification stage. Note that the density of veneer specimens were 0.43 g/cm^3 for the compression at the 3rd plastic stage and 0.46 g/cm^3 for the compression at the densification stage. The difference in density caused the different slops at the linear elastic stage. The springback ratio was 52% for the plastic stage compared to 33% for the compression at the densification stage. The irrecoverable strain with the maximum compression at the plastic stage was about 0.261 (thickness recovery 73.9%) compared to about 0.450 (thickness recovery 55.0%) for the maximum strain at the cell wall densification. In comparison with Figure 5.12, at the third plastic stage (plateau), the level of compression had a significant effect on thickness recovery and springback ratio.

Figures 5.14, 5.15, 5.16 and 5.17 show the relationship of compression strain and irrecoverable strain (strain retained after compression) with regard to the following four temperature levels: namely, 20°C, 50°C, 100°C and 150°C. The average veneer MC was 3%. The irrecoverable strain increased with increasing compression strain and temperature. Note that compared to the

compression at the linear elastic stage, compression at the early plastic stage (right crossing the yield point) resulted in a significant increase in both irrecoverable strain.

Figures 5.18 and 5.19 show the springback ratio of aspen veneer at 3% MC and 6% MC, respectively. First, at both MC levels, veneer compression strain, demonstrated by the compression stage, had a significant effect on the springback ratio. Secondly, compression strain at the linear elastic stage resulted in the largest springback ratio. Compression at the early plastic stage (right crossing the yield point) resulted in a lower springback ratio, leading to a higher thickness loss compared to compression at the linear elastic stage. In addition, the springback ratio decreased with increasing veneer temperature. Furthermore, with the increase of veneer MC, the springback ratio decreased with the largest reduction being in the early plastic stage. At 3% MC, the springback ratio was only reduced slightly from 20°C to 50°C but was reduced more when temperature rose to 100°C or above. In contrast, at 6% MC, the springback ratio decreased noticeably at the four different temperature levels.

Figure 5.20 shows the prediction profiler from the statistical analysis of experiments with the full factorial design. It demonstrated that the compression stage had the largest effect on both springback ratio and thickness recovery, followed by temperature and MC. When temperature was increased from T1 (20°C) to T2 (50°C), both springback ratio and thickness recovery only reduced slightly. When veneer temperature was greater than 50°C, the reduction of springback ratio and thickness recovery became more pronounced.

5.4 Analysis of Veneer Compressive Stress-Strain Relationship

The experimental approach serves two purposes: 1) to determine the veneer basic properties; and 2) to characterize the material behaviour of the veneer during compression. For example, one needs to know veneer density and MC, and the creep behaviour of the veneer under a constant platen pressure in order to predict the creep deformation in addition to that caused by thermo-hydro softening. As well, one needs to know the springback ratio of the veneer in terms of veneer temperature, MC and the maximum compression strain. In contrast, an analytical analysis or theoretical modeling can further advance our understanding of the mechanisms of veneer compression. So far, modeling of veneer transverse (radial) compression has been limited to the application of the modified Hooke's law and use of a strain function to describe the stress-strain

relationship over the whole range of transverse compression. In the case of the veneer, the strain function φ (ε) derived from the modified Hooke's law can be better expressed as:

$$\varphi(\varepsilon) = \sigma / [\varepsilon^* E(\rho, T, MC)] \qquad (5\text{-}17)$$

where σ is the applied stress, ε is strain, and E is the veneer compression modulus, which is a function of veneer density (ρ), temperature (T) and moisture content (MC). If the first stage of progressive contact is ignored, φ(ε) will be 1 at the linear elastic stage. However, if the first stage of non-linear progressive contact is considered, as shown in Figure 5.21, φ(ε) will gradually increase with a maximum value being smaller than 1 at the end of the linear elastic stage. This phenomenon was mainly caused by the delayed elasticity from surface irregularities (roughness) of veneer specimens.

As described in Section 5.3.4, the compressive stress-strain curve can be divided into four stages. Figure 5.22 only shows the first three compression stages, which is believed to be sufficient for simulating veneer compression in plywood and LVL manufacturing. At the second linear elastic stage, the stress-strain relationship can be described as:

$$\sigma = E(\varepsilon - \varepsilon_0) \qquad (5\text{-}18)$$

where ε_0 is the strain intercepting with the axis of strain, which mainly depends on veneer surface roughness. Hence, the strain function at the linear elastic stage can be expressed as:

$$\varphi(\varepsilon) = \sigma / (E^*\varepsilon) = 1 - \frac{\varepsilon_0}{\varepsilon} < 1 \qquad (5\text{-}19)$$

The rougher the surface, the larger the strain ε_0, hence the smaller the φ(ε) at the linear elastic stage. This roughness-dependent strain function drastically increases the complexity of determining veneer deformation in which a single strain function needs to be derived. As a result, the strain function was not pursued in this study. Instead, a modeling approach was attempted to describe the mechanics and compression behaviour of the veneer at the first three compression stages.

As shown in Figure 5.22, for the first stage, namely non-linear progressive contact, we have

$$0 < \varepsilon < \varepsilon_R \quad \text{and} \quad 0 < \sigma < \sigma_R \qquad (5\text{-}20)$$

The subscript R means surface roughness. As described in Chapter 3, at the threshold pressure (stress), veneer surface roughness can be characterized. For the second stage, namely linear elastic, we have

$$\varepsilon_R < \varepsilon < \varepsilon_Y \quad \text{and} \quad \sigma_R < \sigma < \sigma_Y \qquad (5\text{-}21)$$

The subscript Y means the yield point (or proportional limit). For the third stage, namely plastic (or plateau), we have

$$\varepsilon_Y < \varepsilon < \varepsilon_u \quad \text{or} \quad \sigma_Y < \sigma < \sigma_u \qquad (5\text{-}22)$$

The subscript u means the ultimate.

At the first stage of non-linear progressive contact, veneer compression is associated with both elastic strain and plastic (non-elastic) strain. Recall from Figure 5.11, in terms of the springback behaviour, veneers compressed to this stage displayed mixed elasticity and plasticity. The plasticity is mainly exhibited when the strain is from 0 to ε_0 whereas the elasticity is mainly shown when the compression strain is from ε_0 to ε_R. The elastic strain, denoted as ε_m, results from the veneer material deformation. The plastic strain, denoted as ε_g, is mainly caused by veneer surface irregularities (roughness). This plastic strain is mainly associated with veneer geometry change. As demonstrated in Chapter 3 and Figure 5.1, at the early stage of veneer compression, a progressive contact prevails to create contacts of veneer-to-veneer or veneer-to-plate. The stress and strain relationship exactly follows an exponential pattern. Hence the total strain can be written as

$$\varepsilon = \varepsilon_m + \varepsilon_g \qquad (5\text{-}23)$$

The elastic strain obeys Hooke's law, i.e.

$$\varepsilon_m = \frac{\sigma}{E} \qquad (5\text{-}24)$$

The plastic (non-elastic) strain can be expressed as

$$\varepsilon_g = \varepsilon_0 (1 - e^{-\frac{\sigma}{\sigma^*}}) \qquad (5\text{-}25)$$

where ε_0 is the maximum plastic strain, σ^* represents the change rate of geometry with regard to the stress. Substituting Equations (5-24) and (5-25) into Equation (5-23), the strain for the region up to the yield point (first region) can be calculated as follows:

$$\varepsilon = \varepsilon_m + \varepsilon_g = \frac{\sigma}{E} + \varepsilon_0 (1 - e^{-\frac{\sigma}{\sigma^*}}) \qquad (5\text{-}26)$$

As shown in Figure 5.23, two regions are defined in the strain-stress relationship. The second region starts from the yield point and corresponds to the third plastic stage during veneer compression.

As discussed in Chapter 3, when a threshold pressure σ_R is applied, veneer surface roughness can be estimated with a strain (or deformation) ε_R. Hence we have

$$\varepsilon_R = \frac{\sigma_R}{E} + \varepsilon_0 (1 - e^{-\frac{\sigma_R}{\sigma^*}}) \qquad (5\text{-}27)$$

At a threshold pressure, veneer surface roughness is largely suppressed for linear stress-strain behaviour to follow. In other words, the major effect of veneer surface roughness can be eliminated, creating about 80% (or higher) of contact area. By assuming that the veneer exhibits about 95% elasticity at the threshold pressure, we have

$$\sigma_R = E(\varepsilon_R - 0.95\varepsilon_0) \qquad (5\text{-}28)$$

Based on Equations (5-27) and (5-28), we obtain

$$\varepsilon_0 = 1.05(\varepsilon_R - \frac{\sigma_R}{E}) \qquad (5\text{-}29)$$

and

$$\sigma^* \approx \frac{1}{3}\sigma_R \qquad (5\text{-}30)$$

In Equations (5-29) and (5-30), veneer compression E is the function of veneer density, temperature and MC following the regression RSM model in Section 5.3.2. Similar to σ_R, σ^* changes with veneer temperature and MC. For aspen veneer at ambient temperature (20°C) and 3% MC, σ_R is about 1.31 MPa whereas ε_R can be determined based on compression tests under the threshold pressure σ_R. Alternatively, if the average veneer surface roughness is known, the average ε_R can be determined based on the correlation between the minimum compression required and veneer surface roughness as described in Chapter 3. Therefore, Equation (5-26) can be rewritten as:

$$\varepsilon = \varepsilon_m + \varepsilon_g = \frac{\sigma}{E} + \varepsilon_0 (1 - e^{-\frac{\sigma}{\sigma^*}}) = \frac{\sigma}{E} + 1.05 * (\varepsilon_R - \frac{\sigma_R}{E})(1 - e^{-\frac{3\sigma}{\sigma_R}}) \qquad (5\text{-}31)$$

Equation (5-31) provides a fundamental description concerning how veneer compression strain up to the yield point (first region) changes with regard to the applied pressure σ, veneer surface roughness (parameters ε_R and σ_R) and veneer compression E. Note that the veneer compression E is the function of veneer density, MC and temperature.

During plywood and LVL hot-pressing, the strain caused by applied pressure and creeping deformation could exceed the yield point. At this second region ($\varepsilon_Y < \varepsilon < \varepsilon_u$, $\sigma_Y < \sigma < \sigma_u$), as shown in Figure 5.23, the strain increases quickly with a small increase of stress, in which veneer deformation is also a combination of partial elasticity and partial plasticity. Hence, we have

$$\varepsilon = \varepsilon_Y + \Delta\varepsilon \tag{5-32}$$

and

$$\Delta\varepsilon = \Delta\varepsilon_m + \Delta\varepsilon_p \tag{5-33}$$

where $\Delta\varepsilon_m$ and $\Delta\varepsilon_p$ represent the increment of the strain caused by the elastic and plastic deformation of the veneer in this region, respectively. Obviously, the elastic strain increment can be written as

$$\Delta\varepsilon_m = \frac{\sigma - \sigma_Y}{E} \tag{5-34}$$

The plastic strain can be expressed with a power function as follows:

$$\Delta\varepsilon_p = \alpha(\sigma - \sigma_Y)^{n'} \tag{5-35}$$

where α and n' are coefficients. Substituting Equations (5-34) and (5-35) into Equation (5-32), we have

$$\Delta\varepsilon = \frac{\sigma - \sigma_Y}{E} + \alpha(\sigma - \sigma_Y)^{n'} \tag{5-36}$$

Therefore, the strain beyond the yield point is given by

$$\varepsilon = \varepsilon_Y + \Delta\varepsilon = \varepsilon_Y + \frac{\sigma - \sigma_Y}{E} + \alpha(\sigma - \sigma_Y)^{n'} \qquad \sigma_Y < \sigma < \sigma_u \tag{5-37}$$

Equation (5-37) provides a fundamental description concerning how veneer compression strain beyond the yield point (second region) changes with regard to the applied pressure σ and veneer compression E. Note that the veneer compression E and σ_Y are the function of veneer density, MC and temperature, α and n' are coefficients which can be obtained by fitting the stress-strain

data. Based on Chapter 3, the average yield displacement of the aspen veneer is 0.63 mm for average veneer thickness of 3.07 mm, which is equivalent to an average ε_Y of 0.205.

Figure 5.24 shows predicted strain-stress curves compared to their corresponding experimental results for veneers with 3% MC at 50°C and 100°C, respectively. The best fit n value was found to be approximately 3, which seemed to be less dependent on veneer temperature and MC. The α value changed with temperatures, which were 0.95 and 0.75 for 50°C and 100°C, respectively. The results showed that the experimental strain-stress curves and predicted strain-stress relationship agreed very well. As a result, the analytical model developed can be successfully used to describe the compressive stress-strain relationship.

As an example with veneer compression at 3% MC and 50°C, Figure 5.25 demonstrates that the overall strain can be superimposed by elastic deformation and plastic deformation with a reasonable accuracy. At the first stage of progressive contact, the plastic deformation increased exponentially to the maximum whereas the elastic deformation increased linearly. At the beginning of the first stage, the increment of plastic strain was larger. In contrast, at the end of the first stage, the increment of plastic strain was very small. At the second stage of linear elastic, only elastic deformation occurred in which the deformation can be largely recovered. At the third plastic stage, with the buckling or yielding of the cell walls, the plastic deformation dominated in a power function whereas the elastic deformation appeared to be small.

5.5 Conclusions

The mechanical behaviour of aspen veneer in compression perpendicular to the grain (in the radial direction) was experimentally studied and modeled. The effects of veneer density, temperature and MC on the mechanical properties such as compression modulus (E) and yield stress were investigated. A response surface method (RSM)-based model was developed to predict the veneer compression E and yield stress under different combinations of wood density, temperature and MC. The compression E of aspen veneer was significantly affected by veneer density, followed by veneer temperature and MC.

The viscoelastic (creep) behaviour of aspen veneer was also studied. Veneer instantaneous strain was significantly affected by veneer surface roughness and compression *E*. The creep strain was in the range of 0.015 to 0.020 with different pressures. The loading and unloading tests were further conducted under different temperature and MC to investigate the elasto-plastic (springback) behaviour of aspen veneer. The springback ratio and thickness recovery decreased with increasing maximum compression strain (or compression stage), veneer temperature and MC. Both the first stage of progressive contact and the third plastic stage exhibited a mixed behaviour of elasticity and plasticity. An analytical model was developed to describe the compressive stress-strain relationship up to the third plastic stage with a reasonable accuracy, which helps predict the compressive strain (or final panel thickness) and density profile development during plywood/LVL hot pressing in terms of applied pressure, veneer surface roughness, veneer density, temperature and MC.

Table 5.1 Experimental design with a Response Surface Method (RSM)

Experiment run	Coded variables		
	X_1 (Density)	X_2 (MC)	X_3 (Temperature)
1	-1	-1	-1
2	-1	-1	1
3	-1	0	0
4	-1	1	-1
5	-1	1	1
6	0	-1	0
7	0	0	-1
8	0	0	0
9	0	0	0
10	0	0	1
11	0	1	0
12	1	-1	-1
13	1	-1	1
14	1	0	0
15	1	1	-1
16	1	1	1

Table 5.2 Converting coded value to actual value for each variable (normalization)

Variable	Unit	Coded value		
		-1	0	1
X_1 (Density)	g/cm^3	0.350	0.425	0.500
X_2 (MC)	%	0.5	5.0	9.5
X_3 (Temperature)	°C	20	85	150

Table 5.3 The effect of density, MC and temperature on veneer compression modulus and yield stress

Experiment no.	Coded			Actual			Compression modulus (E) (MPa)	Yield stress (MPa)
	Density	MC	Temperature	Density (g/cm^3)	MC (%)	Temperature (°C)		
1	-1	-1	-1	0.35	0.5	20	36.0	4.2
2	-1	-1	1	0.35	0.5	150	20.0	2.0
3	-1	0	0	0.35	5.0	85	28.0	2.5
4	-1	1	-1	0.35	9.5	20	31.0	3.9
5	-1	1	1	0.35	9.5	150	15.8	1.8
6	0	-1	0	0.425	0.5	85	41.0	3.2
7	0	0	-1	0.425	5.0	20	47.0	4.8
8	0	0	0	0.425	5.0	85	28.0	3.5
9	0	0	0	0.425	5.0	85	29.0	3.6
10	0	0	1	0.425	5.0	150	21.0	2.1
11	0	1	0	0.425	9.5	85	25.0	2.3
12	1	-1	-1	0.50	0.5	20	92.0	5.8
13	1	-1	1	0.50	0.5	150	61.6	3.9
14	1	0	0	0.50	5.0	85	58.0	3.7
15	1	1	-1	0.50	9.5	20	80.0	4.8
16	1	1	1	0.50	9.5	150	38.1	3.6

Table 5.4 Analysis of variance for the regression model of veneer compression modulus

Source	DF	Sum of Squares	Mean Square	F ratio
Model	9	7118.5	790.9	47.9
Error	6	99.1	16.5	Prob > $F_{0.001}$
Total	15	7217.5		

Table 5.5 Analysis of variance for the regression model of yield stress

Source	DF	Sum of Squares	Mean Square	F ratio
Model	9	18.03	2.00	10.6
Error	6	1.13	0.189	Prob > $F_{0.005}$
Total	15	19.16		

Table 5.6 The parameters from the log-linear fit for the creep tests

Stress (MPa)	m	β
1.21	0.31	0.007
1.38	0.30	0.008
1.55	0.30	0.009

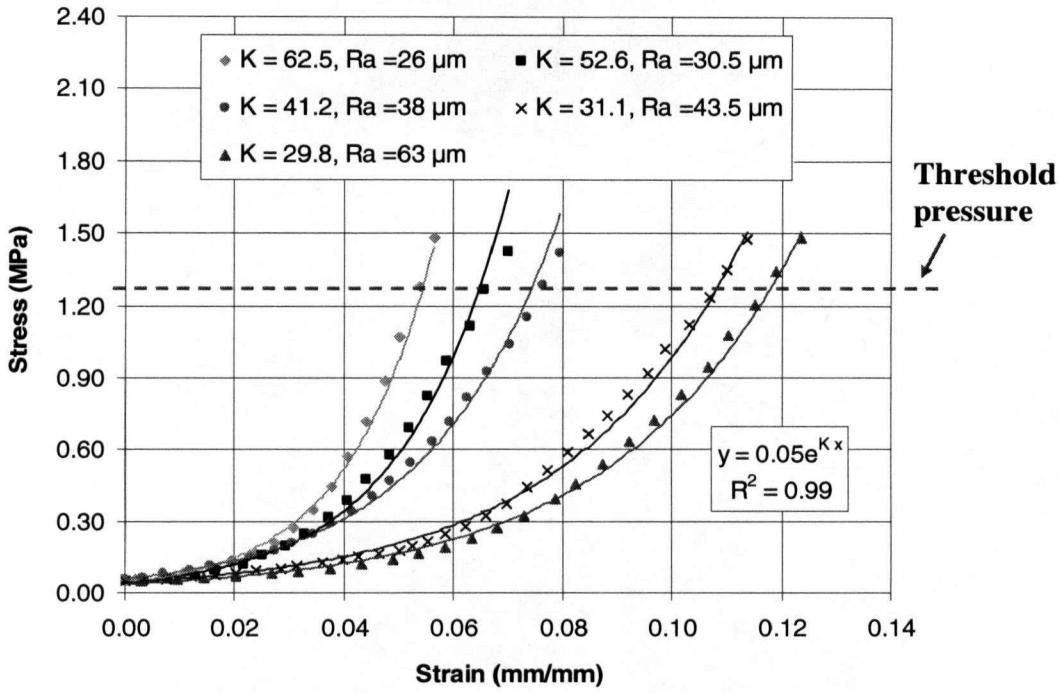

Figure 5.1 The effect of veneer surface roughness on compression

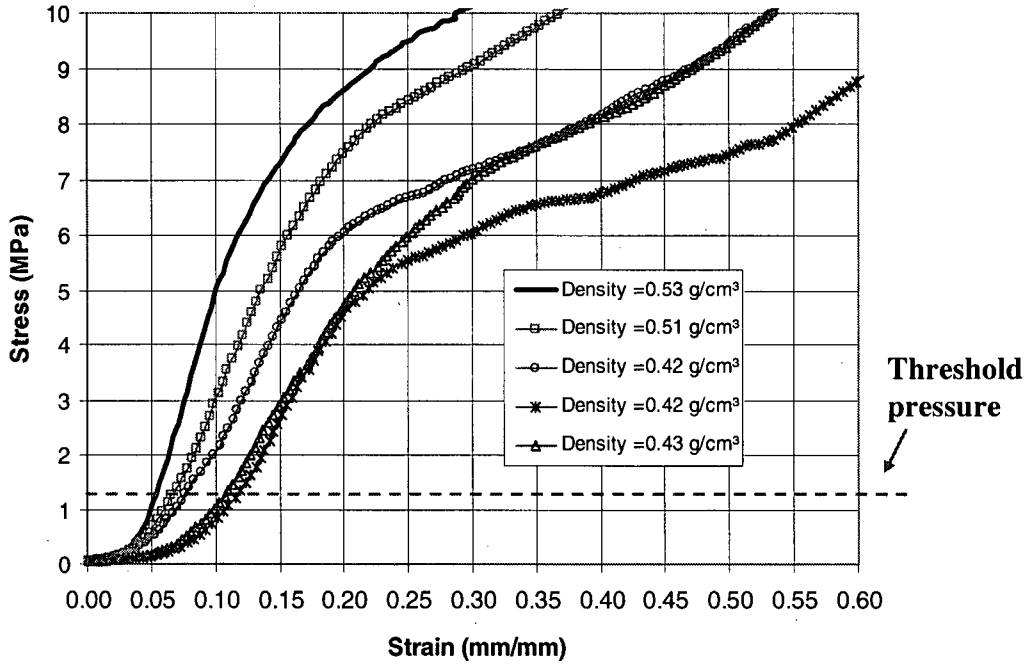

Figure 5.2 The effect of veneer density on compression

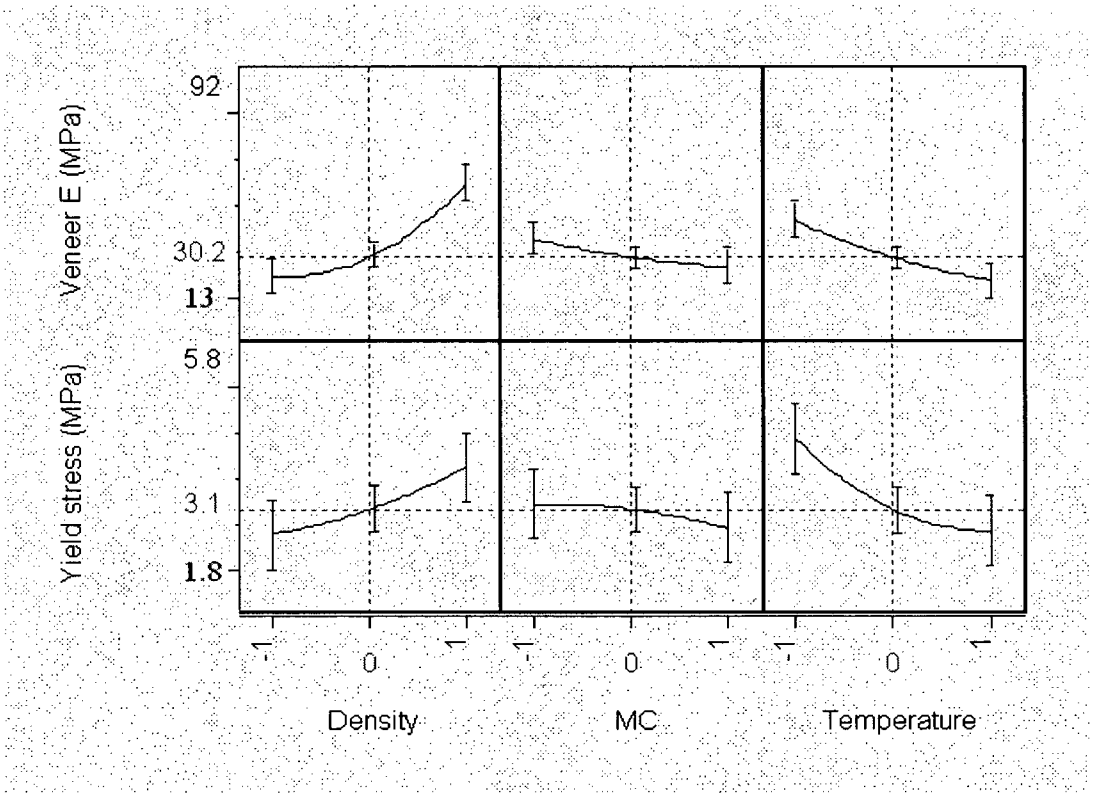

Figure 5.3 Prediction profiler of the three variables on veneer compression modulus and yield stress

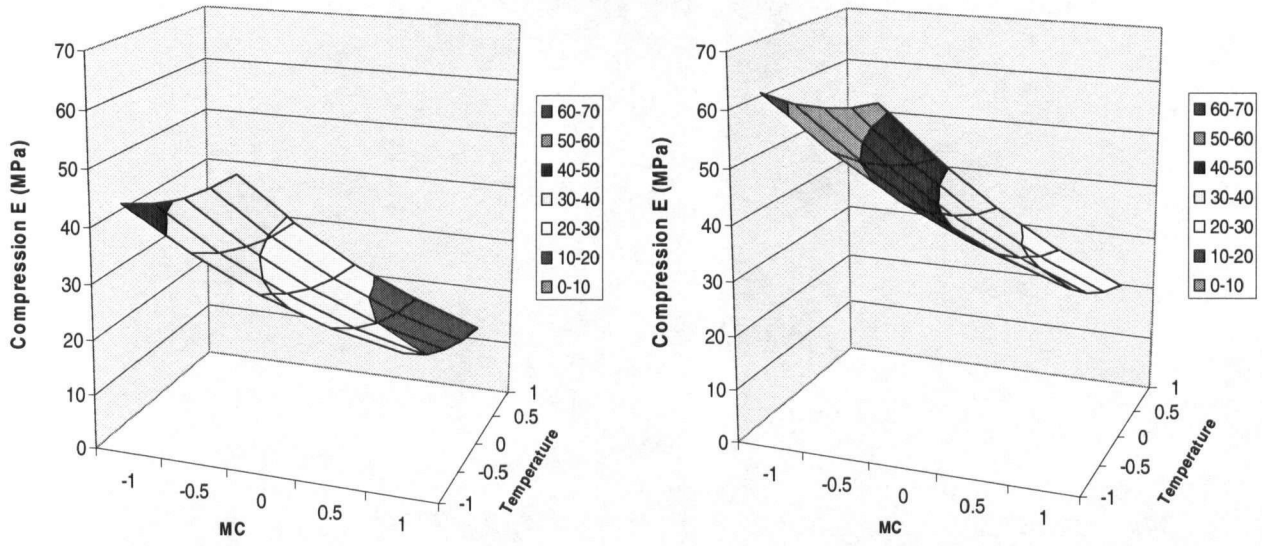

(a) $\rho^* = 0.40$ g/cm^3 (b) $\rho^* = 0.45$ g/cm^3

Figure 5.4 The response of veneer compression modulus in relation to MC and temperature

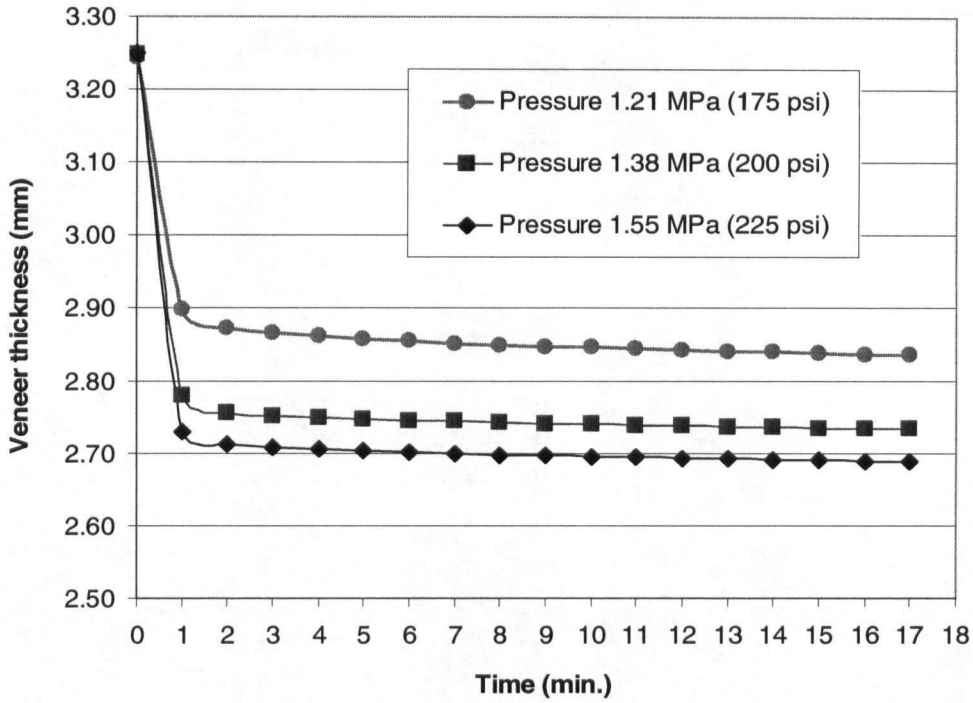

Figure 5.5 The thickness change of aspen veneer with time at the three stress (pressure) levels

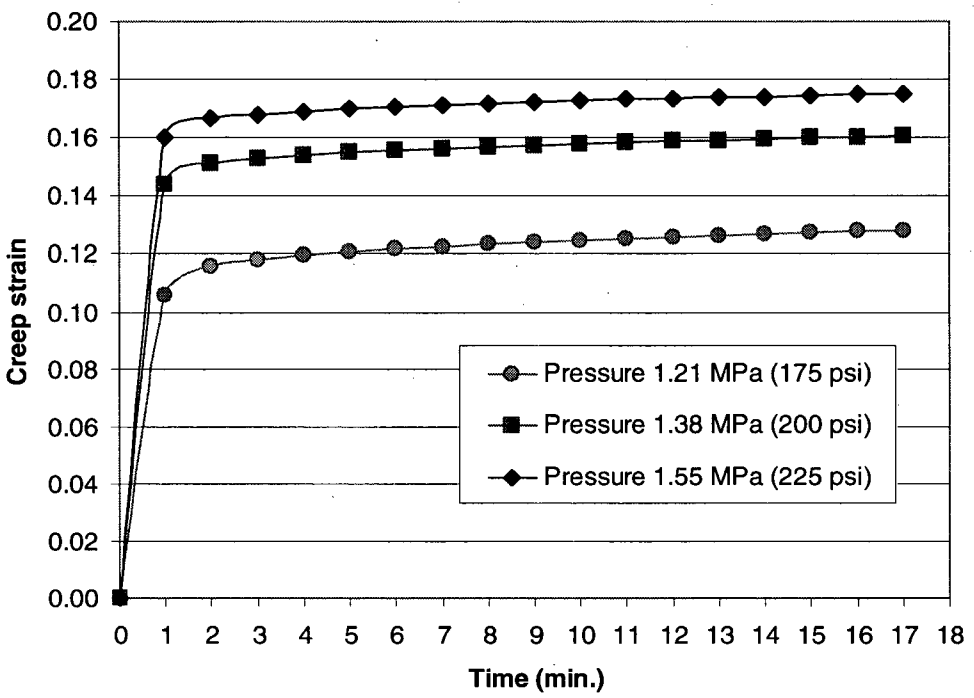

Figure 5.6 The creep strain of aspen veneer with time at the three stress (pressure) levels

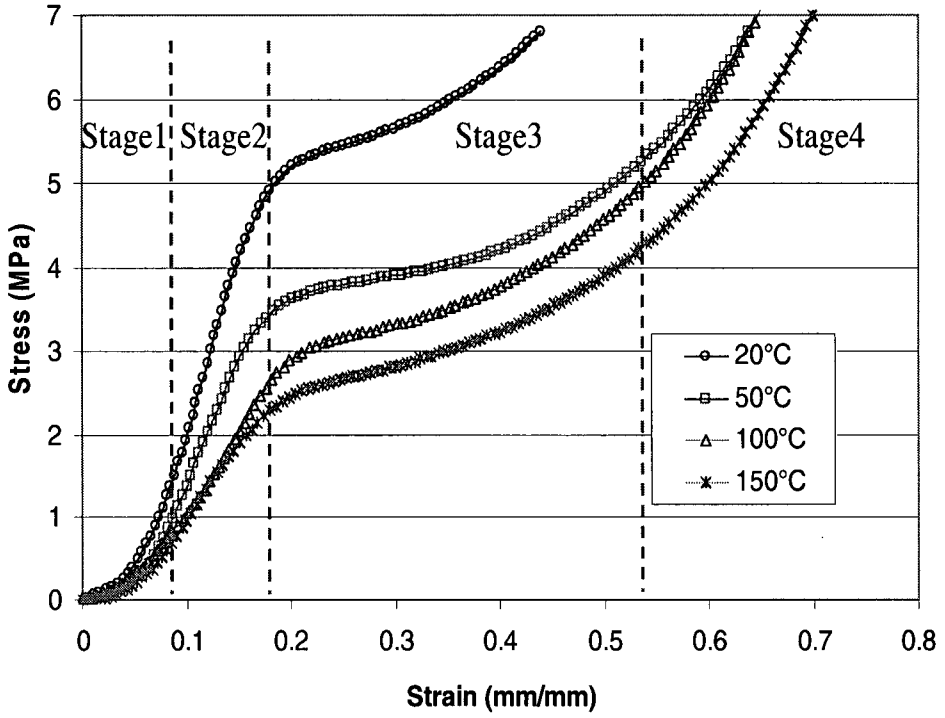

Figure 5.7 Compressive stress-strain relationship at different temperatures

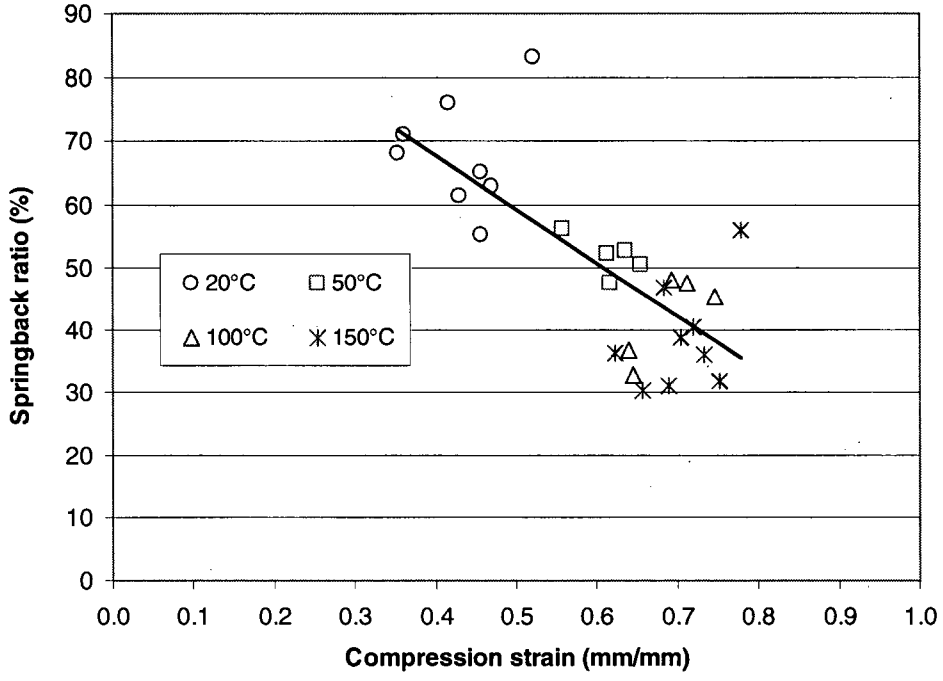

Figure 5.8 Relationship between springback ratio and compression strain

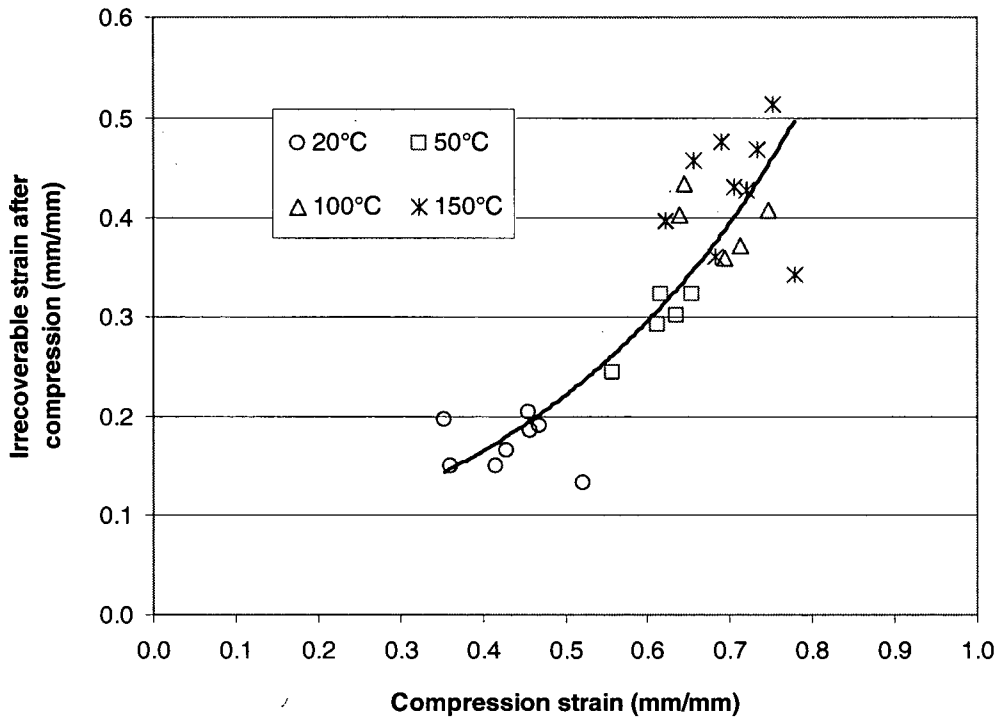

Figure 5.9 Relationship between irrecoverable strain and compression strain

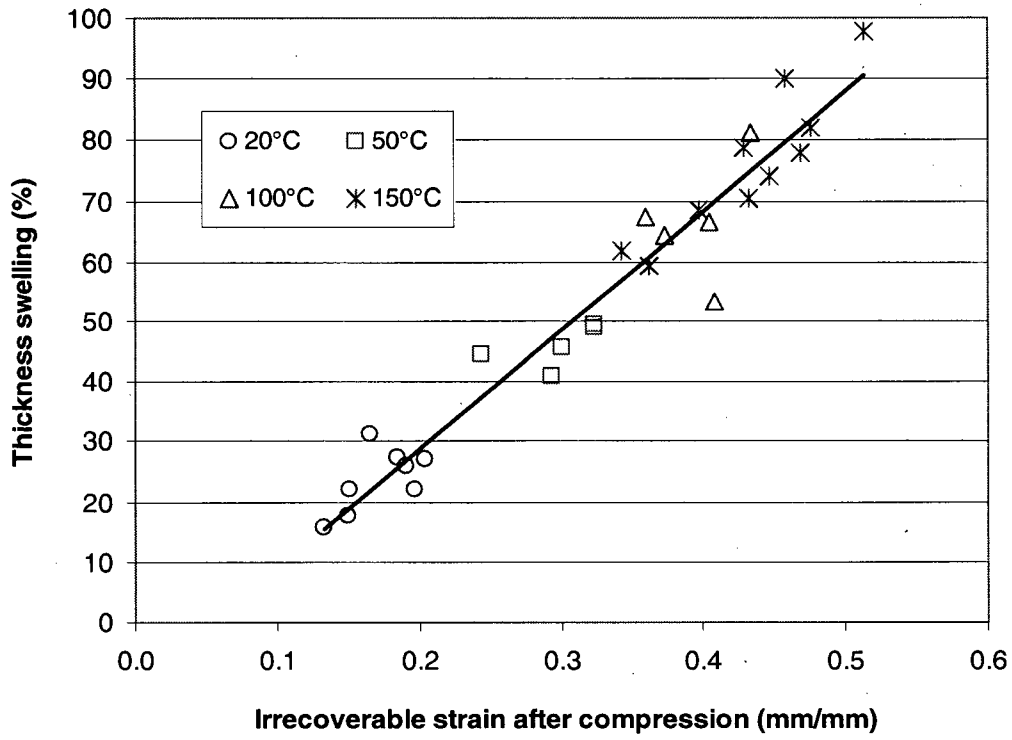

Figure 5.10 Relationship between thickness swell and irrecoverable strain

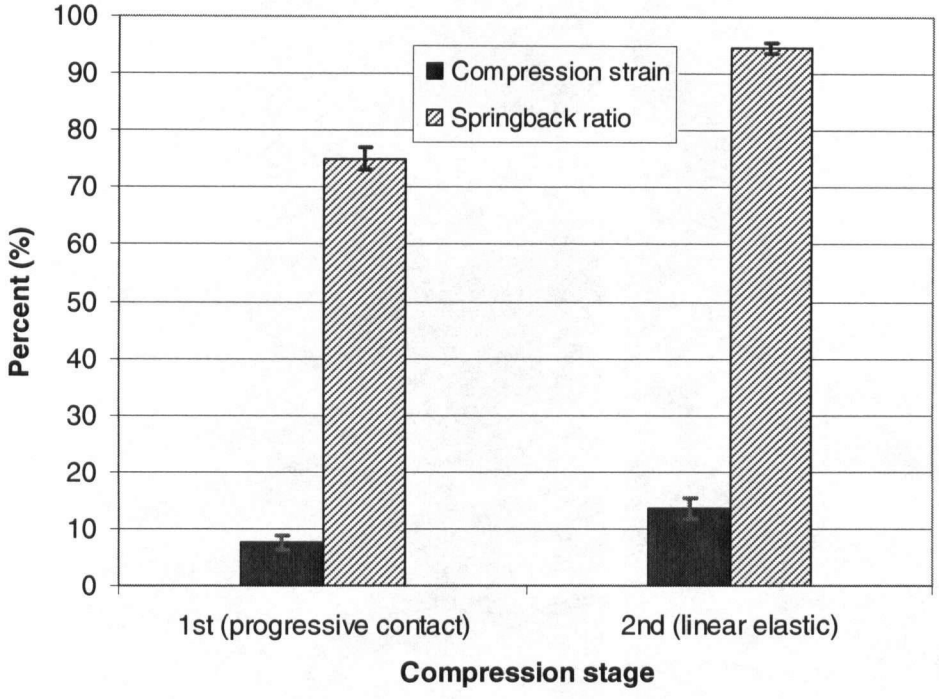

Figure 5.11 Comparing compression strain and springback ratio between the first and second stages (error bar: ± one standard deviation)

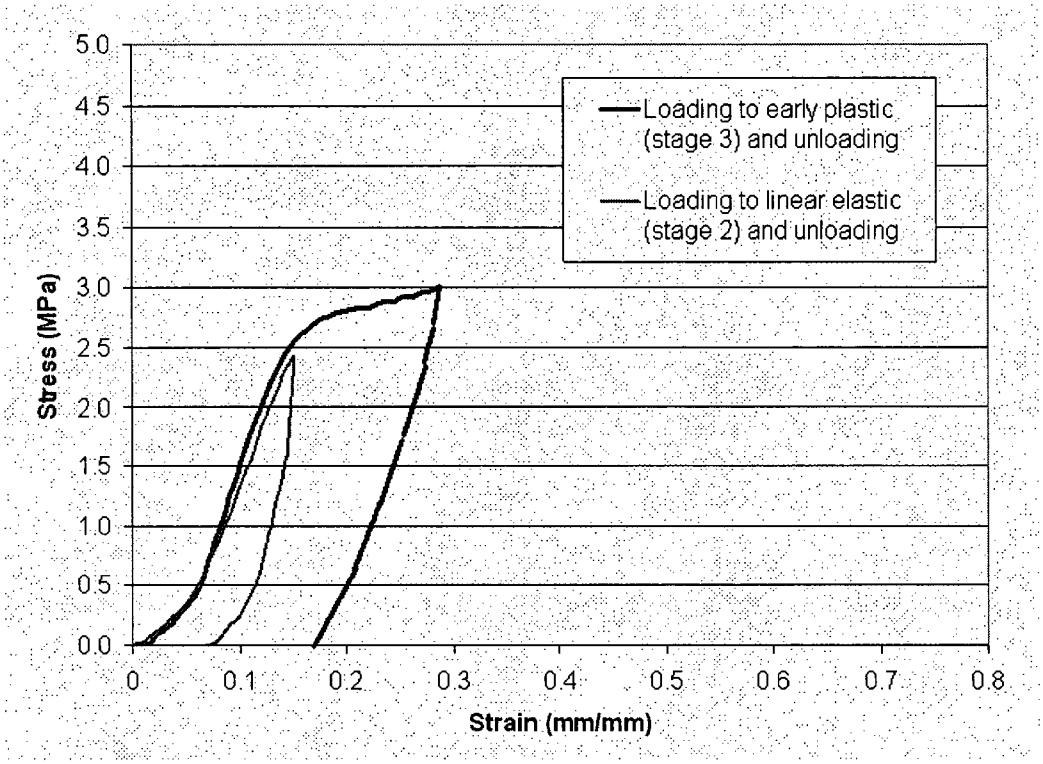

Figure 5.12 Loading to the 2nd linear elastic stage and early plastic stage and unloading

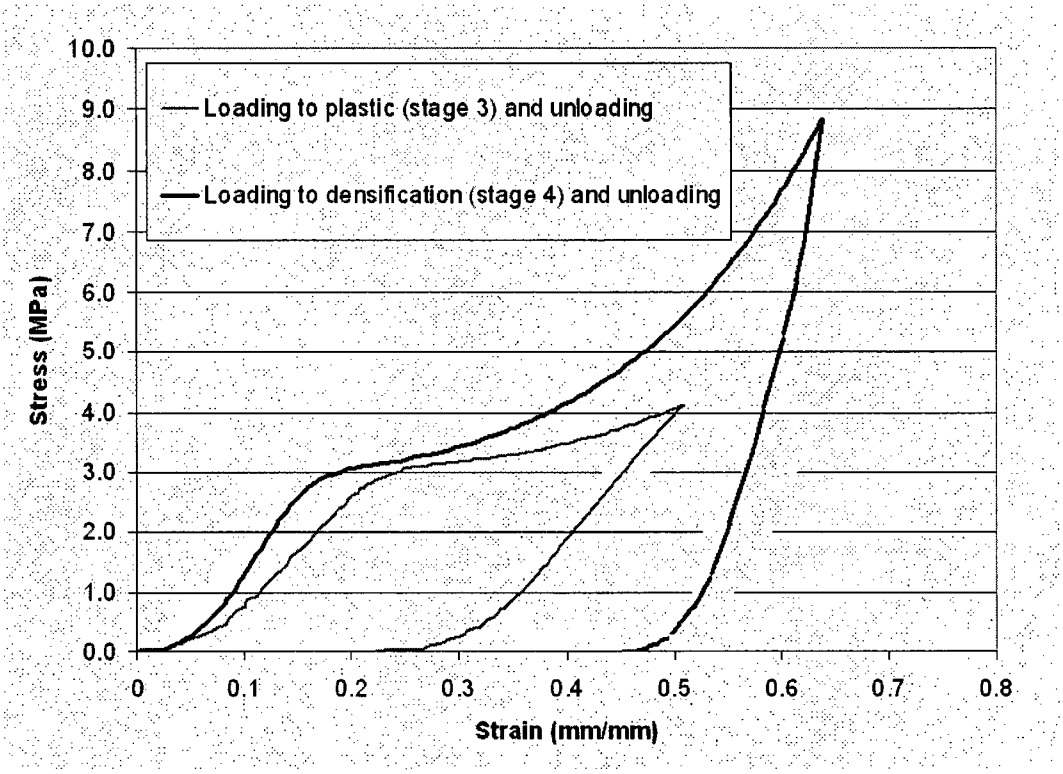

Figure 5.13 Loading to the 3rd plastic stage and 4th densification stage and unloading

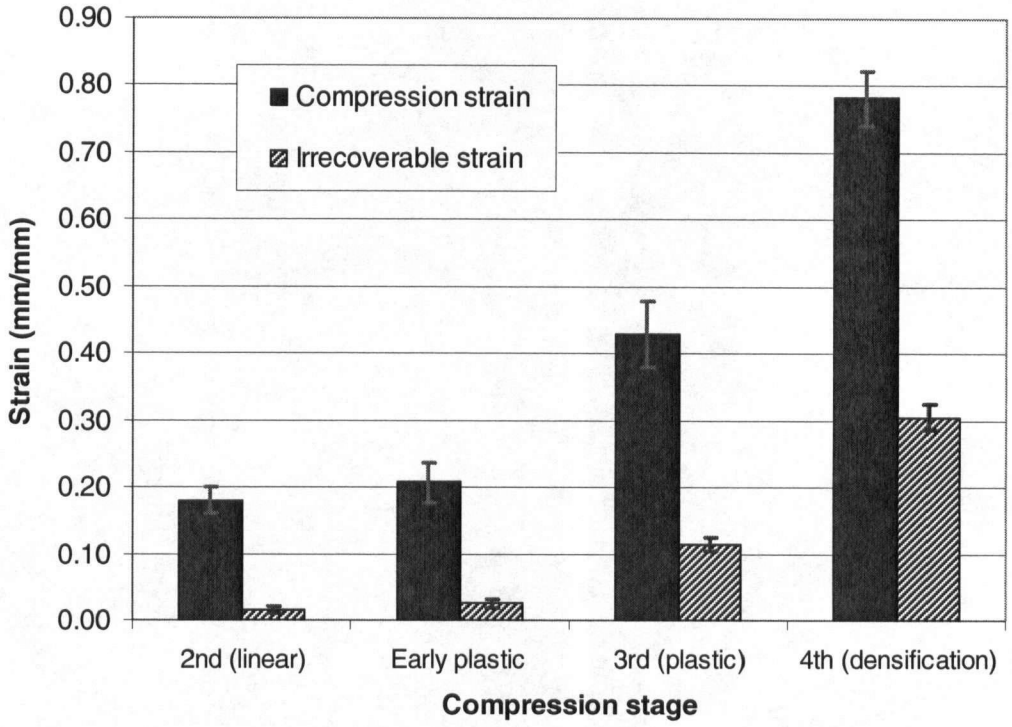

Figure 5.14 Variation of irrecoverable strain at different compression stages (20°C)

(error bar: ± one standard deviation)

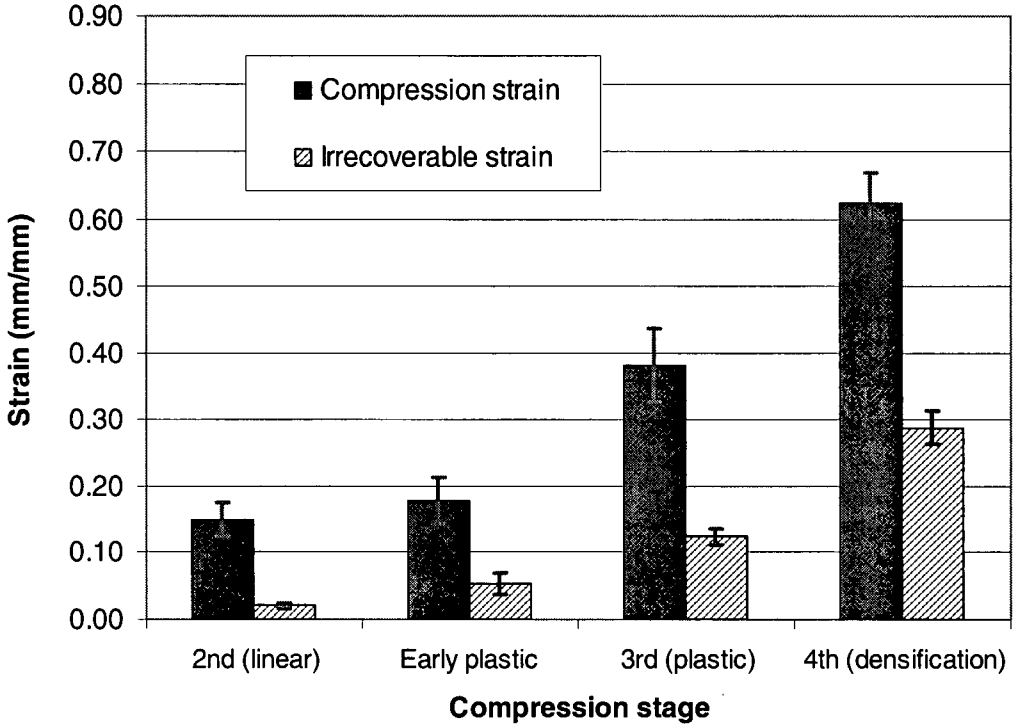

Figure 5.15 Variation of irrecoverable strain at different compression stages (50°C)

(error bar: ± one standard deviation)

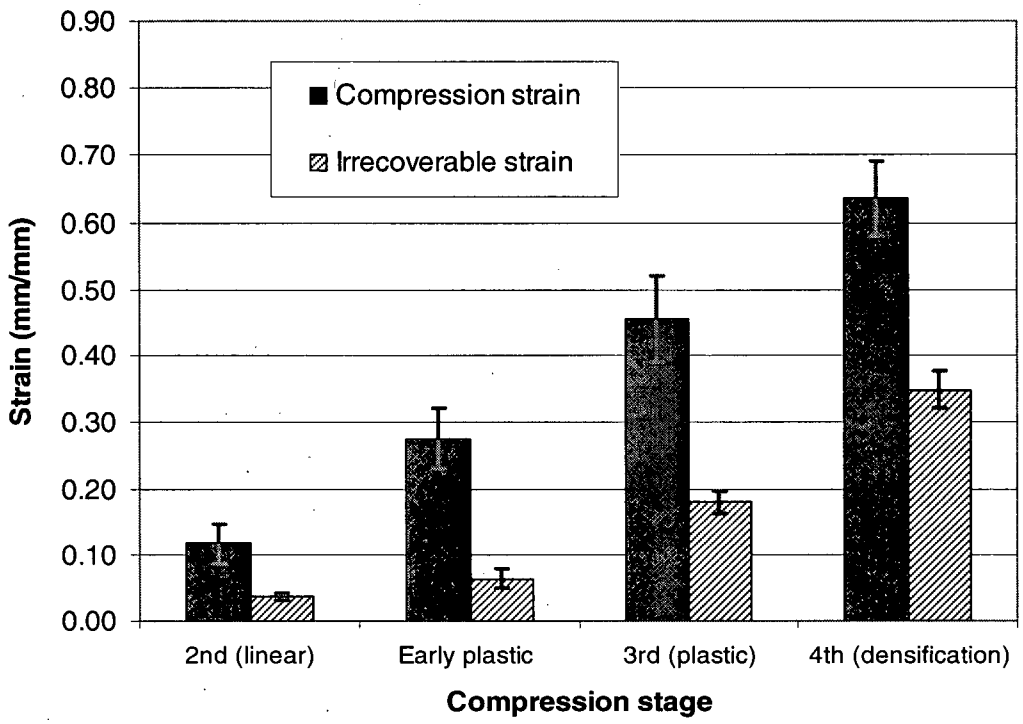

Figure 5.16 Variation of irrecoverable strain at different compression stages (100°C) (error bar: ± one standard deviation)

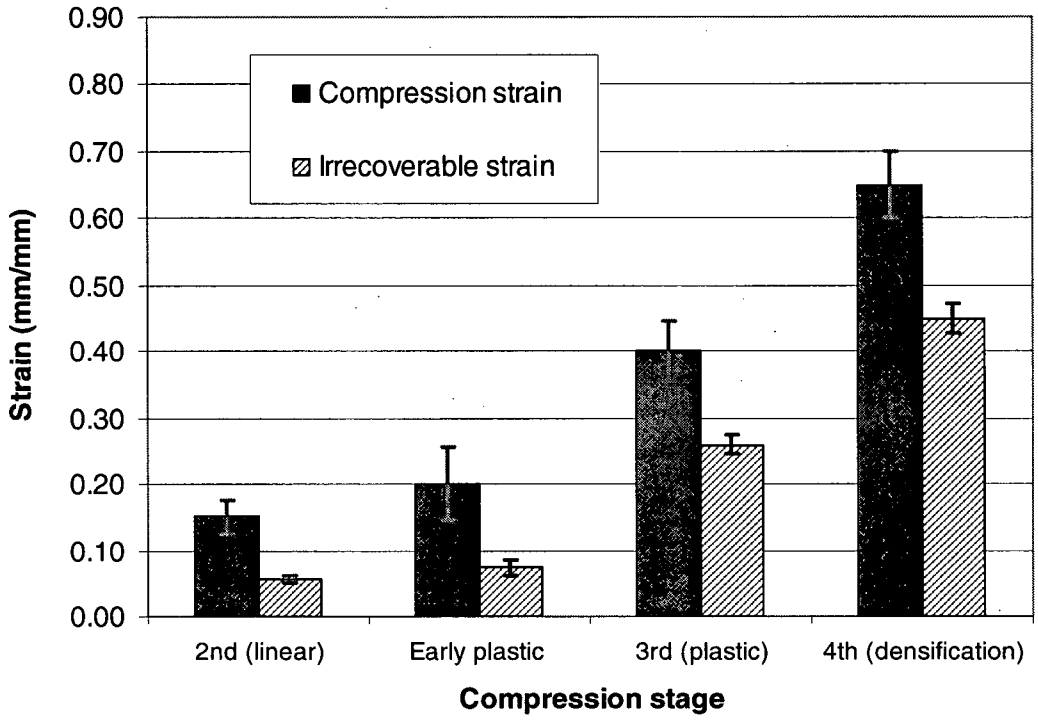

Figure 5.17 Variation of irrecoverable strain at different compression stages (150°C)

(error bar: ± one standard deviation)

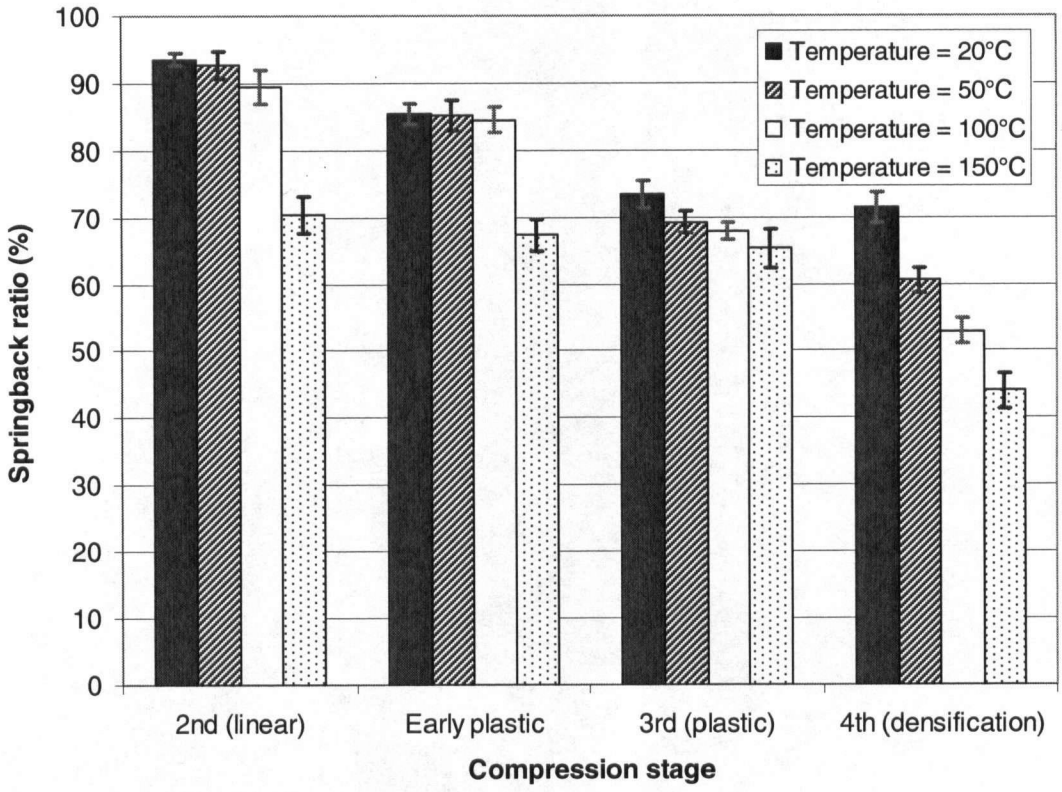

Figure 5.18 Comparing springback ratio at 3% MC in terms of different compression stages (error bar: ± one standard deviation)

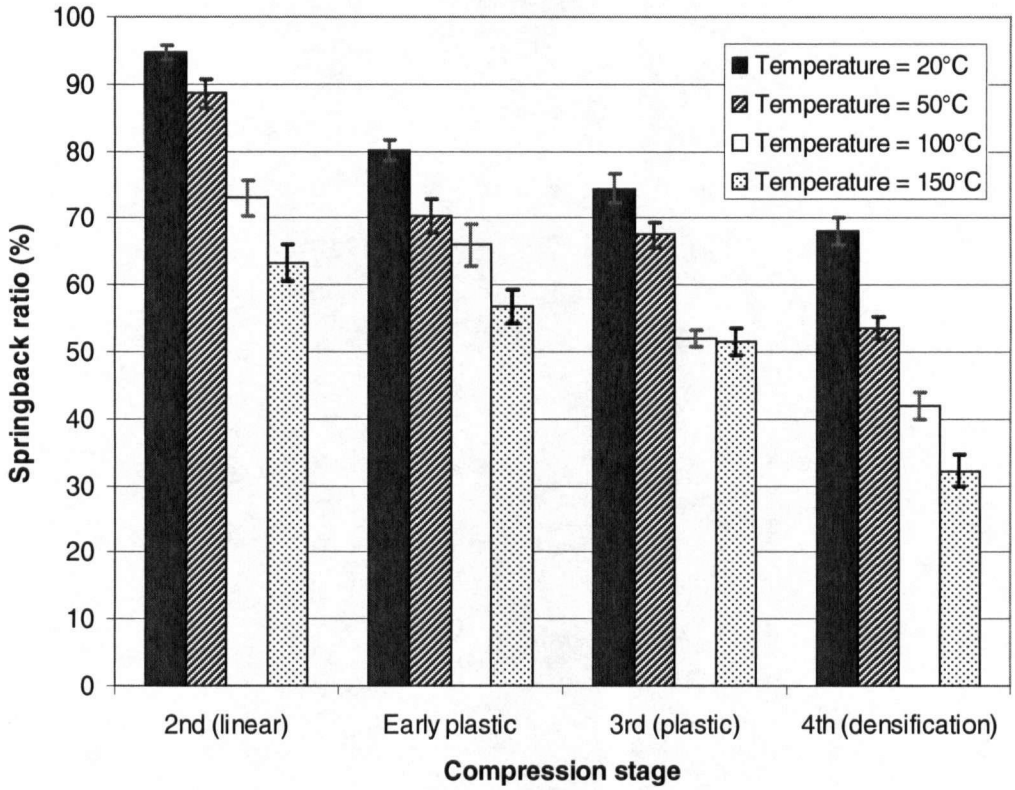

Figure 5.19 Comparing springback ratio at 6% MC in terms of different compression stages (error bar: ± one standard deviation)

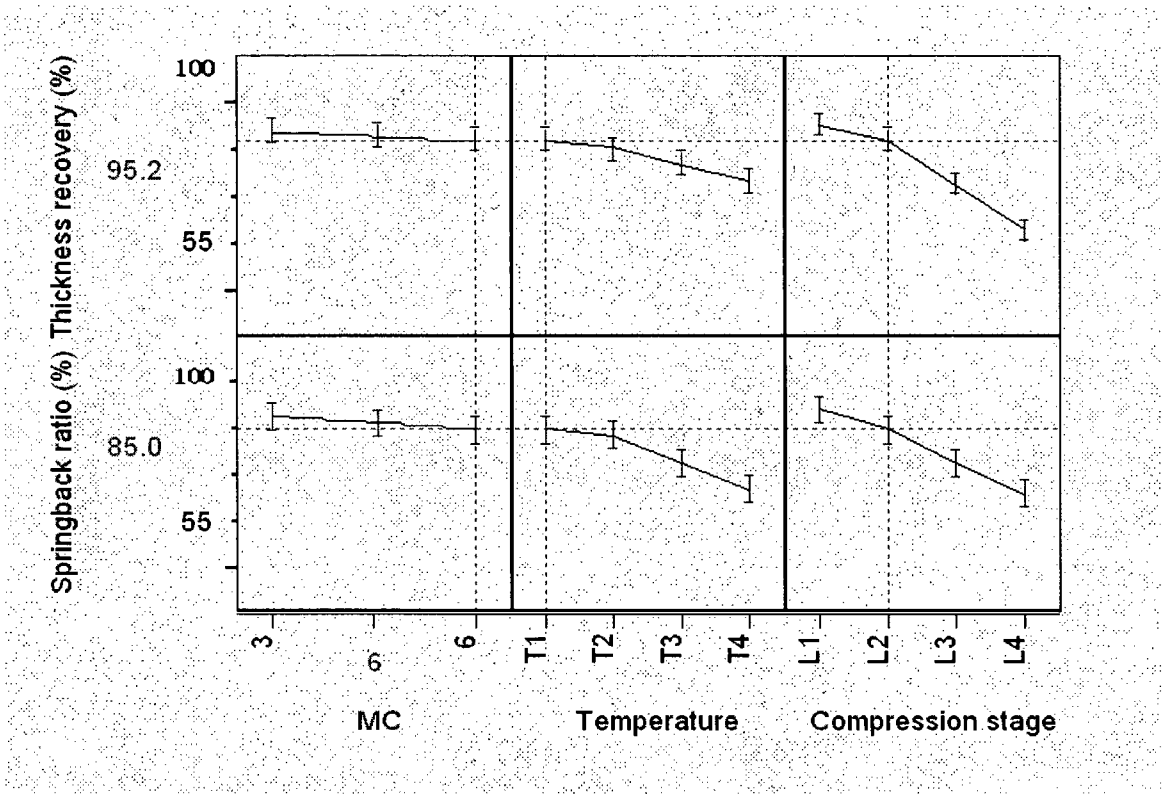

Figure 5.20 Prediction profiler of the three variables on veneer springback behaviour

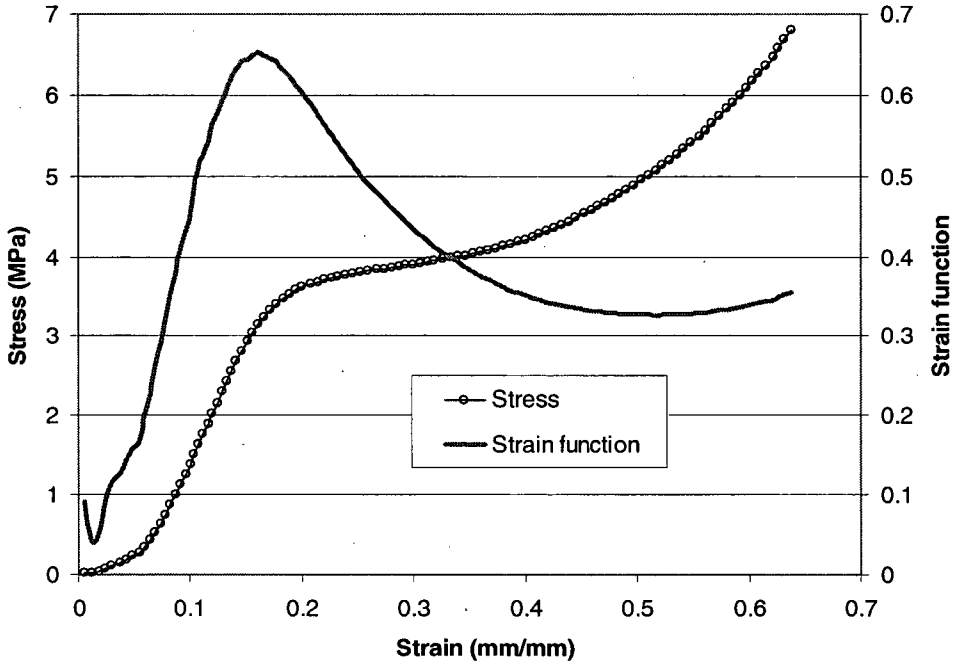

Figure 5.21 The shape of strain function derived from the stress-strain relationship

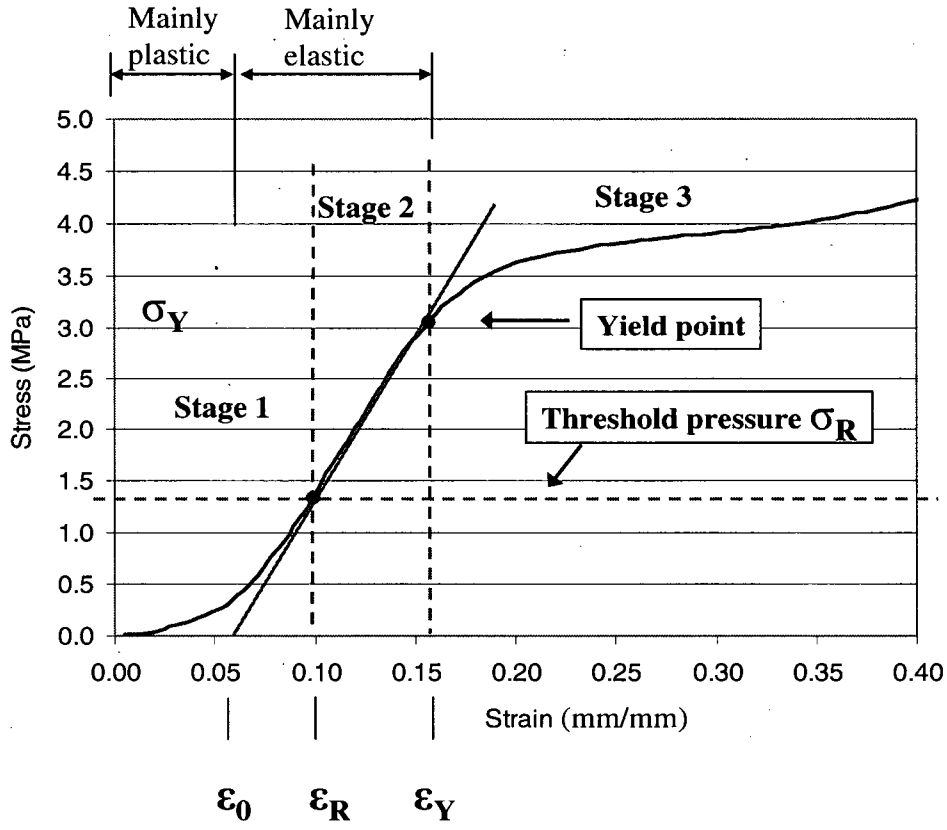

Figure 5.22 Analysis of the stress-strain relationship during veneer compression

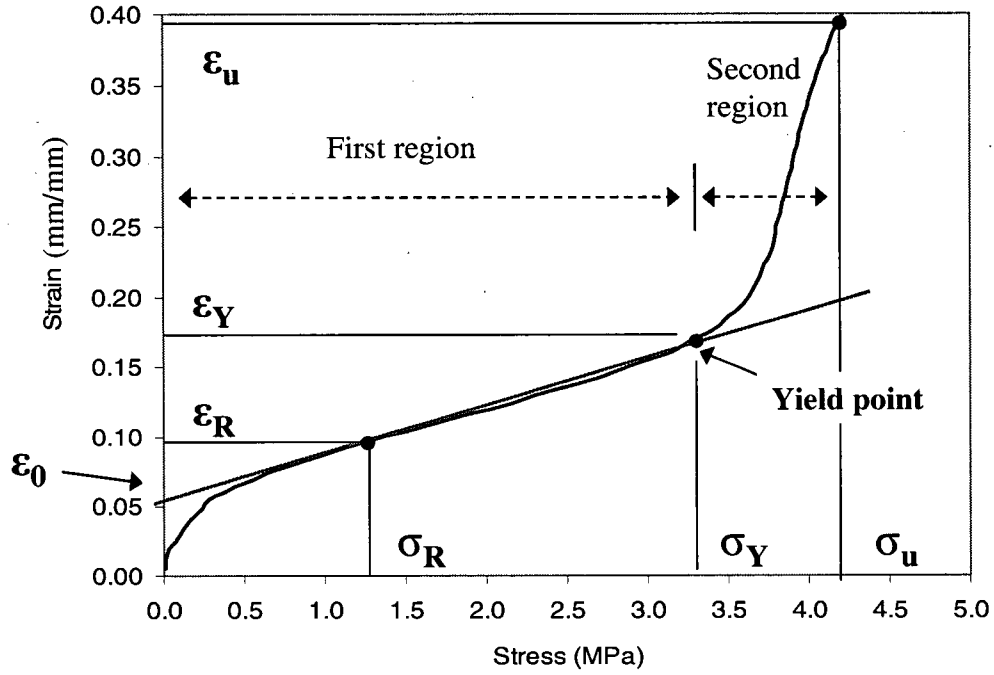

Figure 5.23 Definition of two strain regions for veneer compression

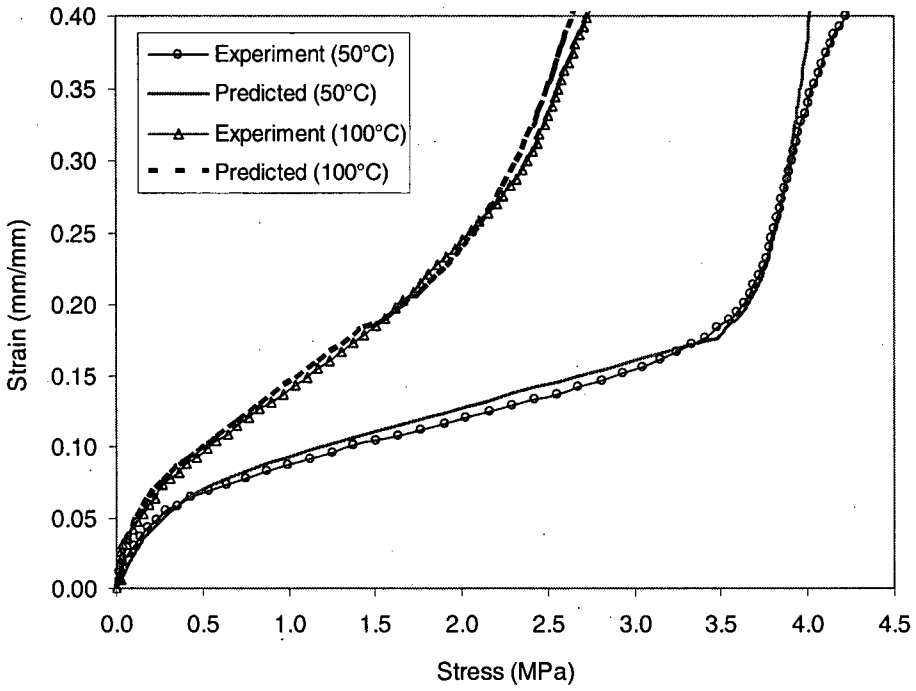

Figure 5.24 Comparison of predicted strain and measured strain for aspen veneer

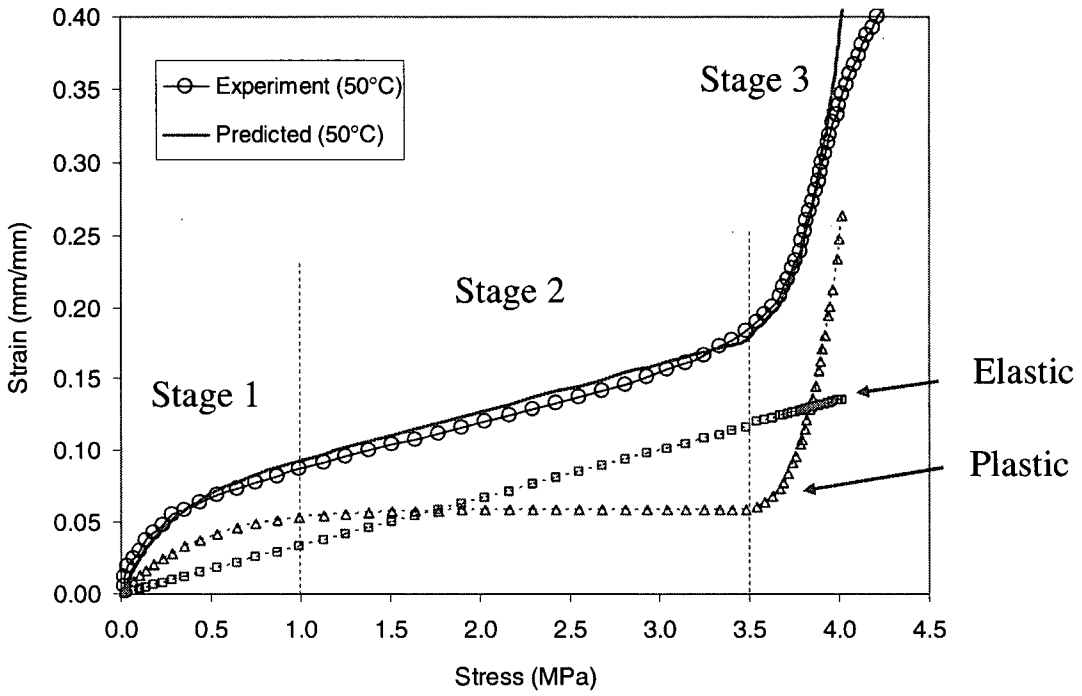

Figure 5.25 Schematic superimposing of elastic strain and plastic strain during veneer compression

5.6 Bibliography

Bodig, J. and B. A. Jayne. 1982. Mechanics of wood and wood composites. Krieger Publishing Company. Malabar, Florida.

Carvalho, L. H., M. N. Costa and C. V. Costa. 2001. Modeling rheology in the hot pressing of MDF: comparison of mechanical models.

Christensen, R. M. 1971. Theory of Viscoelasticity. Academic Press. New York and London.

Dai, C. and P. R. Steiner 1993. Compression behaviour of randomly formed wood flask mats. Wood and Fiber Sci. 25(4):349-358.

Dai, C., C. Yu and P. Hubert. 2000. Modeling vertical density profile in wood composites during hot pressing. Proceedings of the 5th Pacific Rim Bio-Based Composites Symposium. Canberra, Australia. Pp. 220-226.

Dai, C. 2001. Viscoelasticity of wood composite mats during consolidation. Wood and Fiber Sci. 33 (3):353-363.

Gibson, L. J. and M. F. Ashby. 1997. Cellular solids: structure and properties-second edition. Cambridge University Press, Cambridge. UK. 510pp.

Harless, P.E., F.G. Wagner, P. H. Short, R. D. Seale, P. H. Mitchell and D.S. Ladd. 1987. A model to predict the density profile of particleboard. Wood and Fibre Sci. 19(1): 81-92.

JMP® Statistical Discovery Software. 2000. SAS Institute Inc. Cary, NC, USA.

Lang, E. M. and Wolcott M. P. 1996a. A model for viscoelastic consolidation of wood-strand mats. Part I. Structural characterization of the mat via Monte Carlo Simulation. Wood and Fiber Sci. 28 (1):100-109.

Lang, E. M. and Wolcott M. P. 1996b. A model for viscoelastic consolidation of wood-strand mats. Part II. Static stress-strain behaviour of the mat. Wood and Fiber Sci. 28 (3):369-379.

Wolcott, M. P., Kamke F. A. and Dillard, D. A. 1990. Fundamentals of flakeboard manufacture: viscoelastic behaviour of the wood component. Wood and Fiber Sci. 22:345-361.

Godbille F. D. 2002. A simulation model for the hot pressing of particleboard. Ph. D dissertation. The University of New Brunswick. 179pp.

Jimenez, L., I. Perez, M. J. Torre and J. C. Garcia. 2000. Influence of process variables on the properties of pulp and paper sheets obtained by sylphite pulping of olive tree wood. Wood Sci. and Tech. 34: 135-149.

Rosli, W. D., C. P. Leh, Z. Zainuddin and R. Tanaka. 2003. Optimization of soda pulping variables for preparation of dissolving pulps from oil palm fiber. Holzforchung. 57 (1):106-113.

Suo, S. and J. L. Bowyer. 1994. Simulation modeling of particleboard density profile. Wood and Fiber Sci. 26(3):397-411.

Khuri, A. I. and J. A. Cornell. 1996. Response surfaces: Designs and analyses. Second Edition, Revised and Expanded. ISBN: 0-8247-9741-8.

von Haas, G. 1998. Investigation of the hot pressing of wood composite mats under special consideration of the compression behaviour, the permeability, the temperature conductivity and the sorption speed. Hamburg, Germany. Pp. 127-146.

Warren, W. G. and J. R. T. Hailey. 1980. Using response surface methodology to evaluate veneer yield and quality. Wood Sci. 12 (3): 132-140.

Wellons, J. D., R.L.Krahmer, M. D. Sandoe and R. W. Jokerst. 1983. Thickness loss in hot-pressed plywood. Forest Prod. J. 33(1):27-34.

Zhou, X. and C. Dai. 2005. Interaction of temperature and moisture content on flake compression. Proceedings of the 7th Pacific Rim Bio-Based Composites Symposium. Volume II. 116-125. Nanjing, P.R. China.

CHAPTER VI MODELING OF HOT PRESSING BEHAVIOUR OF VENEER-BASED COMPOSITES[3]

6.1 Introduction

As discussed in Chapter 1, the two basic constituent elements in veneer-based composites are layered veneer and glueline. Due to the difference in constituent elements, the hot-pressing schedules for plywood/LVL are different from those for non veneer-based composites such as OSB and MDF. During plywood/LVL manufacturing, the hot pressing process is crucial not only to the productivity and material recovery, but also to the panel quality and performance. Also as demonstrated in Chapter 2, during hot-pressing of veneer-based composites, the permeability of the veneer was significantly reduced with as little as 3-7% compression ratio (CR), which forms a main barrier to the heat convection. The gas was largely trapped inside the panel since its pressures on the surface layer and at the core did not converge, and both gas pressures and temperatures generally kept increasing at the decompression stage. These observations imply that the rate of convection is negligible, and thus heat conduction is dominant. Nevertheless, the rate of heat convection has never been quantified (Bolton and Humphrey 1994). Although the glueline did not act as a main barrier to heat convection for gas and moisture movement, it could provide (thermal) resistance to heat conduction due to its high moisture concentration (Wang 2006) or affect panel stiffness properties (Okuma 1976). The hot pressing efficiency was mainly determined by the temperature of the innermost glueline temperature. Previous studies demonstrated that the moisture from the glue application, normally accounting for 50% to 80% of total moisture in the panel assemblies, affected the rise of the innermost glueline temperature more significantly than the moisture content (MC) from the veneer (Wang 2001b; Wang and Dai 2005). The density near or at the glueline zones was much higher than the density of the veneer. Therefore, during hot-pressing, quantifying the heat and mass transfer behaviour at or near the glueline zone is essential to understand the hot-pressing process. Furthermore, veneer thickness is rather small compared to its length and width; as a result, the heat and mass transfer mainly occurs through-the-thickness. All these results demonstrated that 1) the glueline cannot be excluded in an accurate simulation of heat and mass transfer during plywood/LVL hot-pressing;

[3] A version of this chapter has been accepted for oral presentation and publication.
Wang, B. J., C. Yu, C. Dai and S. Ellis. 2006. A Hot Pressing Simulation Model for Veneer-Based Wood Composites. Proceedings of the 8th Pacific Rim Bio-Based Composites Symposium. Kuala Lumpur, Malaysia. Nov. 20-23. pp236-251.

and 2) a one-dimensional heat and mass transfer model is a good start for hot pressing simulation.

Up to now, the numerical simulation of plywood/LVL hot-pressing processes has not been available (Wellons *et al.* 1983; Zavala 1986; Zavala and Humphery 1996; Wang 2003; Wang and Dai 2005). To help understand the hot-pressing processes, the key objective of this work was to develop a computer simulation model to predict heat and mass transfer and panel densification during plywood/LVL hot-pressing. With the experimentation work conducted from Chapters 2 to 5, further understanding was developed concerning the mechanisms of heat and mass transfer, veneer compression for bonding contact and panel densification. The new knowledge generated lays a foundation for developing an integrated hot pressing simulation model. On the basis of defining wood-glue mix layers through the panel thickness, a finite-difference based plywood/LVL hot-pressing model, VPress®, was developed to simulate, for the first time, the changes of temperature and MC at each veneer ply and glueline, gas pressure and vertical density profile (VDP) throughout the pressing cycle.

6.2 Analysis of Magnitude of Heat Conduction and Convection

As discussed in Chapter 2, the air permeabilities of veneers and gluelines were measured; and the hot pressing behaviour of 5-ply aspen plywood and OSB was compared. The results indicated that during hot pressing of veneer-based composites, compared to heat conduction, heat convection is limited. Previous study by Bolton and Humphrey (1994) also indicated that heat conduction is dominant during plywood hot pressing. A recent study at Forintek demonstrated that the total MC loss of 13-ply aspen LVL after hot pressing ranged from 1-3% on the total weight base (glue + veneer) and 10-25% on the total MC base (Wang 2006), which indicates that after pressing the majority of MC from the veneer and glue remains inside the panel, and vapour evaporation or in-plane and through-the-thickness energy leaking could be limited. For one-dimensional heat and mass transfer in plywood/LVL hot pressing, without considering energy leaking (both in-plane and through-the-thickness) and water phase change, the governing equation of energy conservation can be written for the veneer ply as follows:

$$k\frac{\partial^2 T}{\partial z^2} + \rho_g c_g u_g \frac{\partial T}{\partial z} = \rho c \frac{\partial T}{\partial t} \qquad (6\text{-}1)$$

where T is the temperature, c_g is the specific heat of gas (a mixture of air and vapour), c is the specific heat of the veneer ply depending on veneer MC, ρ_g is the gas volume density, ρ is the density of the veneer ply, and k is the heat conductivity of veneer ply, t is the pressing time, and z is the unit dimension in the panel thickness direction, and u_g is the velocity of gas in the panel thickness direction, which follows Darcy's law as follows:

$$u_g = \frac{K}{\mu}\frac{\partial P}{\partial z} \qquad (6\text{-}2)$$

where K is the air permeability of veneers in the thickness direction, which was obtained from Chapter 1; P is the gas pressure; μ is the viscosity of gas at the room temperature (1.846×10^{-5} $Pa*s$). In Equation (6-1), the first term is energy of the veneer obtained through heat conduction whereas the second term is energy of the veneer obtained through heat convection. To quantitatively validate the conclusion obtained in Chapter 1 that the rate of heat convection is negligible, Equation (6-1) can be rewritten to:

$$\frac{\partial}{\partial z}(k\frac{\partial T}{\partial z} + \rho_g c_g \mu_g T) = \rho c \frac{\partial T}{\partial t} \qquad (6\text{-}3)$$

In general, the conductivity k of aspen veneer is about 0.1 W/(m*K). Also, the ambient temperature and platen temperature are normally 20°C and 150°C, respectively, and c_g is about 2000-3000 J/(kg*K) with an average of 2500 J/(kg*K). For 5-ply plywood (5/8 -in thickness), the half thickness is about 0.008 m. Recall from Chapter 1, the average permeability K of aspen veneer panels is about 4.02×10^{-14} m^2 at a 5% compression ratio (CR), a densification level normally used by plywood industry. Assuming the average gas pressure is 10^5 Pa (1 bar), for half of the 5-ply plywood thickness, the gas velocity u_g can be calculated as:

$$u_g = \frac{K}{\mu}\frac{\Delta P}{\Delta z} = \frac{4.02*10^{-14}}{1.846*10^{-5}}\frac{10^5}{0.008} \approx 0.027 \text{ m/s}$$

As demonstrated in Chapter 2, the effective porosity (void) contributing to the permeability in veneer panels was only 0.05 -0.50% with an approximate value of 0.3% for veneer panels at a 5% CR. Since the water vapour density is about 1 kg/m^3 (Incropera and Dewitt 1990), the effective gas volume density ρ_g is only 0.003 (0.3%*1) kg/m^3. Therefore, based on Equation (6-3), the relative contribution of heat convection (RC) to the total transfer of heat energy can be approximately determined by:

$$RC = \frac{\rho_g C_g \mu_g T}{k\frac{\Delta T}{\Delta z} + \rho_g C_g \mu_g T} \approx \frac{0.003 * 2500 * 0.027 * \frac{(150+20)}{2}}{0.1 * \frac{(150-20)}{0.008} + 0.003 * 2500 * 0.027 * \frac{(150+20)}{2}} * 100\% = 1\%$$

The result indicated that quantitatively, the heat convection only contributes about 1% to the total heat transfer; therefore, the heat conduction is dominant during hot pressing of veneer-based composites. As a result, to simplify the modeling, the effect of heat convection will not be considered.

6.3 General Hypothesis

The model was developed based on the following assumptions:

- heat transfer mainly occurs in the perpendicular-to-thickness direction;
- heat conduction is predominant and heat convection is neglected across the panel thickness but in-plane energy leaking is considered;
- the glue solids are incompressible; and
- pressure control is the mode of the hot-pressing operation.

To simplify the development of a heat and mass transfer model, the following assumptions were also made:

- veneer ply and glueline are homogeneous and uniform along the panel plane;
- the heat and water produced by phenolic formaldehyde (PF) glue during its curing reactions is negligible;
- migration of the phenolic glue to the edge of panel ("squeezing-out") during pressing is negligible.

As discussed, one of the keys to simulate hot-pressing behaviour of veneer-based composites is to characterize the role of the glueline, an interfacial and continuous layer between the two veneer plies. During the course of heat and mass transfer, the glueline effect cannot be ignored since MC from the glue significantly affects the temperature rise in the innermost glueline and, in turn, the hot-pressing time. Figure 6.1 (a) shows a typical X-ray density profile of one 13-ply aspen LVL panel and (b) an enlargement of a portion of the profile at the core. The two peaks represent two glueline zones. The glueline is assumed to include the bulk of the glue, the

interface between the glue and the wood surfaces, and the interphase, which is the glue-penetrated wood layers (Figure 6.2). Thus, the glueline is really a layer of wood-glue mix, which allows for the combined effect of veneer lathe checks, roughness, thickness variation, glue penetration into the veneer and glueline irregularities.

6.4 Modeling of Heat and Mass Transfer

Based on Figure 6.1, it can be estimated that the thickness of the wood-glue mix layer is about 10 - 20% of veneer ply thickness (1/8 -in). The large thickness is mainly due to the glue penetration into the veneer ply through the rough surface and open lathe checks. Therefore, plywood/LVL panels can be conceptualized as a chain series with alternate veneer and wood-glue mix layers, as shown in Figure 6.3. Each veneer layer is defined as the portion of a veneer ply after deducting the partial wood included in the adjacent wood-glue mix layers. For the top and bottom veneer layers, only one side of partial wood needs to be deducted.

6.4.1 Effective Conductivity

The rate at which heat is transferred by conduction, q_k, is proportional to the temperature gradient *(dT/dz)* times the area (A) through which heat is transferred (Incropera and Dewitt 1990):

$$q_k \propto A\frac{dT}{dz} \qquad (6\text{-}4)$$

In this relation, *T(z)* is the local temperature and *z* is the distance in the direction of the heat flow. The actual rate of heat flow depends on the thermal conductivity *k*, which is a physical property of the medium. For conduction through a homogeneous medium, Fourier's law of heat conduction describes:

$$q_k = -\,k A\frac{dT}{dz} \qquad (6\text{-}5)$$

The minus sign is a consequence of the second law of thermodynamics, which requires that heat must flow in the direction from higher to lower temperature.

When two different conducting surfaces are placed in contact, a thermal resistance is present at the interface of the solids. The interface resistance, frequently called the thermal contact

resistance, develops when two materials will not fit tightly together and a thin layer of fluid (possibly air) is trapped between them. The interface resistance is primarily a function of surface roughness, the pressure holding the two surfaces in contact, the interface fluid, and the interface temperature. At the interface, the mechanism of heat transfer is complex. Conduction takes place through the contact points of the solid, while heat is transferred by convection and radiation across the trapped interfacial fluid. If the heat flux through two solid surfaces in contact is q/A and the temperature difference across the fluid gap separating the two solids is ΔT_i, the interface resistance R_i is defined by

$$R_i = \frac{\Delta T_i}{q_k / A} = \frac{\Delta z}{k} \qquad (6\text{-}6)$$

When two surfaces are in perfect thermal contact, i.e., $\Delta z = 0$, the interface resistance approaches zero, and there is no temperature difference across the interface.

To determine the effective conductivity of heat from the wood-glue mix to the veneer layer, the wood-glue mix can be modeled as parallel layers of wood and glue, as shown in Figure 6.4. It is quite possible that the veneer layer may retain some lathe checks with a portion unfilled with the glue. In Figure 6.4, h_v and k_v are thickness and conductivity of the veneer layer, respectively; and h_m amd k_m are the thickness and conductivity of the wood-glue mix, respectively. The total heat resistance of the veneer layer and wood-glue mix layer (R) can be expressed as the sum of heat resistances of the veneer layer (R_v) and wood-glue mix layer (R_m).

$$R = R_v + R_m \qquad (6\text{-}7)$$

Since $R_v = \frac{h_v}{k_v}$, $R_m = \frac{h_m}{k_m}$ and $R = \frac{h_v + h_m}{k_{eff.}}$, we have

$$k_{eff.} = \frac{k_v k_m (h_v + h_m)}{k_v h_m + k_m h_v} \qquad (6\text{-}8)$$

Since the wood-glue mix layer is seen as the parallel series of the wood and glue, the heat resistance (R_m) can be calculated as:

$$\frac{1}{R_m} = \frac{1}{R_{wood}} + \frac{1}{R_{glue}} \qquad (6\text{-}9)$$

By definition, $R_m = \frac{h_m}{k_m}$, $R_{wood} = \frac{h_m}{\alpha k_v}$ and $R_{glue} = \frac{h_m}{\beta k_{glue}}$

Since α, β are volume ratios of wood and glue in the wood-glue mix layer,

$$\alpha + \beta = 1 \qquad (6\text{-}10)$$

Substituting them into Equation (6-9), we have

$$k_m = \alpha k_v + (1 - \alpha) k_{glue} \qquad (6\text{-}11)$$

Again, substituting Equation (6-11) into (6-8), we can get

$$k_{eff.} = \frac{k_v [\alpha k_v + (1-\alpha) k_{glue}]}{k_v \frac{h_m}{h_v + h_m} + [\alpha k_v + (1-\alpha) k_{glue}] \frac{h_v}{h_v + h_m}} \qquad (6\text{-}12)$$

Based on Equation (6-12), if $h_m << h_v$, then $k_{eff.} = k_v$.

For veneer-based composites, h_m is about 20% of total thickness ($h_v + h_m$) (Figure 6.1). Hence, the conductivity of the wood-glue mix layer can be seen as identical to that of the veneer.

6.4.2 Heat Transfer

6.4.2.1 Veneer layer

A lumped finite-element method was used to describe the heat and mass transfer behaviour for veneer-based composites. As shown in Figure 6.5, the veneer layer number is the same as the number of veneer plies n (from 1 to n) for the panel lay-up; whereas the number of wood-glue mix layers is n–1. For the first veneer layer at the bottom, the energy obtained from the bottom platen and from the first layer of wood-glue mix should contribute to the increase of temperature of the veneer layer in a unit time step. During pressing, it is assumed that energy leaking and water phase change mainly occur in the wood-glue mix layers rather than veneer layers. As such, without considering the effect of heat convection, the energy balance equation for the i^{th} veneer layer can be established as:

$$k_{v,i} \frac{T_{m,i-1} - T_{v,i}}{0.5 * (h_{m,i-1} + h_{v,i})} + k_{v,i} \frac{T_{m,i} - T_{v,i}}{0.5 * (h_{v,i} + h_{m,i})} = \frac{d(C_{pv,i} \rho_{v,i} h_{v,i} T_{v,i})}{dt}$$

$$i = 1, 2, \ldots, n \qquad (6\text{-}13)$$

The Euler method can be used to solve a set of above n ordinary differential equations:

$$T_{v,i}^{k+1} = T_{v,i}^{k} + \frac{\Delta t}{C_{pv,i}^{k}\rho_{v,i}^{k}h_{v,i}^{k}}\left\{\frac{2k_{v,i}^{k}}{h_{m,i-1}^{k}+h_{v,i}^{k}}\left(T_{m,i-1}^{k}-T_{v,i}^{k}\right)+\frac{2k_{v,i}^{k}}{h_{m,i}^{k}+h_{v,i}^{k}}\left(T_{m,i}^{k}-T_{v,i}^{k}\right)\right\}$$

$$i = 1, 2, \ldots, n \quad (6\text{-}14)$$

where the superscript k means the previous time and k+1 present time (the k ranges from 0 to required time); Δt is the time step; T_v is the temperature of the veneer layer; T_m is the temperature of the wood glue mix layer; C_{pv} is the specific heat of the veneer layer, which is the function of veneer MC; ρ_v is the density of the veneer layer; h_v is the thickness of the veneer layer; h_m is the thickness of the wood glue mix layer and k_v is the heat conductivity of the veneer layer. On the right hand side, all the variables are known. Note that at k = 0, $T_{v,1}^{0}$, $T_{m,1}^{0}$, and $T_{v,1}^{0}$ are the ambient temperature. Equation (6-14) shows how to calculate the temperatures for n veneer layers, simultaneously when the boundary conditions such as top and bottom platen temperatures are known.

According to Siau (1995), k_v, the heat conductivity of the veneer ply, is a function of veneer density and MC as follows:

$$k_{v,i} = 0.024 + 0.001 * \rho_i * (0.2 + 0.38 * MC_i) \qquad i = 1, 2, \ldots, n \qquad (6\text{-}15)$$

where ρ_i is the veneer density for the i^{th} ply, and MC_i is the veneer MC for the i^{th} ply. Also the specific heat of the veneer ply is a function of veneer MC, which can be determined as follows:

$$C_{pv,i} = 84 + (1113 + MC_i * 4186)/(1 + MC_i) \qquad i = 1, 2, \ldots, n \qquad (6\text{-}16)$$

where MC_i is the veneer MC for the i^{th} ply.

6.4.2.2 Wood-glue mix layer

During plywood/LVL hot-pressing, the MC from the glue will not evaporate easily due to significantly reduced transverse air permeability. That is, the majority of MC in the wood glue mix layer normally remains in the panel. As shown in Figure 6.5, based on the law of energy conservation, without considering the effect of heat convection, the energy increase of the wood-

glue mix layer is acquired from the two adjacent veneer layers by subtracting the in-plane energy leaked. Therefore, for the i^{th} wood-glue mix layer, we have

$$k_{v,i}\frac{T_{v,i}-T_{m,i}}{0.5*(h_{v,i}+h_{m,i})}+k_{v,i+1}\frac{T_{v,i+1}-T_{m,i}}{0.5*(h_{m,i}+h_{v,i+1})}-\dot{q}_i=\frac{d(C_{pm,i}\rho_{m,i}h_{m,i}T_{m,i})}{dt}$$

$$i = 1, 2, \ldots, n-1 \qquad (6\text{-}17)$$

Equation (6-17) can be solved as follows:

$$T_{m,i}^{k+1}=T_{m,i}^{k}+$$

$$\frac{\Delta t}{C_{pm,i}^{k}\rho_{m,i}^{k}h_{m,i}^{k}}\left\{\frac{2k_{v,i}^{k}}{h_{m,i}^{k}+h_{v,i}^{k}}\left(T_{v,i}^{k}-T_{m,i}^{k}\right)+\frac{2k_{v,i+1}^{k}}{h_{m,i}^{k}+h_{v,i+1}^{k}}\left(T_{v,i+1}^{k}-T_{m,i}^{k}\right)-\dot{q}_i\right\}$$

$$i = 1, 2, \ldots, n-1 \qquad (6\text{-}18)$$

where the superscript k means the previous time and k+1 present time (the k ranges from 0 to required time), Δt is the time step, T_v is the temperature of the veneer layer, T_m is the temperature of the wood glue mix layer, C_{pm} is the specific heat of the wood glue mix layer, ρ_m is the density of the wood-glue mix layer, h_v is the thickness of the veneer layer, h_m is the thickness of the wood glue mix layer, k_v is the heat conductivity of the veneer layer, and $\dot{q}_i$ is the energy leaking term. On the right hand side of Equation (6-18), all the variables are assumed known. Note that $\dot{q}_i$ can be approximately expressed as:

$$\dot{q}_i \approx \dot{m}_i * H_{fg} \qquad (6\text{-}19)$$

where H_{fg} is the latent heat, which is from 2100 to 2450 kJ/kg for the temperature ranging from 20°C to 150°C (Incropera and Dewitt 1990), and $\dot{m}_i$ is the mass leaking term in the lateral direction, which can be expressed with a modified Darcy's law as:

$$\dot{m}_i = \frac{K_{L,i}}{\upsilon}\left(\frac{P_{g,i}-P_{atm}}{L}\right) \qquad (6\text{-}20)$$

where $K_{L,i}$ is the lateral permeability of the wood-glue mix layer, υ is the kinetic viscosity of water vapour, which varies from 21.7 to 24.3 (10^{-6} m^2/s) for temperature ranging from 380K to

400K (Incropera and Dewitt 1990), $P_{g,i}$ is the gas pressure at the ith wood-glue mix layer (kPa), P_{atm} is the atmosphere pressure (100 kPa) and L is the panel length (m). Note that $K_{L,i}$ is not easy to measure due to the effect of veneer location and compression, glue spread level and its uniformity. Instead, during panel manufacturing, the total mass leaked is rather easy to measure by subtracting the weight of final panel after hot pressing from the total weight of glued panel assembly.

It was observed that for LVL panels (34 x 24 x 1.5 -in), the vapour was mainly evaporated from the panel length direction during and after pressing. As shown in Figure 6.6, the total weight loss of fourteen 13-ply aspen LVL panels during and after pressing was plotted. The results demonstrated that the weight loss did not change significantly with different levels of glue spread used in this study. With an average pressing time of 20 min, the total weight loss due to gas evaporation was about 0.215 kg which accounts for approximately 20% of total MC. Assuming the $\dot{m}$ for each wood-glue mix layer is the same, the $\dot{m}_i$ can be calculated as:

$$\dot{m}_i = \frac{0.215kg}{24*0.0254(m)*1.5*0.0254(m)*20*60(s)}\frac{1}{12} = 6.43*10^{-4}\left(\frac{kg}{m^2 s}\right)$$

Since the average kinetic viscosity of water vapour υ is about 23.0 (10^{-6} m^2/s), and the average gas pressure P_g is about 2.8 (100 kPa) based on experiments, therefore, based on Equation (6-20), the average lateral permeability $K_{L,i}$ can be determined as:

$$K_{L,i} = \frac{L\upsilon \dot{m}_i}{P_g - P_{atm}} = \frac{34*0.0254(m)*23*10^{-6}\left(\frac{m^2}{s}\right)*6.43*10^{-4}\left(\frac{kg}{m^2 s}\right)}{1.8*10^5\frac{kg*m/s^2}{m^2}*\frac{1}{9.8}} = 7.0*10^{-13}\ (\text{m}^2)$$

i = 1, ..., 12

Compared to the average transverse permeability (4.02 x 10^{-14} m^2) of veneer panels obtained in Table 2.4 of Chapter 2, the average lateral permeability of veneer panels is approximately 16 times greater.

Note also that the wood-glue mix layer has a higher MC concentration but the glue has a smaller specific heat than wood (Incropera and Dewitt 1990). Hence, the specific heat of the wood-glue mix layer can be assumed to be approximately equal to that of the veneer layer.

The gas pressure can be calculated by adding up the partial pressure of air and water vapour (Dai and Yu 2004), i.e.

$$P_g = P_{air} + P_v \qquad (6\text{-}21)$$

Equation (6-21) can be seen as the ideal governing equation for gas pressure P_g. In general, the gas pressure at the wood-glue mix layer is the main concern due to its determining but detrimental effect on panel integrity and quality. According to the state equation of perfect gas, air partial pressure at the wood-glue mix layer can be calculated as follows:

$$P_{air} = \frac{\rho_{air} R T_m}{M_{air}} \qquad (6\text{-}22)$$

where ρ_{air} is the air volume density, R is the universal gas content (8.31 J/mol*K), M_{air} is the air molecular weight (29.0 g/mol), and T_m is the temperature of the wood-glue mix. Note that ρ_{air} is generally dependent on the void space and lateral air permeability of the wood-glue mix layer. Due to the relative large lateral permeability of air during pressing, ρ_{air} can be assumed to stay unchanged with an average value of 1 kg/m^3. Further, based on the definition of relative humidity of wet air, vapour pressure P_v can be calculated by:

$$P_v = RH * P_{sat} \qquad (6\text{-}23)$$

where RH is the relative humidity, and P_{sat} is the saturated gas pressure (Pa). Since the wood-glue mix layer has a high MC concentration, the RH can be assumed constant (100%) during pressing. Note that P_{sat} is only dependent on the temperature of the wood-glue mix layer T_m with the following relationship:

$$P_{sat} = \exp\left\{53.421 - \frac{6516.3}{T_m} - 4.125 \ln T_m\right\} \qquad (6\text{-}24)$$

where T_m is the absolute temperature (K) of the wood-glue mix layer. Equation (6-24) is normally given in a standard steam table (Siau 1995). As a result, gas pressure P_g can be estimated.

The degree of glue cure is the ratio of the mass of cured glue to the initial mass of uncured glue. The general equation from Dai and Yu (2004) was adopted as follows:

$$\frac{d\alpha}{dt} = Ae^{-\frac{\Delta E}{RT}}(1-\alpha)^n \qquad (6\text{-}25)$$

where α is the degree of glue cure, t is the pressing time (s), n is the order of chemical reaction, A is the collision factor (1/s) and ΔE is the activation energy (J/mol) which can be obtained through experiments and R is the universal gas constant, namely, 8.315 J/mol$\cdot k$.

6.4.3 Mass Transfer

6.4.3.1 Veneer layer

During plywood/LVL hot-pressing, the mass of each veneer layer will increase due to the migration of MC from the wood glue mix layer. The veneer density ρ_v, according to the definition, can be written as:

$$\rho_v = \frac{M_v}{V_v} \qquad (6\text{-}26)$$

Here, M_v and V_v are the mass and volume of the veneer layer, respectively. Since the veneer density changes with the pressing time, we can take its derivative against the pressing time (t) as shown below:

$$\frac{d\rho_v}{dt} = \frac{d}{dt}\left(\frac{M_v}{V_v}\right) = \frac{1}{V_v}\frac{dM_v}{dt} + \left(-\frac{M_v}{V_v^2}\right)\frac{dV_v}{dt} \qquad (6\text{-}27)$$

Two factors are attributed to the density change for the veneer layer. One is the absorption of MC from glue; the other is the volume change of the veneer layer during pressing. On the right side of Equation (6-27), the first term represents the density change due to the change of veneer mass; the second term indicates the density change due to the change in the veneer layer volume from pressing. The differential equation for these two changes in veneer density can be expressed as:

$$\Delta\rho_v = \Delta\rho_{v,m} + \Delta\rho_{v,v} \qquad (6\text{-}28)$$

$\Delta\rho_{v,v}$ can be derived based on the experimentation on veneer compression in the previous Chapter 5. $\Delta\rho_{v,m}$ is an increase of MC in the veneer layer which results from the decrease in MC from the wood-glue mixture layers. The value can be derived from the mass balance equation of the wood-glue mix layer in the next section.

6.4.3.2 Wood-glue mix layer

The mass of the wood-glue mix is the sum of mass of both wood interphase and glue. The latter also comprises glue solid and MC. After spreading glue onto the veneer ply, a portion of MC from glue is absorbed by the veneer ply. That is, before pressing, the MC in the veneer ply has already increased. The other portion of MC from the glue gradually migrates into the veneer layer during pressing. This forced migration can be expressed by the following modified Fick's law:

$$\frac{dW\rho_m}{dt} = -K_{diff}\,(W\rho_m - W\rho_v) - \dot{m}_i \qquad (6\text{-}29)$$

K_{diff} is defined as the effective diffusivity of MC, which can be determined through experiments (Incropera and Dewitt 1990), and $\dot{m}_i$ is the mass leaking term in the lateral direction. In Equation (6-29), $W\rho_m$ refers to the water potential or mass of water in a unit volume of wood-glue mix. In this unit, water, wood and glue solids co-exist.

Parameter $W\rho_v$, the water potential in the veneer layer, can be expressed as:

$$W\rho_v = \rho_{veneer,dry} * MC \qquad (6\text{-}30)$$

where $\rho_{veneer,dry}$ is the veneer dry density. For each veneer layer,

$$\rho_{veneer,dry,i} = \frac{\rho_i}{1+MC_i} \qquad i = 1, 2, \ldots, n \qquad (6\text{-}31)$$

where ρ_i and MC_i are density and MC of the i^{th} veneer layer. So Equation (6-31) can be rewritten to be a difference equation as follows:

$$W\rho_{m,i}^{k+1} = W\rho_{m,i}^{k} - K_{diff}(W\rho_{m,i}^{k} - W\rho_{v,i}^{k})\,\Delta t - K_{diff}(W\rho_{m,i}^{k} - W\rho_{v,i+1}^{k})\,\Delta t - \dot{m}_i\,\Delta t \qquad (6\text{-}32)$$

In Equation (6-32), the superscript k means the previous time and k+1 present time.

To estimate the effective diffusivity, 120 aspen veneer sheets (0.86 x 0.61 -m or 34 x 24 -in) were prepared with an average MC of 5%. Eight 13-ply aspen LVL billets were pressed without heat at 1.21 MPa (175 psi) platen pressure for 20 min. Before pressing, the weight of each veneer sheet was measured, then the 2^{nd}, 7^{th} and 12^{th} veneer ply were passed through the glue spreader (water only) to gain 35 - 45 g of water each. After pressing, the weight of each veneer ply was

measured again. As shown in Figure 6.7, the absorbed water from the dry veneer did not cause any noticeable moisture migration. Instead, it was the free water gained from the glue application, the main source of water potential, that caused moisture migration during pressing. In general, the moisture migration from the wetted veneer ply was limited to its adjacent plies. Since the percentage of moisture migration to each adjacent ply was about 20% after pressing for 20 min, the equivalent K_{diff} was approximately $1.67*10^{-4}$ /s.

6.5 Modeling of Panel Densification

During veneer compression, a simple relationship exists as follows for total strain or compression ratio (CR) if there is no glue applied and the mass of the veneer stays unchanged before and after compression:

$$\varepsilon_{total} = \frac{h_0 - h}{h_0} = \frac{V_0 - V}{V_0} \approx \frac{\frac{M}{\rho_0} - \frac{M}{\rho}}{\frac{M}{\rho_0}} = 1 - \frac{\rho_0}{\rho} \qquad (6\text{-}33)$$

where h_0, V_0 and ρ_0 are initial veneer thickness, volume and density, respectively; and h, V, and ρ are thickness, volume and density after compression, respectively; M is the veneer mass. Equation (6-33) indicates that the veneer compression is affected by initial veneer density, and panels assembled with higher density veneer are more difficult to be compressed.

During plywood/LVL hot-pressing, the platen pressure is generally kept constant. Under this constant pressure, panel thickness decreases with a certain level of densification. The first thickness reduction is due to the well-known thermo-hydro softening resulting from the combined effect of veneer temperature and MC on veneer compression *E*; the second thickness reduction arises from the veneer viscoelastic (creep) behaviour. The reduction of total panel thickness, namely total strain change, is the sum of both by taking into account of springback as shown below:

$$\varepsilon_{total} = \varepsilon_p + \varepsilon_v = (1 - S_t) * \varepsilon + \varepsilon_v \qquad (6\text{-}34)$$

where ε is the strain change from thermo-hydro softening before springback, ε_p is the irrecoverable strain (after springback) from thermo-hydro softening; ε_v is the strain change due to creep; and S_t is the springback ratio. As demonstrated in Chapter 5, veneer thickness recovery and springback ratio were different in terms of the stage of compression, temperature and MC.

6.5.1 Panel Compression due to Thermo-Hydro Softening

As demonstrated in Chapter 5, through systematic veneer compression tests, the compressive stress-strain relationship was established at different combinations of density, temperature and MC, and the prediction models were developed for veneer compression E and yield stress. Based on the strain-stress relationship established in Chapter 5, for the first region with the strain up to the yield point ($0 < \varepsilon < \varepsilon_Y$ and $0 < \sigma < \sigma_Y$), we have

$$\varepsilon = \frac{\sigma}{E} + \varepsilon_0 (1 - e^{-\frac{\sigma}{\sigma^*}}) = \frac{\sigma}{E} + 1.05 * (\varepsilon_R - \frac{\sigma_R}{E})(1 - e^{-\frac{3\sigma}{\sigma_R}}) \qquad (6\text{-}35)$$

where σ is the applied stress; E is the veneer compression modulus, which is the function of density, temperature and MC; σ_R is the threshold stress, which is also dependent on temperature and MC; and ε_R is the strain caused by veneer surface roughness, which can be determined under the threshold stress. Note that for any given veneer, the average ε_R is known from the compression tests. Equation (6-35) is used to determine whether the compression stays within the first region or exceeds the first region.

For the second region with the strain beyond the yield point ($\varepsilon_Y < \varepsilon < \varepsilon_u$ and $\sigma_Y < \sigma < \sigma_u$), we have

$$\varepsilon = \varepsilon_Y + \Delta\varepsilon = \varepsilon_Y + \frac{\sigma - \sigma_Y}{E} + \alpha(\sigma - \sigma_Y)^n \qquad (6\text{-}36)$$

where ε_Y is the yield strain with an average of 0.205 for aspen veneer as demonstrated in Chapter 3 (Figure 3.19); α and n are coefficients, determined by fitting the stress-strain curves from the compression tests; and σ_Y is the yield stress, which is the function of density, temperature and MC, as demonstrated in Chapter 5.

Equations (6-35) and (6-36) indicate that the compression strain of any veneer ply due to thermo-hydro softening can be determined based on the work performed in Chapters 3 and 5.

6.5.2 Panel Compression due to Creep

As discussed in Chapter 5, veneer creep strain is dependent on the applied pressure and its own viscous coefficient. Since the latter also changes with the pressing time, a curve fitting technique

is generally used to describe the relationship between the creep strain and time in terms of the applied pressure such as (Bodig and Jayne 1982):

$$\varepsilon_v = \beta t^m \tag{6-37}$$

where β and m are coefficients, which were determined from the creeping experiments. Therefore, the total strain of any veneer ply at any pressing time can be expressed as follows:

$$\varepsilon_{total} = \varepsilon_p + \varepsilon_v = (1 - S_t) * [\frac{\sigma}{E} + 1.05 * (\varepsilon_R - \frac{\sigma_R}{E})(1 - e^{-\frac{3\sigma}{\sigma_R}})] + \beta t^m \tag{6-38}$$

for the strain in Equation (6-35) up to yield point, or

$$\varepsilon_{total} = \varepsilon_p + \varepsilon_v = (1 - S_t) * [\varepsilon_Y + \frac{\sigma - \sigma_Y}{E} + \alpha(\sigma - \sigma_Y)^{n'}] + \beta t^m \tag{6-39}$$

for the strain in Equation (6-35) beyond the yield point.

Note that the temperature and MC of each veneer ply at any pressing time are known by solving the heat and mass transfer equations during hot pressing. With known temperature and MC, the parameters such as veneer compression E, springback ratio S_t, threshold stress σ_R and yield stress σ_Y in Equations (6-38) and (6-39) can be determined. At different combinations of veneer density, temperature and MC, the threshold stress σ_R was determined based on the schematic veneer compression experiments described in Chapter 5 (Table 5.3). The coefficients β and m were platen pressure σ dependent. They might also be affected by veneer temperature and MC. However, compared to the strain caused by thermo-hydro softening, the creep strain caused by elevated veneer temperature and MC on could be relatively small. Hence, it was assumed that the creep strain was mainly affected by platen pressure. The coefficient n' is less temperature and MC dependent whereas coefficient α changes with temperature and MC. Therefore, the change of thickness of each veneer ply at any time step during hot-pressing can be determined as:

$$h_i = (1 - \varepsilon_{total,\,i}) * h_{0,i} \qquad i = 1, 2, \ldots, n \tag{6-40}$$

where $\varepsilon_{total,\,i}$ is the total strain of i^{th} veneer ply; $h_{0,i}$ is the original thickness of i^{th} veneer ply; and n is the total number of veneer plies in the panel. At each time step, the total panel thickness can be written as:

$$h_{panel} = \sum_{i=1}^{n} h_i \qquad (6\text{-}41)$$

In the meantime, the density of each veneer ply at any time step can be determined as follows:

$$\rho_i = W_i / (S^* h_i) \qquad i = 1, 2, \ldots, n \qquad (6\text{-}42)$$

where W_i is the mass of i^{th} veneer ply and S is the area of panel pressed. With this veneer density, the heat conductivity can be updated for recalculating the key parameters such as temperature, MC and gas pressure.

6.6 Typical Prediction Results

6.6.1 Development of VPress® Model

A practical and user-friendly computer simulation model, VPress®, was developed for plywood/LVL hot pressing. The structure of the model is composed of the two major components: a user interface and a finite difference method (FDM) solver. The user interface, as shown in Figure 6.8, defines all the inputs to run the model and allows users to monitor the evolution of key parameters such as temperature, MC, density, and gas pressure at any time step. The FDM solver contains all the calculation algorithms described in Sections 6.4 and 6.5. To solve the complex problem, a modular approach is used for the FDM solver. The pressing process is simulated by the consecutive execution of modules describing various physical, chemical and mechanical phenomena (i.e., heat and mass transfer, glue cure and densification). The modular nature of the proposed model allows for flexible incorporation of any changes that need to be implemented in the future.

6.6.2 Model Input and Output

The input variables for running the model include variables defining panels, boundary conditions and glue parameters, variables defining each layer (veneer ply) and variables controlling the pressing cycles. The predictable variables include the temperature, gas pressure and MC at each individual veneer ply and glueline, and panel density profile. The key feature of the VPress® model is to predict the pressing time needed for the innermost glueline to reach a target temperature to cure the glue, and subsequently control the entire hot-pressing process. Once users specify a target temperature for the innermost glueline of desired plywood/LVL products, the model runs to the required pressing time and then automatically switches to the pre-defined

decompression cycle. This feature helps the users to conduct sensitivity studies of main variables on pressing time, and in turn, manufacturing productivity. The model is also capable of predicting the temperature changes of different locations of veneer plies and wood-glue mix layers (gluelines). Furthermore, the model also provides an option to use pressing time to control the pressing process before the decompression cycle starts.

6.6.3 Model Prediction

6.6.3.1 Temperature

13-ply aspen LVL was chosen as an example with all input parameters defined in Figure 6.8. As shown in Figure 6.9, the temperature rising curves of 13-ply aspen LVL at the second glueline (N4) and the sixth glueline (N12) are predicted. Figure 6.10 compares the temperature curves for the three veneer plies and their associated gluelines. For the same number in the sequence, the temperature of the veneer ply was higher than that of the glueline. Note that the 6^{th} glueline was the innermost whereas the 7^{th} veneer ply was the centre core. The temperature of the 6^{th} glueline was slightly higher than that of the 7^{th} veneer ply. In the 13-ply LVL manufacturing, the pressing productivity was mainly determined by the temperature of the 6^{th} glueline rather than that of the 7^{th} veneer ply.

6.6.3.2 Gas pressure and MC

Figure 6.11 compares the prediction of gas pressure at the three locations of gluelines. The gas pressure at the 1^{st} glueline was higher than that at the 3^{rd} and 6^{th} gluelines, which is mainly due to the difference in temperature. Figure 6.12 shows the prediction of veneer MC at the three veneer plies. Due to the dispersion of MC from the glue and limited evaporation of vapour during hot pressing, veneer MC increased with the surface ply being lower than the inner plies and core. Note that the MC of the surface ply reached a plateau more quickly than that of other plies.

6.6.3.3 Effect of platen pressure on temperature and gas pressure

Since plywood/LVL hot pressing uses a constant pressure control, it is interesting to use the model to examine how the platen pressure affects temperature rising and gas pressure. Figures 6.13 and 6.14 show the effect of platen pressure on temperature and gas pressure of the innermost glueline for 13-ply aspen LVL, respectively. The four platen pressure levels used in the comparison were 1.21, 1.38, 1.55 and 2.0 MPa. Within this range, higher platen pressure

resulted in shorter pressing time required for the innermost glueline to reach a target of 105°C for a full cure of glue; however, higher platen pressure would also lead to higher gas pressure in the innermost glueline due to increased temperature and reduced permeability from higher compression. In general, high gas pressure is not desirable during plywood/LVL hot pressing due to the high tendency of blisters and blows upon press opening. Note that based on the prediction (Figure 6.13), the difference in pressing time between the two pressure levels, 1.21 MPa and 2.0 MPa, was about 80 s, which means an approximate 6.7% difference in manufacturing productivity. However, at the 2.0 MPa platen pressure, the resulting final panel thickness was only 33.0 mm (1.30 -in) compared to 37.5 mm (1.48 -in) at the 1.21 MPa platen pressure. The thin panel is also not desirable since it does not meet the thickness tolerance of the final product. Therefore, to balance manufacturing productivity (pressing time), material recovery (panel thickness) and panel quality (rate of blisters/blows), the platen pressure should be optimized during plywood/LVL hot pressing.

6.6.3.4 Effect of panel size on temperature and gas pressure

Another key feature of the model is to allow examine the effect of panel size on panel internal conditions such as temperature and gas pressure at the innermost glueline. Note that the panels made in the laboratory are generally smaller than those made in the mill due to the size limitation of the press. In plywood/LVL manufacturing, a minimum panel length of 2.44 m (96 -in) is commonly used. During simulation, veneer MC used was 5% and platen pressure was 1.21 MPa (175 psi). Figure 6.15 shows the comparison of temperature rising at the innermost glueline between 0.86 x 0.61 -m (34 x 24 -in) and 2.44 x 1.22 -m (96 x 48 -in) panels from the simulation. It demonstrates that compared to the small panel, the larger panel resulted in a slightly higher temperature at the innermost glueline. This was the net result from less energy leaking and more mass to heat with the larger panel.

Figure 6.16 shows the comparison of gas pressure at the innermost glueline between 0.86 x 0.61-m (34 x 24 -in) and 2.44 x 1.22 -m (96 x 48 -in) panels from the simulation. It demonstrates that compared to the small panel, the larger panel also resulted in a higher gas pressure at the innermost glueline. This was mainly due to less mass leaking in the lateral direction with the larger panel. As a result, the model developed offers a powerful tool to help analyze the effect of the key pressing variables for hot pressing optimization.

6.6.4 Model Validation

As we know, numerical models are an approximation of reality in which many assumptions have been made to obtain the solution. An often neglected part of the modeling process is model validation (or verification). To validate the model, one needs to compare the predictions of the numerical solution with those of an analytical solution. This usually requires choosing a set of simplified conditions for which an analytical solution exists. A common heat transfer problem for which an analytical solution exists is that of the heat flow into a semi-infinite plate with an isothermal boundary condition (Smith 2006). The analytical solution to the problem is:

$$\frac{T(x,t)-T_s}{T_0-T_s} = erf\left(\frac{x}{2\sqrt{\alpha t}}\right) \qquad (6\text{-}43)$$

where T_s is the surface temperature (°C);

T_0 is the initial temperature (°C);

T(x, t) is the temperature at time t with a distance of x above the lower plate (°C);

erf (z) is the error function encountered in integrating the normal distribution defined by:

$$\text{erf}(z) = \frac{2}{\sqrt{\pi}}\int_0^z e^{-t^2}dt = \frac{2}{\sqrt{\pi}}\left(z-\frac{1}{3}z^3+\frac{1}{10}z^5-\frac{1}{42}z^7+\frac{1}{216}z^9+\cdots\right)$$; and

α is the thermal diffusivity which is given by $\frac{k}{\rho C_p}$, where k is the conductivity, ρ is the density and C_p is the specific heat.

By rearranging, we have (Smith 2006):

$$T(x, t) = (T_0 - T_s)\,\text{erf}\left(\frac{x}{2\sqrt{\alpha t}}\right) + T_s \qquad (6\text{-}44)$$

To validate the heat transfer model, we need to match boundary conditions of the numerical solutions with those for which the analytical solutions exist. Therefore, for the numerical simulation of the plywood/LVL hot pressing, only one lower platen was assumed heated, i.e., T_s and T_0 were chosen as 150°C and 20°C, respectively. Veneer density was 400 kg/m^3 and veneer MC was selected as 5% to calculate veneer conductivity (k) and specific heat (C_p) following Equations (6-15) and (6-16), respectively. Normally, dry veneer thickness (1/8 -in thick) was about 3.25 mm, hence x was chosen as 1.63 mm (a half of the veneer thickness) and 3.25 mm (about the center of wood-glue mix layer) from the heated lower platen.

Figure 6.17 compares the predictions of the numerical solution with those of an analytical solution for 13-ply LVL hot pressing with one platen being 150°C (heated) and the other being 20°C (unheated). For a distance of 1.63 mm from the heated platen, the two solutions agreed very well. For a distance of 3.25 mm from the heated platen, the temperature of an analytical solution was only slightly higher than that of a numerical solution. The discrepancy is mainly due to the fact that the analytical solution did not take the glue spread and panel densification into account.

Secondly, to validate the mass transfer during plywood/LVL hot pressing, one simple case, i.e., panel cold pressing, was taken. For 13-ply LVL, veneer original MC was 5% and a glue spread level was 160 g/m^2. The model was used to predict temperature and MC change of veneer inner plies and surface plies. As shown in Figure 6.18, the temperature of all veneer plies was the same as the ambient temperature (20°C), whereas veneer MCs for the surface plies and inner plies were quite different. It is true that the veneer gains MC from the glue during cold pressing (see Figure 6.7). In general, only one glueline contributes to the MC increase of each of the two surface plies whereas two gluelines contribute to the MC increase of each of the eleven inner plies. Since there is no MC loss from the cold pressing, the MC of surface plies increased from 5% to about 8% whereas the MC of inner plies increased from 5% to about 11.5%. This indicates that during plywood/LVL pressing, the veneer MC gained from glue is normally greater than veneer original MC, which would have a significant effect on heat and mass transfer, as demonstrated in Figure 1.6.

To further validate the model, one hundred and fifty 0.86 x 0.61 -m (34 x 24 -in) aspen veneer sheets were cut with an average MC of about 5%. The reason to use small sheets was to accommodate the size of hot press (35 x 35 -in). For each veneer sheet, the thickness, length, width and weight were measured. Veneer sheets were then sorted-out based on the density groups (high, medium, low and random). Ten LVL panels were prepared with different experimental variables. As an example, 13 veneer sheets were selected as the low density group with an average density of 0.40 g/cm^3 to make a 13-ply aspen LVL panel. The glue spread was 160 g/m^2 per single glueline (all the other conditions were the same as the VPress® input in Figure 6.8). During hot-pressing, the 2nd and innermost glueline temperatures were measured by thermocouples and monitored by the PressMan® software. Figure 6.19 shows the comparison of

the temperatures at the 2nd and innermost gluelines between the model prediction and experiments. It can be seen that the model predictions of temperatures at the 2nd and innermost gluelines agreed well with the experimental temperature measurements. The other panels showed similar results.

Similar to non veneer-based wood composites such as OSB and MDF, vertical density profile (VDP) has a drastic effect on stiffness and strength of plywood/LVL products. Examining density formation helps understand the mechanism of panel densification and effect of hot-pressing strategies on panel performance (Wong 1999). Figure 6.20 shows the density profile (batch average) through the thickness of 13-ply aspen LVL with veneer density of 0.401 g/cm^3. Figure 6.21 shows the density profile change from the VPress® simulation at the two pressing times, namely 300s and 1100s. By comparison, it can be seen that the VPress® captured the trend of vertical density formation with the same magnitude of peak density in the glueline. The actual peak density of the gluelines was slightly lower than that from the prediction, which is mainly due to the misalignment of the gluelines from individual samples and/or a higher glue penetration into the veneer than assumed.

6.7 Conclusions

From this work, a hot-pressing simulation model, VPress®, was developed for the first time to simulate the heat and mass transfer and panel densification during hot pressing of veneer-based wood composites. By introducing wood-glue mix layers, the role and contribution of distinct gluelines to the heat and mass transfer during hot-pressing was quantified. This simulation model is capable of showing several important characteristics of the hot-pressing processes of veneer-based composites such as effect of glue spread level, veneer MC and density as well as pressing control parameters on heat and mass transfer and panel compression. The model can capture the trends of temperature, gas pressure, MC and panel density during hot pressing. Experiments were conducted using several different variables to validate the model. Specifically, the predicted temperature profiles of veneer plies and gluelines (especially at the innermost glueline) agreed well with the experimental measurements. Hence, the model can be used to evaluate the sensitivity of the key material and manufacturing variables on hot-pressing time (manufacturing productivity), panel compression (material recovery) and vertical density profile (panel stiffness). Once customized in industry, the model will allow users to optimize the production

balance between productivity, panel densification and panel quality or stiffness. This hot-pressing model is the first step to help further understand the plywood/LVL manufacturing processes and in turn to facilitate the optimization of the hot pressing process.

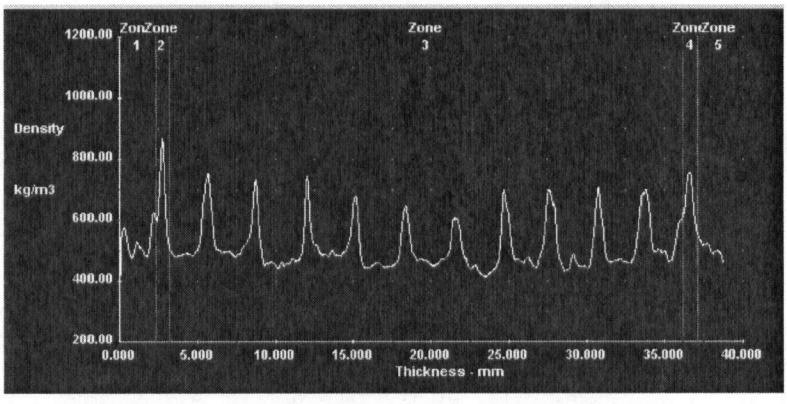

(a) An entire density profile with 12 gluelines

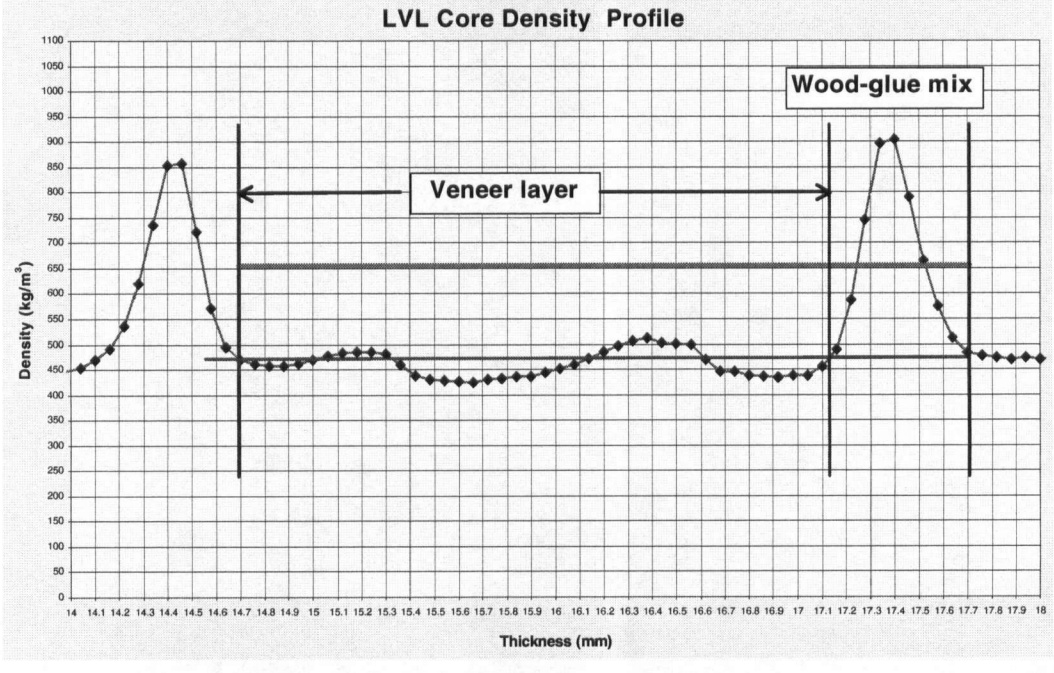

(b) An enlargement of the two gluelines

Figure 6.1 Typical LVL X-ray density profile

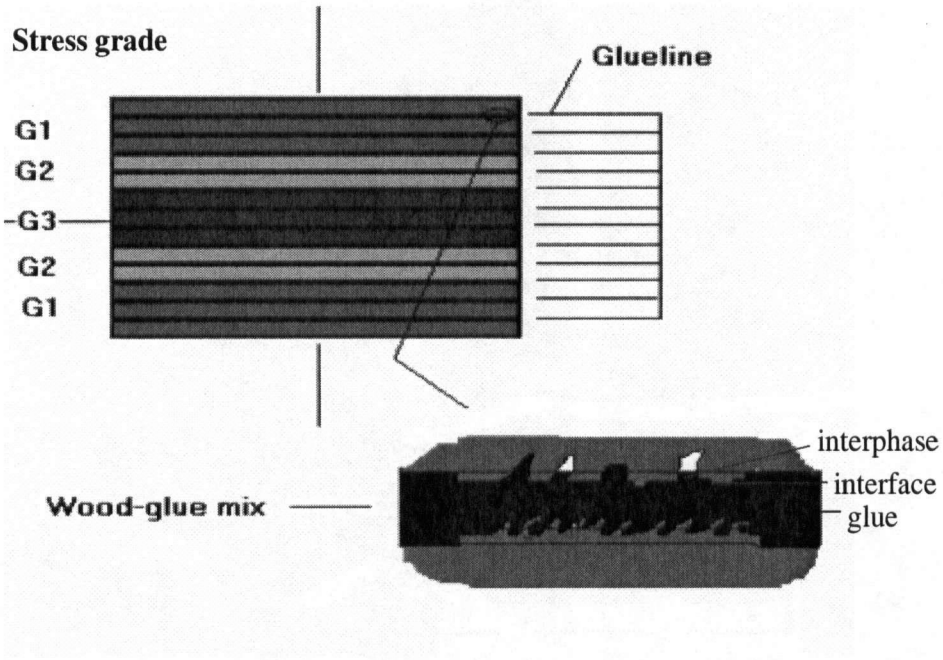

Figure 6.2 Defining glueline as wood-glue mix through the panel thickness

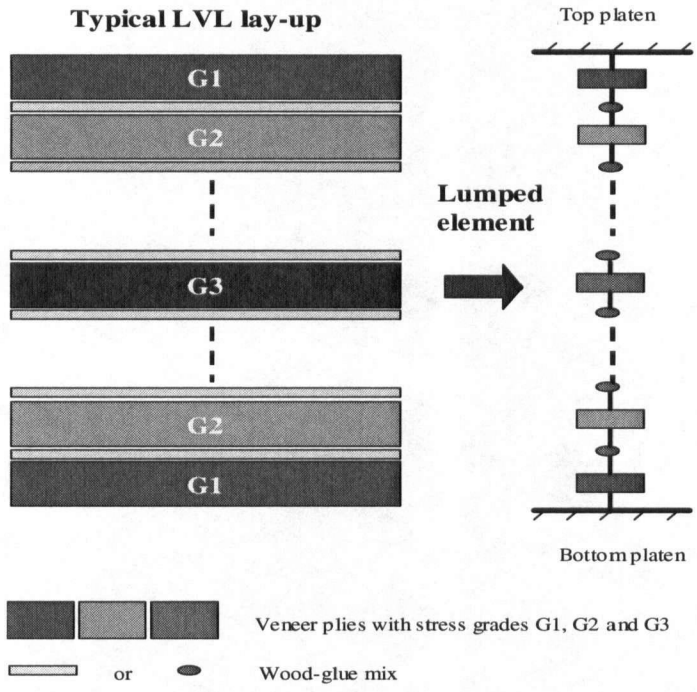

Figure 6.3 Conceptualizing a typical LVL lay-up as lumped elements

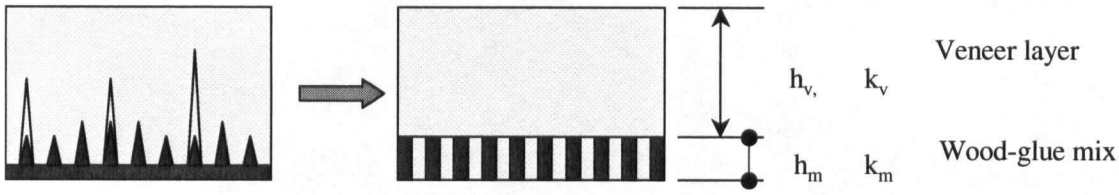

Figure 6.4 Modeling wood-glue mix as parallel layers of wood and glue to determine effective conductivity

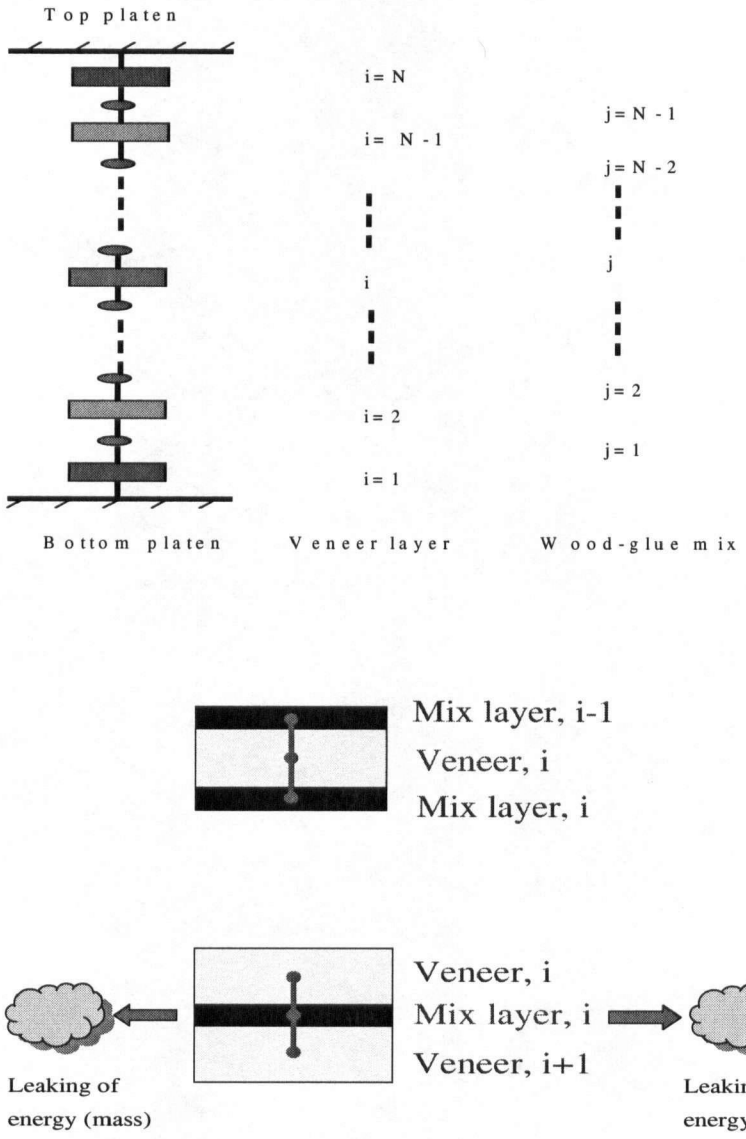

Figure 6.5 Discretization of veneer layer and wood-glue mix through the panel thickness

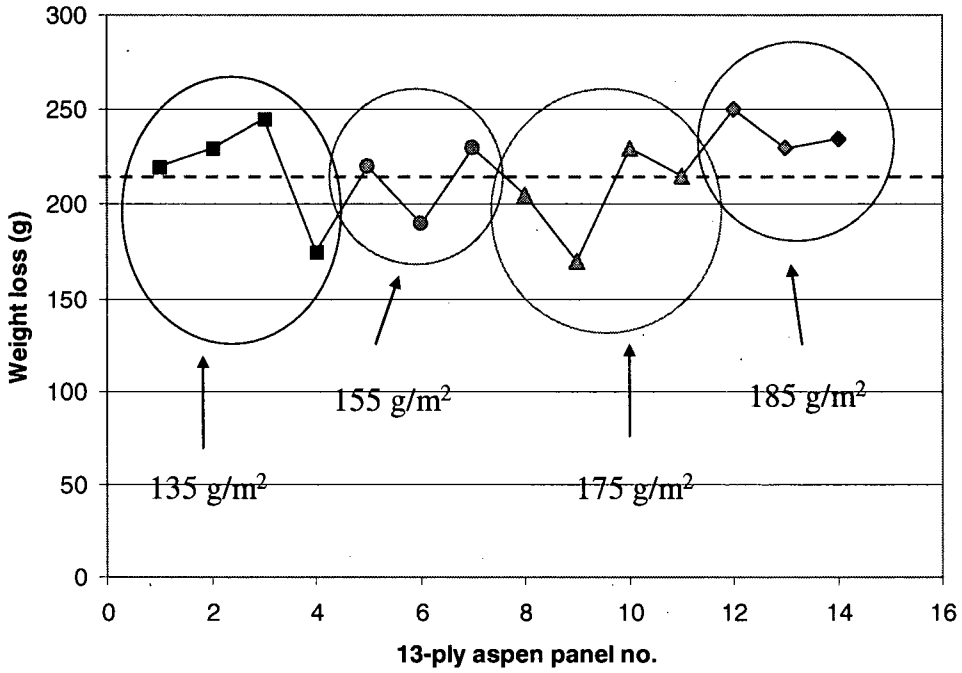

Figure 6.6 Weight losses of 13-ply aspen LVL after pressing with different levels of glue spread

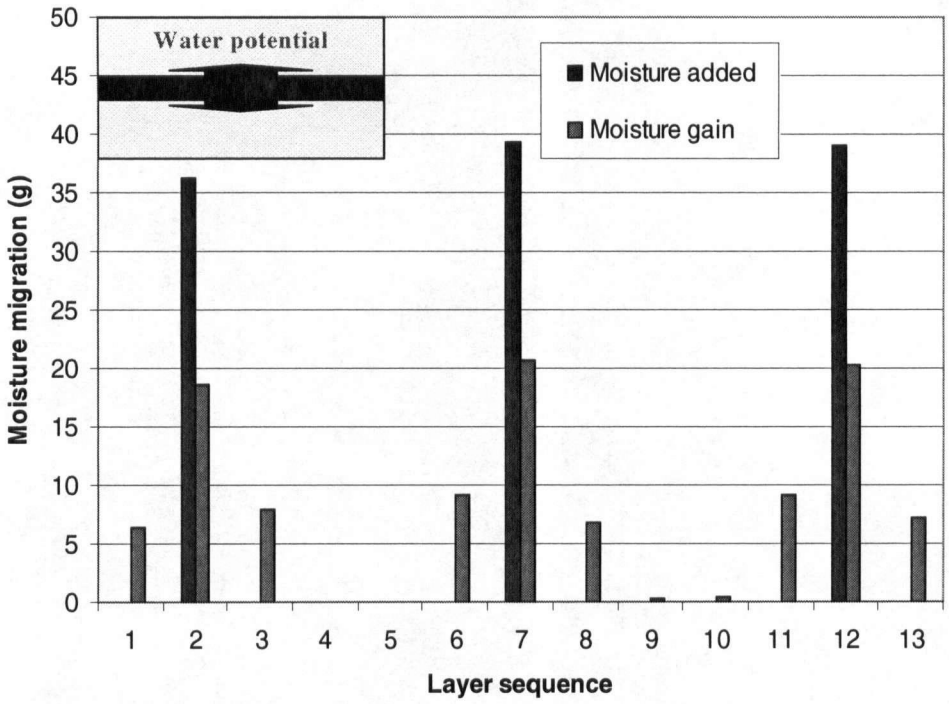

Figure 6.7 Moisture migration of 13-ply aspen LVL after cold pressing

a) Variables defining panel

b) Variables defining each veneer ply

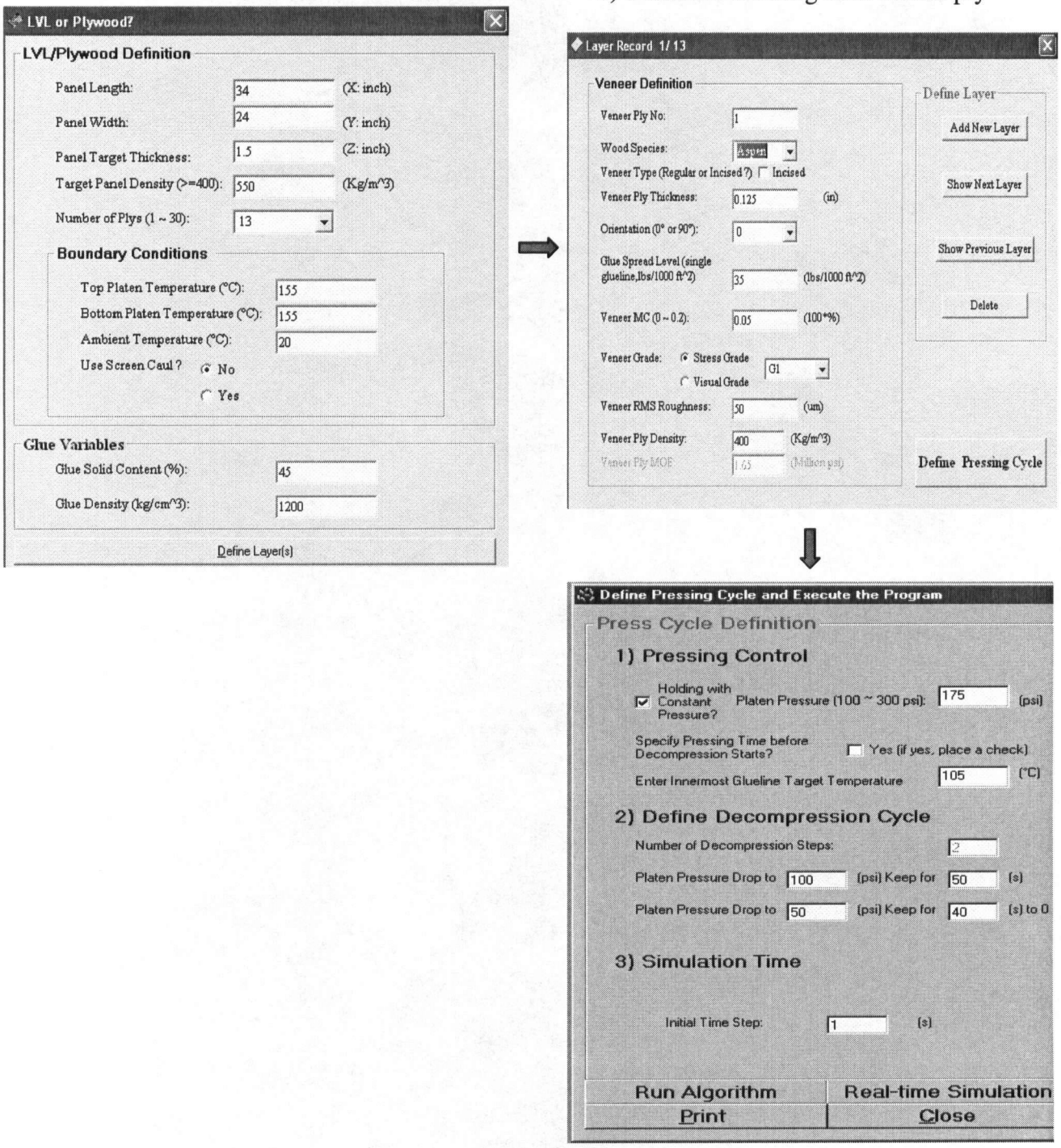

c) Variables defining pressing schedule

Figure 6.8 Input user interfaces of VPress® model

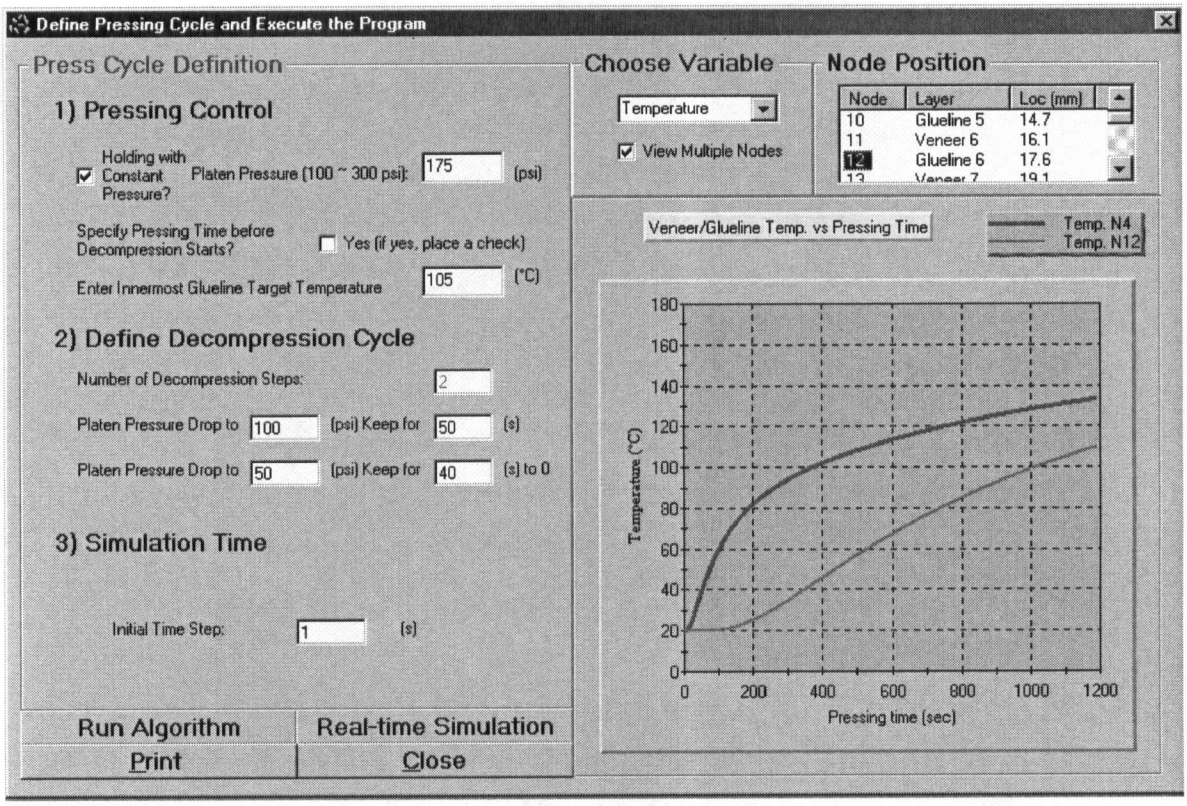

Figure 6.9 Prediction of temperatures at the 2nd and 6th gluelines

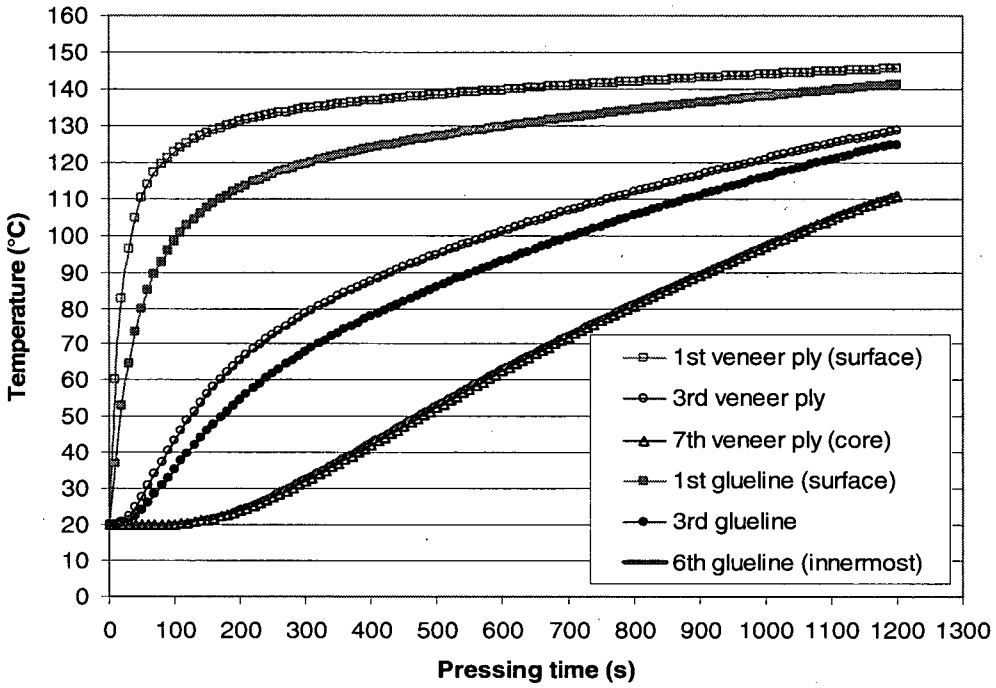

Figure 6.10 Prediction of temperatures of the three veneer plies and three gluelines

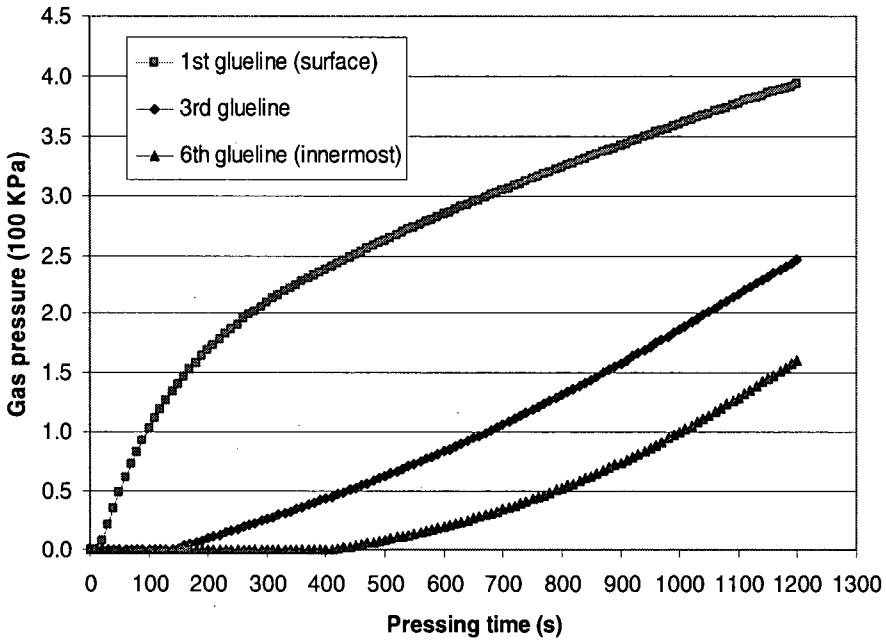

Figure 6.11 Prediction of gas pressure at the three locations of gluelines

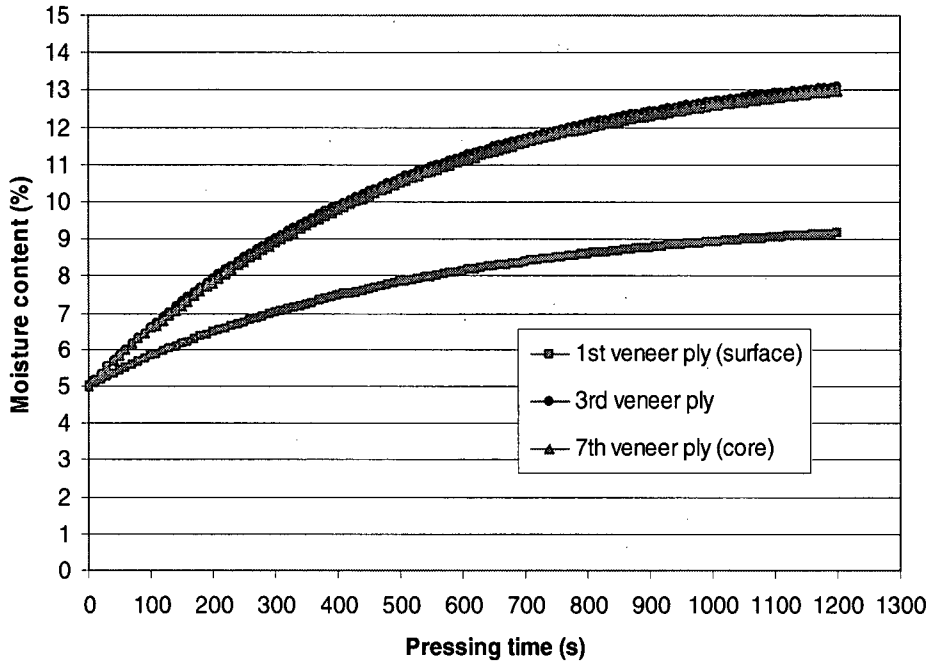

Figure 6.12 Prediction of veneer MC at the three locations of veneer plies

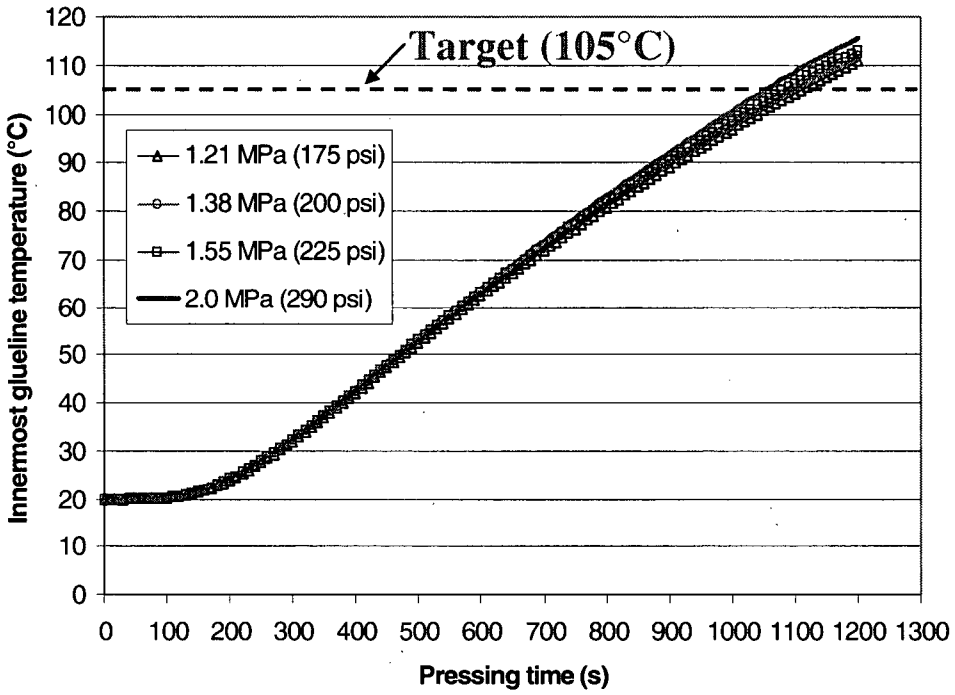

Figure 6.13 Predicted effect of platen pressure on the innermost glueline temperature

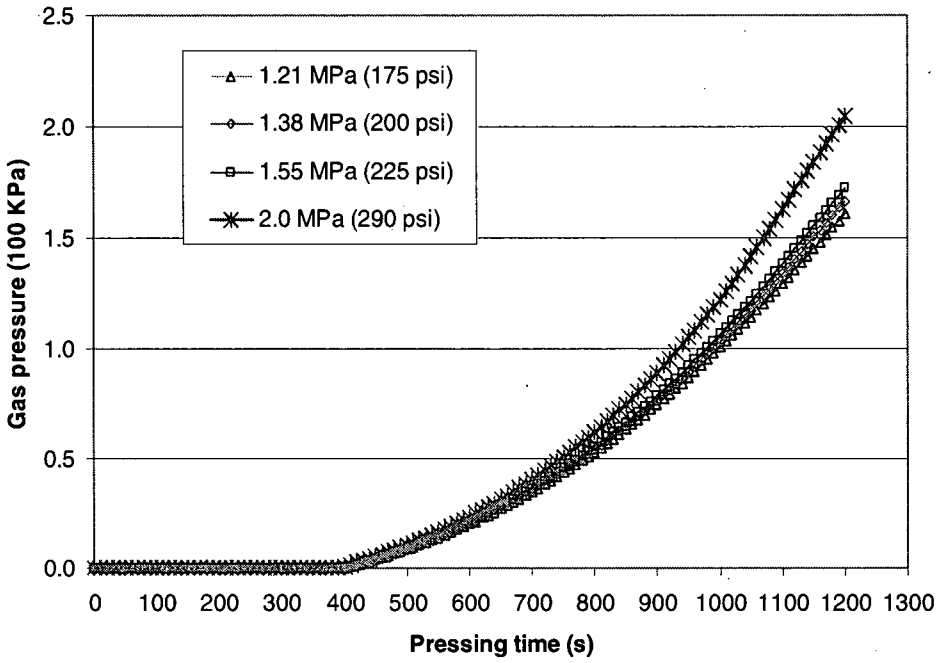

Figure 6.14 Predicted effect of platen pressure on gas pressure at the innermost glueline

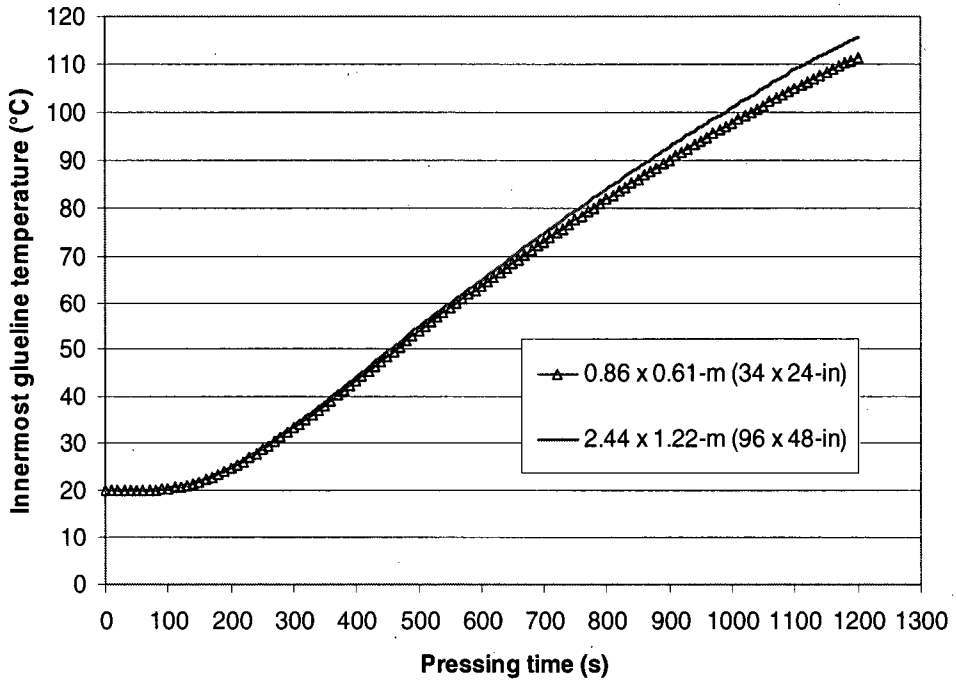

Figure 6.15 Predicted effect of panel size on the innermost glueline temperature

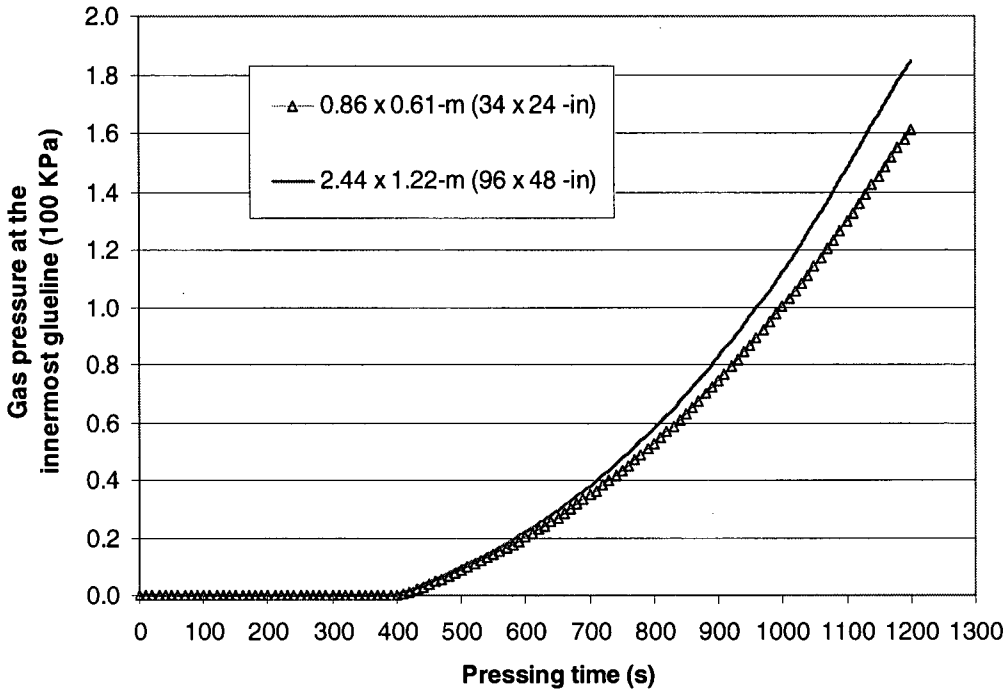

Figure 6.16 Predicted effect of panel size on gas pressure at the innermost glueline

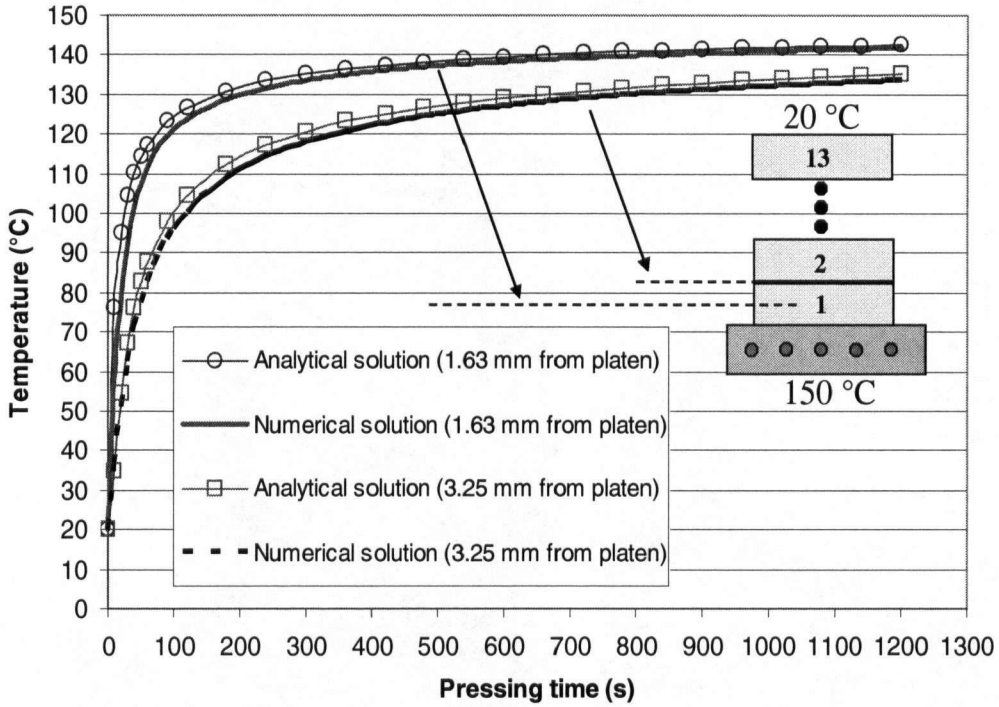

Figure 6.17 Comparison of a numerical solution with an analytical solution for heat transfer

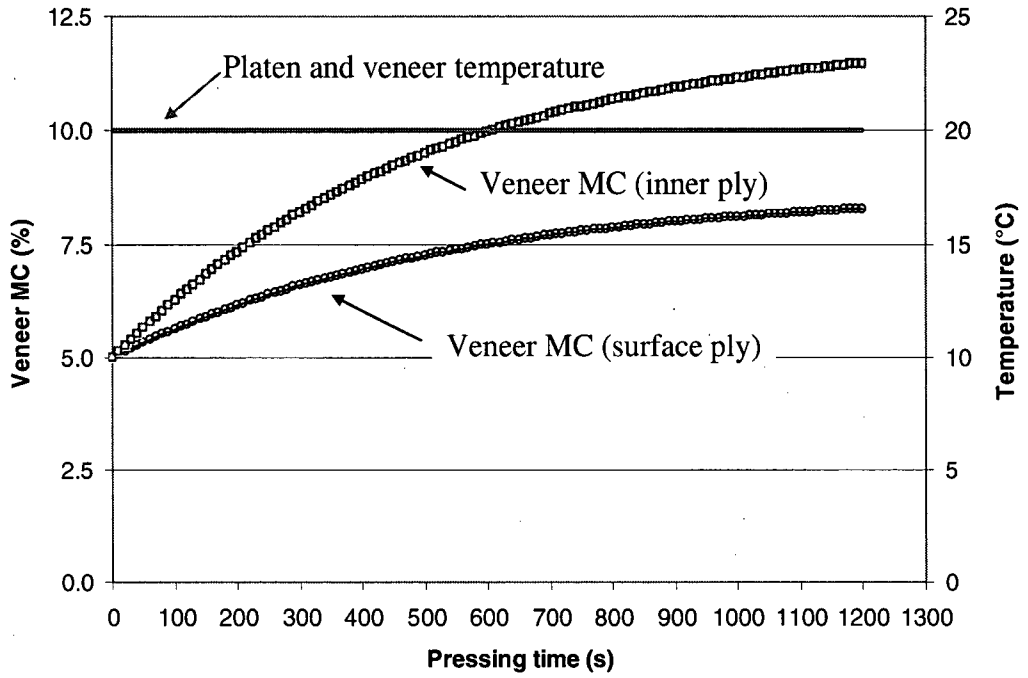

Figure 6.18 Predicted veneer temperature and MC from cold pressing

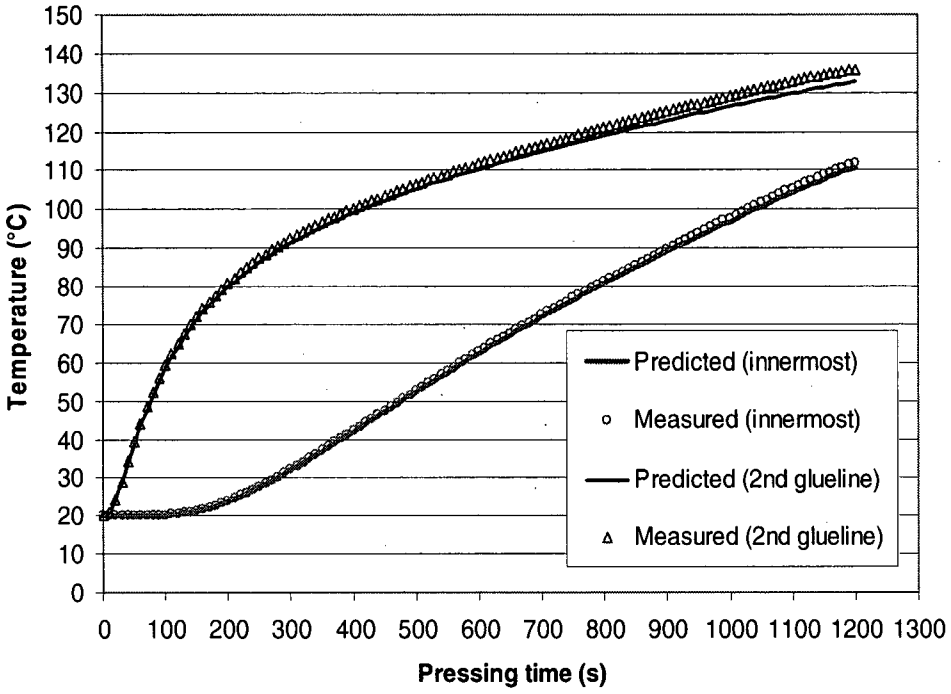

Figure 6.19 Comparison of temperatures at the 2nd and innermost gluelines

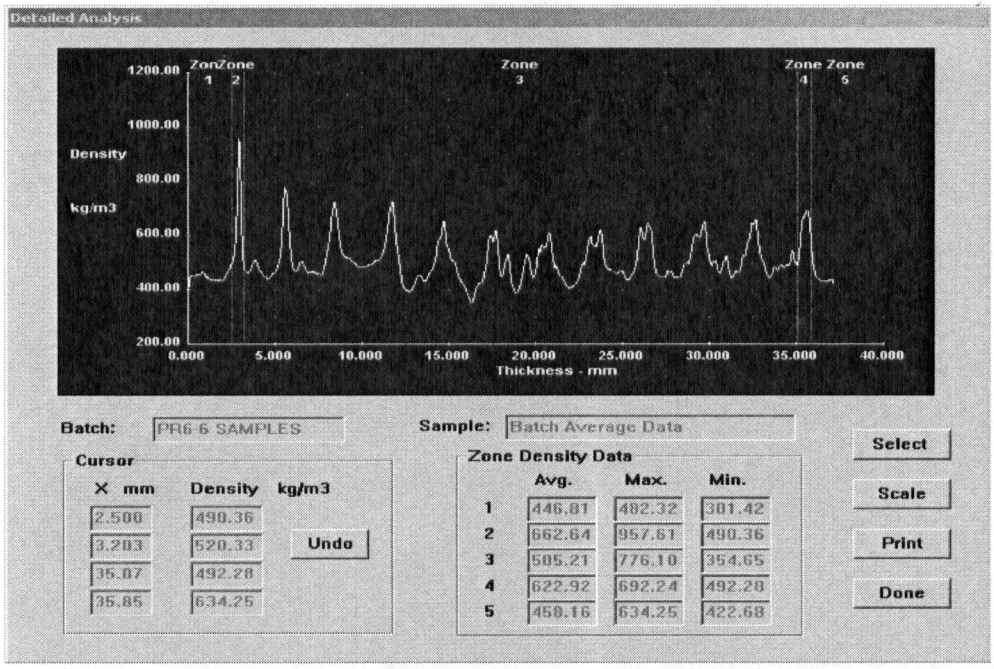

Figure 6.20 Density profile of 13-ply aspen LVL (batch average)

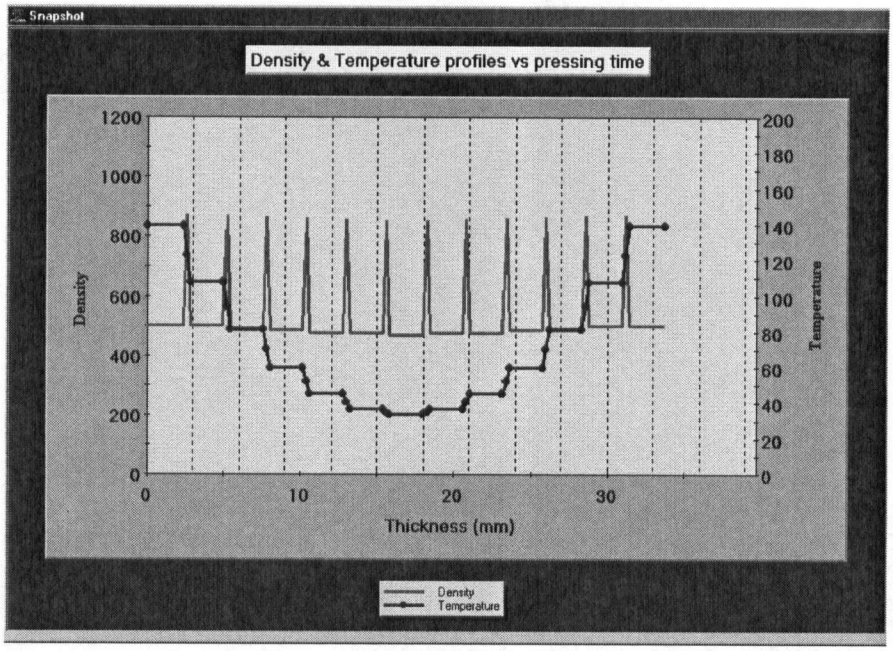

a) at 300 s

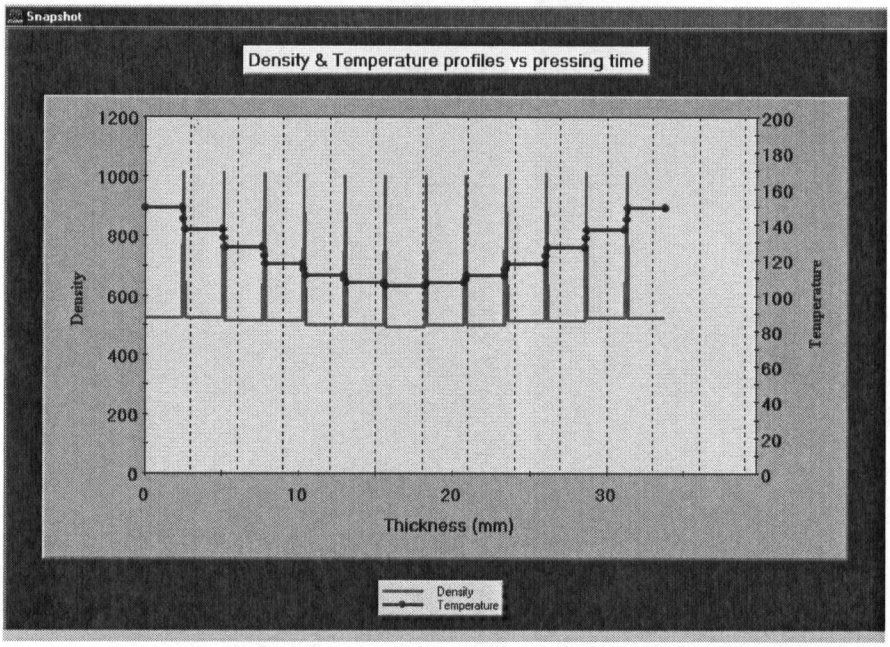

b) at 1100 s

Figure 6.21 Simulated density and temperature profiles with VPress®

6.8 Bibliography

Bolton, A. J. and P. E. Humphrey. 1994. The permeability of wood-based composite materials. Part 1. A review of the literature and some unpublished work. Holzforschung. 48: 95-100.

Dai, C. and C. Yu. 2004. Heat and mass transfer in wood composite panels during hot-pressing: Part I. A physical-mathematical model. Wood and Fibre Sci. 36(34): 585-597.

Gindl, W. 2001. SEM and UV-microscopic investigation of glue lines in Parallel PSL. Holz als Roh. 59: 211-214.

Incropera, F. P. and D. P. Dewitt. 1990. Fundamentals of heat and mass transfer. 3rd Edition. John Wiley & Sons, Inc. New York.

Kreith, F. and M. S. Bohn. 2001. Principals of heat transfer-6th edition. Pacific grove, CA 93950. USA. 700pp.

Okuma, M. 1976. Plywood properties influenced by the glueline. Wood Sci. and Tech. 10: 57-68.

Siau, J. F. 1995. Wood: Influence of moisture on physical properties. Department of Wood Science and Forest Products, Virginia Polytechnic Institute and State University. ISBN No: 0-9622181-0-3. 227pp.

Smith, G. 2006. Course note of Wood 341: Unsteady-state heat transfer. Dept. of Wood Science, The University of British Columbia.

Wang, B. J. 2001a. Characterizing aspen veneer for Plywood/LVL products Part 1: stress grades of veneer. Forintek Canada Corp. Report-2019 (5). 14 pp.

Wang, B. J. 2001b. Characterizing aspen veneer for Plywood/LVL products Part 2: pressing strategies and strength. Forintek Canada Corp. Report-2019 (6). 41 pp.

Wang, B. J. 2003. Hot-pressing behaviour of 5-ply Douglas-fir and spruce plywood. Forintek Canada Corp. Report-2019 (7). 28 pp.

Wang, B. J. and C. Dai. 2005. Hot-pressing stress graded aspen veneer for laminated veneer lumber. Holzforschung. 59(1): 10-17.

Wang, B. J. 2006. Experimentation on new method of plywood/LVL hot-pressing. Funded by Forest Innovation Investment (FII), B. C. Canada. Unpublished results.

Wellons, J. D., R. L. Krahmer, M. D. Sandoe and R. W. Jokerst. 1983. Thickness loss in hot-pressed plywood. Forest Prod. J. 33(1):27-34.

Wong, E. D. 1999. Effects of density profile on the mechanical properties of particleboard and fiberboard. Review article from author.

Zavala, D. 1986. Analysis of process operative within plywood during hot-pressing. Ph.D dissertation. Oregon State University.

Zavala, D. and P. Humphery. 1996. Hot pressing veneer-products: the interaction of physical process. Forest Prod. J. 46 (1): 69-77.

CHAPTER VII CONCLUDING REMARKS AND RECOMMENDATIONS

7.1 General Summary and Conclusions

The key objective of the present work was to understand the unique hot pressing behaviour of veneer-based wood composites such as plywood and LVL and then, for the first time, to develop a hot pressing simulation model. The main differences in constituent elements, panel structure and hot pressing behaviour between veneer-based and non veneer-based wood composites have been identified and analyzed. Several key issues in the plywood/LVL hot pressing processes have been tackled.

To determine the mechanism of heat and mass transfer during hot-pressing of veneer-based composites, the air permeabilities of the two basic constituent elements, veneer and glueline, were first characterized. Extensive experiments were conducted to investigate transverse air permeability of aspen veneer and phenol formaldehyde (PF) glueline as well as aspen plywood and strandboard. The laminate permeability theory was adopted to determine the relative contribution of the veneer and glueline to panel permeability. A concept of effective porosity was also proposed based on the classic Carman-Kozeny theory to explain the difference in panel permeability and resulting hot pressing behaviour. It was found that effective porosity was only 0.05-0.50% compared to 50 -70% of total voids in veneer panels, and veneer compression rather than curing gluelines served as the main barriers to gas and moisture movement during hot pressing. Furthermore, the relative magnitude of heat conduction and heat convection was quantified in which the heat convection contributed approximately only 1% to the total transfer of heat energy. As a result, during plywood/LVL hot pressing, the heat conduction is predominant and the heat convection is negligible.

To examine fundamentals of veneer-to-veneer contacts for bonding, aspen veneer transverse compression tests were conducted under ambient and controlled temperature and MC conditions in terms of veneer surface roughness, load applied and densification. Based on the experimental results, a revised wood transverse compression theory was proposed to include the first stage of "progressive contact", and a novel method was developed for assessing veneer surface roughness/quality on an area basis. This first stage of compression, largely overlooked in the previous studies with non veneer-based composites, was demonstrated to be essential in the

plywood/LVL manufacturing. Note that the first stage of compression from wood strands could also shed light on the manufacture of low density OSB. Through analyses of glue coverage under different loads, the veneer-to-veneer contact area was experimentally investigated. The minimum compression required for achieving adequate veneer-to-veneer contacts for bonding development was defined, and the true yield displacement or strain was established. With the revised wood transverse compression theory, the compression behaviour of wood constituent elements such as veneers and strands can be directly linked to the densification and performance of resulting panel products. Based on veneer surface roughness/quality and compressibility, the optimum panel densification was predicted and validated for performance plywood/LVL products. Furthermore, based on contact mechanics, classic Hertz theory and modified Greenwood and Tripp's theory, a theoretical model was developed to predict veneer-to-veneer contact area in terms of veneer surface roughness and compression. The model provides further understanding as to how veneer surface roughness and compression affect veneer-to-veneer bonding contacts in a 3-D domain.

To understand the mechanism of panel densification, the aspen veneer compressive stress-strain relationship was first established in terms of veneer surface roughness and density. A statistical model based on a response surface methodology (RSM) was then developed to predict veneer compression Young's modulus and yield stress with regard to veneer density, temperature and moisture content (MC). In addition, veneer creeping tests were conducted to determine the panel deformation due to viscous creep; and veneer loading and unloading tests were conducted to understand the springback behaviour of the veneer at different compression stages to determine the irrecoverable veneer deformation due to thermo-hydro softening. Finally, an analytical model was developed to describe the compressive stress-strain relationship in terms of veneer density, temperature and MC. For the first time, this model took into account the effect of veneer surface roughness for prediction of total panel densification during plywood/LVL hot pressing.

To develop a one-dimensional hot-pressing simulation model, the effect of the glueline on heat and mass transfer was determined. A concept of a wood-glue mix layer was proposed, and the effective conductivity was then modelled and determined. The theories of heat and mass transfer and solid mechanics were applied to develop the finite-difference based model in conjunction with the experimental results. The numerical solutions of the model were successfully validated with the analytical solutions and experimental results. The model is capable of predicting some

important physical and mechanical behaviour such as the changes of temperature and gas pressure for all veneer plies and gluelines through the panel thickness, and the formation of the vertical density profile during hot-pressing. The outcome of this research provides insight into how to optimize the plywood/LVL hot pressing processes for increased productivity and material recovery, and improved panel quality and performance.

7.2 Recommendations and Further Studies

The hot-pressing simulation model developed was based on an integrated approach through material characterization and theoretical analysis. In the present work, all experimental results were based on aspen veneer, a diffuse-porous hardwood with no obvious growth ring. For other species, due to their differences in cell structure such as rays and growth rings, the compression behaviour under ambient and controlled temperature and MC environments could be significantly different. To apply the model to the other species, further experimental work is needed to characterize their material behaviour for the model input. Insight into the mechanism of compressive deformation can be observed at the cell level directly with a scanning electron microscope (SEM). To improve the prediction of veneer-to-veneer contact area in terms of veneer surface roughness and compression, a study is needed to modify the existing theoretical contact model to consider the resin flow, plastic deformation and lateral expansion. The difference in compression behaviour and bonding contacts between parallel-ply veneer assembly (LVL) and cross-ply veneer assembly (plywood) should be further explored. The relationship between the contact area, actual bonding area and gluebond performance needs to be examined. The present study used only one loading rate (2 mm/min) for all compression tests and one density level for veneer viscous creeping tests. Further studies are needed to investigate the effect of loading (strain) rate on veneer compression modulus (E) and the effect of veneer density, temperature and MC on creep deformation (Bodig and Jayne 1982; Wolcott *et al.* 1990; Dai 2001).

Since veneer surface roughness has a drastic effect on the required panel compression ratio (CR), a better process control of log conditioning and veneer peeling is recommended to reduce veneer surface roughness. As well, it seems to be beneficial to sort veneer sheets based on surface roughness for making panels with different CRs. As a result, plywood thickness loss and glue

consumption could be significantly reduced for increased material recovery and reduced manufacturing cost.

Currently, panel delamination is the most urgent issue for plywood as a sub-flooring product resulting from a low percent wood failure. Based on this study, it appears so crucial that an optimum control of panel compression (or densification) should be addressed in the plywood/LVL production. In this way, adequate veneer-to-veneer bonding contacts can be achieved to help prevent panel delamination without increasing glue spread and sacrificing material recovery. However, bondability of veneers needs to be further studied. This study assumed bonding is only related to veneer surface contacts. Obviously, veneer surface properties are also very important as they can affect the bonding through their effects on glue penetration, wetting, spreading and even curing. By considering the surface bondability, one can factor into the model the effects of veneer temperature at glue application, assembly time and MC variations, and so on.

As the first step, the present work developed a one-dimensional plywood/LVL hot-pressing simulation model by considering an in-plane energy leaking term in the lateral direction. However, the actual hot-pressing process is very complex with coupled physical, chemical and mechanical changes. As well, this process involves many material variables, process variables and pressing control variables. To make the model prediction more accurate, it is deemed necessary to quantify the lateral (length or width) air permeability in terms of veneer location and compression. In this way, the in-plane convective energy transfer per unit volume can be more accurately determined as follows:

$$q_x = \rho_g c_g u_x \frac{\partial T}{\partial x} \qquad (7\text{-}1)$$

$$q_y = \rho_g c_g u_y \frac{\partial T}{\partial y} \qquad (7\text{-}2)$$

where q_x, q_y are the energy transfer in the length and width directions, respectively; T is the temperature, c_g is the specific heat of gas (a mixture of air and vapour), ρ_g is the gas volume density, and x and y are the unit dimension in panel length and width directions, respectively, and u_x and u_y are the air velocities in the length and width directions, respectively, which are given by:

$$u_x = \frac{K_x}{\mu}\frac{\partial P}{\partial x} \qquad (7\text{-}3)$$

$$u_y = \frac{K_y}{\mu}\frac{\partial P}{\partial y} \qquad (7\text{-}4)$$

where K_x and K_y are the air permeabilities of the veneer in the length and width directions, respectively; P is the gas pressure; μ is the viscosity of gas (about 1.846 x 10^{-5} $Pa*s$). In addition, the energy involved in localized phase change from water to vapour can be quantified in the model. Furthermore, the time-dependent water diffusion (moisture migration) during pressing can be more accurately characterized. By considering these additional factors, a more comprehensive two or three dimensional plywood/LVL hot-pressing simulation model, as demonstrated for OSB products (Dai and Yu 2004), can be developed.

To make the hot-pressing simulation model, VPress®, more useful and practical, efforts are needed to determine the effects of the hot-pressing process and resulting panel densification on panel quality and stiffness properties. Further work is needed to refine the algorithm and continue to upgrade the VPress® simulation model.

7.3 Bibliography

Bodig, J. and B. A. Jayne. 1982. Mechanics of wood and wood composites. Krieger Publishing Company. Malabar, Florida.

Dai, C. 2001. Viscoelasticity of wood composite mats during consolidation. Wood and Fiber Sci. 33 (3):353-363.

Dai, C. and C. Yu. 2004. Heat and mass transfer in wood composite panels during hot-pressing: Part I. A physical-mathematical model. Wood and Fibre Sci. 36(34): 585-597.

Wolcott, M. P., F. A. Kamke and D. A. Dillard. 1990. Fundamentals of flakeboard manufacture: viscoelastic behaviour of the wood component. Wood and Fiber Sci. 22:345-361.